Cholesterol Transport in the Hair Follicle:

A Novel Determinant of Hair Growth

Megan Alexandra Palmer

A thesis submitted to the University of Huddersfield in partial fulfilments of the requirements for the degree of Doctor of Philosophy

Department of Biological and Geographical sciences,

School of Applied Sciences,

The University of Huddersfield

September 2020

Table of contents

Table of figures

Table of tables

List of abbreviations

5αR	5α-reductases
7DHC	7-dehydrocholesterol
7DHCR	7-dehydrocholesterol reductase
AA	Alopecia areata
AGA	Androgenic alopecia
ABC	ATP binding cassette
ACAT	Acetyl-CoA acetyltransferase
APO	Apolipoprotein
AR	Androgen receptor
ATPB	ATP synthase subunit beta, mitochondrial marker
A.U.	Arbitrary units
BODIPY	Boron-dipyrromethene
BMP	Bone morphogenetic protein
BSA	Bovine serum albumin
CE	Cholesterol esters
CH25H	Cholesterol 25-hydroxylase
Co	Cortex
CS	Cholesterol sulfate
CTS	Connective tissue sheath
CTX-FITC	Cholera toxin-FITC conjugate
Cu	IRS cuticle
CYP	Cytochrome P450 family cleaving enzymes
DAPI	4′,6-diamidino-2-phenylindole
DHCR24	24-dehydrocholesterol reductase
DHT	Dihydrotestosterone
DKK1	Dickkopf-1
DP	Dermal papilla
EdU	5-ethynyl-2'-deoxyuridine
EBP	EBP cholestenol delta-isomerase
ER	Endoplasmic reticulum
ERK	Extracellular signal-regulated kinases
FC	Free cholesterol

FFA	Frontal fibrosing alopecia
FGF	Fibroblast growth factor
β-gal	β-galactosidase
GK5	Glycerol kinase 5
HC	Hair shaft cuticle
HDL	High density lipoprotein
He	Henle's layer
HF	Hair follicle
Hh	Hedgehog
HMG-CoA	3-hydroxy-3-methylglutaryl-CoA
HMGCR	HMG-CoA reductase
HMGCS	HMG-CoA synthase
Hu	Huxley's layer
HS	Hair shaft
IFAP	Ichthyosis follicularis with alopecia and photophobia
INSIG	Insulin-induced gene
IRS	Inner root sheath
JAK	Janus kinase family
KFSD	Keratosis follicularis spinulosa decalvans
KRT	Keratin
LAMP1	Lysosomal associated membrane protein 1
LDL	Low density lipoprotein
LDLR	Low density lipoprotein receptor
LEF1	Lymphoid enhancer binding factor 1
LPP	Lichen planopilaris
LSS	Lanosterol synthase
LXR	Liver X receptor
LXRE	LXR response element
MBTPS	Membrane bound transcription factor eptidase
MβCD	Methyl-β-cyclodextrin
NPC	Niemann-Pick disease, type C
NR0B1	Nuclear receptor subfamily 0 group B member 1
NR5A1	Nuclear receptor subfamily 5 group A member 1
ORS	Outer root sheath

PCA	Primary cicatricial alopecia
PCM	Pre-cortical matrix
PDI	Protein disulfide isomerases
PPAR	Peroxisome proliferator-activated receptor
PPRE	Peroxisome proliferator response element
RXR	Retinoid X receptor
SC5D	Sterol-C5-desaturaseare
SCARB1	Scavenger receptor class B type 1
SCAP	SREBP cleavage-activating protein
Shh	Sonic hedgehog
siRNA	Small interfering RNA
SG	Sebaceous gland
SREBP	Sterol regulatory element binding proteins
STAR	Steroidogenic acute regulatory protein
STARD	STAR-related lipid transfer domain proteins
STAT	Signal transducer and activator of transcription family
SULT2A1	Sulfotransferase family 2A member 1
SULT2B1b	Sulfotransferase family 2B member 1 isoform b
TGFβ	Transforming growth factor β
TUNEL	Terminal deoxynucleotidyl transferase dUTP nick end labelling

Abstract

The importance of cholesterol in hair follicle (HF) biology is underscored *via* links between cholesterol and both the pathogenesis of alopecias and hair growth. Defects in at least one ATP binding cassette (ABC) transporter (ABCA5) alter intracellular cholesterol distribution, leading to congenital hypertrichosis. The underlying mechanisms by which cholesterol levels, and cholesterol transport and compartmentalisation, influence keratinocyte behaviour within HF cell populations is largely unknown. The aim of this study was to characterise the routes of cholesterol transport within the HF and the effects for modulation of cholesterol levels on hair growth and cycling.

Primary keratinocytes isolated from the outer root sheath (ORS) of plucked human HFs were utilised as a model cell system, along with organ cultured human HFs, to examine their responsiveness to cholesterol loading *via* free cholesterol and depletion *via* methyl-β-cyclodextrin. Exogenous cholesterol loading in addition to siRNA-mediated knockdown of ABCA5 was performed in ORS keratinocytes. Exploration into cholesterol-sensitive target genes, cholesterol compartmentalisation and cellular behaviour were identified *via* numerous assays.

Liver X receptor (LXR) agonism demonstrated active regulation of *ABCA1* and *ABCG1*, but not *ABCA5* or *SCARB1*, in human HFs and ORS keratinocytes *via* qPCR, in addition to LXR regulating cholesterol efflux to apolipoprotein A1 and high-density lipoprotein. ABCA5 co-localised to intracellular organelles with cholesterol loading. Western blotting analysis of ABCA5 revealed additional isoforms at 300 and 400 kDa. The HFs capability to handle excess cholesterol and cholesterol depletion, along with small increases and decreases in Wnt signalling targets, respectively was detected. Methyl-β-cyclodextrin revealed a reduction in cell viability and cellular senescence *via* β-galactose staining, but no changes in proliferation. Immunofluorescence microscopy in human HF sections revealed differential expression of ABC transporters across the hair cycle. SCARB1 was highly expressed in the dermal papilla basement membrane. Staining for free cholesterol (filipin) revealed prominent cholesterol striations within the basement membrane of the hair bulb. *ABCA5* siRNA revealed a dysregulation in cholesterol homeostasis, and partial recovery of cholesterol homeostatic genes with LXR agonist T0901317 was detected. Filipin staining and live BODIPY cholesterol immunofluorescence microscopy revealed reduction of endo-lysosomal cholesterol with ABCA5 knockdown. Analysis of oxysterols *via* liquid chromatography mass spectrometry revealed significant differences in 25-hydroxycholesterol and 7-β-hydroxycholesterol following cholesterol loading in ORS keratinocytes with ABCA5 knockdown.

The maintenance of cholesterol homeostasis is vital for normal cellular function. As a pre-cursor for steroid hormone synthesis and regulator of signalling pathways associated with HF growth and cycling (i.e. Wnt/β-catenin, Shh), changes in cellular cholesterol could have wide-ranging implications for skin and hair biology. These results demonstrate the capacity of human HFs for cholesterol transport and trafficking. Furthermore, data shown here demonstrate a role for ABCA5 in the intracellular compartmentalisation of free cholesterol in primary HF keratinocytes. Reduced movement of cholesterol to APOA1 could indicate an indirect role for ABCA5 in the delivery of free cholesterol for ABCA1-mediated efflux. Crucially, the loss of normal homeostatic response to excess cholesterol delivery, following ABCA5 knockdown, suggests an impact on LXR-mediated transcriptional activity. We therefore speculate that the loss of ABCA5 leads to impaired endo-lysosomal cholesterol transport and thus alterations in signalling pathways such as JAK/STAT and Shh which could lead to alterations in hair growth. Further research should investigate the role of ABCA5 in modulating cholesterol homeostasis with a focus on signalling pathways associated with HF morphogenesis and cycling.

Copyright statement

i. The author of this thesis (including any appendices and/ or schedules to this thesis) owns any copyright in it (the "Copyright") and she has given The University of Huddersfield the right to use such Copyright for any administrative, promotional, educational and/or teaching purposes.

ii. Copies of this thesis, either in full or in extracts, may be made only in accordance with the regulations of the University Library. Details of these regulations may be obtained from the Librarian. This page must form part of any such copies made.

iii. The ownership of any patents, designs, trademarks and any and all other intellectual property rights except for the Copyright (the "Intellectual Property Rights") and any reproductions of copyright works, for example graphs and tables ("Reproductions"), which may be described in this thesis, may not be owned by the author and may be owned by third parties. Such Intellectual Property Rights and Reproductions cannot and must not be made available for use without permission of the owner(s) of the relevant Intellectual Property Rights and/or Reproductions.

Acknowledgements

I would like to thank my supervisor Dr Iain Haslam for his support and guidance throughout this PhD, especially for your encouragement and mentorship over the past four years. I would like to thank my co-supervisor Dr Nikolaos Georgopoulos for his support. A big thank you to Dr Irundika Dias for collaborating on the oxysterol lipidomic work. Thank you to my fellow lab member Sarah, especially for staying with me on many occasions into the night dissecting hair follicles. Thank you to my undergraduate placement student Liam for all your hard work.

A big thanks to all my friends on "Girl street" for always being there for a chat, and to eat a whole cake with just a spoon when the times called for it! All your encouragement and support has helped me along this journey we have taken together. I can't wait to celebrate all of our accomplishments together.

A big thank you to Ellie, I have very much enjoyed our chats on the trips to Huddersfield, and for always answering my random science questions. Very much appreciate the times I have stayed in your spare room, our trips to the theatre and yoga together.

A massive thank you to Steffen who has put up with a lot of moaning about writing over the last six months. Thank you for being there for me and engaging with my midnight talks about science and life.

Thank you to all my family for all your support on this journey, your encouragement and love is what has moulded me into the person I am today. Thank you, Mum, for always making sure I am taking care of myself and not getting lost in work. Thank you, Dad, for always asking me if I can answer my own questions.

Finally, I would like to dedicate this thesis to my grandad Dr Rex Palmer whose encouragement and support I could not have done without. You are my inspiration as a scientist, and I aspire to follow in your footsteps!

Publications

Palmer, MA, Blakeborough, L, Harries, M, Haslam, IS. Cholesterol homeostasis: Links to hair follicle biology and hair disorders. Exp Dermatol. 2019; 00: 1–13. https://doi.org/10.1111/exd.13993.

- Conceptual design and writing of the manuscript
- This publication has been incorporated into Chapter 1, and figures used clearly referenced

Palmer, MA, Smart, E, Haslam IS. Localisation and regulation of cholesterol transporters in the human hair follicle: mapping changes across the hair cycle. Histochemistry and cell biology. (Submission under review)

- Experimental design, performed and analysed the experiments, wrote the manuscript
- This publication has been developed from Chapter 5, including Chapter 3: Section 3.2.3

Palmer, MA, Dias, I, Smart, E, Haslam IS. Cholesterol homeostasis in hair follicle keratinocytes is disrupted by impaired ABCA5 activity. (Publication in preparation)

- Experimental design, performed and analysed the experiments, wrote the manuscript
- This publication has been developed from Chapter 6: including Chapter 3: Figure 3.9

Oral presentations

Palmer, MA., Haslam, IS. Cholesterol Transport in the Hair Follicle: A Novel Determinant of Hair Growth. North of England Cell Biology Forum. August 2018, The University of Huddersfield, UK

Poster presentations

Palmer, M.A., Haslam, I.S. A bioimaging approach to determine the impact of ABCA5 knockdown on intracellular cholesterol distribution in hair follicle keratinocytes: Comparisons between endpoint and live imaging of cholesterol distribution. NEUBIAS Conference & Symposium. March 2020, Bordeaux, France

Palmer, M.A., Haslam, I.S. Filipin staining identifies distinct membrane staining patterns in human hair follicle keratinocytes. North England cell biology forum. September 2019, University of Manchester, UK

Palmer M.A., Haslam I.S. Cholesterol homeostasis is disrupted by ABCA5 knockdown in outer root sheath keratinocytes. World Congress of Hair Research. April 2019, Sitges, Spain

Palmer, M.A., Haslam, I.S. Cholesterol transport in the hair follicle: A novel determinant of hair growth (Poster and flash presentation). Structure and mechanism of membrane proteins. August 2018, Birmingham, UK

Palmer, M.A., Haslam, I.S. Cholesterol transport in the hair follicle: A novel determinant of hair growth. North England cell biology forum. September 2017, University of Hull, UK

Chapter 1:   Introduction

1.1 Rationale

Cholesterol is vital to the functioning of all animal cells and has particular importance in cutaneous tissues. Cholesterol functions in the regulation of membrane fluidity through partitioning into the phospholipid bilayer, therefore forming an essential component of cell membranes (Ohvo-Rekilä *et al.*, 2002), in addition to regulation of cell signalling *via* for example, activation of the Wnt/β-catenin pathway and modulation of hedgehog protein (Hh) biogenesis (Incardona and Eaton, 2000, Sheng *et al.*, 2014).

The importance of cholesterol is emphasized by the capability of all vertebrate cells in *de novo* biosynthesis (Cortes *et al.*, 2014). Furthermore, circulatory lipoproteins (i.e. high density lipoprotein [HDL] or low density lipoprotein [LDL]) provide additional sources of cholesterol, and membrane efflux pumps facilitate the removal of excess cholesterol (by for example ATP-binding cassette transporter (ABC) A1 and ABCG1). Physiological feedback loops are integral in maintaining the narrow concentration range for a balance in cellular cholesterol levels, through control of cholesterol efflux, biosynthesis, and uptake.

Within peripheral tissues the roles for cholesterol have been previously reported. In the skin, cholesterol is a precursor for the synthesis of local steroid hormones (Thiboutot *et al.*, 2003, Inoue *et al.*, 2012, Payne and Hales, 2004), influences keratinocyte differentiation (Elbadawy *et al.*, 2011, Jiang *et al.*, 2005, Spörl *et al.*, 2010), melanogenesis (Schallreuter *et al.*, 2009, Lee *et al.*, 2016), barrier repair (Tsuruoka *et al.*, 2002), corneocyte desquamation (Jiang *et al.*, 2005), and is important in maintaining epidermal permeability barrier (Feingold, 2009, Wertz, 2000). Yet investigations into the role of cholesterol in the hair follicle (HF) have yet to be fully explored. Whereas the impact of lipids on HF biology are recognized, through the association of the HF with the lipid-rich sebaceous gland (SG), the precise functions regulated by cholesterol are not as well understood. Reports of both hair loss and hair growth with cholesterol-modulatory drug therapies have been made, along with associations between sterol levels and certain hair disorders (Ali and Martin, 2010, Lattouf *et al.*, 2015, Robins, 2007, Cervantes *et al.*, 2018, Lee, 2000, Robb-Nicholson, 1998).

A greater understanding of the control of cellular cholesterol in the HF and the potential impact on the hair cycle may identify novel targets for regulating hair growth and the treatment of hair disorders linked to disordered sterol homeostasis or sterol-sensitive signalling pathways (DeStefano *et al.*, 2014, Evers *et al.*, 2010, Panicker *et al.*, 2012).

This chapter will introduce the following topics:

1. HF anatomy and cycling
2. Mechanism of cholesterol homeostasis
3. The role of cholesterol in signaling pathways associated with HF cycling
4. The role of cholesterol in keratinocyte biology
5. Cholesterol associated hair pathologies

1.2   The human hair follicle

1.2.1   Anatomy of the hair follicle

The human HF is a cyclical mini organ, which along with the SG and arrector pili muscle makes up the pilosebaceous unit of the skin. HFs are composed of a series of concentric keratinocyte layers with a central hair shaft (HS), all of which are encapsulated by a mesenchymal connective tissue sheath (CTS) (Schneider *et al.*, 2009) (Figure 1.1). The HF is comprised of an upper permanent portion which is continuous with the epidermis in the infundibulum, along with the isthmus containing a resident population of adult stem cells, residing within a region known as the 'bulge' (Cotsarelis *et al.*, 1990). In addition, there is a lower portion that undergoes remodelling during the hair cycle, which can be split into the suprabulb and bulb (Schneider *et al.*, 2009).

Within the deepest portion of the HF located within the hypodermis, the bulb region contains transient amplifying cells known as matrix keratinocytes, which rapidly proliferate and differentiate to produce the various layers of the inner root sheath (IRS) and keratinised HS itself (Hsu *et al.*, 2014) (Figure 1.1 red box). These hair matrix cells must undergo a tightly regulated process of differentiation as they proliferate and migrate upwards, establishing the IRS and trichocytes that form the HS.

In human HFs, the bulge region can be defined as CD200 and keratin (KRT) 15 positive as well as Connexin 43 negative region (Purba *et al.*, 2014). These slow cycling cells are predominantly quiescent (Lyle *et al.*, 1998). In the mouse Sox9 expression is essential in maintaining the HF stem cell niche (Kadaja *et al.*, 2014), whereas human studies have shown that in addition to the bulge Sox9 expression is predominantly in the sub-bulge region along with the matrix (Purba *et al.*, 2015). Formation of the outer root sheath (ORS), the outermost keratinocyte cell layer of the HF, differs in that the bulge cells migrate in a downwards manner and proliferate (Oshima *et al.*, 2001, Purba *et al.*, 2017) to repopulate the ORS in both human and mouse. In addition murine studies suggest the bulge region slowly repopulates the germinative pool of matrix keratinocytes (Huang *et al.*, 2019a). Furthermore, human melanocyte stem cell population is found within the bulge region of HFs. (Gola *et al.*, 2012).

The companion layer (Figure 1.1 red box) is a single layer of cells residing between the ORS and IRS, in the mouse it has been shown that the companion layer is transcriptionally similar to the ORS (Joost *et al.*, 2020), yet is highly associated with Henle's layer (He). Morphologically it is distinct with specific KRT75 expression in both human and mouse (Wang *et al.*, 2003, Winter *et*

al., 1998) and appears to function in the movement of the IRS with the hair growth against the immobile ORS (Harland and Plowman, 2018).

The IRS is comprised of three layers (Figure 1.1 red box), He, Huxley's layer (Hu) and the IRS cuticle (Cu). He is a single layer of cells, that undergoes terminal cornification at the distal portion of the bulb (Joshi, 2011). These plate-like cells form a structural support of the IRS, and differ morphologically to the elongated Hu, which contains approximately 2-4 layers of cells which cornify at the Adamson's fringe (Harland and Plowman, 2018). As the IRS layers differentiate trichohyalin granules accumulate, which disappear during cornification (Harland and Plowman, 2018, Joshi, 2011). Together with the Cu, the IRS functions in the structure and shape of the HS (Harland and Plowman, 2018, Joshi, 2011, Hashimoto, 1988).

The HS is comprised of the HS cuticle (HC), cortex (Co) and the medulla (Figure 1.1 red box), which express KRT85, a specific HF keratin. The HC cells are originally oval in shape, which elongate and produce a greater number of trichohyalin granules as they move distally (Hashimoto, 1988). The overlapping structure of HC cells is highly associated with the Cu (Harland and Plowman, 2018, Hashimoto, 1988). Additionally, within the bulb the dendritic processes of melanocytes come into contact with the Co cells (and to a lesser extent the medulla) (Slominski *et al.*, 2005). Here pigmentation of the HS occurs through the transfer of melanin granules from mature melanosomes to the HS keratinocytes (Slominski *et al.*, 2005) through phagocytosis (Harland and Plowman, 2018).

In the human HF, the dermal papilla (DP) is an onion shaped ball of densely packed inductive fibroblasts, surrounded by the matrix keratinocytes (Figure 1.1). These specialised fibroblasts communicate with the HF epithelium to influence both hair growth and cycling (Schneider *et al.*, 2009). The DP is classified as the signalling centre of the HF, and cross talk between the DP and secondary hair germ initiates new hair growth. In addition signalling occurs between the DP and the transient amplifying cells which defines the fate of the matrix keratinocytes (Lei *et al.*, 2017).

Separating the mesenchymal and epithelial portions of the HF is the basement membrane, a region rich in extracellular matrix proteins (Joubeh *et al.*, 2003). The basement membrane can be broken down into two components, the keratinocytes connect with the lamina lucida containing α6 and β4 integrins along with collagen XVII (Beiu *et al.*, 2019), and the lamina densa containing collagen IV, laminin-332 and laminin-551 (Gao *et al.*, 2008, Imanishi *et al.*, 2010, Sugawara *et al.*, 2007) which anchor to collagen VII filaments within the dermal fibroblast population (Beiu *et al.*,

2019). A thickening of the basement membrane surrounding the DP distally is present along with thickening during catagen (Couchman and Gibson, 1985).
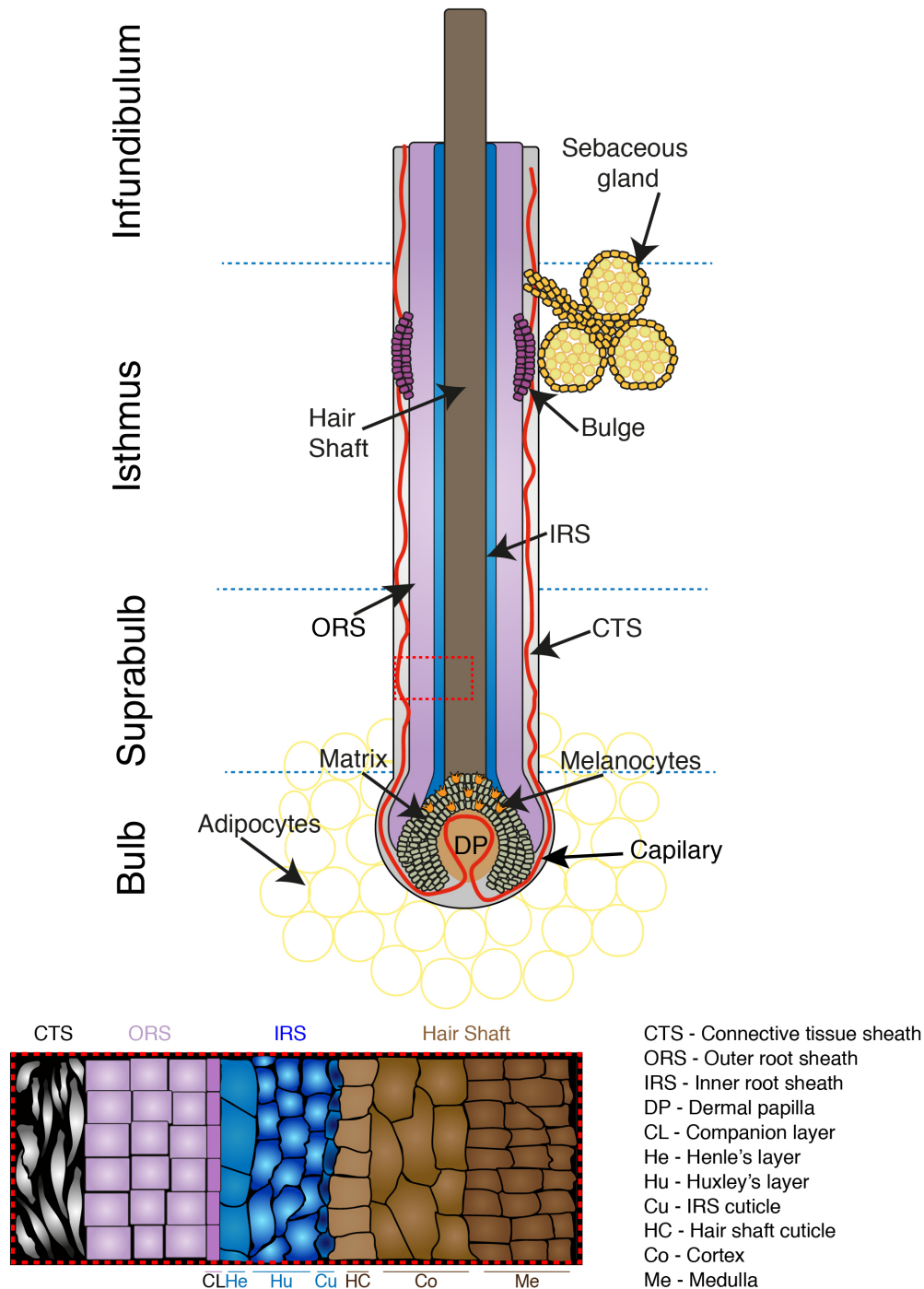
Figure 1.1 Schematic representation of the human hair follicle. The anagen VI HF is comprised of concentric layers of keratinocytes encompassing of the hair shaft, IRS and ORS. Surrounded by a fibroblast layer, the CTS, containing the vasculature supply to the HF. The bulb region of the HF is located proximally and contains the signalling centre of the HF, DP, and highly proliferative matrix keratinocytes. Distal to the bulb the HF can be broken down into the suprabulb, isthmus and infundibulum regions. Within the isthmus the ORS contains the K15/CD200+ bulge region of keratinocytes, proximal to the sebaceous gland. Red dashed box represents the differences in cell morphology of the individual HF layers (image generated in Adobe Illustrator®)

1.2.1.1 **The hair cycle**

As detailed in Figure 1.2, the HF is a cyclically regenerating mini-organ that undergoes regular periods of growth (anagen), regression (catagen) and relative quiescence (telogen) (Oh *et al.*, 2016). This process of initial hair growth and cycling is tightly regulated by numerous signalling pathways (Schneider *et al.*, 2009), and it is therefore important to gain an understanding of how both the anatomy of the HF is altered and the signalling involved to give insight into how cholesterol may alter HF growth and cycling.

1.2.1.2 **Hair follicle morphogensis**

Initial HF growth occurs *in utero* with the formation of the placode; this process is driven through Wnt/β-catenin, noggin and transforming growth factor β (TGFβ) signalling (Schneider *et al.*, 2009). Subsequently the formation of the DP occurs through sonic Hh (Shh) signalling, along with the hair germ formed through increased fibroblast growth factor (FGF) (Chiang *et al.*, 1999). Furthermore, proliferation and differentiation are driven through numerous signalling pathways including Wnt/β-catenin, Shh, noggin and notch in the HF peg to produce a keratinous HS (Schneider *et al.*, 2009).

1.2.1.3 **Catagen**

Following initial hair growth, apoptosis-mediated regression occurs. Catagen can be broadly subcategorised into three stages: early, mid and late (Kloepper *et al.*, 2010). This period of hair growth results in the rapid regression of the HF and is present in 5-10% of scalp hair (Oh *et al.*, 2016). Initiated through FGF5 signalling in mice (Suzuki *et al.*, 2000), early catagen can be identified through a loss of melanin production in the pre-cortical matrix (PCM) and melanin incontinence where leaking of pigmentation into the DP occurs (ectopic melanin) (Oh *et al.*, 2016, Stenn and Paus, 2001, Tobin, 2011). The previously onion shaped DP reduces to become an almond shape through migration of DP fibroblasts into the DP stalk (Oh *et al.*, 2016). The surrounding matrix keratinocytes undergo apoptosis (Stenn and Paus, 2001) and a general reduction in cell number and volume of the HF bulb is noted (Kloepper *et al.*, 2010). A progression of apoptosis occurs during mid-catagen where a reduction to few matrix keratinocytes encasing the DP takes place. The remnants of the ORS and IRS form the epithelial strand and the HS begins the formation of the brush-like club hair (Oh *et al.*, 2016). Late catagen reveals a shortened epithelial strand which draws the now rounded DP towards the bulge, leaving a CTS trail behind (Oh *et al.*, 2016). Migration of the bulge stem cell region to encapsulate the club hair also occurs. In addition to FGF5, many other factors have been identified as catagen inducing such as; Wnt

inhibition through dickkopf WNT signalling pathway inhibitor 1 (DKK1) (Kwack *et al.*, 2012), TGFβ (Hibino and Nishiyama, 2004) and bone morphogenetic protein (BMP) inhibition through Noggin (Guha *et al.*, 2004).

1.2.1.4   **Telogen**

A period of relative "quiescence" occurs following catagen, where predominantly neither proliferation nor apoptosis is occurring, and equates for 1-2% of human scalp hairs (Oh *et al.*, 2016). The HF, now two thirds the size during Anagen VI, has condensed to lie within the dermis. The HF epithelium can be characterised into the KRT15 and CD200 positive outer bulge, and the inner bulge which surrounds the club hair (Hawkshaw *et al.*, 2020). Additionally, the formation of the secondary hair germ (SHG) separates the club hair from the DP.

Previously thought to be entirely quiescent, the telogen stage of the hair cycle is now known to be integral to maintenance of the HF stem cell niche and preparation for the regeneration of the HF (Geyfman *et al.*, 2015). Telogen can be separated into two phases, refractory and competent telogen. Refractory telogen is defined by high BMP and FGF signalling, with TGFβ signalling absent. In comparison, during competent telogen BMP and FGF signalling switches to low, with high levels of TGFβ present (Geyfman *et al.*, 2015).

1.2.1.5   **Anagen**

Initiation of new anagen, and therefore new hair growth is induced through Wnt signalling (Hawkshaw *et al.*, 2020). Anagen can be categorised into 6 stages (Oh *et al.*, 2016), starting with proliferation of the bulge and SHG in Anagen I, leading to development and differentiation of the concentric HF layers (Oh *et al.*, 2016). Pigmentation occurs by Anagen IV, the distinct onion shaped DP being detectable by Anagen V (Oh *et al.*, 2016). The majority of HF *in situ* are in Anagen VI where they remain for a number of years (Stenn and Paus, 2001).
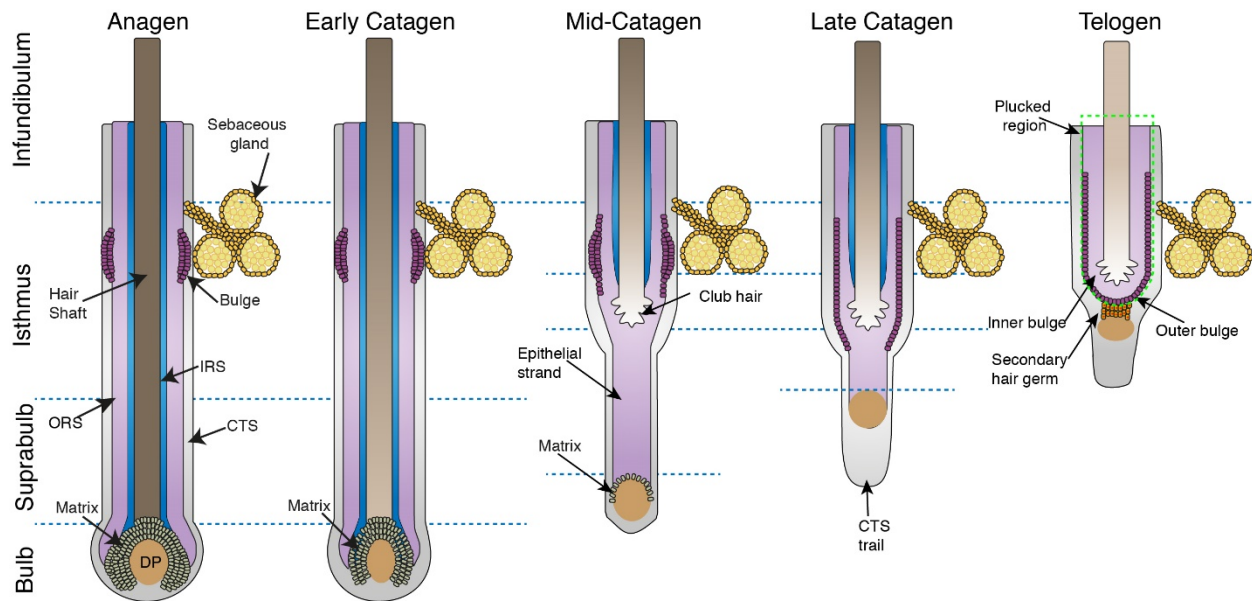
Figure 1.2 Schematic representation of the hair cycle. The cyclical mini-organ goes through periods of growth (anagen), apoptosis-mediated regression (catagen) and relative quiescence (telogen). Early catagen is represented by a loss of pigmentation in the hair shaft, loss of matrix keratinocytes and a transition from the onion shaped DP in anagen to an almond shape for early catagen. Further regression occurs during mid-catagen to reveal the epithelial stand and formation of the club hair, along with migration of bulge keratinocytes. The development of the CTS trail occurs during late catagen. During telogen the DP is condensed, bulge keratinocytes have migrated and surrounded the club hair (outer bulge) along with the production of the secondary hair germ and a CTS trail present. Plucked telogen follicles are represented by the dashed green line, in which the fibroblast layers, sebaceous gland and secondary hair germ are retained in the scalp (image generated in Adobe Illustrator®).

1.3 Cholesterol homeostasis

Cellular cholesterol metabolism has been covered in detail in many excellent reviews (Aye *et al.*, 2009, Ikonen, 2008, Incardona and Eaton, 2000, Klappe *et al.*, 2009, Quazi and Molday, 2011). This section is therefore restricted to summarising the generic mechanisms involved in the regulation of cellular cholesterol levels.

1.3.1 *De novo* cholesterol synthesis

As summarised in Figure 1.3 the initial steps in cholesterol synthesis start in the mitochondria with the formation of Acetoacetyl-CoA from two molecules of Acetyl-CoA initiated by Acetyl-CoA acetyltransferase (ACAT) 2. 3-hydroxy-3-methylglutaryl-CoA (HMG-CoA) is produced through the modification of Acetyl-CoA and Acetoacetyl-CoA by HMG-CoA synthase (HMGCS) in the mitochondria (Ikonen, 2008, Incardona and Eaton, 2000).

The remaining steps predominantly occur in the endoplasmic reticulum (ER) where the rate-limiting enzyme HMG-CoA reductase (HMGCR) forms mevalonic acid. A series of further enzymatic reactions in the mevalonate pathway are required to produce Squalene (Goldstein and Brown, 1990). Squalene is transformed into squalene 2,3-epoxide by squalene epoxidase (SQLE) Another series of enzymatic reactions occur and lanosterol synthase (LSS) generates lanosterol (Sharpe and Brown, 2013, Hubler *et al.*, 2018).

Here two pathways are available, in the Bloch pathway cytochrome P450 cleaving enzymes (CYP) CYP51A1 (Bloch, 1992) facilitates the next step, whereas 24-dehydrocholesterol reductase (DHCR24) in initiates the Kandutsch-Russell pathway (Kandutsch and Russell, 1960). In both pathways EBP cholestenol delta-isomerase (EBP) is utilised in the reduction of zymosterol (Mitsche *et al.*, 2015). Further reductions by sterol-C5-desaturaseare (SC5D) form either dehydrodesmosterol or 7-dehydrocholesterol (7DHC). In the Kandutsch Russell pathway the cholesterol precursor 7DHC is reduced by 7DHC reductase (7DHCR) to form cholesterol (Ikonen, 2008), whereas desmosterol is formed in the Bloch pathway requiring an additional step by DHCR24 to form cholesterol (Mitsche *et al.*, 2015). An alternative pathway for cholesterol synthesis can be achieved in peroxisomes from the initial Acetyl-CoA step up to the mevalonate pathway, where squalene will move into the ER for the remainder of the synthesis pathway (Thompson and Krisans, 1990).
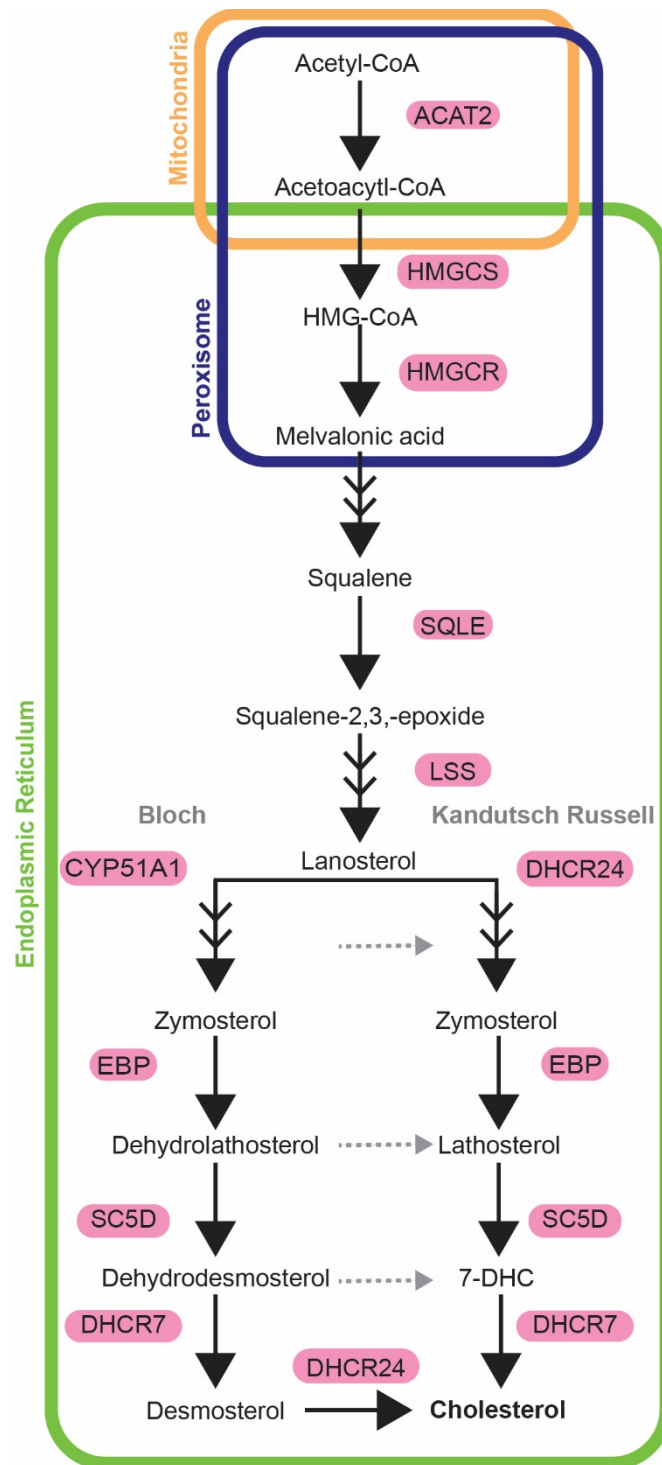
Figure 1.3 Cholesterol biosynthesis pathways. *De novo* cholesterol synthesis occurs through a series of defined reactions in the endoplasmic reticulum, enzymes outlined in pink, dashed grey arrows show cross over paths mediated by DHCR24 between the Bloch and Kandutsch Russell pathways.

1.3.2 Cholesterol uptake

Uptake in the peripheral tissues occurs primarily through the binding of LDL to the LDL receptor (LDLR) on cell membranes and undergoes receptor-mediated endocytosis (Ikonen, 2008). Scavenger receptor class B member 1 (SCARB1) primarily functions in the uptake of free cholesterol (FC) and cholesterol esters (CE) from circulating HDL (Rhainds and Brissette, 2004). CD36 belongs to the same family as SCARB1 and is also involved in the uptake of cholesterol in enterocytes (Nassir *et al.*, 2007), though expression in the skin is less well defined (Westergaard *et al.*, 2001). There is evidence that both of the receptors can mediate bi-directional cholesterol trafficking, and SCARB1 has been shown to increase cholesterol to the lipid rafts (Rhainds and Brissette, 2004). Niemann-Pick disease, type C (NPC) 1 like intracellular cholesterol transporter 1 is a dominant cholesterol transporter in the intestine, however expression is unknown in the skin or hair (Davies *et al.*, 2005).

1.3.3 Cholesterol efflux

ABC transporters play an important role in the transport of lipids, with the ABCA family involved in cholesterol efflux. ABCA1 is a well characterised cholesterol transporter and is ubiquitously expressed. It meditates the efflux of excess cholesterol from cells to apolipoproteins (APO), in particular APOA1, for the formation of nascent HDL for reverse cholesterol transport (Klappe *et al.*, 2009, Quazi and Molday, 2011). ABCA7 is another cholesterol transporter known to be located in the skin, particularly in late differentiating keratinocytes (Quazi and Molday, 2011, Kielar *et al.*, 2003). ABCG1, another ubiquitous ABC transporter known to be expressed in the skin, is characterised in transport of cholesterol to HDL (Jiang *et al.*, 2010). Other ABC transporters known to transport cholesterol are ABCB1, ABCG4, and the heterodimeric ABCG5/ABCG8 (Quazi and Molday, 2011). ABCA5 (DeStefano *et al.*, 2014, Ye *et al.*, 2010) and ABCA2 (Mack *et al.*, 2007) have putative roles in cholesterol movement. In addition to cholesterol uptake, cholesterol efflux to HDL *via* SCARB1 is also known (Shen *et al.*, 2018b).

1.3.4 Intracellular cholesterol transport

Intracellular trafficking of cholesterol can occur through two mechanisms: vesicular and non-vesicular. Vesicular transport requires a cytoskeleton along with ATP to facilitate the movement. Non-vesicular transport occurs through hydrophobic cavity transporter proteins, such as steroidogenic acute regulatory protein (STAR) and through spontaneous resorption which is

thought to be processed through as yet unidentified specialist proteins (Soccio and Breslow, 2004).

Although the ER is the site of cholesterol synthesis, it is a cholesterol poor environment. Nascent cholesterol is rapidly exported from the ER to the plasma membrane, a cholesterol-rich site. A small amount of the export occurs through vesicular mechanisms produced by the Golgi. However, the transport is more likely to occur through non-vesicular mechanisms. Caveolin 1 and 2 along with sterol carrier protein 2 have been shown to facilitate this, in addition with caveolin like cholesterol chaperones (Incardona and Eaton, 2000). Lipid droplet formation occurs from excess cholesterol produced from the ER (Ikonen, 2008, Soccio and Breslow, 2004).

Excess cholesterol accumulated in the plasma membrane returns to the ER for esterification, through a different route other than nascent cholesterol. Sphingomyelinase facilitates the release of cholesterol from the plasma membrane through the formation of vesicles. This can occur without ATP; however, ATP is required for the vesicles to become late endosomes and lysosomes which can be transported back to the ER. Mediated through the Golgi, this can be achieved both by non- vesicular or vesicular routes (Soccio and Breslow, 2004).

Mitochondria are also cholesterol poor organelles, however they contain two important P450 type enzymes within the inner membrane which are integral to the function of cholesterol in hormone synthesis. CYP11A1 converts cholesterol to pregnenolone which is post modified to create sterol hormones. CYP27A1 converts cholesterol into 27-hydroxycholesterol which functions in reverse cholesterol transport due to being an LXR agonist, represses sterol regulatory element binding protein (SREBP) intermediates in the synthesis of bile acid and is a more soluble form of cholesterol to be transported within the plasma. Multiple sources of cholesterol are presented to mitochondria, some of which are: lipid droplets, late endosomes and lysosomes (Ikonen, 2008, Soccio and Breslow, 2004). STAR-related lipid transfer domain protein (STARD) 3 is located on the surface of late endosomes and interacts with NPC intracellular cholesterol transporter 2 (NPC2) to assist transport into the mitochondria (Wustner and Solanko, 2015). STARD4 is said to transport cytoplasmic FC and cholesterol oxides from lysosomes to the outer membrane of mitochondria (Elbadawy *et al.*, 2011, Ikonen, 2008). STAR facilitates the movement from the outer to the inner membrane of the mitochondria, through the binding of cholesterol with the peripheral benzodiazepine receptor (Ikonen, 2008, Soccio and Breslow, 2004).

1.3.5   Regulation

Regulation of cholesterol homeostasis occurs through numerous nuclear receptors, two main mechanisms are: SREBPs, or ligand-activated retinoid X receptor (RXRs) heterodimerising with liver X receptor (LXRs), as summarised in Figure 1.4.

In cholesterol poor environments SREBP cleavage-activating protein (SCAP) facilitates transport of SREBP2 from the ER to the Golgi for processing. The proteolytic fragmented SREBP2 is produced through two enzymatic reactions by membrane bound transcription factor peptidase (MBTPS)1 and MBTPS2. SREBP2 then moves to the nucleus, initiating the transcription of HMGCR and the LDLR, amongst other genes which increase cellular cholesterol levels (Figure 1.4A). SREBP-mediated transcription is downregulated through Insulin-induced gene (INSIG) and SCAP binding in sterol-rich environments. This is initiated through the binding of FC to SCAP and oxysterols to INSIG. SREBP transport is blocked and expression of downstream targets inhibited (Figure 1.4B) (Shimano and Sato, 2017). Additionally INSIG can also act through binding to the sterol sensing domain of HMGCR, resulting in enzyme degradation (Sever *et al.*, 2003)

In cholesterol-rich environments activation of the LXR/RXR pathway occurs, through oxysterols and retinol binding respectively, initiating the transcription of ABC transporters and APO, along with the downregulation of transcription of cholesterol synthesis genes. Two isoforms of LXR exist, LXRα and LXRβ, both of which are expressed in the skin and hair (Russell *et al.*, 2007, Schmuth *et al.*, 2004). Ligand activated LXR binds to the LXR response element (LXRE) in target genes to initiate transcription (Zhao and Dahlman-Wright, 2010).

In addition RXR can also heterodimerise with peroxisome proliferator-activated receptor (PPAR), which in turn initiates binding to the peroxisome proliferator response element (PPRE) (Gupta *et al.*, 2015, Ramot *et al.*, 2015), initiating the transcription of numerus downstream target genes including those associated with gluconeogenesis, ketogenesis, mitochondrial oxidation, lipoprotein metabolism and cholesterol catabolism (Mandard *et al.*, 2004). In addition PPAR activation functions in enhancing proliferation of peroxisomes, which act as secondary sites for cholesterol synthesis (Gupta *et al.*, 2015, Karnik *et al.*, 2009). Furthermore, PPAR activation has been shown to increase ABCA1 expression, although this is likely to be in an LXR-mediated manner (Ogata *et al.*, 2009).
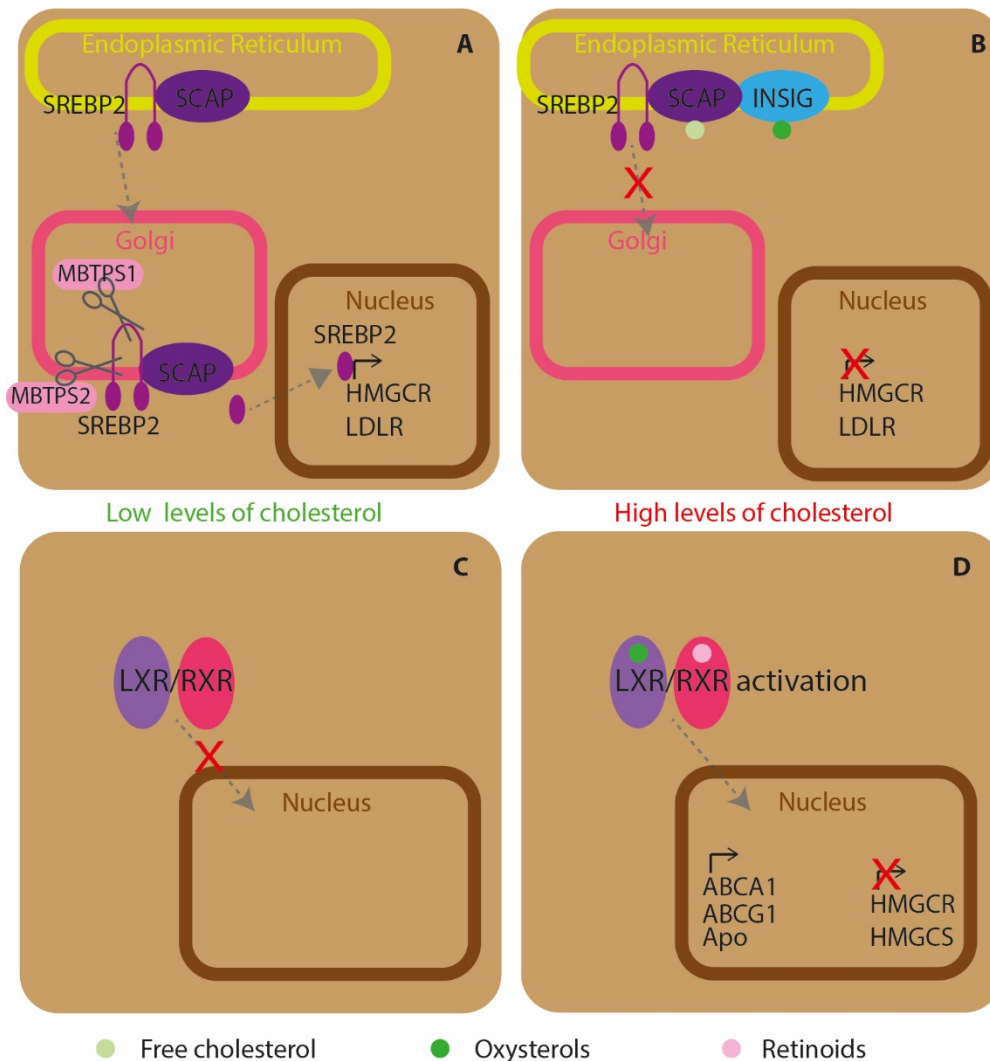
Figure 1.4 Regulation of cholesterol homeostasis. Schematic representation of SREBP2-mediated regulation (A) during low cholesterol leading to SREBP2 processing and transcription of cholesterol synthesis and uptake genes, whereas (B) during high levels of cholesterol INSIG prevents the movement of SCAP/SREBP2 to the Golgi. (C) LXR/RXR-mediated regulation is inactive with low sterol levels, (D) during high cholesterol activation of LXR/RXR with oxysterol and retinols initiates the transcription of cholesterol efflux genes.

1.3.6   Cholesterol metabolism

Oxysterols have many functions including transcriptional regulation of cholesterol homeostasis through SREBP2 and LXR (Olkkonen *et al.*, 2012), keratinocyte differentiation (Hanley *et al.*, 2000), apoptosis (Lordan *et al.*, 2009), and 25-hydroxycholesterol has been shown in Shh signalling through interactions with smoothened (Corcoran and Scott, 2006). The generation of oxysterols can occur through either enzymatic synthesis in the ER and mitochondria, or through autoxidation through reactive oxygen species (Olkkonen *et al.*, 2012) as shown in Figure 1.5.

In the mitochondria, CYP27A1 facilitates the addition of a hydroxy group to the 27th carbon to form 27-hydroxycholesterol, and is important both in bile acid production (Chiang, 1998) and vitamin-D metabolism (Nemazannikova *et al.*, 2019). In addition, 27-hydroxycholesterol is a selective oestrogen receptor modulator (DuSell *et al.*, 2008).

Within the ER multiple enzymes which facilitate cholesterol metabolism are present. For example; CYP3A4 forms 4-β-hydroxycholesterol, CYP46A1 generates 24-hydroxycholesterol, and cholesterol 25-hydroxylase (CH25H) forms 25-hydroycholesterol, which is further oxidised to form 7-α-dihydroxycholesterol by CYP7B1 (Olkkonen *et al.*, 2012).

Autoxidation of the 7th carbon atom of cholesterol can produce 7-β-hydroxycholesterol, 7-ketohydroxycholesterol, in addition autoxidation of the 5th and 6th carbon atoms forms 5-6-epoxycholesterol. Moreover accumulation of these oxysterols can lead to apoptosis (Lordan *et al.*, 2009).

In addition to oxysterols, esterification of cholesterol through ACAT1 and ACAT2 is one mechanism cells apply to reduce high ER cholesterol levels (Ikonen, 2008). Sulfation of 25-hydroxycholesterol is achieved through sulfotransferase family 2B member 1 isoform b (SULT2B1b) to produce 25-hydroxycholesterol 3-sulfate, which is further sulphated by the sulfotransferase family 2A member 1 (SULT2A1) to produce 25-hydroxycholesterol di-sulfate (Ren *et al.*, 2014). This process is reversible by steroid sulfatase (Elias *et al.*, 2014), and cholesterol sulfate (CS) has been shown to induce differentiation in the skin (Elias *et al.*, 2014, Hanley *et al.*, 2001, Hanyu *et al.*, 2012).

Synthesis of pregnenolone in the mitochondria by CYP11A1 is the initial first step in steroidogenesis. Further enzymatic reactions occur in the ER with CYP17A1 (Payne and Hales, 2004, Hu *et al.*, 2010). Indeed steroidogenic enzymes are present in the HF (Slominski *et al.*, 2013) as discussed further in Section 1.5.3 Hu *et al.* (2010) have reviewed the utilisation of cholesterol sources in the production of steroid hormones, which will not be covered in as much detail here.
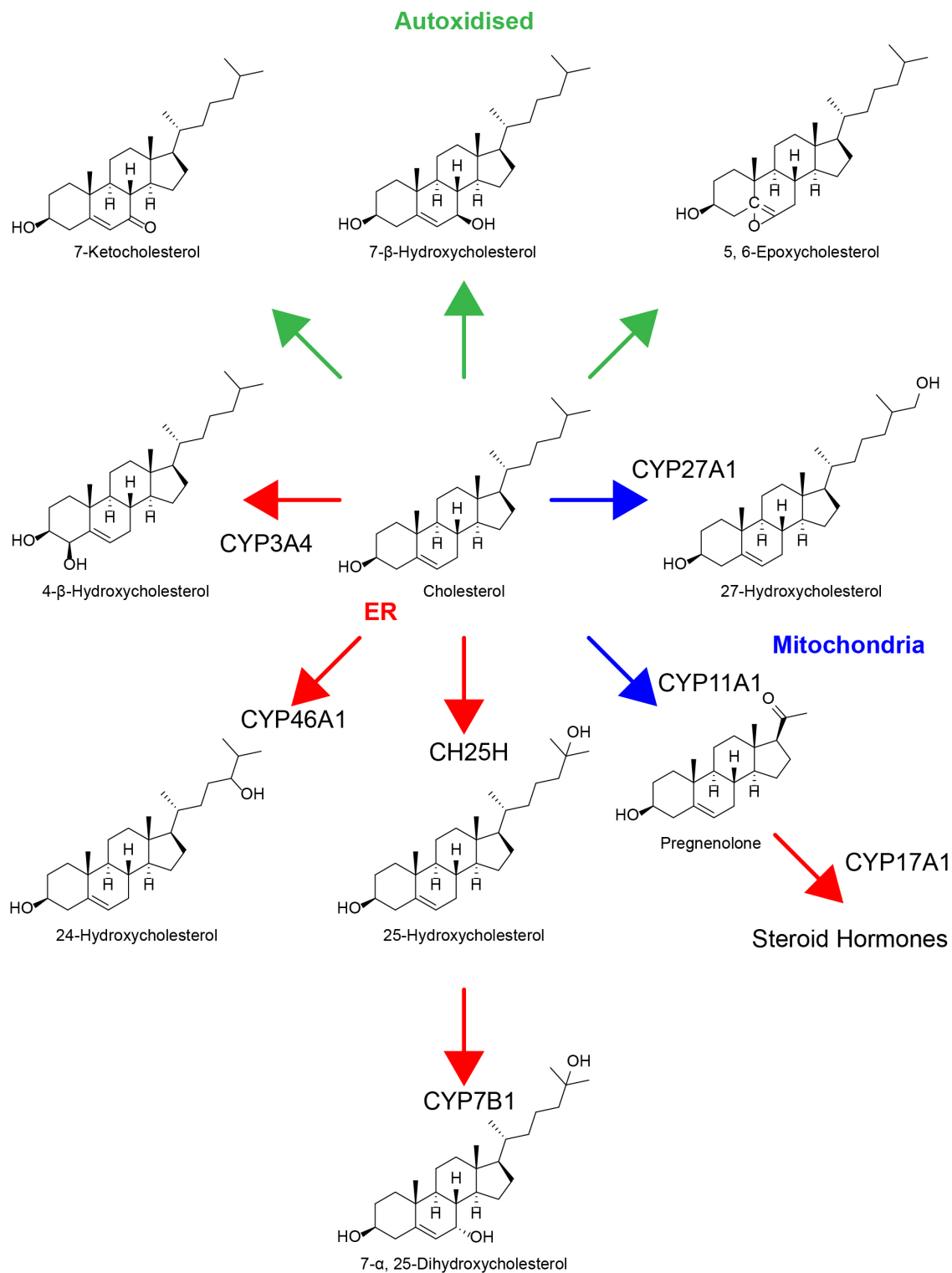
Figure 1.5 Cholesterol metabolism. Structure of cholesterol and its oxysterol metabolites, along with steroid precursor pregnenolone. Green arrows indicate autoxidation, red arrows enzymatic reactions within the ER and blue arrows within mitochondria.

1.3.7 Specific cholesterol transporters

In characterising cholesterol homeostasis in the HF, investigations will focus on three ABC transporters, two of which are ubiquitously expressed and known in the skin: ABCA1 (Deng *et al.*, 2019, Jiang *et al.*, 2006) and ABCG1 (Jiang *et al.*, 2010, Marko *et al.*, 2012). Along with examination of ABCA5, a putative cholesterol transporter implicated in congenital hypertrichosis (DeStefano *et al.*, 2014, Hayashi *et al.*, 2017). Additionally, the bi-directional cholesterol transporter SCARB1, which has also been identified in the skin (Crivellari *et al.*, 2017, Muresan *et al.*, 2018, Sticozzi *et al.*, 2012) will be explored. Therefore, this section focuses on these specific transporters in more detail.

1.3.7.1 ABCA1

ABCA1 is the first member of the ABCA family, characterised for their transport of lipids (Quazi and Molday, 2011). The large 254 kDa membrane protein contains six transmembrane domains for both the N-terminal and C-terminal, two nuclear binding domains and two extracellular domains between the first and second transmembrane domain of each terminal containing disulfide bonds which is essential for the APOA1 binding region (Hozoji *et al.*, 2009).

ABCA1 plays a role in the formation of nascent HDL in conjunction of cholesterol efflux to APOA1 (Denis *et al.*, 2004b). In addition to cholesterol, ABCA1 can also facilitate the movement of sphingomyelin, phosphatidylcholine, phosphatidylserine, sphingolipid-I-phosphate and 25-hydroxycholesterol (Quazi and Molday, 2011).

Cellular localisation is predominantly noted in the plasma membrane, however intracellular localisation of ABCA1 to endosomes (Neufeld *et al.*, 2001), ER and Golgi (Quazi and Molday, 2011) is also known, which facilitates the movement of intracellular cholesterol to the plasma membrane for efflux (Neufeld *et al.*, 2001). ABCA1 expression in anagen HFs has been previously detected (Haslam *et al.*, 2015) in addition to murine epidermis, foreskin keratinocytes (Jiang *et al.*, 2006) and HaCaT cells (Sticozzi *et al.*, 2010).

Tangier disease results from loss-of-function mutations in ABCA1, phenotypically patients present with an accumulation of CE within macrophages and low levels of circulating HDL and APOA1 (Ceccanti *et al.*, 2016).

1.3.7.2 ABCG1

Unlike the ABCA family, ABCG family contains half transporters, these half transporters homo- or heterodimerise to form a functioning transporter (Quazi and Molday, 2011). ABCG1 is a 75 kDa

protein composed of six transmembrane domains and a nucleotide binding domain located within the N-terminal containing walker A and walker B motifs (Hardy *et al.*, 2017). Post-translational modifications include cystine palmitoylation, which is important for the trafficking of ABCG1 from the ER to the plasma membrane (Gu *et al.*, 2013)

Contrasting evidence has been reported for LXR agonism enhancing plasma membrane localisation of ABCG1 (Wang *et al.*, 2006, Xie *et al.*, 2006). Intracellular ABCG1 has also been suggested to participate in endosomal transport, facilitating the movement of cholesterol from the ER to the plasma membrane (Tarling and Edwards, 2011). In addition to functioning in efflux of cholesterol to HDL (Wang *et al.*, 2008), ABCG1 can also efflux oxysterols (Engel *et al.*, 2007). It is hypothesised that ABCG1 enhances cholesterol efflux to HDL without direct binding, but through increases of plasma membrane pools to enable desorption to HDL (Phillips, 2014).

Currently there are no mutations of ABCG1 linked to disease, however overexpression of ABCG1 does occur in Tangier disease, a mechanism to counteract the loss of ABCA1 function (Lorkowski *et al.*, 2001).

1.3.7.3 ABCA5

ABCA5 is a lesser known ABC transporter, part of the subcluster of ABCA family of proteins on chromosome 17q24.3 including ABCA6, ABCA8, ABCA9 and ABCA10. The function and allocrite have yet to be determined, however the putative cholesterol transporter is implicated in congenital hypertrichosis (DeStefano *et al.*, 2014, Hayashi *et al.*, 2017) making it the most physiologically relevant cholesterol transporter to study in the HF.

Although crystal structural analysis has yet to be investigated, three splice variants are known including a 187 kDa full transporter and two half transporters of 99 kDa and 104 kDa. Structural analysis in rat revealed sixteen transmembrane domains, an N terminal comprised of two sections, where a cytoplasmic loop separates the first two transmembrane domains, followed by a subsequent six transmembrane domains. In addition two nuclear binding domains are present, the first separated from the second by eight transmembrane domain C terminal (Petry *et al.*, 2003). 90% homology between the rat and human ABCA5 is documented, including highly conserved walker A and walker B motifs (Petry *et al.*, 2003). Studies revealed 200 and 220 kDa protein expression in rat (Petry *et al.*, 2006) and 215 kDa in human (DeStefano *et al.*, 2014), suggesting post-transcriptional glycosylation modifications, with predictions of three N-linked glycosylation sites of asparagine (www.uniprot.org, 2020).

Transcriptional control of ABCA5 has been detected with PPAR agonist pioglitazone (Mak, 2014) but not LXR agonism (Mak, 2014, Fu *et al.*, 2015), and indeed PPAR binding sites are predicted (www.genecards.org, 2020). Furthermore miR-205, a putative PPARγ target (John *et al.*, 2012), has been found to reduce ABCA5 expression. Extracellular signal-regulated kinases (ERK)-mediated silencing of ABCA5 has also been found (Shukla *et al.*, 2010). Arsenite induced oxidative stress has shown a decrease in ABCA5 expression (Zhao *et al.*, 2019), and Huang *et al.* (2019b) hypothesise a role for ABCA5 in detoxification metabolism. *ABCA5* is decreased in sorcin knockdown, a calcium homeostasis protein (Gao *et al.*, 2015), and therefore calcium levels may be important in ABCA5 expression.

Sphingomyelin treatment in neuroblastoma cell line SK-N-SH increases *ABCA5* expression, and therefore ABCA5 may play a role in the transportation of sphingomyelin (Kim and Halliday, 2012). ABCA5 capacity in APOE-mediated cholesterol efflux has been measured in SK-N-SH cells (Fu *et al.*, 2015), furthermore, *Abca5*$^{-/-}$ mice show no change in APOA1 efflux but a reduction in cholesterol efflux to HDL (Ye *et al.*, 2008), demonstrating a role for ABCA5 in cholesterol efflux.

In disease, ABCA5 is upregulated in cancer stem-like cells (Huang et al., 2009), overexpression is correlated to prostate cancer (Karatas *et al.*, 2016), and presence in urine can be used as a premalignant detection of prostate cancer (Hu *et al.*, 2007). High expression of ABCA5 can be used as a prognostic marker in acute myeloid lymphoma (Niu *et al.*, 2019, Varatharajan *et al.*, 2017), whereas Wu *et al.* (2009) report a lower expression of ABCA5 in acute myeloid lymphoma than in normal bone marrow. Low ABCA5 expression in conjunction with high ABCA1 is associated with a poor prognosis in ovarian cancer (Hedditch *et al.*, 2014), and post treatment in breast cancer ABCA5 is down regulated (Hlaváč *et al.*, 2013). Expression of ABCA5 increases with age in Parkinson's disease (Kim and Halliday, 2012), in addition to associations with lysosomal disease (Kubo *et al.*, 2005).

Tissue expression is ubiquitous, with high levels of expression being reported in the testis, (Annilo *et al.*, 2003, Petry *et al.*, 2006), brain (Fu *et al.*, 2015, Ohtsuki *et al.*, 2007, Tachikawa *et al.*, 2018), liver (Quezada *et al.*, 2008, Ohtsuki *et al.*, 2007, Takenaka *et al.*, 2013), pancreas (Ohtsuki *et al.*, 2007) and skin (DeStefano *et al.*, 2014, Tachikawa *et al.*, 2018, Takenaka *et al.*, 2013, Haslam *et al.*, 2015). Intracellular localisation has previously been documented for ABCA5 with distribution to lysosomes (Kubo *et al.*, 2005) and Golgi (Petry *et al.*, 2006).

1.3.7.4 SCARB1

SCARB1 is a bi-directional cholesterol transporter (Shen *et al.*, 2018b) composed of 520 amino acids (isoform 3), with an eleven amino acid cytoplasmic N terminal, a twenty amino acid transmembrane domain, a large extracellular ectodomain with eleven N-linked glycosylation sites, multiple cystine residues and a HDL binding region. The second transmembrane domain and large C terminal is integral for oligomerisation (Shen *et al.*, 2018a). Predominantly the protein is detected as monomers in rats (Shen *et al.*, 2018b), however homo-dimers and oligomers have been noted (Sahoo *et al.*, 2007). Furthermore, oligomerisation has been shown to increase functional capacity of cholesterol efflux. Specifically, SCARB1 can facilitate the movement of both FC and CE to and from HDL (de la Llera-Moya *et al.*, 1999, Luo *et al.*, 2010) in addition to triglycerides and phospholipids. The protein has several additional functions, including bacterial detection (Guo *et al.*, 2014), transport of carotenoids (Shyam *et al.*, 2017) and vitamins (Reboul *et al.*, 2011, Reboul *et al.*, 2006).

The promoter region of SCARB1 contains multiple transcription factor binding sites including SREBP1 (Shen *et al.*, 2018a), LXR (Malerød *et al.*, 2002) and NR5A1 (nuclear receptor subfamily 5 group A member 1) (Cao *et al.*, 1997). Contrasting evidence has been provided for LXR activation of SCARB1 where both increases and decreases of expression have been shown (Komaromy *et al.*, 1996). Amongst steroidogenic tissues trophic hormones have been shown to be integral in inducing the transcription of SCARB1 (Rigotti *et al.*, 1996), which is mediated through NR5A1 (Lopez *et al.*, 1999). Indeed these transcription factors have been previously detected in HFs, and the HF contains enzymes that indicate it may be capable of steroidogenesis (Patel *et al.*, 2001, Slominski *et al.*, 2013), therefore SCARB1 may be regulated by numerous mechanisms in the HF.

SCARB1 expression in skin (Muresan *et al.*, 2019), sebocytes (Crivellari *et al.*, 2017) and keratinocytes (Sticozzi *et al.*, 2012, Tsuruoka *et al.*, 2002) have been previously studied. Expression is prominent in basal layer of the epidermis (Tsuruoka *et al.*, 2002), and may function in epidermal barrier function (Muresan *et al.*, 2019) and wound healing (Muresan *et al.*, 2018).

1.4 Links between cholesterol and common signalling pathways which regulate hair follicle growth and cycling

As discussed in Section 1.2, HF growth and cycling are tightly regulated by numerous signalling pathways. Furthermore, cholesterol modification of these pathways and cholesterol-rich lipid rafts are important for signal transduction (Incardona and Eaton, 2000). Disruption of these pathways are associated with hair pathologies, for example hypertrichosis simplex is correlated with a mutation in a Wnt inhibitor (APC down regulated 1) (Shimomura *et al.*, 2010), downregulation of Wnt/β catenin signalling has been reported in alopecia universalis, alopecia areata (AA) (Lim *et al.*, 2014) and androgenic alopecia (AGA) (Lu *et al.*, 2016), and the treatment of basal cell carcinoma with Hh inhibitors results in alopecia (Fecher and Sharfman, 2015).

Lipid modification of Wnt/βCatenin and Notch pathways are important in membrane targeting of these proteins (Stenn and Karnik, 2010, Incardona and Eaton, 2000). Furthermore selection of the Wnt/β-catenin pathway over non-canonical Wnt (Sheng *et al.*, 2014) is associated with cholesterol binding to dishevelled through membrane localisation of Wnt (Sheng *et al.*, 2014). In fact simvastatin treatment results in reductions to Wnt inhibitor and catagen inducer (Kwack *et al.*, 2012) DKK1 (Pontremoli *et al.*, 2018) along with enhanced Wnt signalling (Gao *et al.*, 2016).

A mouse model of Smith-Lemli-Opitz syndrome, a condition with mutated DHCR7, which demonstrates a parallel decrease in Shh transduction is associated with reduction in cholesterol levels (Cooper *et al.*, 2003). In addition cholesterol acts downstream of Hh at the level of smoothened and patched 1, and ligand binding of cholesterol to smoothened activates the transcription of downstream Hh targets (Tang *et al.*, 2007, Huang *et al.*, 2016). Furthermore, cholesterol is associated with post-translational modification of Hh proteins (Porter *et al.*, 1996) and the secretion of Hh ligands (Burke *et al.*, 1999). As Hh signalling is important to HF morphogenesis and cycling, with the onset of anagen alterations to interfollicular cholesterol levels may affect the hair cycle through delayed anagen onset.

TGFβ1 treatment in keratinocytes resulted in increase of HMGCR and cholesterol levels (Yamane *et al.*, 2016), as TGFβ is associated both with catagen induction and the switch from refractory to competent telogen, induction of cholesterol synthesis may be important for initiation of hair cycle stages.

Cholesterol depletion through methyl-β-cyclodextrin (MβCD) results in an upregulation of BMP6 through the disruption of lipid rafts (Mathay *et al.*, 2011). BMP family is associated with delayed

anagen onset (Hsu *et al.*, 2011) and the inhibition of bulge cell proliferation during telogen (Lee and Tumbar, 2012). In addition inhibition of ABCA1 and ABCG1, resulting in the reduction of cholesterol efflux in macrophages is associated with the upregulation of BMP signalling (Feng *et al.*, 2014). Furthermore BMP signalling is important in bulge stem cell activation (Plikus *et al.*, 2008) and regulating postnatal hair cycle (Guha *et al.*, 2004), thus cholesterol levels may play an important role in BMP signalling during the hair cycle.

1.5 Roles of cholesterol in keratinocyte behaviour

The roles of cholesterol have not yet been explored in the HF, and although epidermal keratinocyte differentiation is distinct from HF keratinocyte populations it can be used to provide insight. Therefore, this section focuses on the physiological response of epidermal keratinocytes to modulation in cholesterol.

1.5.1 Cholesterol regulates keratinocyte proliferation and differentiation

Lipids are integral factors in epidermal barrier function and as such, extensive investigations have explored the role of lipid metabolism in epidermal keratinocytes (see Feingold and Elias (2014)). The influence of cellular cholesterol levels on both keratinocyte differentiation and proliferation has been explored in many studies (Hanley *et al.*, 2000, Hanley *et al.*, 2001, Hanyu *et al.*, 2012, Jans *et al.*, 2013, Ponec *et al.*, 1985, Ponec *et al.*, 1987). Disruption of membrane cholesterol in lipid raft formation through cyclodextrin-mediated cholesterol depletion, increases keratinocyte proliferation along with causing a loss of early and late differentiation markers KRT1, KRT2 and KRT10 (Spörl *et al.*, 2010). In correlation Mathay *et al.* (2011) demonstrate a downregulation of filaggrin gene expression with MβCD disruption of lipid rafts. Fundamentally, these studies show that normal keratinocyte behaviour is inherently linked to cholesterol status.

In contrast neither FC nor its precursor mevalonate were able to induce keratinocyte differentiation. Furthermore, oxysterols (25-hydroxycholesterol and 22R-hydroxycholeserol) have been shown to upregulate involucrin and transglutaminase 1 (Hanley *et al.*, 2000). As oxysterol activates LXR, which has previously been detected in regulation of keratinocyte differentiation (Hanley *et al.*, 2000, Schmuth *et al.*, 2004), it is important to distinguish between different sterol forms. Culture of human HFs *ex vivo* with LXR agonist T0901317 has previously been reported to reduce hair growth, in addition to reducing proliferation of epidermal keratinocytes (Russell *et al.*, 2007).

CS is present in the stratum granulosum at high levels and regulates desquamation in the stratum corneum. CS increases the expression of differentiation markers, involucrin, filaggrin, transglutaminase 1 and loricrin (Feingold and Jiang, 2011, Strott and Higashi, 2003, Elias *et al.*, 2008). Mild impairment of barrier function is detected with X-linked ichthyosis, a disease associated with loss-of-function mutation in steroid sulfatase, an enzyme responsible for the removal of sulfate from sterols. Inhibition of cholesterol synthesis and reduction of cholesterol levels is detected with excess CS (Elias *et al.*, 2008). In addition to controlling cellular cholesterol

levels and keratinocyte differentiation, agonism of LXR and PPAR has been shown to regulate SULT2B1b, an enzyme involved in CS synthesis (Jiang *et al.*, 2005). No hair phenotype is reported for autosomal recessive congenital ichthyosis, which is linked to a mutation in SULT2B1b, (Heinz *et al.*, 2017).

The maintenance of skin health therefore relies on maintenance of sterol isoforms and cholesterol metabolism, however the regulatory activity of CS and oxysterols within HF keratinocytes has yet to be defined. Indeed, CS is an integral lipid of hair fibres (Wertz and Downing, 1988), HMGCR activity in human HFs is reduced with 25-hydrocholesterol treatment (Smythe *et al.*, 1998), yet the functional significance is unclear. Hair clippings from patients with elevated serum LDL revealed no change in total cholesterol, yet an increase in CS levels (Brosche *et al.*, 2001). As desquamation does not occur in the HF, there must be an alternative role for CS in the HF (i.e. adhesion and/or differentiation of the trichocytes within the HS).

The evidence from epidermal keratinocyte demonstrates that cholesterol and its products are associated with differentiation, moreover dysfunction can lead to impairment of the epidermal barrier. It is therefore reasonable to hypothesise an important role of cholesterol-mediated differentiation in the HF and formation of the HS. Indeed, some reports into the indirect or direct influence of cholesterol on HF biology have been made, which are outlined below.

1.5.2   Sources of cholesterol in the hair follicle: uptake versus *de novo* biosynthesis

The predominant route for increasing cellular cholesterol levels in peripheral tissues is through uptake from circulatory lipoproteins. Indeed, the HFs proximity to multiple sources of exogenous cholesterol is demonstrated in Figure 1.1, yet it remains unclear if this is of importance for HF biology. Both the SG and adipocytes surrounding the HF contain stores of cholesterol (Table 1.1) and are capable of *de novo* cholesterol synthesis. In fact Nicu *et al.* (2019) suggest cholesterol efflux from adipocytes could be capable of modulating the hair cycle. It should be noted that although the expression of HMGCR in sebocytes is known, the cholesterol biosynthesis pathway is ceased at squalene, with high levels of squalene present (Picardo *et al.*, 2009).

Microvasculature runs throughout the CTS and capillary loops are present within the DP (Ellis and Moretti, 1959), providing the HF with a potential source of circulatory lipoproteins. Although expression of LDLR in HFs has been previously shown, Brannan *et al.* (1975) suggest these are non-functional, as no differences were detected for HMGCR activity in healthy *versus* hypercholesterolemic patients. However, it cannot be ruled out that when intrafollicular cholesterol

levels are lacking, the presence of LDLR may indicate that uptake of exogenous cholesterol from LDL can occur. Furthermore, it is suggested that *de novo* synthesis is the predominant pathway for the epidermis to increase cellular cholesterol levels (Slominski *et al.*, 2013). Therefore, despite multiple surrounding sources of exogenous cholesterol, it is likely that the HF also replenishes intrafollicular cholesterol in the same manner.

All cells are capable of *de novo* cholesterol biosynthesis, and the HF is likely to increase intrafollicular cholesterol in this manner. High expression is reported in the HF for the enzyme DHCR24 (Brannan *et al.*, 1975, Mirza *et al.*, 2009, Smythe *et al.*, 1998), which facilitates the conversion of desmosterol to cholesterol in the Bloch pathway (Figure 1.3). Furthermore, both cholesterol and desmosterol are present in the HS of mice, in fact at a higher level than in the skin (Evers *et al.*, 2010, Mirza *et al.*, 2009, Serra *et al.*, 2010). The authors suggest that during HS formation cholesterol is incorporated opposed to coating *via* secretions from the SG, suggesting synthesis is occurring in the HF during formation of the HS.

Table 1.1 Composition of sterols as percentage of total lipids in the human hair follicle and sebaceous gland (Palmer *et al.*, 2020)

Lipid	Hair Shaft	IRS	HF	Sebum	SG
Cholesterol	3.9-5.5%	2.5%	3.7%	7.0%	3.4%
Cholesterol esters	8.5-19.1%			27.8%	
Cholesterol sulfate	5.7-17.0%			1.4%	
Squalene	2.9%				19.0%
References	(Lee, 2011, Coderch *et al.*, 2008, Masukawa *et al.*, 2005, Cruz *et al.*, 2013, Wertz, 2000)	(Lee, 2011)	(Lee, 2011)	(Coderch *et al.*, 2008)	(Puhvel *et al.*, 1975)

1.5.3 Importance of cholesterol homeostasis in steroid hormone biosynthesis

Steroidogenesis is predominantly observed in the gonads and adrenal glands, and although the skin is also reported to be a steroidogenic tissue, it is important to note that this activity is considerably lower (less than 1%) (Slominski *et al.*, 2013). Crucially, numerous steroidogenic enzymes are expressed in the HF (Figure 1.7), most importantly CYP11A1, which catalyses the rate-limiting step (conversion of cholesterol into pregnenolone) in steroid hormone production (Thiboutot *et al.*, 2003, Slominski *et al.*, 2013). This initial step in steroid biosynthesis occurs in

the inner mitochondrial membrane, where cholesterol levels are comparatively low. Members of the STAR family facilitate the delivery of cholesterol to this inner membrane (Figure 1.7) leading to a concomitant increase in pregnenolone synthesis, which can then be utilised by steroidogenic enzymes in the ER (Slominski *et al.*, 2013).

Androgens, oestrogens and glucocorticoids are the major steroid hormone products of cholesterol in the skin (Inoue *et al.*, 2012, Zouboulis, 2009, Zouboulis *et al.*, 2007, Feingold *et al.*, 1983). In particular, the testosterone metabolite dihydrotestosterone (DHT), which plays a role in the onset of AGA, is formed in the cutaneous tissues, including the HF.

The significance between uptake of endocrine-produced circulating steroid hormones, which are subsequently metabolised *in situ* (for example to DHT) and *de novo* steroidogenesis within the HF has yet to be concluded. A large reduction in plasma androgens is detected in pre-pubertal castrated patients, correlating to the lack of secondary sexual hair growth (vellus to terminal formation driven through androgens), and these patients do not develop AGA (Hamilton, 1960, English, 2018). Furthermore, AGA can be induced through testosterone injection in pre-pubertal castrated patients, suggesting intrafollicular DHT levels arise predominantly from metabolism of circulating androgens. In this respect, the role of cholesterol in *de novo* steroidogenesis as a replacement of circulatory testosterone does not appear to be adequate to drive AGA or formation of secondary hair.

Taves *et al.* (2011) suggest that within peripheral tissues *de novo* steroid hormone synthesis functions in autocrine or paracrine signalling. In this case, regulation of hair growth and cycling from modulatory signals could occur from relatively low levels of intrafollicular androgen synthesis. In fact, Kretzschmar *et al.* (2015) report crossover of androgen receptor (AR) and Wnt/β-catenin signalling, where a concomitant reduction of Wnt/β-catenin signalling is detected from high levels of DHT induced AR activity in the balding scalp. In this way, links between signalling pathways associated with hair growth and cycling could be modulated by fluctuations in steroidogenesis because of alterations to intrafollicular cholesterol levels. Indeed, preliminary evidence reported by Nicu *et al.* (2019) suggested that cholesterol release from dermal adipocytes during catagen is increased, leading to the hypothesis that increased cholesterol uptake may lead to an increase in steroidogenesis in the HF and has impact on anagen to catagen transition (Nicu *et al.*, 2019).

Increased expression of 5α-reductase (5αR) isoforms have been detected in female patterned hair loss with normal circulating androgen levels (Sánchez *et al.*, 2018). 5αR function in the

formation of DHT from testosterone, suggesting metabolism of steroid hormones rather than *de novo* synthesis is linked with the onset of female patterned hair loss.

Inoue *et al.* (2012) detected an association between decreased hair density and increased expression of STAR within the frontal area of the scalp. In addition, higher testosterone and oestrogen levels are correlated to higher expression of STAR (Inoue *et al.*, 2012). Furthermore, HF localisation of the steroidogenesis regulatory nuclear receptors NR5A1 and NR0B1 (nuclear receptor subfamily 0 group B member 1) have been found in the DP, ORS, IRS and matrix (Patel *et al.*, 2001) (Figure 1.6). In addition, the authors speculate that conversion of sterols into DHT may be induced by oxysterol activation of NR5A1 and NR0B1 (Patel *et al.*, 2001). Although intrafollicular androgen production does not appear to be sufficient to cause DHT-sensitive AGA, little to no difference in circulatory DHT levels were detected in patients with AGA (Hannen *et al.*, 2011, Nikolakis *et al.*, 2016, Slominski *et al.*, 2013, Zhang *et al.*, 2018, Urysiak-Czubatka *et al.*, 2014). Therefore, it cannot be fully determined if cholesterol plays a role in intrafollicular steroidogenesis or oxysterol induced metabolism of testosterone to DHT in androgen-sensitive alopecias.

Given that cutaneous tissues have the ability to utilise cholesterol for steroid hormone synthesis, and in conjunction with the reliance on rate-limiting cholesterol trafficking, alterations in cholesterol homeostasis have the capacity to dysregulate normal HF biology. However, the role of *in situ* metabolism of circulating sterols (i.e. androgens, oestrogens, or glucocorticoids) versus *de novo steroidogenesis* within the HF remains to be elucidated.

Gene		Adipocytes	CTS	ORS	IRS	Matix	DP	Basal Sebocytes	Differentiating Sebocytes
CYP11A1	Pregnalone/ 20(S)-Hydroxycholesterol synthesis	■						■	
HSD3B	Progestagens/Androgens synthesis	■						■	
CYP17A1	Synthesis of androgens from progestagens	■		■	■			■	
HSD17B	Synthesis of testosterone	■		■				■	
5αR	Synthesis of dihydroxytestosterone	■		■	■		■		■
CYP19	Synthesis of estrogens from androgens	■		■	■		■		■
HSD11B1	Glucocorticoid synthesis	■							
NR0B1	Inhibitor of NR5A1	■		■	■	■	■	■	■
NR5A1	Transcription factor (StAR, CYP19, CYP17A1)	■		■	■	■	■	■	
STAR	Cholesterol movement to mitochondria	■		■					
STS	Removes sulfate from cholesterol sulfate	■					■		■
HMGCR	Cholesterol biosynthesis pathway	■	▨	▨	▨	▨	▨	▨	▨
LDLR	Cellular uptake of cholesterol	■	▨	▨	▨	▨	▨	▨	▨
ABCA1	Cholesterol efflux transporter	■		■	■	■	■		

Figure 1.6 Hair follicle expression of cholesterol homeostatic and steroidogenesis proteins. Filled boxes indicated known localisation of gene/protein. Striped boxes indicated that the gene/protein is known to be present in pilosebaceous unit but the pattern of expression is yet to be defined. Empty boxes indicate the expression of a specific gene/protein is yet to be reported (Adapted from Palmer *et al.* (2020)).

1.6 Associations between cholesterol and hair pathologies

1.6.1 Cholesterol synthesis is dysregulated in primary cicatricial alopecia

Altered cholesterol status has been associated with primary cicatricial alopecias (PCA), a group of inflammatory hair loss disorders characterised by permanent HF loss and formation of scar-like fibrous tissue (Panicker *et al.*, 2012). The hallmarks of PCA include inflammation and the influx of immune cells, yet the underlying mechanisms remain unclear. Recently evidence pointing towards dysregulation in lipid homeostasis has been shown to have a role.

In particular, both lesional and non-lesional scalp tissue from PCA patients demonstrated a significant downregulation of genes involved in cholesterol biosynthesis (Panicker *et al.*, 2012). This included DHCR7, which catalyses the final step in cholesterol biosynthesis (Figure 1.3) as well as EBP. Furthermore, mutations in EBP cause Conradi-Hunermann syndrome, a disorder where scarring hair loss is seen (see section 1.6.6). A pro-inflammatory response was noted with either the addition of exogenous 7DHC or inhibition of DHCR7 to human primary ORS keratinocytes or *via* topical application to mouse back skin, including upregulation of toll-like receptor and interferon signalling networks. Additionally TGFβ, an established inducer of catagen (Hibino and Nishiyama, 2004) and fibrosis (Imanishi *et al.*, 2018), was also upregulated with the inhibition of cholesterol biosynthesis (Panicker *et al.*, 2012).

Ultimately, in these murine models abnormal cycling and loss of HF growth resulted from inhibition of cholesterol synthesis, with an increase in markers associated with catagen induction (TGFβ1), a downregulation of stem cell markers (SOX9) alongside epidermal thickening and follicular plugging (Panicker *et al.*, 2012). Therefore, the conclusion is drawn that the inflammatory response associated with macrophage recruitment and, ultimately, HF destruction in PCA patients is mediated through the accumulation of cholesterol precursors (Panicker *et al.*, 2012). Consequently, a direct link between PCA and HF sterol status is evident.

Of relevance to this is the evidence linking sex steroid responses to frontal fibrosing alopecia (FFA), a form of PCA primarily observed in women (Harries *et al.*, 2018). Indeed, a predisposition in post-menopausal women to the development of FFA is associated with oestrogen activity levels or the decline in dehydroepiandrosterone (Tziotzios *et al.*, 2016, Gaspar, 2016, Harries *et al.*, 2018).

The steroid hormone metabolising enzyme CYP1B1 plays a role in the oxidative metabolism of oestradiol and oestrone, but may also metabolise xenobiotics such as the oral contraceptive

(Tziotzios *et al.*, 2016). Furthermore, a recent GWAS identified a missense mutation in CYPB1 linked with pathogenesis of FFA (Tziotzios *et al.*, 2016). Additionally, in Pomeranian dogs, CYP1B1 has been associated with alopecia X (Brunner *et al.*, 2017). Although this could indicate a role for metabolism of steroid hormones in the development of hair disorders such as FFA, direct evidence of steroidogenesis within the HF is still required. Whether reduced *de novo* steroidogenesis is directly related to changes in intrafollicular cholesterol levels in FFA has yet to be determined but remains a possibility.

1.6.2 Peroxisome proliferator-activated receptor dysregulation in primary cicatricial alopecia pathogenesis

The development of PCA has also been associated with the dysregulation or dysfunction in the PPAR family (Karnik *et al.*, 2009, Harnchoowong and Suchonwanit, 2017). Expression and function of specific PPAR isoforms in the HF have been made, PPARα is associated with HF survival (Billoni *et al.*, 2000), PPARβ/δ is linked with HF morphogenesis (Di-Poi *et al.*, 2004, Icre *et al.*, 2006), in addition PPARγ agonism is involved with keratinocyte differentiation through increased KRT15 in the bulge, reduction of IL-6 as well as catagen induction (Ramot *et al.*, 2015).

A significant reduction in PPARγ expression has been detected in scalp tissue from patients with lichen planopilaris (LPP; a form of PCA characterised by follicular inflammation and fibrosis) both for affected and unaffected HFs (Karnik *et al.*, 2009). This is associated with a downregulation of the cholesterol homeostasis genes HMGCR, HMGCS1 and ACAT, as well as decreased peroxisome numbers, resulting in reduced cholesterol synthesis (Karnik *et al.*, 2009). Furthermore, a downregulation of cholesterol homeostasis genes *Hmgcr, Hmgcs1, sterol O-acyltransferase 1* and *Dhcr24* has been detected in *Ppary* knockout mice, which phenotypically develop scarring alopecia (Karnik *et al.*, 2009). This evidence supports the role of dysregulation to cholesterol homeostasis as a potential factor in the pathogenesis of LPP.

Although PPAR activation is associated with lipid homeostasis, other properties of PPARγ activity such as anti-inflammatory effects and a role in immune regulation (Straus and Glass, 2007), along with epithelial to mesenchymal transition inhibition (Reka *et al.*, 2010, Imanishi *et al.*, 2018), also likely play an important role in disease development (Harries *et al.*, 2018). Interestingly, pioglitazone (a PPARγ agonist) is now successfully being used to treat LPP, with over 50% response rates recorded (Mesinkovska *et al.*, 2015).

1.6.3 Mutations in cholesterol synthesis cause autosomal-recessive hypotrichosis simplex

Recently, whole exome sequencing in autosomal-recessive hypotrichosis simplex identified mutations in cholesterol biosynthesis enzyme LSS (see Figure 1.3) (Romano *et al.*, 2018). Five separate mutations were detected which resulted in either loss of protein or cytoplasmic localisation of the ER enzyme, causing loss-of-function. Romano *et al.* (2018) hypothesise that inflammation from accumulation of cholesterol precursors and lipid modifications of Wnt or Hh proteins may be causative of the sparse scalp hairs, which may include eyebrows and eyelashes in some patients.

1.6.4 Accumulation of cholesterol precursors causes abnormal hair growth in mice

Abnormal murine HF morphogenesis occurs in epidermal-specific double knockout of Insig (epi-*Insig*-DKO). Histological examination revealed the dissociation of the DP from the hair bulb, along with hair kinking and keratin plugging (Evers *et al.*, 2010). As discussed in Section 1.3.5, INSIG is integral in the regulation of cholesterol synthesis through both inhibition of SREBP2 translocation and proteolytic degradation of HMGCR (Sever *et al.*, 2003). Furthermore, the significant increase in sterol precursors detected was hypothesised to be the causative factor (Evers *et al.*, 2010). Statin treatment resulted in the reversal of the morphological HF defects, along with significantly reducing sterol precursors. Given the similarities in hair phenotype between the epi-*Insig*-DKO and *Shh*$^{-/-}$ mice, Evers *et al.* (2010) suggest an impairment of Shh signalling. As discussed in Section 1.4, this hypothesis fits well with cholesterol modification of Shh pathway, and therefore effecting hair growth and morphogenesis.

Mirza *et al.* (2009) report a reduction in HFs and epidermal thickening is present, along with the accumulation of desmosterol in the epidermis in *Dhcr24*$^{-/-}$ mice, although this model resulted in fatality within 24-hours. In comparison a viable *Dhcr24*$^{-/-}$ mouse with no hair or skin phenotype was reported by Wechsler *et al.* (2003), with very low levels of cholesterol and an accumulation of both liver and circulatory desmosterol. Dhcr7 deficient mice show a significant accumulation in 7-dehyrodesmosterol and reduction in both desmosterol and cholesterol levels within the hair, however no hair phenotype was reported (Serra *et al.*, 2010).

Table 1.2 Mutations in cholesterol homeostasis leading to hair and skin diseases (Palmer *et al.*, 2020)

Mutation	Gene function	Disease	Hair Phenotype	References
ABCA12	Ceramide transporter, regulatory function in ABCA1 expression	Harlequin Ichthyosis	Sparse and brittle hair shafts	(Ahmed and O'Toole, 2014)
ABCA5	Putative cholesterol transporter	Congenital Hypertrichosis	Excessive hair growth throughout the body	(DeStefano *et al.*, 2014, Hayashi *et al.*, 2017)
EBP	Conversion of Zymosterol in cholesterol biosynthesis pathway	Conradi–Hünermann syndrome	Follicular atrophoderma and patchy scarring alopecia	(Has *et al.*, 2000, Ikegawa *et al.*, 2000, Lambrecht *et al.*, 2014, Martanova *et al.*, 2007, Morice-Picard *et al.*, 2011, Steijlen *et al.*, 2007, Braverman *et al.*, 1999)
LSS	Synthesis of lanosterol from squalene-2,3-epoxide	Autosomal-recessive hypotrichosis simplex	Sparse scalp hair, may include eyebrows and eyelashes	(Romano *et al.*, 2018)
MBTPS2	Cleavage of SREBP2	IFAP	Non-progressive alopecia	(Araujo *et al.*, 2015, Bornholdt *et al.*, 2013, Fong *et al.*, 2015, Izumi *et al.*, 2013, Megarbane and Megarbane, 2011, Ming *et al.*, 2009, Nemer *et al.*, 2017, Oeffner *et al.*, 2009, Wang *et al.*, 2014b)
		KFSD	Cicatricial alopecia	(Aten *et al.*, 2010, Fong *et al.*, 2012, Zhang *et al.*, 2016a)
Steroid Sulfatase	Reduces cholesterol sulfate levels	X-linked ichthyosis	Normal	(Elias *et al.*, 2014)
SULT2B1b	Synthesis enzyme of cholesterol sulfate	Congenital ichthyosis	Normal	(Heinz *et al.*, 2017)

1.6.5 Congenital hypertrichosis and cholesterol

Mutations in ABCA5 have been identified in congenital hypertrichosis, a condition resulting in excessive hair growth across the body (DeStefano *et al.*, 2014, Hayashi *et al.*, 2017). As discussed in Section 1.3.7.3, ABCA5 is a putative cholesterol transporter and indeed a dysregulation of cholesterol homeostasis was also observed (DeStefano *et al.*, 2014).

DeStefano *et al.* (2014) reported cholesterol accumulation in the lysosomes, along with lysosomal dysfunction in patient derived keratinocytes. Additionally, ABCA5 was highly expressed in the HF, which was significantly reduced in patient HFs. Although direct mechanistic studies were not performed, DeStefano *et al.* (2014) hypothesise that cholesterol modifications of signalling pathways (i.e. Wnt or Shh) may be a causative factor in the hair overgrowth. Furthermore, an enlargement of HFs was detected in patients leading to similarities to HF bulbs from Noggin-overexpressing mice (DeStefano *et al.*, 2014). Indeed, the likely importance of cholesterol transport and trafficking needed for maintenance of intrafollicular cholesterol levels for normal hair growth is highlighted through this study.

1.6.6 Other hair phenotypes

Conradi–Hünermann syndrome is caused by mutations to cholesterol biosynthesis enzyme EBP (see Figure 1.7A) (Braverman *et al.*, 1999, Ikegawa *et al.*, 2000, Morice-Picard *et al.*, 2011, Steijlen *et al.*, 2007), resulting in the accumulation of cholesterol intermediates, causing patients to develop patchy scarring alopecia (Ikegawa *et al.*, 2000, Lambrecht *et al.*, 2014, Martanova *et al.*, 2007, Morice-Picard *et al.*, 2011, Steijlen *et al.*, 2007).

Mutations in MBTPS2 (cleavage of SREBP2 see Figure 1.7B) have been found in multiple rare skin disorders; X-linked form of Olmsted syndrome (Haghighi et al., 2013) where patients have sparse, brittle hair (Duchatelet and Hovnanian, 2015). Ichthyosis follicularis with alopecia and photophobia (IFAP) syndrome (Araujo *et al.*, 2015, Bornholdt *et al.*, 2013, Fong *et al.*, 2015, Izumi *et al.*, 2013, Megarbane and Megarbane, 2011, Ming *et al.*, 2009, Nemer *et al.*, 2017, Oeffner *et al.*, 2009, Wang *et al.*, 2014b, Haslam *et al.*, 2015) patients present with non-progressive non-cicatricial alopecia. Keratosis follicularis spinulosa decalvans (KFSD) (Aten *et al.*, 2010, Fong *et al.*, 2012, Zhang *et al.*, 2016a) has a progressive cicatricial alopecia phenotype.

Progressive hair loss is found with mutations in glycerol kinase 5 (GK5) in mice and is associated with increased cholesterol levels, the mechanism is thought to be through inhibition of SREBP (Zhang *et al.*, 2017).

Mutations in ABCA12 result in a rare skin condition, Harlequin ichthyosis (Ahmed and O'Toole, 2014, Thomas *et al.*, 2006), with sparse, brittle hair (Basel-Vanagaite *et al.*, 2007). In addition to transporting ceramide, ABCA12 has also been associated with post-transcriptional regulation of cholesterol transporter ABCA1 (Fu *et al.*, 2013).

Furthermore, links between circulatory cholesterol levels and AGA have been explored in a number of studies, in particular focusing on cardiovascular disease risk and metabolic syndrome (Arias-Santiago *et al.*, 2010a, Arias-Santiago *et al.*, 2010b, Ellis *et al.*, 2001, Guzzo *et al.*, 1996, Sasmaz *et al.*, 1999, Sharma and Jindal, 2014, Sharma *et al.*, 2013, Trevisan *et al.*, 1993, Acibucu *et al.*, 2010, Agamia *et al.*, 2016, Bakry *et al.*, 2015, Banger *et al.*, 2015, Chakrabarty *et al.*, 2014, El Sayed *et al.*, 2016, Thakare, 2016, Kim *et al.*, 2017).
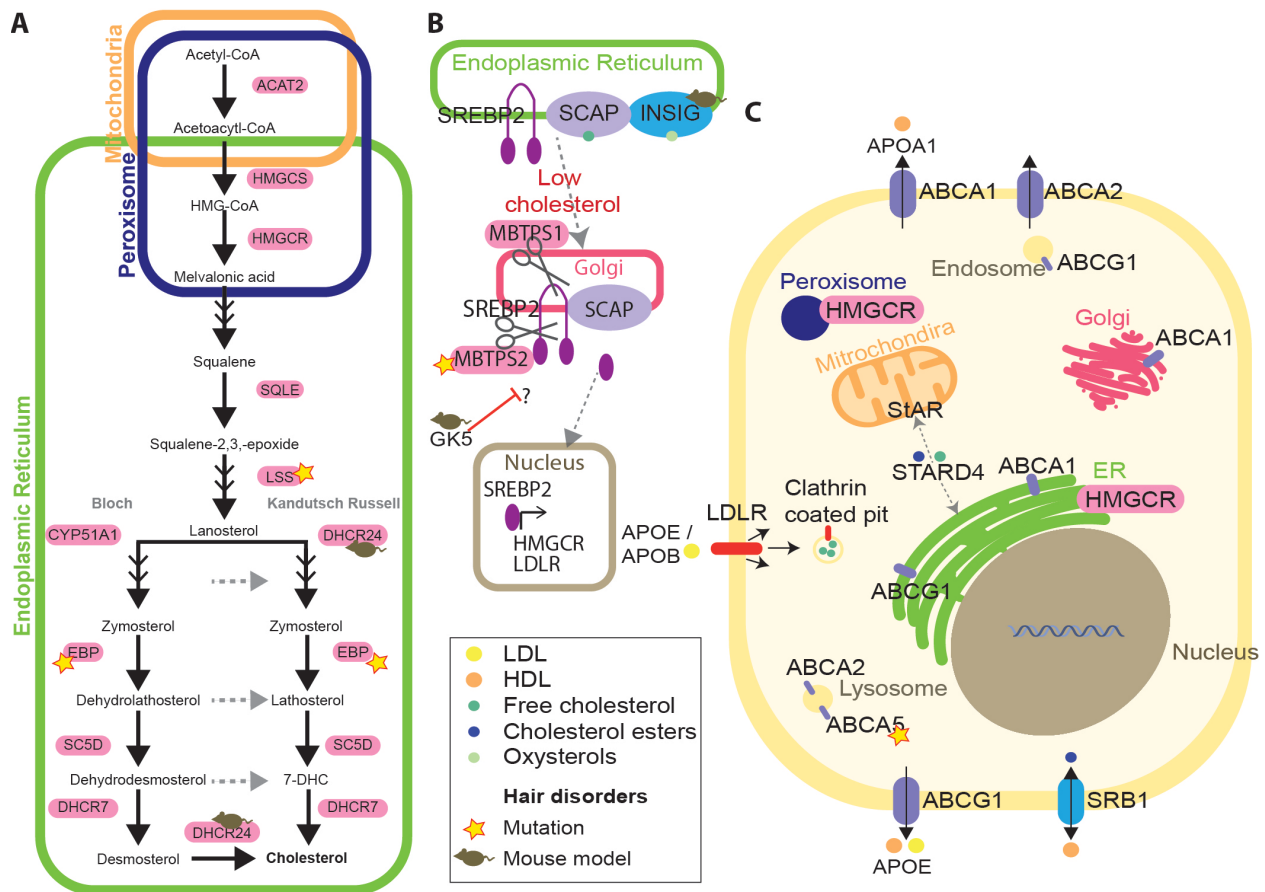
Figure 1.7 Cholesterol homeostasis in the hair follicle: identification of known mutations and knockout mouse models associated with hair disorders. (A) A summary of cholesterol biosynthesis, (B) SREBP2-mediated cholesterol regulation, C) Representation of putative cholesterol transport and trafficking routes in hair follicle keratinocytes, including known mutations (as indicated by stars) or mouse models with a hair phenotype (indicated by mouse) (Palmer *et al.*, 2020).

1.7 Modulation of cholesterol homeostasis in the hair follicle

1.7.1 Associations between statin treatment and hair growth

Inhibition of HMGCR *via* statins is used to reduce serum cholesterol levels and contrasting links have been made with both hair loss and the treatment of alopecias. Although links have been made between statin use and hair loss, there is no definitive evidence. In one case study, a 38-year-old female taking 10 mg daily oral atorvastatin (amongst other medications) reported hair loss. Suspension of the medication resulted in a reversal of the hair loss, however it returned two weeks after re-introduction of atorvastatin, therefore leading to the conclusion by Segal (2002) that atorvastatin has a causal link to hair loss. Given the rapid pace of onset, it is likely that this points towards anagen effluvium, as opposed to telogen effluvium (drug-induced hair loss). Additionally, another case study reported alopecia with atorvastatin use in a female patient in the parietal and vertex regions (Mohammad-Ali *et al.*, 2015). In comparison a larger study by Smeeth *et al.* (2009) had no conclusive evidence for the role of statins in hair loss.

Whereas Lattouf *et al.* (2015) report regrowth of hair in patients with AA, universalis and totalis with a combinational treatment of simvastatin and ezetimibe (inhibits enterocyte uptake of cholesterol through Niemann-Pick C1-Like 1), a varied response of hair regrowth has also been reported (Ali and Martin, 2010, Cervantes *et al.*, 2018, Lattouf *et al.*, 2015, Robins, 2007) and no benefits have been shown for severe AA (Loi *et al.*, 2016, Freitas Gouveia and Trueb, 2017). It should be noted that as well as reducing cholesterol synthesis, statin treatment also results in an inhibitory effect in the JAK/STAT pathway (Janus kinase family/ signal transducer and activator of transcription family), along with an immunomodulatory effect (Cervantes *et al.*, 2018). Therefore, the direct mechanisms behind statin-induced hair regrowth cannot be fully determined without further examination.

1.8 Hypothesis, aims and experimental design

The importance of cholesterol to normal cell function is well established and recent evidence has suggested a crucial role for cholesterol in maintaining normal hair growth. Given the hydrophobicity of cholesterol, facilitated movement across and between membranes is essential for this important molecule to fulfil its diverse roles. No study has yet described the mechanisms for cholesterol uptake, trafficking and compartmentalisation in the HF.

1.8.1 Hypothesis

Altered cholesterol homeostasis can disrupt human hair growth and cycling.

1.8.2 Aims

This project has the following aims:

1. To determine the expression and activity of cholesterol transport proteins in human HF keratinocytes, with a particular focus on the ABC transporter superfamily.
2. To investigate how modulation of cholesterol level impacts on HF biology, using human HF keratinocytes and organ-cultured human HFs.
3. To determine the expression of cholesterol transport proteins and compartmentalisation of cholesterol across the human hair cycle.
4. To investigate how modulation of ABCA5 impacts on HF biology, using human HF keratinocytes to give insight into potential mechanisms of hypertrichosis.

1.8.3 Methodology and experimental design

Cell culture offers a pragmatic tool for testing preliminary hypotheses and generating experimental cues that can then be further investigated in more complex model systems. In this project the characterisation of specific target genes and proteins for cholesterol transport utilised the culture of primary ORS keratinocytes that were isolated from plucked human HFs following a method developed by Bodo *et al.* (2005). ORS keratinocytes create a cell model which can be specifically applied to the HF. These primary cells require a specialised Epilife media and can only be cultured for 3-5 passages before they begin to senesce. In addition, they lack the 3D complexity of the human HF and the mesenchymal-ectodermal interactions that occur in the intact tissue. Therefore, in addition, human HFs were cultured *ex vivo* in isolation, allowing the development of this research within a tissue-specific model. Human HF organ culture therefore had the benefit of

providing a more physiologically and clinically relevant model system than can be found in the 2D cell culture models.

To determine the expression and activity of cholesterol transport proteins, the impact of cholesterol loading (using exogenous FC), along with MβCD to deplete cholesterol levels, were examined in ORS keratinocytes. The gene expression changes of specific proteins involved in cholesterol transport (outlined in Section 1.3.7) were detected by qPCR, along with protein expression *via* western blotting. In addition, LXR agonist T0901317 was utilised as positive control to alter the transcription of cholesterol efflux genes. The cellular localisation of cholesterol transport proteins were determined by immunofluorescence staining. The activity of these transporters was measured using a fluorescence cholesterol efflux assay.

To investigate how modulation of cholesterol level impacts on HF biology, both ORS keratinocytes and human HFs were cultured with FC and MβCD. Alterations in cholesterol distribution were measured using filipin to detect changes in FC, and cholera toxin-FITC (CTX-FITC) conjugate was utilised to measure lipid raft abundance. Investigations in the cellular proliferation, apoptosis, senescence, hair cycling and Wnt signalling were performed.

To determine the expression of cholesterol transport proteins and compartmentalisation of cholesterol across the hair cycle, freshly isolated HFs were staged in accordance to Oh *et al.* (2016), and immunofluorescence staining of ABCA1, ABCG1, ABCA5, SCARB1 and HMGCR, in addition to filipin staining for FC, were performed. In addition, gene expression changes were detected *via* qPCR following T0901317, FC and MβCD treatments.

Finally, to investigate how modulation of ABCA5 impacts on HF biology, using primary HF keratinocytes to give insight into potential mechanisms of hypertrichosis, siRNA transfections were performed in primary ORS keratinocytes. Investigations into intracellular cholesterol distribution were performed using filipin and BODIPY cholesterol in conjunction with organelle markers. Gene expression changes were investigated in ABCA5 knockdown keratinocytes following exogenous FC loading. Furthermore, oxysterol levels were detected using mass spectrometry.

Chapter 2:   Materials and methods

2.1 Isolation and culture of primary outer root sheath keratinocytes

2.1.1 Human dermal fibroblasts

Human dermal fibroblasts (HDF) (gifted from Tamás Biro, University of Debrecen, Hungary) were grown in Dulbecco's Modified Eagle's Medium (DMEM) – high glucose (Sigma-Aldrich, Dorset, UK) supplemented with 10% FBS (heat inactivated; South American origin) (Gibco™, Massachusetts, USA), 2 mM L-glutamine (Lonza, Basel, Switzerland) and 1% penicillin/streptomycin (Lonza) (100 IU and 100 µg/ml), at 3000 cells/cm^2 until confluency. Sub-culture was achieved *via* incubating with 0.25% trypsin-EDTA (Gibco™) for 5-minutes, followed by centrifugation at 200 g for 5-minutes.

A 400 µl/ml stock of mitomycin C (Acros Organics, Geel, Belgium) was prepared by reconstitution into serum-free DMEM. Confluent HDF cells were treated with 4 µg/ml mitomycin C for 24-hours and sub-cultured into 35 mm petri dishes containing 35,000 cells per dish. Feeder layers were used 2-6 days post seeding.

2.1.2 Preparation of outer root sheath keratinocyte isolation media

Penicillin G (Alfa Aesar™, Massachusetts, USA) was prepared at 6.7 mg/ml (10,000 units/ml) in distilled water. Ascorbyl-2-phosphate (Sigma-Aldrich) was prepared at 29 mg/ml in serum-free DMEM. Adenine (Alfa Aesar™) was prepared by adding 48.6 mg to 300 µl NaOH (4 M), subsequently 1 ml of water and 1 ml of HCl (1 M) were added, then the solution was made up to 40 ml with distilled water. Human epidermal growth factor (Sigma-Aldrich) was prepared 10 ng/ml in PBS with 1% bovine serum albumin (BSA) (Fisher Bioreagents™, Leicestershire, UK). Hydrocortisone (Acros Organics) was prepared by adding 25 mg to 5 ml of 95% ethanol, 4 ml of this solution was added to serum free DMEM. 13.65 mg of Triiodothyronine (Sigma-Aldrich) was added to 1.5 ml NaOH (1 M), then made up to 100 ml with distilled water. 1 ml of this solution was added to 99 ml of PBS. Cholera toxin (Sigma-Aldrich) was prepared by adding 1 mg to 1.18 ml of sterile water. 1 ml of the previous solution was added to 99 ml of DMEM supplemented with 10% FBS. All solutions were filter-sterilised and stored at -20°C.

Table 2.1 Composition of outer root sheath keratinocyte isolation media

Component	Stock	Final concentration	Supplier
DMEM		43.1%	Sigma-Aldrich
DMEM : Ham's F12 (1:1)		43.1%	Lonza
FBS		10%	Gibco™
Insulin	10 mg/ml	5.0 µg/ml	Sigma-Aldrich
Hydrocortisone	0.4 mg/ml	0.4 µg/ml	Acros Organics
Adenine	1.215 mg/ml	2.4 µg/ml	Alfa Aesar™
Triiodothyronine	2 µM	2 nM	Sigma-Aldrich
Cholera Toxin	0.1 µM	0.1 nM	Sigma-Aldrich
Epidermal growth factor	10 µg/ml	10 ng/ml	Sigma-Aldrich
Ascorbyl-2-phosphate	100 mM	1 mM	Sigma-Aldrich
Penicillin G	10000 UI/ml	100 UI/ml	Alfa Aesar™
Gentamycin	50 mg/ml	25 µg/ml	Gibco™
L-Glutamine		1%	Lonza

2.1.3   Isolation of outer root sheath keratinocytes

5-10 HFs were plucked from consenting donors (in accordance with ethical review *via* the School of Applied Sciences, University of Huddersfield) and incubated for 30-minutes at 37°C in fully supplemented ORS keratinocyte media (Table 2.1). Follicles were washed twice with PBS containing 100 µg/ml gentamycin. Follicles were incubated with 0.25% trypsin-EDTA (Gibco™) for up to 60-minutes, periodic agitation with vigorous pipetting and vortexing was performed every 10-minutes until the ORS keratinocytes were removed from the HF (Figure 2.1B). Trypsin was inactivated using fully supplemented ORS keratinocyte media, and the suspension spun at 200 g for 8-minutes. Cells were seeded onto HDF feeder layers in 35 mm petri dishes. Media was changed after 5-6 days, as previously described (Aasen and Izpisua Belmonte, 2010, Bodo *et al.*, 2005, Haslam *et al.*, 2017, Limat and Noser, 1986). Subculture was achieved through incubation with 1x TrypLE Express (Gibco™) and subsequent growth performed in Epilife media (Gibco™) supplemented with human keratinocyte growth supplement (HKGS) (Gibco™).

2.1.4   Subculture

Cells were washed two times with PBS-gentamycin, then incubated with TrypLE Express (Gibco™) for 5-10-minutes. Inactivation was achieved through dilution and cells were centrifuged

for 8-minutes at 200 g. Cells were re-suspended in Epilife media supplemented with human keratinocyte growth supplement (HKGS) (Gibco™) and seeded at 1 x10^4 cells per cm^2.
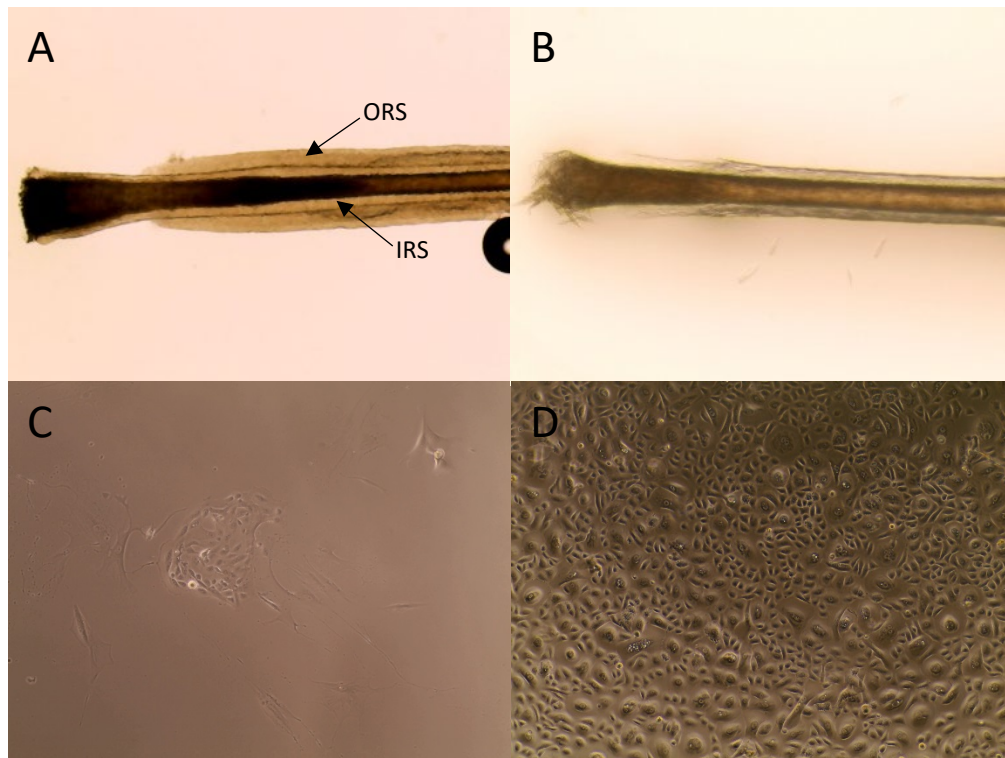
Figure 2.1 Isolation of outer root sheath keratinocytes from plucked hair follicles. (A) Plucked HF showing ORS and IRS. (B) ORS removed by incubation with TrypLE. (C) Colony formation of freshly isolated ORS keratinocytes on feeder layers. (D) Passage 3 ORS keratinocytes.

2.1.5   Cell culture treatments

FC (Sigma-Aldrich) was reconstituted in 100% ethanol to form a 10 mM stock. Cells were treated for 24 or 72-hours.

MβCD was prepared fresh in media at 1 mM or 5 mM concentration. Cells were treated for 1-hour and then fresh media was replaced for a 23-hour recovery period.

T0901317 (Sigma-Aldrich) stock was prepared at 10 mM in DMSO, cells were treated at 5 μM for 24 or 72-hours.

2.1.6   siRNA transfections

10 ml of 5x siRNA buffer solution was prepared in the following procedure to final concentrations of 60 mM KCL, 6 mM HEPES-pH 7.5 and 0.2 mM MgCl$_2$. 3 ml of nuclease-free water was added

to 224 mg of potassium chloride, 72 mg HEPES (Sigma-Aldrich) and 2 mg magnesium chloride. 2 M nuclease-free potassium hydroxide was prepared using 600 mg of potassium hydroxide pellets dissolved in 5 ml of nuclease-free water. The pH of the 5x siRNA buffer solution was adjusted to 7.5 using 2 M potassium hydroxide and the volume adjusted to 10 ml using nuclease-free water. The solution was sterile-filtered prior to use.

Pre-designed SMARTpool ON-TARGETplus siRNA were obtained from Dharmacon (Horizon, Cambridge, UK). Non-targeting (NT) #1 5 nmol (D-001810-01-05) and Human ABCA5 (L-004345-01-0005) siRNA were resuspended in 1x siRNA buffer to form a 10 µM stock, aliquoted and stored at -20°C.

Cells were seeded at $2x10^5$ per ml into respective wells and incubated overnight. Subsequent to transfections Lipofectamine™ RNAiMAX Transfection Reagent (Invitrogen™, Massachusetts, USA) and siRNA were diluted in Opti-MEM™ I Reduced Serum Medium (Gibco™), complexed together at 1:1 ratio and incubated for 5-minutes prior to transfection. Media was removed from cells and replaced with fresh Epilife. siRNA Lipofectamine complexes were added dropwise to wells to a final concentration of 10 nM siRNA and incubated for 8-hours. Media was aspirated and replaced with fresh Epilife media.

A further 16-hour incubation was performed, then cells were treated with 25 µM FC or 5 µM T0901317 for 24-hours (or appropriate vehicles) for RNA, lipidomic and immunocytochemistry analysis. Alternatively, protein lysates were analysed 72-hours after initial transfection *via* western blotting, or EdU (5-ethynyl-2'-deoxyuridine) incorporation was performed as described in Section 2.5.8.

2.1.7   MTT assays

Cells were seeded at $0.8x10^4$ per well in 96 well plates and treated for 72-hours with FC or T0901317, or 1-hour with MβCD with 23-hours recovery. 3-(4,5-Dimethylthiazol-2-yl)-2,5-Diphenyltetrazolium Bromide (MTT) (Invitrogen™) was reconstituted at 5 mg/ml in PBS. Assay was performed as per manufacturers' instructions. Absorbance was measured using a Magellan plate reader at 540 nm excitation.

2.1.8   Caspase 3/7 assay

Cells were seeded into black-walled 96 well plates at $1x10^4$ cells per well and incubated overnight. Next cells were treated with 1 mM MβCD for 1-hour either containing CellEvent™ Caspase-3/7 Green Detection Reagent (Invitrogen™) added at 1:1000 dilution, or media was replaced with

fresh media containing the Caspase-3/7 reagent. Fluorescence was measured at 0, 12 and 24-hours using 488 nm filter on BMG Labtech FLUOstar plate reader.

2.2 Tissue Culture

Temporal scalp skin was obtained *via* surplus material from face lift surgeries (Caltag Medsystems Ltd, Buckingham, UK). Samples were shipped overnight on ice and received within 24-hours of surgery. Storage of samples was in accordance with the Human Tissue Act 2004 in the Huddersfield Skin & Hair Biobank. Donor information is provided in Table 2.2 and Table 2.3.

Table 2.2 Details of hair follicle donors for cultured follicles in Chapter 4

Donor	FC [Age (ID) Gender]	MβCD [Age (ID) Gender]	T0901317 [Age (ID) Gender]
1	54 (001) M	32 (016) M	65 (017) F
2	60 (004) M *	65 (017) F	60 (018) F
3	64 (008) M †	69 (019) F	53 (021) F
4	65 (017) F	53 (021) F	64 (023) F
5	69 (019) F ‡		

* indicates donor was on daily Atorvastatin treatment. † indicates culture was for sectioned tissue only. ‡ indicated culture was for RNA extraction only. ID is the donor number and gender is represented by M for male and F for female.

Table 2.3 Details of hair follicle donors for freshly isolated tissue in Chapter 5

	Donor	Anagen [Age (ID) Gender]	Early Catagen [Age (ID) Gender]	Mid-Catagen [Age (ID) Gender]	Telogen [Age (ID) Gender]
ABCA1	1	65 (002) M	**65 (002) M**	60 (018) F	**(007)***
	2	69 (019) F	25 (003) M	**69 (019) F**	(009) *
	3	**59 (022) F**	55 (020) F	-	(013) *
	4	-	-	-	30 (015) M
ABCG1	1	54 (001) M	25 (003) M	60 (018) F	**(013) ***
	2	69 (019) F	60 (004) M †	**69 (019) F**	(014) *
	3	**59 (022) F**	**69 (019) F**	-	30 (015) M
	4	-	-	-	-
ABCA5	1	**65 (002) M**	**25 (003) M**	60 (018) F	**(005) ***
	2	69 (019) F	60 (004) M †	**69 (019) F**	(009) *
	3	59 (022) F	69 (019) F	-	30 (015) M
	4	-	-	-	-
SCARB1	1	65 (002) M	**65 (002) M**	60 (018) F	(007) *
	2	**60 (018) F**	60 (004) M †	**69 (019) F**	(013) *
	3	69 (019) F	69 (019) F	-	**(014) ***
	4	-	-	-	-
HMGCR	1	65 (002) M	25 (003)	60 (018) F	**(009) ***
	2	69 (019) F	**55 (006)**	**69 (019) F**	(012) *
	3	**59 (022) F**	60 (018)	-	30 (015) M
	4	-	-	-	-
Filipin	1	**65 (002) M**	**25 (003) M**	60 (018) F	(005) *
	2	69 (019) F	60 (004) M †	**69 (019) F**	(009) *
	3	59 (022) F	60 (018) F	-	**30 (015) M**
	4	-	-	-	-

Bold text indicates the donor from which images in the manuscript are shown, * donor age not supplied. † indicates donor was on daily Atorvastatin treatment. ID is the donor number and gender is represented by M for male and F for female.

2.2.1 Microdissection

Scalp skin was pinned onto a cork dissection board (Figure 2.2A) and strips of HFs were obtained using no.7 watchmakers' forceps and a no.11 scalpel blades (Figure 2.2B). Strips were then further dissected by removing the epidermis (Figure 2.2C) to amputate the HFs below the bulge. Isolation of individual HFs was performed using no.15 scalpel blades and clean-up of surrounding subcutaneous fat and dermis was achieved (Figure 2.2D).
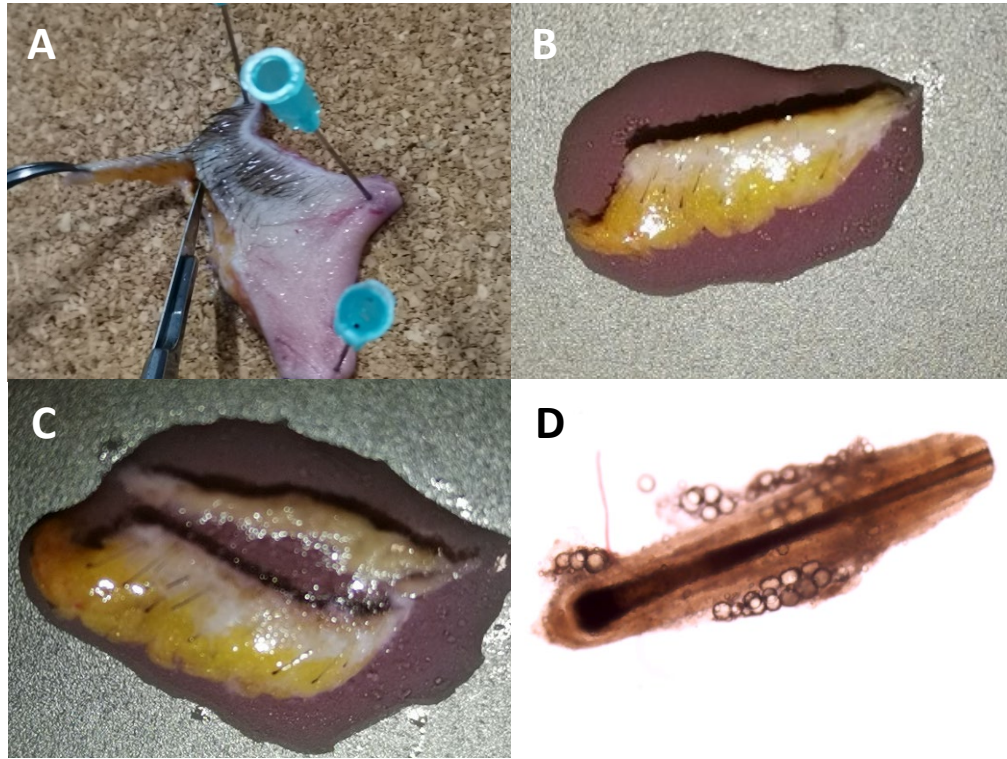
Figure 2.2 Isolation of hair follicles from temporal scalp skin. (A) Dissection of skin to form strips (B). (C) removal of the epidermis from strips. (D) removal of surrounding dermis and subcutaneous fat from follicles.

2.2.2 Culture

HFs were cultured in accordance to (Langan *et al.*, 2015, Philpott *et al.*, 1989, Philpott, 2018) in Williams E medium (Gibco™) supplemented with 1% penicillin-streptomycin, 1% L-glutamine, 10 µg/ml insulin and 10 ng/ml hydrocortisone. Prior to treatment HFs were incubated overnight to acclimatise. The following day the media was replaced with fresh HF media containing either 25 µM FC and incubated for 24-hours, or 5 mM MβCD and incubated for 1-hour with 23-hours recovery time.

2.2.3 Staging

Prior to culture, isolated HFs were staged in accordance to Oh *et al.* (2016) and Kloepper *et al.* (2010). Freshly isolated anagen, early catagen, mid-catagen and plucked telogen HFs were frozen in Richard-Allan Scientific™ Neg-50™ Frozen Section Medium (Thermo Scientific™) using liquid nitrogen, then stored at -80°C until sectioning. For RNA extraction HFs were placed into RNAlater™ Stabilization Solution (Invitrogen™) and stored at 4°C prior to RNA extraction. For culture anagen VI HFs were selected.

2.3 Gene expression analysis

2.3.1 RNA extractions

Cells from 12 well plates were detached using TrypLE as described in Section 2.1.4. RNA was extracted from cell pellets using ReliaPrep™ RNA Miniprep Systems (Promega, Wisconsin, United States) as per manufacturers' instructions. Alternatively, extraction using RNeasy mini plus kit (QIAGEN, Hilden, Germany) was used per manufacturers' instructions, including the addition of β-mecapthoethanol (Sigma-Aldrich) to lysis buffer. RNA was eluted in 15 µl of nuclease-free water.

For HFs RNeasy micro plus kit (QIAGEN) was used per manufacturers' instructions, including the addition of β-mecapthoethanol to lysis buffer. 5-10 HFs were used as starting material, tissue disruption was performed using a 1.5 ml micro centrifuge tube and pestle (Fisher) with a pestle pellet cordless motor (Kimble®, New Jersey, USA), followed by homogenisation *via* TissueRuptor II (QIAGEN). Samples were eluted in 14 µl of nuclease-free water.

Concentrations were measured using a Nanodrop™ 2000 (Thermo Scientific™), along with purity as measured by the 260/280 nm absorbance ratio. RNA was either stored at -80°C or proceeded straight to Section 2.3.2.

2.3.2 cDNA Synthesis

Tetro™ cDNA synthesis kit (Bioline, London, UK) was used to convert between 100 ng to 1 µg of RNA in DNA tetrad 2 thermocycler (Bio-Rad, California, USA) as per manufacturers' instructions.

2.3.3 qPCR

TaqMan™ gene expression assays (Applied biosciences™, Massachusetts, USA) (Table 2.4) were used with either TaqMan™ gene expression master mix (Applied biosciences™) or PrecisionFast master mix (PrimerDesign, Southampton, UK). Each reaction used 1-10 ng of cDNA (vehicle controls and treatment were consistent per donor) and cycling was set up according to manufacturers' guidelines. StepOnePlus™ real time PCR machine (Applied biosciences™) was used to run qPCR. Expression levels were calculated using PPIA as the reference gene, in accordance with the ΔΔCT method.

Table 2.4 TaqMan™ gene expression assays

Gene	Product code
ABCA1	Hs01059118_m1
ABCA5	Hs00363322_m1
ABCG1	Hs00245154_m1
AXIN2	Hs00610344_m1
HMGCR	Hs00168352_m1
LEF1	Hs01547250_m1
PPIA	Hs99999904_m1
SCARB1	Hs00969821_m1
SREBP2	Hs01081784_m1

2.4   Cholesterol efflux assay

2.4.1   Preparation of solutions

1 M HEPES (Sigma-Aldrich) solution was prepared by diluting in distilled water and pH was adjusted to 7.4 using NaOH. 10 mM HBSS (Lonza) HEPES solution was prepared. Cholic acid solution was made at 1% in pure methanol. PSC833 (Sigma-Aldrich) stock was prepared at 4 mM in DMSO. BLT-1 (Sigma-Aldrich) was prepared at 10 mM stock solution in DMSO. MβCD was prepared at either 25 mM or 5 mM stock solution in HBSS+HEPES. APOA1 (Life Technologies™, Massachusetts, USA) was supplied at a concentration of 2.12 mg/ml. HDL (Merck, Darmstadt, Germany) was supplied at a concentration of 11.4 mg/ml. ACAT inhibitor stock solution was prepared at 16 mg/ml in DMSO. BODPIY (Boron-dipyrromethene) Cholesterol (TopFluor® Cholesterol; Avanti lipids, Alabama, USA) was complexed at a molar ratio of 1:10 with 25 mM MβCD to make a 2.5 mM stock. Solution was sonicated in a water bath at 37°C for 30-minutes, then placed into an orbital shaker for 2-hours. Stock solution was stored at -20°C and sonicated in a water bath at 37°C for 30-minutes prior to use.

2.4.2   Assay

ORS keratinocytes were seeded at 2×10^4 cells per well in a 48 well plate and grown for 3 days, with two replicate wells per treatment. Cells were washed in Epilife and then incubated with BODIPY Cholesterol (25 µM) for 2-hours in the dark. Cells were washed in Epilife and equilibrated for 24-hours with ACAT inhibitor (2 µg/ml). Cells were washed in HBSS+HEPES and efflux was initiated by adding cholesterol acceptors, APOA1 (10 µg/ml) in HBSS+HEPES or HDL (25 µg/ml) with or without PSC833 (5 µM) or BLT-1 (10 µM) for 4-hours. Positive control efflux was initiated with 5 mM MβCD incubation. For background efflux, HBSS+HEPES was added to cells with or without PSC833 (5 µM) or BLT-1 (10 µM). Media was removed and measured in black-walled 96 well plates (excitation filter 485/20 nm, emission filter 528/20 nm).

Time-0-monolayers were incubated with 1% cholic acid for 1-hour at room temperature on a plate shaker. Cells were scraped using a pipette tip and fluorescence of the cell suspension was measured (excitation filter 485/20 nm, emission filter 520/20 nm). Efflux calculations were achieved through subtracting the fluorescence values of the background efflux from the cells treated with the cholesterol acceptor and divided by the time-0-monolayers.

2.5 Immunofluorescence and histochemical staining

2.5.1 Preparation of cells

Cells were seeded onto 13 mm tissue culture treated coverslips (Sarstedt, Nümbrecht, Germany) by adding a 30 µl droplet of cell suspension containing 66.6×10^4 cells per ml and incubated for 2-hours to ensure adherence to the centre of the coverslip. Next, 500 µl of media was added per well and cells were incubated overnight prior to treatments or fixation (details below in Table 2.5). Post fixation, cells were washed three times in PBS and stored at 4°C until staining.

2.5.2 Preparation of frozen tissue sections

Snap-frozen HFs as described above in Section 2.2.3 were mounted using Richard-Allan Scientific™ Neg-50™ Frozen Section Medium (Thermo Scientific™) into a CM1900 cryostat (Lecia, Wetzlar, Germany). Sections were made at 7 µm thickness and placed onto Superfrost™ Plus slides (Thermo Scientific™). Sections were stored at -80°C until use.

2.5.3 Antibody staining

All tissue sections were air-dried for 10-minutes before fixation in the following Table 2.5, blocking was performed at room temperature with either 10% normal goat serum (NGS) (Sigma-Aldrich) diluted in respective buffer or 2.5% normal horse serum (NHS) (Vector® Laboratories, Peterborough, UK). Primary antibodies (see Table 2.5) were diluted in either 2% NGS or 2.5% NHS (for vector) and incubated overnight at 4°C. Washes with PBS or TBS (see Table 2.5) were performed three times for 5-minutes in tissue sections or three dip washes in 5 ml Bijou tubes for coverslips. Secondary antibody incubations were performed for 45-minutes at room temperature with Alexa Fluor Goat IgG (H+L) Cross-Adsorbed Secondary Antibody (Invitrogen™). Alternatively, for ABCA1 and ABCG1, VectaFluor™ Excel Amplified DyLight® 488 IgG Kit (Vector® Laboratories) was used. In the case of dual immunofluorescence staining Vector secondary antibodies and subsequent blocking were performed prior to additional primary antibody staining to prevent chances of cross reactivity. Nuclear counterstaining was performed by incubating for 1-minute with 1 µg/ml 4′,6-diamidino-2-phenylindole (DAPI).

Table 2.5 Antibody protocols for immunofluorescence

Antibody [clone]	Fixative	Block	Wash	Primary dilution	Secondary Antibody	Secondary dilution	Product code
ABCA1 [AB.H10]	1:1 Acetone: Methanol	2.5% NHS	TBS-T	1:25	VectaFluor excel anti-Mouse 488	N/A	ab18180 (abcam)
ABCA5	100% Acetone	10% NGS	PBS	1:200	Goat anti-Rabbit 594	1:200	ab99953 (abcam)
ABCG1 [EP1366Y]	1:1 Acetone: Methanol	2.5% NHS	TBS-T	1:50	VectaFluor excel anti-Rabbit 488	N/A	ab52617 (abcam)
SCARB1 [EPR20190]	100% Acetone	10% NGS	PBS	1:200	Goat anti-Rabbit 594	1:1000	ab217318 (abcam)
HMGCR	100% Acetone	10% NGS	PBS	1:100	Goat anti-Rabbit 594	1:200	13533-1-AP (proteintech®, Manchester, UK)
Laminin-332 [P3H9-2]	Any of the above or 4% paraformaldehyde	10% NGS	PBS	1:1000	Goat anti-Mouse 488 Goat anti-Mouse 568	1:200	ab78286 (abcam)
CD200 [OX-104]		10% NGS	PBS/TBS	1:200	Goat anti-Mouse 488	1:200	MCA1960GA (Bio-Rad, California, USA)
ATPB [3D5]		10% NGS	PBS/TBS	1:1000	Goat anti-Mouse 488	1:200	ab14730 (abcam)
PDI [RL90] †		10% NGS	PBS/TBS	1:200	Goat anti mouse 488	1:500	ab2792 (abcam)
LAMP1 [H4A3]		10% NGS	PBS/TBS	1:200	Goat anti mouse 488	1:200	ab25630 (abcam)

† Official gene symbol: PH4B

2.5.4   Filipin staining

In order to examine the localisation of cellular FC filipin iii streptomyces, a naturally fluorescent antibiotic was utilised. The antibiotic filipin iii is a naturally fluorescent probe, which binds to the 3-β-hydroxy group of sterols, making it selective in detecting FC and not CE (Maxfield and Wüstner, 2012) (see Figure 2.3).

4% paraformaldehyde (Sigma-Aldrich) (w/v) was prepared in PBS and mixed on a heated stirrer at 100°C for 2-hours. Solution was cooled prior to use. Filipin (F4767; Sigma-Aldrich) was reconstituted at a concentration of 10 mg/ml in DMSO, aliquoted and stored at -80°C protected from light.

Tissue sections were air-dried for 10-minutes before fixation, whereas coverslips were immediately fixed. Filipin staining was performed subsequent to fixation in 4% paraformaldehyde for 10-minutes, followed by washes in PBS. A 10-minute quenching step was performed with 1.5 mg/ml glycine. A working concentration of filipin was prepared at 100 µg/ml in PBS with 10% FBS added for 2-hours at room temperature. For dual immunofluorescence staining, quenching was performed subsequent to secondary antibody staining as described in Section 2.5.3. Lastly, coverslips or slides were mounted using Faramount aqueous mounting media (DAKO, Agilent, California, USA) and left to set until hardened. Images were acquired immediately, and all stages were performed protected from light.
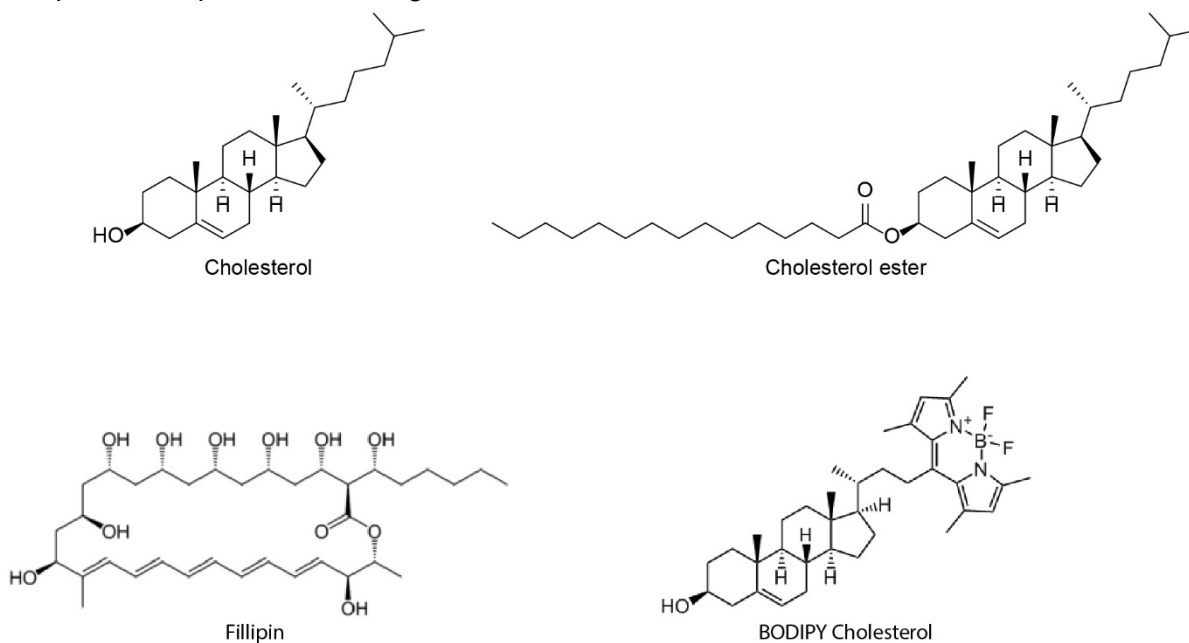
Figure 2.3 Structure of cholesterol, cholesterol esters and fluorescent probes.

2.5.5 Live cholesterol imaging

Cells were seeded into micro-Insert 4 Well in 35 mm µ-Dish with ibidi treat polymer coverslips (ibidi, Planegg, Germany) at 2×10^4 cells per ml. Cells were incubated overnight and siRNA transfections were achieved as described above in Section 2.1.6. Following this, cells were washed once in HBBS-Hepes and then incubated first with step 1 as per manufacturers' instructions (outlined in Table 2.6), washed again with HBSS-Hepes and incubated with step 2 (diluted in HBSS-Hepes). A subsequent wash with HBSS-Hepes was performed, then in step 3 BODIPY cholesterol was diluted in HBSS-Hepes and added directly before imaging.

Table 2.6 Live cell imaging protocol

Step	Product	Product code	Dilution	Incubation time
1	ER Staining Kit - Red Fluorescence - Cytopainter	ab139482 (abcam)	1:500	15-minutes
2	Mitochondrial Staining Reagent - Blue - Cytopainter	ab219940 (abcam)	1:500	30-minutes
	LysoTracker™ Deep Red	L12492 (Invitrogen™)	1:20000	
3	TopFluor cholesterol	810255 (Avanti lipids)	25 µM	N/A

2.5.6 Masson's Fontana

Silver nitrate stock solution was prepared using 10% silver nitrate (Honeywell, North Carolina, USA) in distilled water, ammonium hydroxide (Fisher) was added dropwise until the solution turned brown and back to clear again. The stock solution was left in the dark for 24-hours to develop. The working solution was used at 1:4 dilution in distilled water.

Slides were air-dried for 10-minutes, then fixed in a 2:1 ethanol: glacial acetic acid mixture for 10-minutes. Slides were placed into silver nitrate working solution and microwaved for 2-3-minutes, Followed by incubation with 5% sodium thiosulfate (Fisher) solution for 1-minute. Counter staining with Mayer's Haematoxylin (Sigma-Aldrich) was performed for 2-minutes.

2.5.7 Ki67 / TUNEL

Tissue sections were air-dried for 10-minutes. ApopTag® Fluorescein *In situ* Apoptosis Detection Kit (Merck) was utilised to detect apoptosis *via* TUNEL (terminal deoxynucleotidyl transferase dUTP nick end labelling). Fixation in 1% paraformaldehyde for 10-minutes was initially performed, followed by post-fixation with ethanol-glacial acetic acid (2:1) for 5-minutes. Slides were washed

with PBS and followed by incubating in equilibration buffer for 5-minutes. TdT enzyme was diluted in reaction buffer 30/70, then tissue sections were incubated in a humidified chamber for 1-hour at 37°C. Stop solution was prepared at 1:35 dilution and slides were incubated for 10-minutes at 37°C. Following washes with PBS, slides were blocked in 10% NGS for 20-minutes and incubated with primary Rabbit anti-Ki67 antibody [SP6] (ab16667) at 1:200 dilution in 2% NGS in a humidified chamber at 4°C overnight. Following washes with PBS, sections were incubated with fluorescein-labelled anti-digoxigenin-antibody at 52% dilution in blocking solution provided in the kit. Incubation was performed for 30-minutes at room temperature, followed by washes with PBS. Alexa Fluor Goat anti-rabbit IgG 594 (H+L) Cross-Adsorbed Secondary Antibody (Invitrogen™) was incubated for 45-minutes at room temperature in a 1:200 dilution in 2% NGS. Subsequent washes in PBS and counterstaining with DAPI at 1 μg/ml was performed.

2.5.8   EdU click iT

Cells were seeded onto coverslips as described in section 2.1.4, then fixation media was aspirated and fresh media containing 10 μM EdU was incubated for 4-hours. Following this, cells were washed in PBS and fixed in 4% formaldehyde for 15-minutes. Click-iT™ reaction was performed as per manufacturer's instructions for Invitrogen™ Molecular Probes™ Click-iT™ EdU Alexa Fluor™ 594 Imaging Kit.

2.5.9   β-galactosidase senescence staining

Chromogenic senescent staining was performed as described in Debacq-Chainiaux *et al.* (2009), using the optimal pH 6 conditions to detect senescence β-galactosidase (β-gal) activity (Dimri *et al.*, 1995). Cells were seeded as described in Section 2.1.4, after treatment cells were washed once in PBS and fixed in 2% formaldehyde with 0.2% glutaraldehyde (v:v) in PBS for 5-minutes at room temperature. X-gal (Thermo Scientific™) was diluted in N, N-dimethylformamide immediately before use (Acros Organics). X-gal solution was made up in distilled water as described in Table 2.7 and incubated overnight at 37°C. Following PBS and methanol washes, coverslips were mounted with Faramount aqueous mounting media onto glass slides before imaging.

Table 2.7 X-gal solution

Total	Stock	Working concentration
Citric acid/Sodium phosphate (1:5) pH 6.0	200 mM	40 mM
Potassium Hexacyanoferrate (II) trihydrate (1:20)	100 mM	5 mM
Potassium Hexacyanoferrate (III) (1:20)	100 mM	5 mM
Magnesium Chloride (1:500)	1 M	2 mM
Sodium Chloride (1:10)	1.5 M	150 mM
X-gal (1:20)	20 mg/ml	1 mg/ml

2.6 Image acquisition and analysis

2.6.1 Widefield microscopy

Fluorescence widefield microscopy was used to image Ki67 TUNEL staining in HF tissue sections, EdU staining ORS cells. Images were acquired on Axio observer Z1/7 microscope (Zeiss, Oberkochen, Germany) using the Zen Blue software suite and a Plan-Aprochromat 63x/1.4 Oil DIC M27 objective. Images were acquired using the Zeiss AxioCam 305 mono camera.

Masson Fontana brightfield images were acquired using either the above-mentioned microscope or a fully automated Leica DM6000B (Leica Microsystems, Wetzlar, Germany) equipped with the LAS X software, a HC PL FLUOTAR 10x/0.30 dry objective and a DCF 490 colour camera. Cell senescence images were taken on the Lecia microscope or an EVOS™ XL Core Imaging system (ThermoFisher™).

2.6.2 Confocal microscopy

Confocal microscopy was performed using a Zeiss laser scanning microscope 880 Axio-Observer using Zen Black v2.3 software for acquisition (Zeiss). For HFs tile scan images were performed with a Plan-Aprochromat 40x/1.4 Oil DIC M27 objective and 10% overlap between tiles. For all images the following settings were used: digital gain 1.0, detector offset 0, binning 1x1 and averaging 1. Scaling of either 0.04x0.04 µm or 0.07x0.07 µm per pixel was used. A diode 405 nm, the 488 nm-line of an Argon458/488/514nm, a diode 561 nm and a HeNe 594 nm laser were used at a range of 1-3%, detector gain setting varied from 600-800. Images were acquired using a 34-channel detector comprised of two high-sensitivity red and blue PMT confocal detectors and a 32 channel GaAsP spectral detector.

2.6.3 Image processing

Airyscan processing was performed in Zen Black software. Zen Blue v2.3 was utilised for image stitching; histogram image processing and gamma correction were applied to all images universally. Regions of interests were selected from the tile scan images, scale bars donate 50, 10 or 5 µm as shown in figure legends.

2.6.4 Ki67 / TUNEL analysis

To analyse proliferation and apoptosis, the ImageJ FIJI (Schindelin *et al.*, 2012) cell counter tool was utilised. Analysis was performed as described in Kloepper *et al.* (2010). Auber's line was

determined, and a line drawn at this level; numbers of cells below this line, along with the DP and DP stalk were counted. Ki67+ DAPI were counted in the matrix cells below Auber's line, whereas TUNEL+ DAPI were counted in the whole bulb, DP and DP stalk.
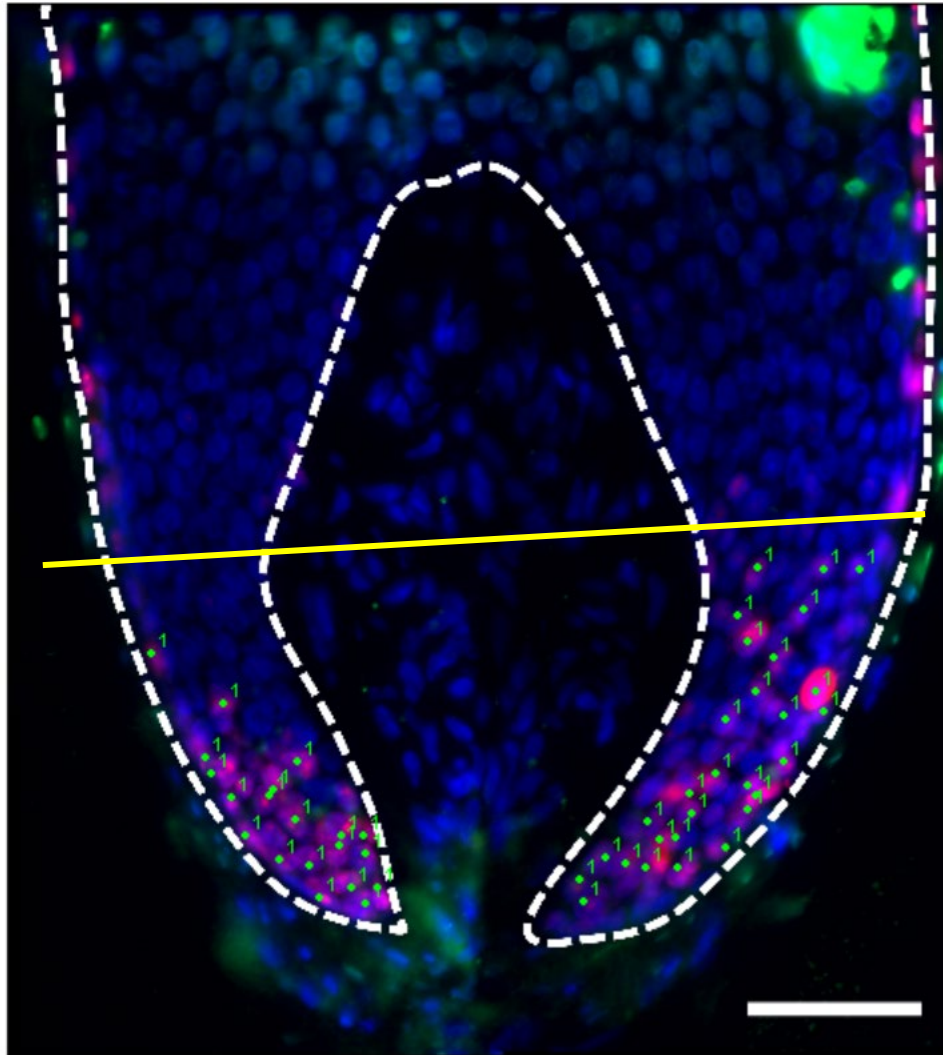
Figure 2.4 Ki67 / TUNEL analysis. Representative image showing Ki67+ cells counted below Auber's line (yellow line). Epithelial region shown by white dashed line.

2.6.5   Masson's Fontana analysis

Images acquired for Masson's Fontana staining were analysed in ImageJ FIJI, by converting to 8-bit, then inverting grayscale. Epithelial components of the bulb were outlined using the polygon line tool (Figure 2.5) and mean pixel intensity (arbitrary units; a.u.) was measured. Furthermore, the number of Melanin clumps were counted, along with the presence of ectopic Melanin in the DP or DP stalk.
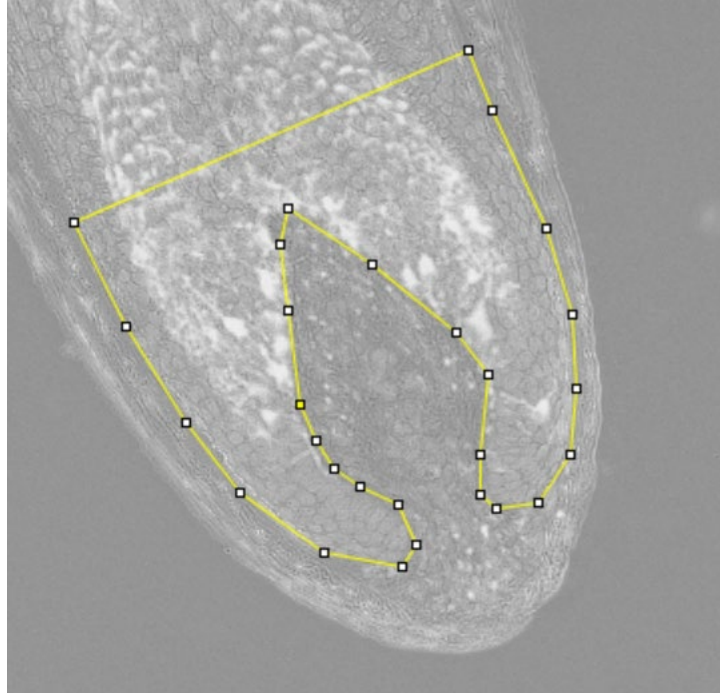
Figure 2.5 Masson Fontana analysis. Inverted image showing epithelial region drawn with polygon tool in ImageJ.

2.6.6 Image segmentation for counting cells and pixel intensity per cell

Image segmentation was performed using pixel classifier in ilastik (Berg *et al*., 2019). Annotations for background and cells were performed manually (Figure 2.6) and batch processing applied to the data set to produce probability scores. Binary processing, including close and fill hole functions, were performed, and particles were analysed to produce ROIs per cell, then number of ROIs were recorded (Appendix 10). Alternatively, analyse particles was redirected to original image to measure pixel intensity per cell (Appendix 11).
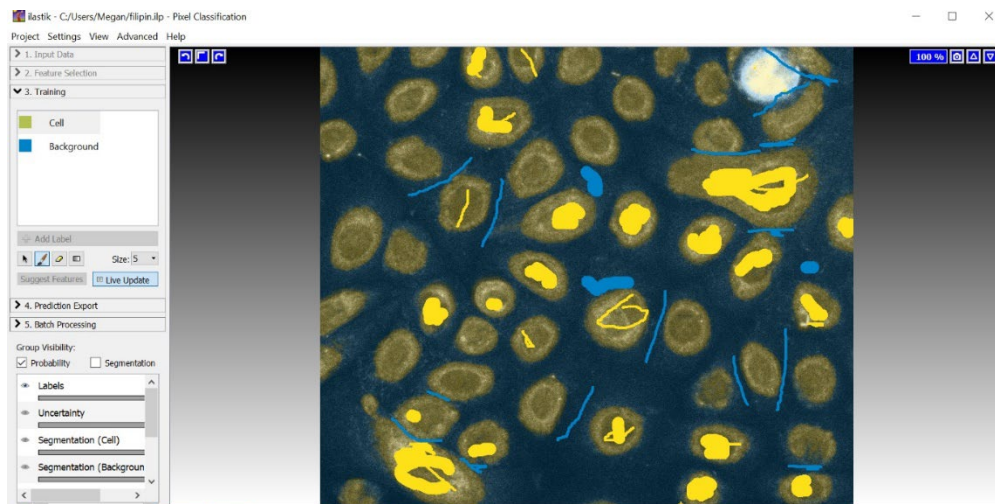
Figure 2.6 Representation of ilastik segmentation.

2.6.7 Intracellular distribution

To determine the co-localisation of either ABCA5, filipin or BODIPY to intracellular markers ImageJ FIJI was used. Macros were written to automatically determine the mean pixel intensity within the masked area of the organelle. First the organelle images were converted to 8-bit, then a threshold was set (normalised across each donor and staining). Images were converted to mask, and then either the ABCA5, filipin, BODIPY opened and converted to 8-bit. Measurements were set to redirect the area to the signal image. Analyse particles was run to overlay mask and summarise information (Figure 2.7). Mean pixel intensity measurements were taken per image (Appendix 12), and averages taken per donor.
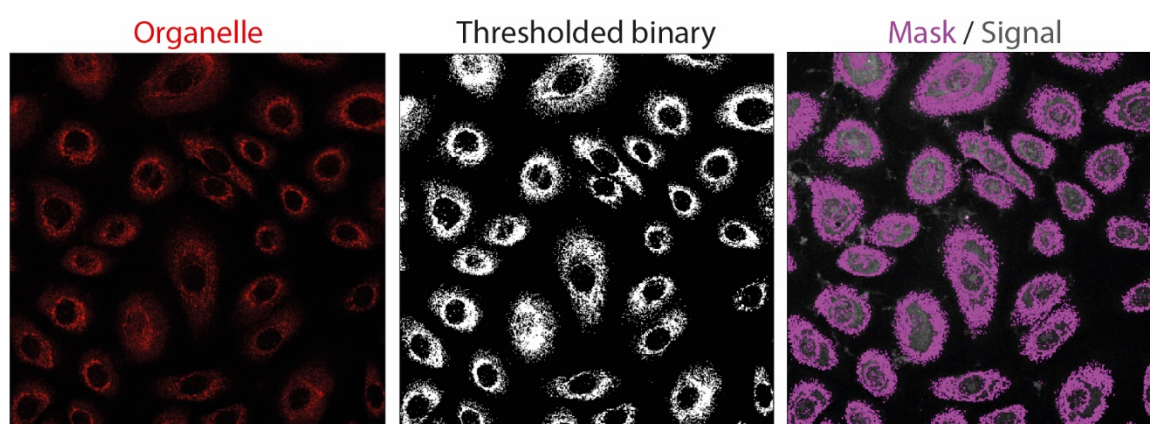
Figure 2.7 Co-localisation masking. Representation original organelle marker (red), binary image from thresholding (white), Mask from analyse particles (Magenta) on signal image (grey).

The BIOP JaCoP plugin was utilised to generate Pearson and Mander's co-efficients, image analysis was performed using auto-thresholding (Appendix 13).

2.6.8 Live imaging and 3D image processing

To acquire live images, confocal airyscan microscopy was used and additional filters were applied to prevent cross talk in quad staining as shown in Table 2.8. These settings were optimised using single-stained cells to ensure correct localisation.

Table 2.8 Image acquisition settings for live cholesterol tracking

Marker	Excitation/Emission	Laser	Filter
Mitochondria	350/490	405	
BODIPY Cholesterol	495/507	488	BP 450/60 + BP 522.5/55
Endoplasmic Reticulum	~560/650	561	BP 450/60 + LP 605
Lysosome	647/668	633	

Images were acquired with a LD LCI Plan-Aprochromat 40x/1.2 Imm Korr IC M27 objective with a Z-stage Piezo and glycerol immersion using fast Airyscan. Z-stack settings for 20 µm from the centre were optimised for complete coverage of all 4 regions and allowed for changes in Z position over time. Six time points were acquired over a period of 3-hours. 3D airyscan processing followed using Zen Black. Image registration was performed using Zen Blue to correct for Z-drift. Images were split into separate time points subsequent to image analysis.

Prior to running macros, the Bio-formats plugin was configured to open CZI images in windowless mode with channel splitting selected following opening the images. Intensity of BODIPY cholesterol per cell was measured using maximum intensity projections and mean pixel intensity was measured and normalised to cell counts (Appendix 14). Image analysis for co-localisation was performed as described in Section 2.6.7 on maximum intensity projections (Appendix 15).

2.7 Western blotting

2.7.1 Protein lysis

Radioimmunoprecipitation assay (RIPA) buffer was prepared to final concentrations of 150 mM sodium chloride, 0.1% (v/v) triton x 100 (Sigma-Aldrich), 0.5% (w/v) sodium deoxycholate (Alfa Aesar™), 0.1% (w/v) sodium dodecyl sulphate (Fisher BioReagents™), 50 mM Tris-HCL pH 8.0 (Fisher BioReagents™) and protease inhibitor tablet (Pierce™, Massachusetts, USA). The solution was aliquoted and stored at -20°C.

Cells were seeded into 3 wells of a 6 well plate prior to treatment. Following treatments, media was aspirated, and cells were washed in ice-cold PBS. PBS was aspirated and cells were lysed in 200 µl of RIPA buffer. Cell lysates were sonicated for six times 5-seconds on ice using a probe sonicator. Samples were then centrifuged at 13539 g for 20-minutes at 4°C. Supernatants were removed from pellets and proceeded to protein quantification.

Alternatively, siRNA knockdown samples were prepared from the cytosolic fraction prepared from nuclear extraction kit as described in Section 2.9.1.

2.7.2 Bradford Coomassie assay

To quantify protein amounts samples were diluted 1:20 in ultrapure water. Pierce™ Coomassie (Bradford) Protein Assay (Thermo Scientific™) was used as per manufacturers' instructions. 5 µl of samples were added to 96 well assay plates with 250 µl of Coomassie reagent and incubated for 10-minutes. BSA was diluted to produce a set of standards ranging from 2 mg/ml to 25 µg/ml as described in manufacturer's instructions. Absorbance was measured at 595 nm on a FLUOstar plate reader (BMG Labtech, Ortenberg, Germany). A 4-parameter fit standard curve was created using MARS Data Analysis Software (BMG) to calculate sample concentrations.

2.7.3 SDS-Page

40-100 µg of cell lysates were prepared with NuPAGE™ LDS Sample Buffer (Invitrogen™) and Bolt™ Sample Reducing Agent (Invitrogen™) for a final concentration of 50 mM dithiothreitol (DTT), samples were not heated unless otherwise stated. Samples were separated on NuPAGE™ 3-8% Tris-Acetate Protein Gels (Invitrogen™) at 150 V for 1-hour in 1x NuPAGE™ Tris-Acetate SDS Running Buffer (Invitrogen™) using a mini gel tank (Life Technologies™). Adequate protein separation was monitored using Chameleon® Duo Pre-stained Protein Ladder (Licor®, Nebraska, USA).

2.7.4   Transfer

Transfer to PVDF membranes with iBlot™ 2 transfect stacks was achieved using iBlot™ 2 Gel Transfer Device (Life Technologies™) following the modified P0 protocol. 20 V for 1-minute, followed by 23 V for 4-minutes and 25 V for 5-minutes were applied.

2.7.5   Western blotting

Membranes were blocked for 1-hour at room temperature using Intercept® TBS blocking buffer (Licor®). Primary antibodies were incubated overnight at 4°C on a rocker, concentrations are detailed in Table 2.9 below. Following three 5-minute washes in TBS, secondary antibodies Goat anti-mouse IgG (H+L) Alexa Fluor® 790 (Invitrogen™) or Goat anti-rabbit IgG (H+L) Alexa Fluor® 680 (Invitrogen™) were incubated for 1-hour at room temperature. Membranes were imaged using an Odyssey scanner (Licor®).

Table 2.9 Western blot antibody dilutions

Antibody	Primary dilution	Species	Product code
ABCA1	1:500	Mouse	ab18180 (abcam)
ABCA5	1:500	Rabbit	ab99953 (abcam)
ABCG1	1:500	Rabbit	ab52617 (abcam)
SCARB1	1:1000	Rabbit	ab217318 (abcam)
β-actin	1:40000	Rabbit	ab8227 (abcam)
β-actin	1:40000	Mouse	MAB1501 (Merck)

2.7.6   Analysis

Densitometry analysis was performed using Image studio lite (Licor®). Blot scans were imported, and the draw rectangle tool was utilised to calculate intensity of each protein of interest and β-Actin as reference protein. Background calculations are automatically subtracted, and the signal values were taken. Final values of densitometry were acquired by normalising the protein amount to β-Actin.

2.8   Flow cytometry

2.8.1   Cholera toxin FITC

In order to examine lipid raft cholesterol, CTX-FITC was used as a tool to detect lipid raft marker GM1 gangliosides (Kellie *et al.*, 1983). CTX-FITC (Sigma-Aldrich) was reconstituted at 2.5 mg/ml stock in water. Cells were seeded at 10×10^4 per ml in 24 well plates prior to siRNA transfection. Cells were washed twice in ice cold PBS and then fixed with 1% PFA (w/v) for 5-minutes on ice. Following fixation cells were washed twice in ice-cold PBS containing 3% BSA, then incubated with 6 µg/ml CTX-FITC (Sigma-Aldrich) for 30-minutes at room temperature. Two more washes in-ice cold PBS with BSA were performed before cells were scraped in 1x ice-cold PBS. Flow cytometry analysis was performed using a Guava® easyCyte™ SL 5 flow cytometer (Merck).

2.8.2   Annexin V and propidium iodide

Cells were seeded at 10×10^4 cells per well in 24 well plates and treated with MβCD as described in Section 2.1.5. In addition, a positive control of 2 mM hydrogen peroxide was used to induce apoptosis. Cells were washed once in PBS, then incubated with TrypLE for 10-minutes and centrifuged at 500 g for 5-minutes at 4°C. Cell pellets were washed in ice-cold PBS and then centrifugation was repeated. Supernatant was removed and cell pellets were resuspended in 100 µl of ice-cold annexin V binding buffer. Samples were incubated with annexin V and propidium iodide for 15-minutes as described in manufacturers' instructions for TransDetect® Annexin V-FITC/PI Cell Apoptosis Detection Kit (TransGen Biotech, Beijing, China). Cell suspensions were made to a final volume of 500 µl before immediately detecting fluorescence *via* flow cytometry. Individual single staining in positive and negative control cells was used to adjust quadrant settings. Counts obtained for unstained cells were categorised alive, annexin V only-staining as early apoptotic, dual annexin V as well as propidium iodide-staining as late apoptotic and necrotic for propidium iodide only-stained cells.

2.9 SREBP2 Transcription factor assay

2.9.1 Nuclear protein fractionation

Cells were seeded at 4×10^4 cells per cm^2 into three wells of a 6 well plate and scraped in ice-cold PBS. Nuclear fractions were isolated using Nuclear Extraction kit (ab113474; abcam) as per manufacturers' instructions. Protein concentration was measured using Bradford Coomassie (Section 2.6.2) and the isolate immediately frozen at -80°C.

2.9.2 Assay

Nuclear fractions were thawed and immediately used for the assay with 30 µg of protein per reaction. SREBP2 assay was measured *via* ELISA method as per manufacturers' instructions using SREBP2 transcription factor assay kit (abcam; ab133111). Absorbance was measured at 450 nm on a BMG Labtech SPECTROstar Nano.

2.10 Lipidomic analysis

Cells were seeded at 4×10^4 per cm^2 in three wells of a 6 well plate subsequent to transfection (as described above in Section 2.1.6). After 48-hours incubation 25 µM FC was added for 24-hours. Cells were lysed using 1xTrypLE for 10-minutes and centrifuged at 200 g for 8-minutes. Supernatant was removed and pellets were immediately snap-frozen on dry ice. Samples were shipped on dry ice to Dr Irundika Dias (Aston University, Birmingham, UK) for extraction. Cholesterol and oxysterols were measured by liquid chromatography–mass spectrometry as described in Dias *et al.* (2016).

2.11 Statistical analysis

Graphs and statistical analysis were performed using Prism (GraphPad, California, USA). Shapiro-Wilk test was performed to test for normality. One sample t-tests, unpaired t-test and one-way ANOVA were used to detect statistical significance for data with a normal distribution. Kruskal Wallis tests or Wilcoxon test was performed for data without a normal distribution. Significance is denoted by * P≤0.05, ** P≤0.01, *** P≤0.001.

Chapter 3: Determining the expression and activity of cholesterol transporters in human hair follicle keratinocytes

3.1 Introduction

As highlighted in Chapter 1, cholesterol has long been suspected in influencing hair growth (Palmer *et al.*, 2020). Yet the mechanisms by which cholesterol homeostasis are maintained have not been explored in the HF. Cholesterol homeostasis is tightly regulated by a host of proteins involved in efflux (Aye *et al.*, 2009), intracellular trafficking (Soccio and Breslow, 2004), uptake, synthesis and metabolism (Zhao and Dahlman-Wright, 2010, Ikonen, 2008, Krisans, 1992, Rhainds and Brissette, 2004). This study focused on ABC transporter-mediated cholesterol movement, including two ubiquitously expressed and well documented cholesterol transporters; ABCA1 and ABCG1 (Quazi and Molday, 2011, Tarling *et al.*, 2013). The putative cholesterol transporter ABCA5, which shows high expression levels in the skin and is implicated in a form of congenital hypertrichosis (DeStefano *et al.*, 2014, Hayashi *et al.*, 2017) was also examined. The functionality of bi-directional cholesterol transporter SCARB1, which facilitates movement of CE to and from circulating HDL was measured (Shen *et al.*, 2018b), alongside mRNA expression of the rate-limiting cholesterol biosynthesis enzyme HMGCR to give insight into the HF capability to synthesise cholesterol.

HF mRNA expression of *ABCA1, ABCA5* and *ABCG1* have been previously reported, and protein localisation of ABCA1 has been explored in anagen HFs by Haslam *et al.* (2015). ABCA5 protein and mRNA location has been reported in anagen and late catagen HFs (DeStefano *et al.*, 2014).

This chapter aims to determine the mechanisms by which primary HF-derived keratinocytes modulate cholesterol transport activity. The following elements were examined:

1. The impact of cholesterol loading or depletion on transporter expression levels
2. Cellular localisation of transporters in ORS keratinocytes
3. The response of cholesterol transporters to LXR activation
4. The routes by which cholesterol efflux occurs in ORS keratinocytes

3.2 Results

3.2.1 Characterising cholesterol transport genes in response to cholesterol loading and depletion

Firstly, the transcriptional response of genes involved in cholesterol homeostasis was examined. ORS keratinocytes were exposed to a physiological concentration of cholesterol (25 µM) (Shiigi *et al.*, 2008) for 24 or 72-hours (Figure 3.1 A,B respectively). A trend towards increased expression of *ABCA1*, *ABCG1* and *SCARB1* was seen at both time points. Responses between donors showed substantial variability and, as such, only the increase in *SCARB1* expression following 72-hours FC loading reached the level of significance (P=0.047). No changes were observed for *ABCA5* or *SREPB2*. *HMGCR* did not respond to 24-hours of FC loading, however significant reductions were detected at 72-hours (P=0.002).

To further investigate cholesterol homeostasis, cholesterol depletion was performed using 1 mM MβCD for 1-hour, followed by a 23-hour recovery period (Figure 3.1C). All cholesterol transporters (including *ABCA5*) were significantly reduced under these conditions. No change was detected in the cholesterol synthesis gene *HMGCR*.

Following this, the effects of altering cellular cholesterol levels on protein expression and cholesterol efflux were examined.

A

24h FC loading

B

72h FC loading

C

1mM MβCD cholesterol depletion
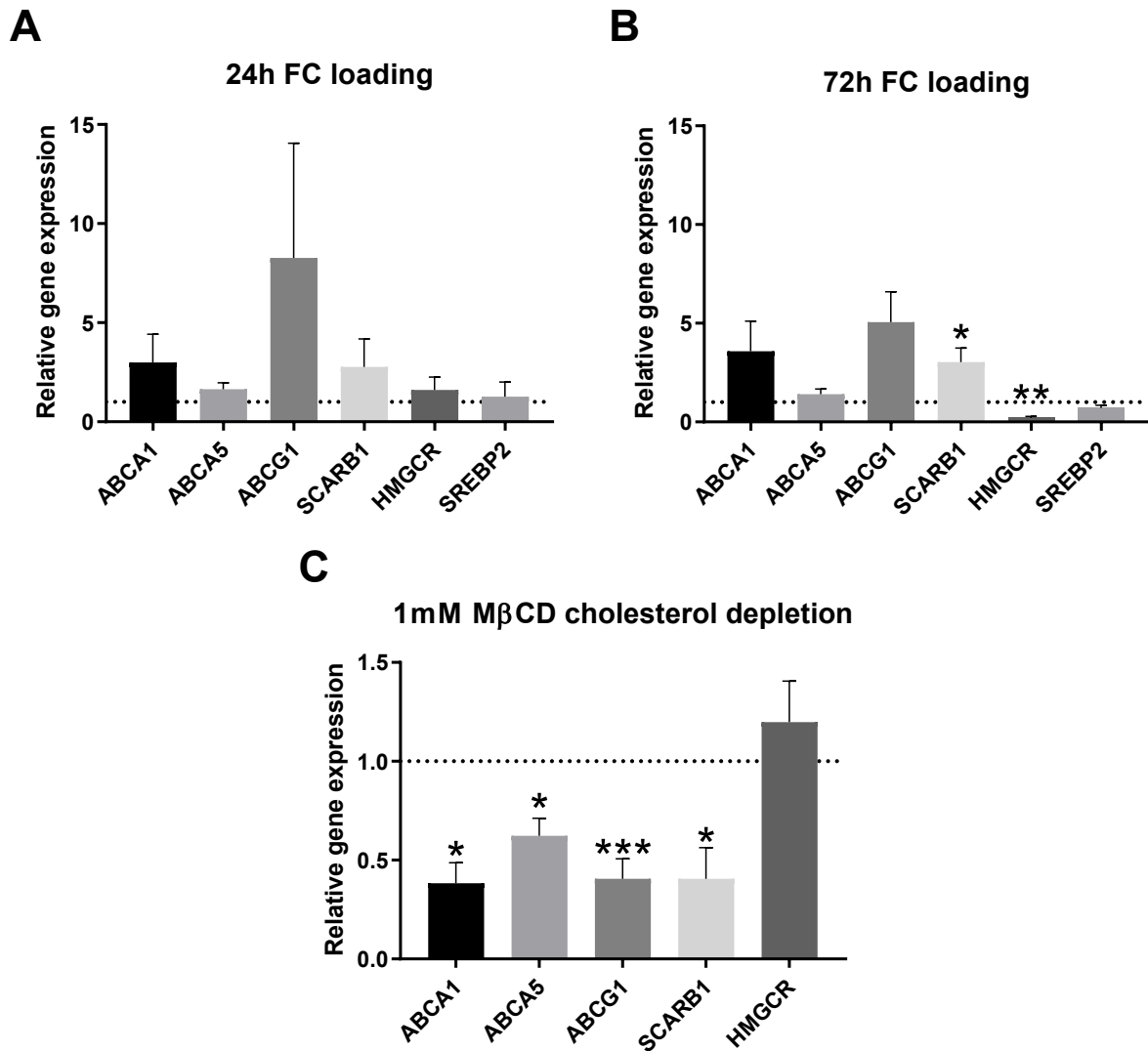
Figure 3.1 Initial screening of cholesterol transporters in response to cholesterol loading and depletion. Gene expression changes in ORS keratinocytes treated with 25 µM FC for (A) 24-hours, (B) 72-hours or (C) 1 mM MβCD for 1-hour + 23-hours recovery. Gene expression reported relative to vehicle control and normalised to *PPIA*. Data are mean ± SEM for n=5 or 6 donors. One-sample t-test performed; significance denoted by * P≤0.05, ** P≤0.01, *** P≤0.001.

3.2.2 Quantification of protein expression and activity of cholesterol transporters

Western blotting was used to examine total protein abundance following loading with FC for 72-hours, or depleting cholesterol for 1-hour with MβCD (Figure 3.2). No changes in ABCA1, ABCG1 or SCARB1 protein were detected following cholesterol loading, as confirmed by densitometry

analysis (Figure 3.2A). Small increases were found in the glycosylated form of ABCA1 for both FC and MβCD (Figure 3.2B).

ABCA5 immunoblotting detected multiple bands (Figure 3.3). Predicted isoforms for ABCA5 occur at both 99 and 187 kDa, and previous studies have detected glycosylated bands at approximately 220 kDa in both human and rat (DeStefano *et al.*, 2014, Petry *et al.*, 2003). However, data presented here shows bands at much higher molecular weights of approximately 300 and 400 kDa, of which the 400 kDa band increases in intensity with both FC loading and MβCD depletion (Figure 3.3A). There is evidence that other ABC transporters form tetramers and oligomers in the active forms in membranes (Denis *et al.*, 2004a, Trompier *et al.*, 2006, Xu *et al.*, 2004). To further investigate these additional high molecular weight proteins, additional western blots were performed with or without a higher concentration of reducing agent (500 nM DTT), and heat was applied to reduce oligomerisation. Figure 3.3B demonstrates that in the absence of both DTT and heat, both 400 and 99 kDa bands were present. With the addition of either heat and/or DTT a mixture of bands were present between 300 and 99 kDa, with a loss of the 400 kDa band.

Cholesterol loading resulted in no change in the 99, 187 and 300 kDa bands, however an increase was detected for the 400 kDa band in 3 out of 4 donors (mean 3.16, ± SEM 1.17). Whereas MβCD treatment resulted in a significant reduction in the 187 kDa band, increases in the 300 plus and the 400 kDa bands were detected, albeit with varied donor responses (fold change ranges 0.33-5.7 and 0.32-14.13 respectively).

Next, the activity of cholesterol efflux transporters was measured using BODIPY-labelled cholesterol, with efflux to the cholesterol acceptors APOA1 and HDL (Figure 3.2). Efflux to HDL increased when cells were loaded with FC and reduced following MβCD treatment. In contrast, a reduction in efflux to APOA1 was observed with FC loading and an increase following MβCD treatment.

Subsequently, modulation of cholesterol transport following activation of LXR with the synthetic agonist T0901317 was investigated.
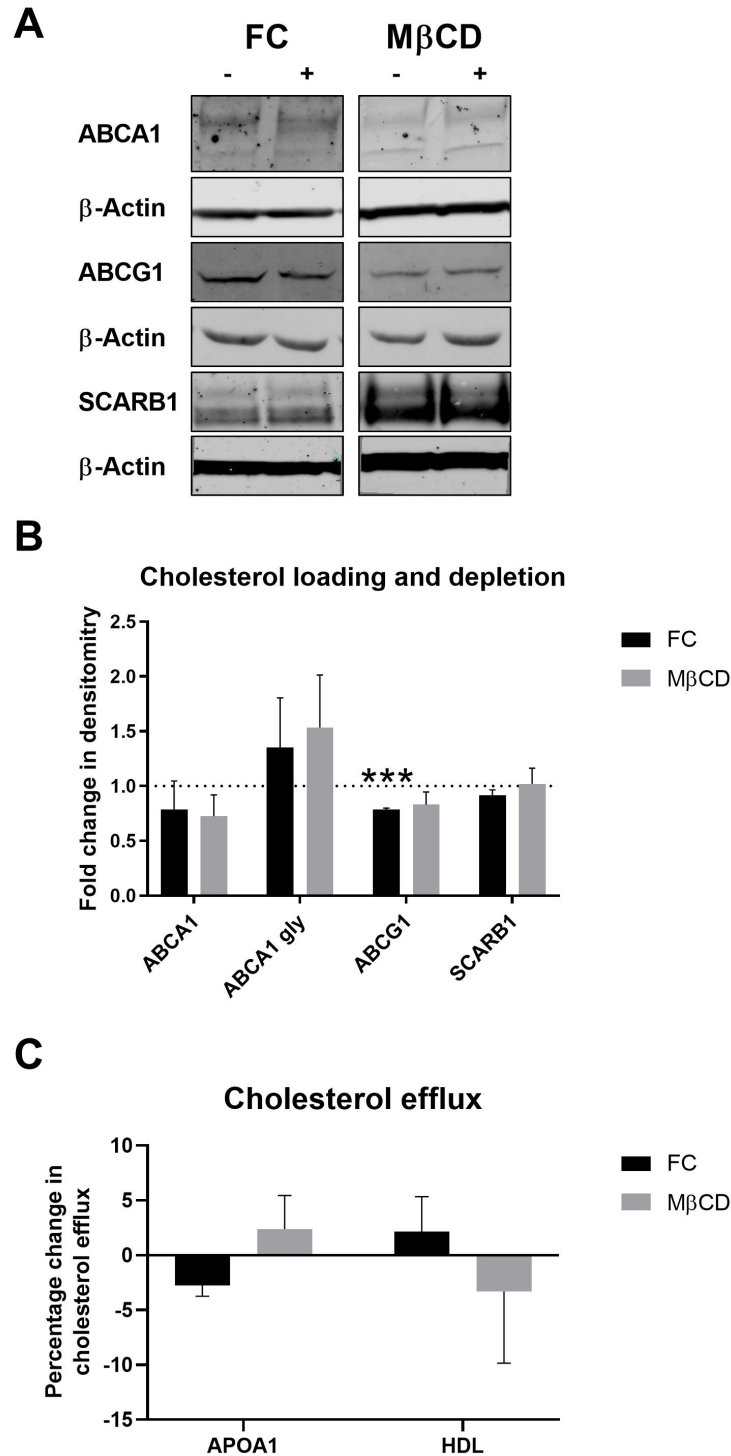
Figure 3.2 Western blot analysis and activity of cholesterol transporters in cholesterol loaded or depleted outer root sheath keratinocytes. Protein expression changes in ORS keratinocytes treated with 25 µM FC for 72-hours, or 1 mM MβCD for 1-hour + 23-hours recovery (A). Protein densitometry values relative to reference protein β-Actin. Cholesterol efflux changes in ORS keratinocytes treated with 25 µM FC for 72-hours or 1 mM MβCD for 1-hour with a recover period of 23-hours (B). Data are mean ± SEM for n=4 donors. One-sample t-test performed; significance denoted by *** P≤0.001.
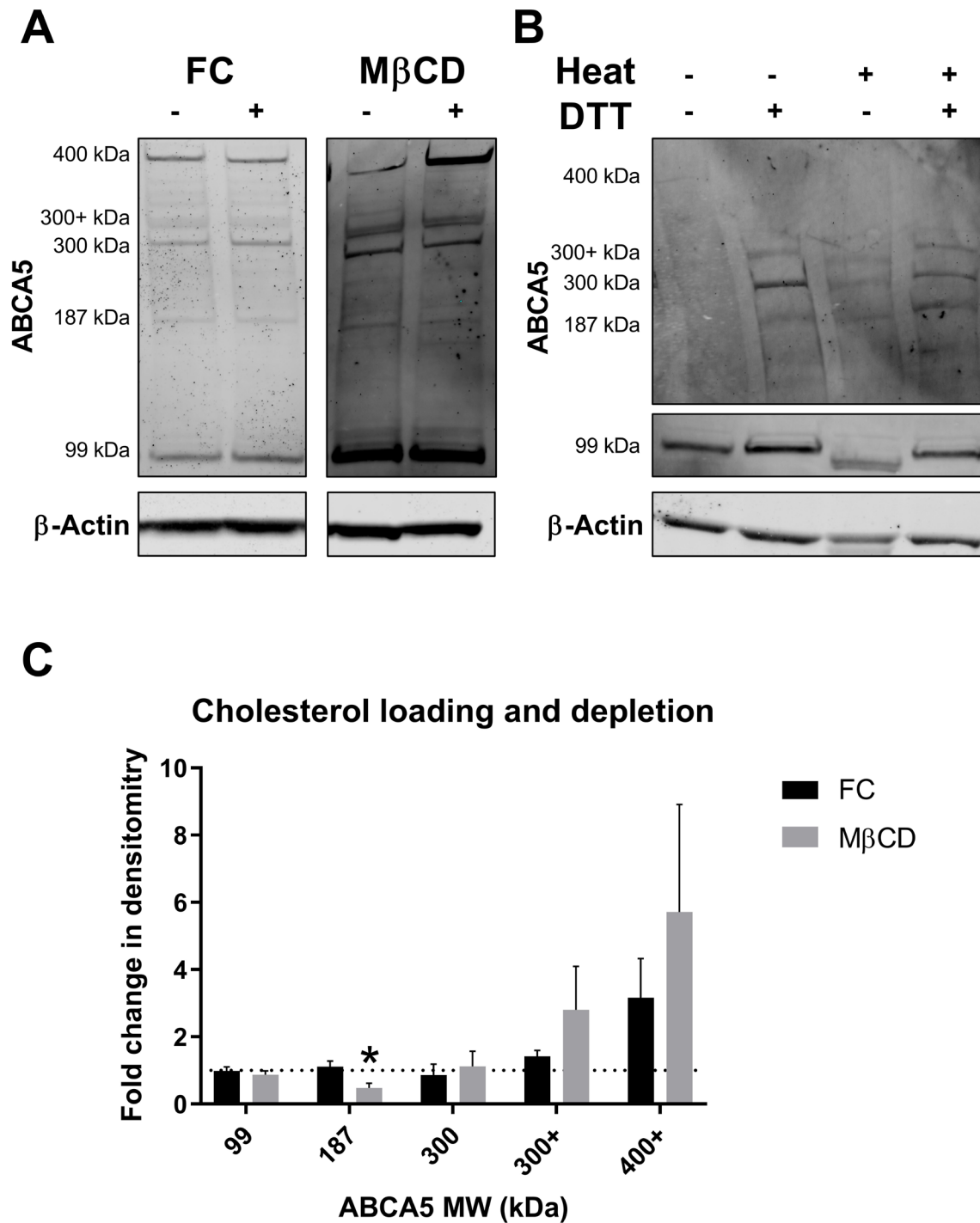
Figure 3.3 Western blot analysis of ABCA5 in cholesterol loaded or depleted cells. ABCA5 protein expression changes in ORS keratinocytes treated with 25 μM FC for 72-hours, or 1 mM MβCD for 1-hour + 23-hours recovery (A) or control samples either prepared with or without heating at 80°C and 500 μM DTT. Protein densitometry values relative to reference protein β-Actin. Data are mean ± SEM for n=4 donors. One-sample t-test performed; significance denoted by P *<0.05.

3.2.3   Effects of liver X receptor activation and inhibition of cholesterol transporters

The control of cholesterol homeostasis is tightly regulated by LXR, therefore ORS keratinocytes were treated with 5 µM T0901317 (an LXR agonist) for 24-hours. Significant increases in the expression of both *ABCA1* and *ABCG1* were seen, whereas *ABCA5* and *SCARB1* showed small, non-significant increases in mRNA levels, and no change was seen for *HMGCR* (Figure 3.4A). To confirm these gene expression changes at the protein level, ORS keratinocytes were treated with T0901317 for 72-hours. Western blotting revealed a 9-fold increase in ABCA1 total protein abundance (P=0.071), a 4-fold increase in ABCG1 (P=0.085) and no change for SCARB1 (Figure 3.4B). ABCA5 showed no changes in the 99, 187 and 300 kDa isoforms, however the 400 kDa tetramer showed a varied increase from 2.5-fold to 54.8-fold (n=4) following LXR agonism (Figure 3.4C).

Cholesterol efflux was measured following T0901317 treatment, with the addition of the non-specific ABC transport inhibitor PSC899 and specific SCARB1 inhibitor BLT-1 (Raldua and Babin, 2007). ABCA1-mediated cholesterol efflux to APOA1 significantly increased with 72-hour LXR activation and decreased with 5 µM PSC833 treatment (Figure 3.5A). Efflux to HDL was significantly inhibited by both PSC833 and BLT-1 (Figure 3.5B), suggesting that both ABCG1 and SCARB1 can function in cholesterol efflux to HDL in ORS keratinocytes. T0901317 treatment significantly increased efflux to HDL, though to a lesser extent than that to APOA1.

These results suggest that all three transport proteins examined ABCA1, ABCG1 and SCARB1, are involved in cholesterol efflux in ORS keratinocytes. As these proteins are known to be expressed both intracellularly and within the plasma membrane in a cell-type dependent manner (Tsuruoka *et al.*, 2002, Schroder *et al.*, 2007, Sticozzi *et al.*, 2012, Sticozzi *et al.*, 2010, Santamarina-Fojo *et al.*, 2001, Tarling and Edwards, 2011), immunolocalisation studies were next performed to assess their subcellular distribution in ORS keratinocytes.
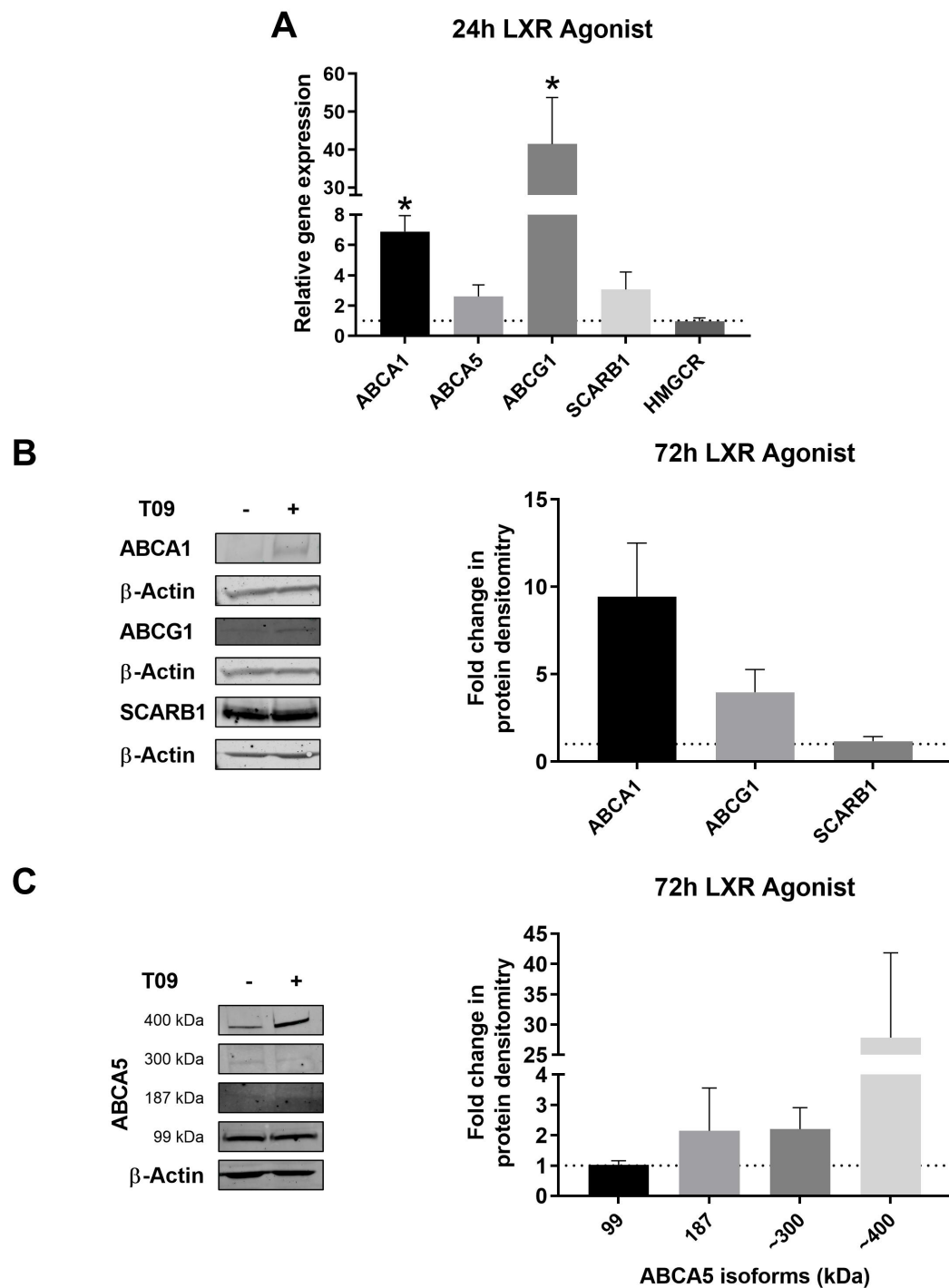
Figure 3.4 Liver X receptor activation of cholesterol transporters in outer root sheath keratinocytes. Gene expression changes in ORS keratinocytes treated with 5 µM T0901317 for 24-hours (A). Gene expression reported relative to vehicle control and normalised to *PPIA*. Protein expression changes ORS keratinocytes treated with 5 µM T0901317 for 72-hours (B, C). Protein densitometry values relative to reference protein β-Actin. Data are mean ± SEM for n=4 or 6 donors. One-sample t-test performed; significance denoted by * P≤0.05.
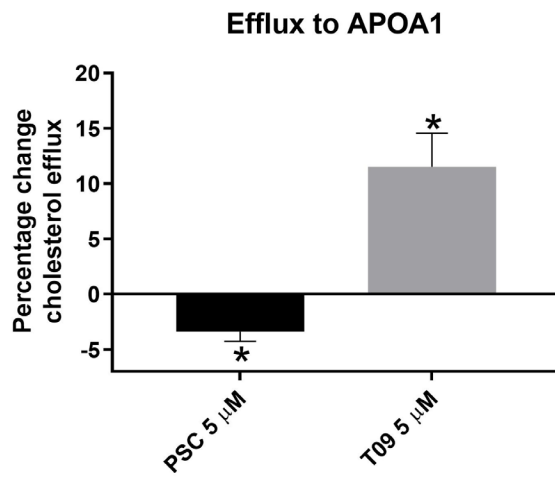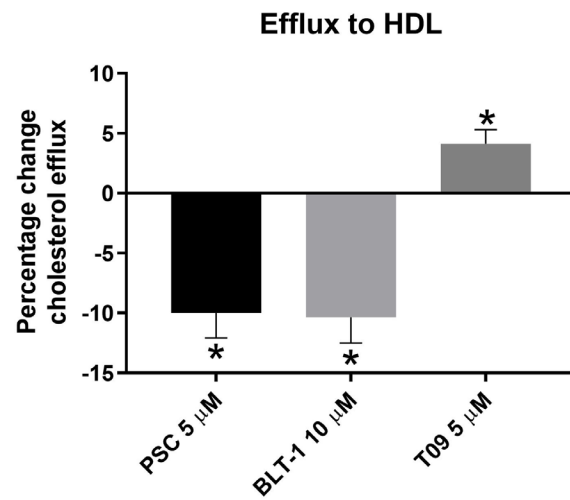
Figure 3.5 Cholesterol efflux in outer root sheath keratinocytes. Cholesterol efflux changes in ORS keratinocytes treated with 5 µM T0901317 for 72-hours, 5 µM PSC833 for 24-hours or 10 µM BLT-1 for 24-hours to APOA1 (A) or HDL (B). Data are mean ± SEM for n=4 or 6 donors. One-sample t-test performed; significance denoted by * P≤0.05.

3.2.4 Immunolocalisation of cholesterol transporters in outer root sheath keratinocytes

Figure 3.6 shows the intracellular distribution of ABCA1, with a similar pattern observed for ABCG1. To more accurately determine the sub-cellular localisation of ABCG1, dual immunocytochemistry was performed with endo-lysosomal marker LAMP1 (lysosomal associated membrane protein 1) and ER marker PDI (Protein disulfide isomerases). Cells were loaded with 25 µM FC prior to staining to determine whether this altered transporter expression or localisation.

There was little to no localisation of ABCG1 to endo-lysosomes, however clear co-localisation to ER was seen (Figure 3.7); FC loading did not alter the cellular localisation of ABCG1. Previous reports have described conflicting data as to the impact of LXR agonism, describing increases in plasma membrane localisation (Wang *et al.*, 2006) or no impact (Xie *et al.*, 2006). In this study, treatment with T0901317 did not change co-localisation to the ER.
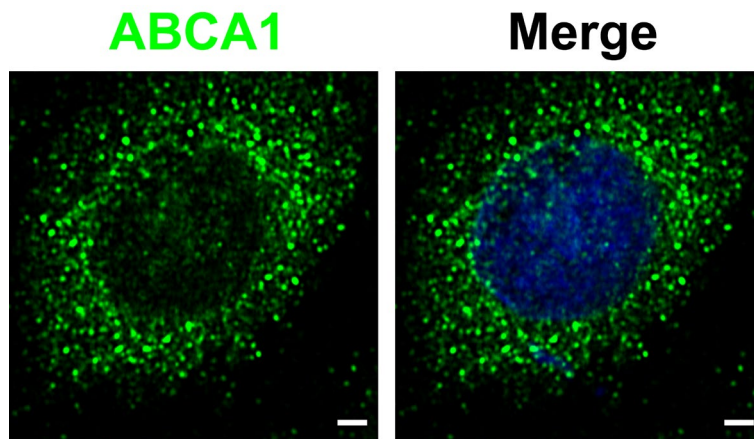
Figure 3.6 Immunocytochemistry staining of ABCA1 in outer root sheath keratinocytes. ABCA1 immunolocalisation (Green) in ORS keratinocytes, counterstained with DAPI (blue). Scale bars 2 µm.
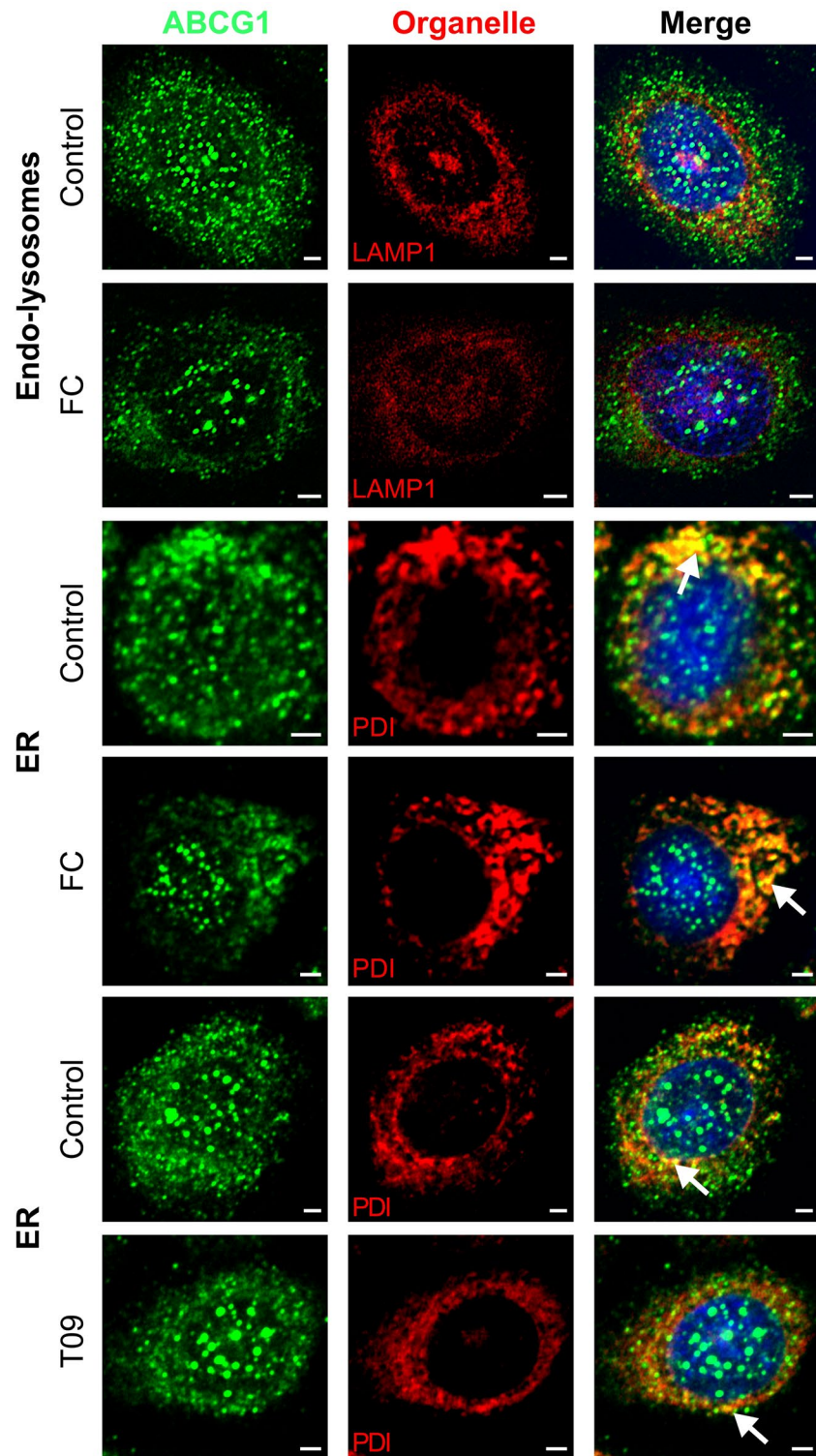
Figure 3.7 Immunocytochemistry detection of ABCG1 in outer root sheath keratinocytes co-localises to endoplasmic reticulum. Dual immunocytochemistry staining of ABCG1 (green) with endo-lysosomal marker LAMP1 (red) and ER marker PDI (red) in ORS keratinocytes treated with 25 μM FC or 5 μM T0901317 for 72-hours. Counterstained with DAPI (blue), white arrows represent co-localisation of ABCG1 to ER. Scale bars 2 μm.

SCARB1 staining demonstrated substantial co-localisation with LAMP1 in the endo-lysosomal compartment, as demonstrated by the white arrows (Figure 3.8).
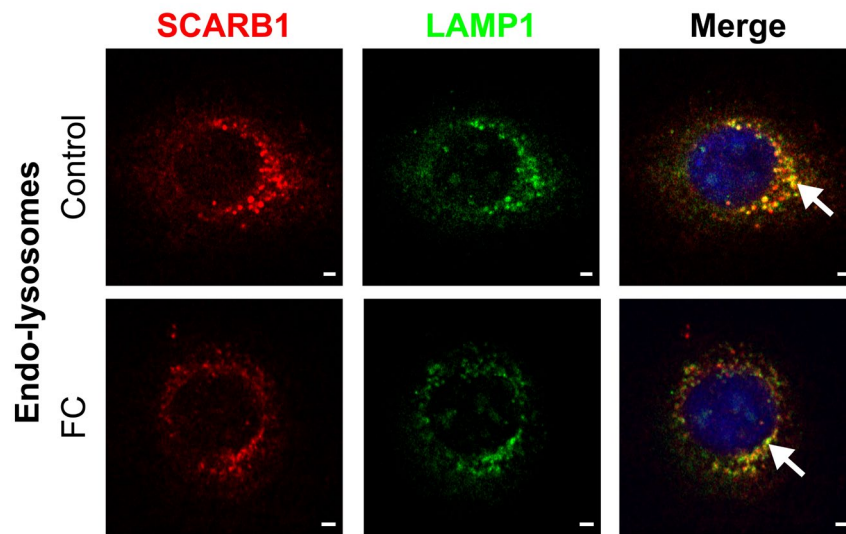
Figure 3.8 Immunocytochemistry detection of SCARB1 in outer root sheath keratinocytes co-localises to endo-lysosomes. Dual immunocytochemistry staining of SCARB1 (red) with endo-lysosomal marker LAMP1 (green) in ORS keratinocytes treated 25 µM FC for 72-hours. Counterstained with DAPI (blue), white arrows represent co-localisation of SCARB1 to endo-lysosomes, scale bars represent 2 µm.

Similarly, the intracellular localisation of ABCA5 was examined by dual immunostaining with organelle markers: LAMP1, PDI and ATPB (ATP synthase subunit beta, mitochondrial marker). Figure 3.9 demonstrates co-localisation to endo-lysosomes was apparent under control conditions. Moreover, 72-hours FC loading increased the intensity of all three organelle markers. Image analysis was performed through generating a threshold mask of these intracellular organelle markers and intensity of ABCA5 staining was measured within the masked area (Figure 3.10). This analysis resulted in a 1.99-fold increase detected for endo-lysosomal ABCA5, with 2.65-fold increase in ER ABCA5 (P=0.044), and a 3.31-fold increase for mitochondrial ABCA5 following FC loading. Total ABCA5 pixel intensity resulted in a 2.76-fold increase (P=0.008 Wilcoxon rank test) with FC loading.
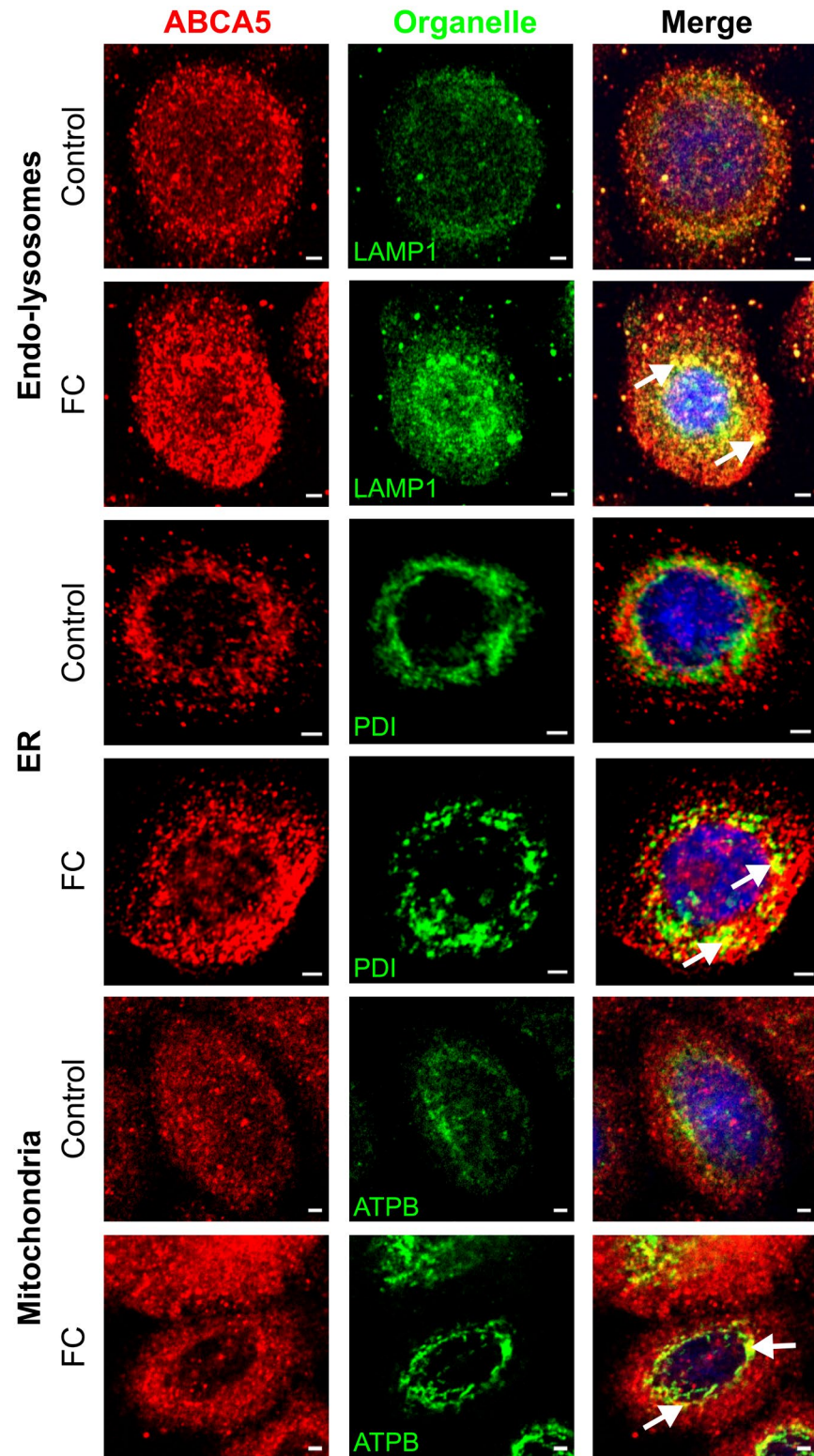
Figure 3.9 Immunocytochemistry detection of ABCA5 in outer root sheath keratinocytes co-localises to intracellular organelles with free cholesterol treatment. Dual immunocytochemistry staining of ABCA5 (red) with endo-lysosomal marker LAMP1 (green), ER marker PDI (green) and mitochondrial marker ATPB (green) in ORS keratinocytes treated with 25 µM FC for 72-hours. Counterstained with DAPI (blue), white arrows represent co-localisation of ABCA5 when treated with FC to endo-lysosomes, ER and mitochondria. Scale bars represent 2 µm.

ABCA5 co-localisation with 72h FC
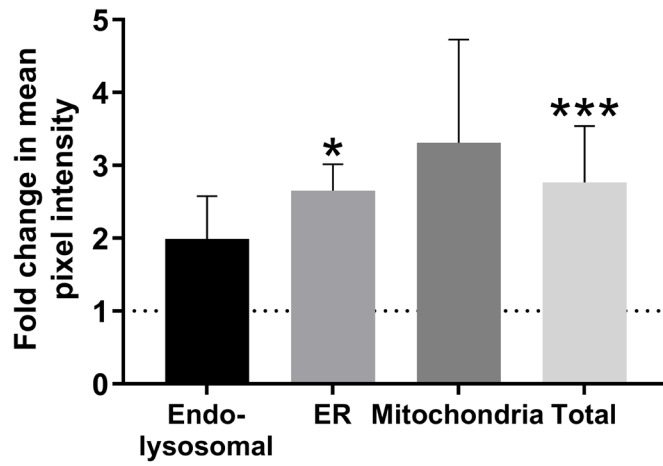
Figure 3.10 Quantification of ABCA5 immunocytochemistry. Image analysis for fold change in mean pixel intensity of ABCA5 masked to organelle marker or total pixel intensity. Data are mean ± SEM for n=3 or 9 (total). One-sample t-test performed; significance denoted by * P≤0.05, *** P≤0.001.

3.3 Discussion

The homeostatic balance of cholesterol is essential for maintaining normal cellular function and both sustained excess cholesterol levels (Yao and Tabas, 2000, Tabas, 2002) and cholesterol depletion can lead to apoptosis (Bang *et al.*, 2005, Park *et al.*, 2009). Cholesterol has been suspected of influencing HF growth and cycling, yet this has not been systematically explored. Here, primary ORS keratinocytes were utilised as a relevant model cell type to characterise the expression and regulation of cholesterol transporters in the HF epithelium.

In examining transcriptional changes following exogenous cholesterol addition or removal, *ABCG1* was observed to be consistently dynamically regulated. These results correlate with previous studies in human foreskin keratinocytes, where *ABCG1* was found to be upregulated following 22-hydroxycholesterol treatment and downregulated with statin treatment (Jiang *et al.*, 2010). Cholesterol efflux from ABCG1 to HDL is well documented (Zanotti *et al.*, 2008) and the reported increase of cholesterol efflux to HDL with both FC loading and LXR activation correlate to this function in the HF. *ABCA1* expression increased by a numerically smaller magnitude of increase in response to cholesterol loading compared with *ABCG1*, however donor variability in response meant that differences were not significant. ABCA1 expression has also been demonstrated in foreskin keratinocytes (Jiang *et al.*, 2006) along with HaCaT cells (Sticozzi *et al.*, 2010) and is upregulated following addition of 22R-hydroxycholesterol and 25-hydroxycholesterol (Jiang *et al.*, 2006).

Following 72-hours LXR agonism, significant increases in both *ABCA1* and *ABCG1* gene expression were observed. Whereas FC loading would be expected to increase levels of oxysterols and therefore indirectly activate LXR (Björkhem, 2002, Fu *et al.*, 2001), these data suggest that direct targeting of the LXR pathway with a synthetic agonist results in a more robust transcriptional response. Likewise, protein expression of ABCA1 and ABCG1 is upregulated, which was not observed following FC loading alone. These data confirm the activity of the LXR pathway in ORS keratinocytes, which has previously been shown to upregulate these transporters in numerous cell and tissue types including primary keratinocytes (Jiang *et al.*, 2010, Jiang *et al.*, 2006, Fu *et al.*, 2001, Zanotti *et al.*, 2008).

Protein localisation of ABCA1 was detected with a distribution peripheral to the nucleus; however, as co-localisation studies were not explored, it is not possible to say to which compartments ABCA1 is distributed within ORS keratinocytes. ABCA1 is known for both intracellular transport and cholesterol efflux (Quazi and Molday, 2011, Tarling *et al.*, 2013, Santamarina-Fojo *et al.*,

2001), with additional work needed to explore its specific localisation and cholesterol transport function within ORS keratinocytes.

ABCG1 was co-localised with the ER marker PDI. ABCG1 has been highlighted to be involved with endosomal intracellular transport, and the hypothesis of Tarling and Edwards (2011) suggests trafficking away from the ER. Indeed precipitation of ABCG1 and PDI did not occur (Tarling and Edwards, 2011), however co-localisation to the ER has been reported with Brefeldin A treatment (an antiviral which inhibits protein transport form ER-Golgi) (Neufeld *et al.*, 2001). The ER functions in both the packaging and degradation of ABC transporters (Nikles and Tampe, 2007), so this localisation of ABCG1 may be indicative of dimerisation occurring. Pandzic *et al.* (2017) demonstrated ABCG1 localisation to actin filaments, and indeed cholesterol:MβCD complex has been shown to significantly increase ABCG1 presence in the plasma membrane. Previous studies have detected heterodimerisation of ABCG1 to ABCG4 (Hegyi and Homolya, 2016) and speculated that dimerization would occur within the ER prior to trafficking to the plasma membrane. Furthermore, previous reports detected LXR agonism enhancing plasma membrane localisation of ABCG1 (Wang *et al.*, 2006), whereas this study did not detect changes in cellular distribution following 72-hours treatment with T0901317, in correlation with results reported by Xie *et al.* (2006). It remains unknown if ABCG1 is facilitating ER cholesterol transport, or indeed co-localisation indicates quaternary processing and dimerization. Further work investigating loss of ABCG1 function and ER cholesterol could aid in determining this.

Regulation of *SCARB1* gene expression appears to be consistent in the function of cholesterol efflux, with significant increases in gene expression with cholesterol loading (at 72-hours) and significant reduction with cholesterol depletion. This bi-directional transporter has been shown to efflux CE to HDL (Luo *et al.*, 2010), and in previous studies regulation *via* 25-hydroxycholesterol loading and statin-mediated cholesterol depletion in human foreskin keratinocytes is consistent with the data reported in this chapter (Tsuruoka *et al.*, 2002). However, the authors speculate that SCARB1 can also have a role in CE uptake from HDL in the basal epidermis due to the increase in mRNA following barrier disruption (Tsuruoka *et al.*, 2002). LXR agonism did not alter gene or protein expression of SCARB1; previous studies have shown both increases and decreases with LXR agonism (Komaromy *et al.*, 1996, Rigotti *et al.*, 1996, Shen *et al.*, 2018b). Here, SCARB1 did not localise to the plasma membrane, matching other data produced in keratinocytes (Crivellari *et al.*, 2017). Cholesterol loading in ORS keratinocytes did not alter the distribution of SCARB1 and, as protein densitometry studies did not change either, it appears that the chosen time course or concentration may have been insufficient to induce an LXR response. This

confirms previous keratinocyte data with expression at the nuclear periphery (Sticozzi *et al.*, 2012) and endo-lysosomal localisation (Schroder *et al.*, 2007).

To determine changes in the activity of these transporters in response to cholesterol levels, a BODIPY-cholesterol efflux assay was utilised. APOA1 was used as the acceptor for measuring ABCA1-mediated efflux, whereas HDL provided a relevant acceptor to determine ABCG1/SCARB1-mediated efflux. The use of a specific SCARB1 inhibitor, BLT-1 (Raldua and Babin, 2007), aided in determining if this transporter functions primarily in an efflux or uptake capacity in this cell type. Individually, the inhibition of ABC transporters and SCARB1 reduced cholesterol efflux to both APOA1 and HDL, with LXR activation increasing efflux to the acceptors. This contrasts with the cholesterol loading and depletion experiments, which showed little impact on cholesterol efflux. An explanation for this can be found in the expression data which, as described, shows that direct LXR agonism has a more robust and consistent impact on ABCA1 and ABCG1 expression levels in comparison to the cholesterol loading and depletion experiments.

The data showed very little alterations in protein expression following FC and MβCD treatments. It may be that the conditions used in loading or depleting cholesterol were not optimal to produce significant changes in cholesterol transporter expression. What is more, a reduction in cholesterol synthesis, suggested by the reduced HMGCR expression at 72-hours could have counteracted the impact of excess cholesterol, thereby reducing the dynamic regulation of the transporters. Indeed, previous studies have demonstrated that cholesterol synthesis can be dynamically regulated in both keratinocytes (Siefken *et al.*, 2000, Harris *et al.*, 2000) and the HF (Karnik *et al.*, 2009), the latter occurring specifically in patients with LPP, a form of cicatricial alopecia.

The results presented in this chapter are consistent with previous studies by Seeree *et al.* (2019), where no significant changes in expression were detected with 10 μM FC loading, however a slight drop in APOA1 efflux and increase in HDL efflux were observed. Also, the authors reported that efflux to HDL was of a greater magnitude than APOA1, which is commonly reported within other cell types (Daffu *et al.*, 2015, Gu *et al.*, 2016, Wang *et al.*, 2014a, Seeree *et al.*, 2019).

As previous studies in keratinocytes have used oxysterols to initiate alterations in ABC transporter responses, concentrations for cholesterol loading were obtained from different cell types. Ranges upwards from 10 μg/ml have been shown to increase protein expression (Spann *et al.*, 2012). However, in some cell types the concentrations have needed to be higher (Choi *et al.*, 2003, Hsieh *et al.*, 2014, Seeree *et al.*, 2019). Previous studies in HaCaT cells have included concentrations

of 1-2% MβCD to disrupt lipid rafts and induce apoptosis. This study explored 1 mM MβCD concentration to investigate alterations to cholesterol transporters, which is equivalent to a concentration of 0.13%. Using a higher concentration to deplete cholesterol resulted in an inability to obtain sufficient RNA or protein content to analyse. Studies using 1 mM MβCD have shown reductions in ABCA1 and ABCG1 (mRNA and protein) but not SCARB1 in smooth muscle cells (Coisne *et al.*, 2016). Although Coisne *et al.* (2016) detected no change in percentage of cholesterol efflux for smooth muscle cells, aortic bovine endothelial cells showed a significant reduction. This suggests that modulation of cholesterol efflux in response to loading or depletion can vary substantially between cell types and experimental conditions.

As the data in this chapter detected significant reductions in mRNA with MβCD it could be postulated that a 24-hour time period was not sufficient enough to detect changes in protein abundance or cholesterol efflux. Indeed, ABC transporters are large transmembrane proteins which undergo post-translational modifications in which homodimerisation (e.g. ABCG1) (Nakamura *et al.*, 2004) and glycosylation occur (Czuba *et al.*, 2018). In addition, processing and degradation has been shown to take time and be integral to function, where the half-life of ABC transporters (ABCB1 and ABCB4) are reported as 5 days in hepatocytes (Kipp *et al.*, 2001). SCARB1 largely exists as monomers, however oligomerisation has been detected (Landschulz *et al.*, 1996). ABCA1 functionally exists as homodimers (Denis *et al.*, 2004a, Trompier *et al.*, 2006) and higher order oligomers are processed through ATP binding (Trompier *et al.*, 2006). Both the packaging of dimers and degradation of ABC transporters occurs within the ER (Nikles and Tampe, 2007). Furthermore, phosphorylation *via* cAMP or protein kinases of ABC transporters has been shown to be important to efflux functionality and protein stability (Haidar *et al.*, 2002, Watanabe *et al.*, 2019). Palmitoylation is essential for ABCA1 membrane localisation and therefore efflux capacity (Singaraja *et al.*, 2009). Additionally, ABCA5 is reported to be acetylated at three lysine residues (K614, K620 and K1438) (Czuba *et al.*, 2018, Lundby *et al.*, 2012). Further repeats should investigate additional FC and MβCD concentrations and time points for cholesterol loading and depletion, along with investigations into the post-translational modification status, and modulation *via* additional treatments such as cAMP.

Immunolocalisation studies reported in this chapter show no plasma membrane localisation for any of the transporters investigated. In contrast, cholesterol efflux assays showed the functional capacity for transporter-mediated efflux. It may be that cell-cell contact is needed to encourage plasma membrane localisation, and in fact an increase in ABCG1 expression was reported with keratinocyte differentiation both *in vitro* and in the murine epidermis. Yet, in contrast, neither gene

(Kielar *et al.*, 2003) nor protein expression of ABCA1 changes with keratinocyte differentiation (Jiang *et al.*, 2006). Addition of Ca^{2+} to culture media would allow a longer culture developing method, however this would induce differentiation in an epidermal phenotypic manner. ORS cells have been noted to migrate into the epidermis during wound healing (Zhou *et al.*, 2018), and HF derived differentiation mechanisms are poorly understood *in vitro.* Further investigations with the use of serum, lipoproteins or differentiation should be investigated to see if plasma membrane localisation can be detected.

Little is known of the role of ABCA5 in keratinocytes or other cell types. Research by Ye *et al.* (2010) showed an upregulation of *ABCA5* following addition of oxidised LDL but not β-vLDL in bone marrow derived-macrophages *in vitro* from $Ldl^{-/-}$ mice. Furthermore, cholesterol efflux to HDL, but not APOA1 was reduced in macrophages derived from $Abca5^{-/-}$ mice (Ye *et al.*, 2010). Keratinocytes derived from congenital hypertrichosis patients with *ABCA5* mutations show reduced ABCA5 protein expression and endo-lysosomal cholesterol accumulation (DeStefano *et al.*, 2014). Results in this chapter show no change in ABCA5 expression following FC loading or LXR activation, though a significant drop in mRNA levels was seen after cholesterol depletion.

There are three known isoforms of ABCA5, one encoding a full transporter of 187 kDa, and two half transporters of 99 and 105 kDa. Bioinformatics analysis of the antibody epitope used here is only predicted to detect both the 187 and 99 kDa isoforms. The detection of additional bands of a higher molecular weight than anticipated for ABCA5 could suggest that the half transporter can oligomerise to form trimers and tetramers. Although no previous studies on ABCA5 have reported this, members of ABCD family (peroxisome) (Geillon *et al.*, 2017), ABCG2 (Xu *et al.*, 2004) and ABCA1 (Denis *et al.*, 2004a) have been shown to form oligomers. The presence of the half transporter subunit alone was hypothesised by Petry *et al.* (2003) to either form a functioning transporter as a homo or heterodimer, or be involved in regulatory functions. In correlation with previous studies (Fu *et al.*, 2015) these data shows that neither gene nor protein expression of ABCA5 is regulated by LXR agonism. However, loss of both the 300 and 400 kDa isoforms with protein denaturation techniques indicate in a role of LXR agonism in post-translational modification with the detection of an increase in the predicted tetramer band.

By investigating ABCA5 immunofluorescence, prominent intracellular localisation was observed. Previous studies have shown co-localisation of Abca5 to endo-lysosomes, amongst other intracellular organelles, in mice (Kubo *et al.*, 2005). Noticeably, only a low level of co-localisation of ABCA5 to intracellular organelles was detected under control conditions, with the addition of

FC inducing co-localisation to endo-lysosomes, ER and mitochondria. This may indicate that ABCA5 is important in the intracellular trafficking and packaging of cholesterol in ORS keratinocytes, rather than in cholesterol efflux. It is likely to function alongside other intracellular sterol binding proteins, such as STARD4 (Elbadawy *et al.*, 2011) amongst other StAR related proteins, and NPC1 and NPC2 (Soccio and Breslow, 2004), which have similar roles in regulating cholesterol movement.

Chapter 3 has demonstrated the presence of four cholesterol transporters, ABCA1, ABCA5, ABCG1 and SCARB1, within ORS keratinocytes. Functional efflux assays show efflux to APOA1 and HDL acceptors, and that LXR-mediated regulation of these processes can occur. Immunofluorescence co-localisation studies have shown the presence of ABCG1 in the ER, and SCARB1 amongst endo-lysosomes. Furthermore, the first evidence of oligomeric ABCA5 is presented, along with dynamic changes in localisation in response to cholesterol loading. Next the impact of cholesterol levels on HF growth, cycling and keratinocyte behaviour will be examined.

Chapter 4: Determining the mechanisms by which altered cholesterol levels impact keratinocyte behaviour, and hair follicle organ culture

4.1 Introduction

Chapter 3 demonstrated HF keratinocytes ability to modulate cholesterol homeostasis through regulation of cholesterol transport proteins. Previous studies have shown that modulating cholesterol levels can alter the differentiation and proliferation status in epidermal keratinocytes (Jans *et al.*, 2004, Mathay *et al.*, 2011, Spörl *et al.*, 2010). In addition, cholesterol modification of signalling proteins associated with hair cycling is reported to be integral to these signalling cascades (Reis *et al.*, 2016, Sheng *et al.*, 2014).

This chapter focuses on how exogenous cholesterol loading and depletion impacts the behaviour of primary ORS keratinocytes, specifically investigating cholesterol distribution, cellular proliferation, apoptosis, and senescence. These experiments were repeated using human HF organ culture, where anagen VI to catagen like transition, pigmentation, proliferation, and apoptosis were examined. Preliminary analysis on the impact of cholesterol loading on Wnt signalling was also performed.

This chapter aims to determine if altering cholesterol levels impacts on keratinocyte and HF behaviour. The following elements were examined:

1. Does cholesterol loading or depletion alter subcellular cholesterol distribution?
2. Does cholesterol loading or depletion alter the intrinsic behaviour of ORS keratinocytes?
3. Does cholesterol loading or depletion effect HF growth?

4.2 Results

4.2.1 Excess cholesterol accumulates in endo-lysosomes and cholesterol depletion alters lipid rafts

First the distribution of FC was measured using filipin staining. The antibiotic filipin iii is a naturally fluorescent probe, which binds to the 3-β-hydroxy group of sterols, making it selective in detecting FC and not CE (Maxfield and Wüstner, 2012). ORS keratinocytes were treated with 25 µM FC for 24-hours (Figure 4.1A) and co-localisation with the endo-lysosomal marker LAMP1 was investigated. FC loading increased filipin staining intensity, resulting in a 68.1 ± 14.8 increase in mean pixel intensity (a.u.) per cell (P=0.010). Endo-lysosomal cholesterol was quantified through examining the co-localisation *via* measuring mean pixel intensity masked to endo-lysosomes (Figure 4.1B); a 20.9 ± 4 increase in mean pixel intensity (a.u.) was detected within endo-lysosomes (P=0.006).

In addition, Pearson's co-efficient was utilised to measure the correlation of pixels detected for endo-lysosomes and cholesterol, where as Mander's co-efficient was used to measure the co-occurrence of the endo-lysosomes and cholesterol relative to pixel intensity (Aaron *et al.*, 2018, Mascalchi and Cordelières, 2019). Mander's 1 (M1) co-efficient detects the overlap of channel 1 (LAMP1) with channel 2 (filipin), and Mander's 2 (M2) detects signal co-occurrence of channel 2 in channel 1. Pearson's co-efficient (Figure 4.1C) revealed no significant changes in correlation, whereas M1 showed a significant decrease (P=0.007) in proportional co-occurrence of LAMP1 to filipin, and M2 showed a significant increase (P=0.036) in filipin in LAMP1 co-occurrence to FC loading.
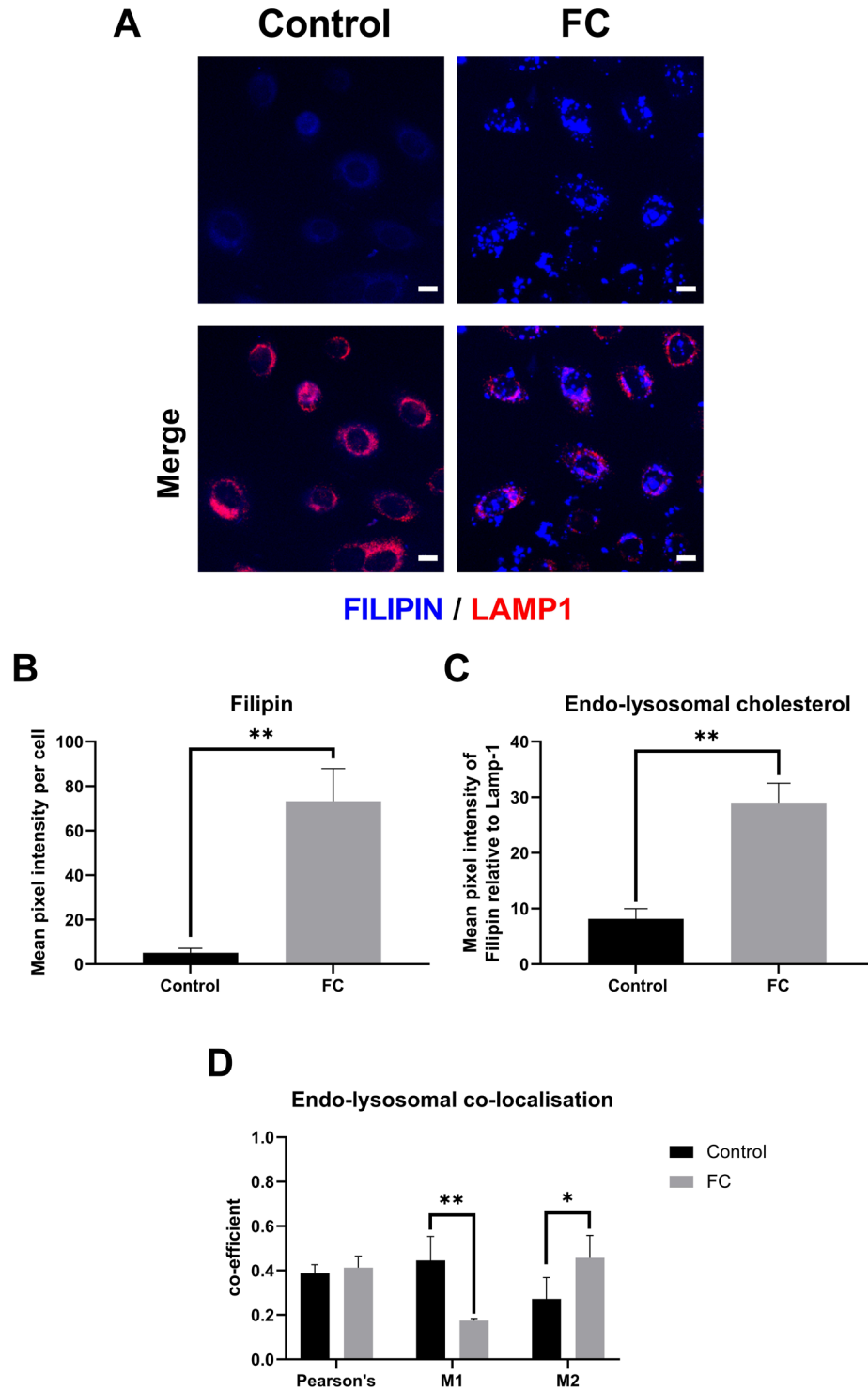
Figure 4.1 Filipin staining in outer root sheath keratinocytes detects endo-lysosomal accumulation with cholesterol loading. Filipin staining (blue) in ORS keratinocytes treated with 25 µM FC for 24-hours (A). Dual immunocytochemistry staining with endo-lysosomal maker LAMP1 (red). Scale bars represent 10 µm. Image analysis for mean pixel intensity (a.u.) per cell (B) or masked to organelle marker (C). Pearson's and Mander's (M1 & M2) co-localisation co-efficient (D). Data are mean ± SEM for n=3. Unpaired t-test or two-way ANOVA performed; significance denoted by * P≤0.05 ** P≤0.01.

To investigate the effects of reduced cellular cholesterol, ORS keratinocytes were treated with 1 mM MβCD for 1-hour, and filipin staining was performed following a 23-hour recovery period (Figure 4.2A). Figure 4.2B shows a mean, non-significant reduction of -7.7 ± 10.7 in mean pixel intensity (a.u.) of filipin per cell.
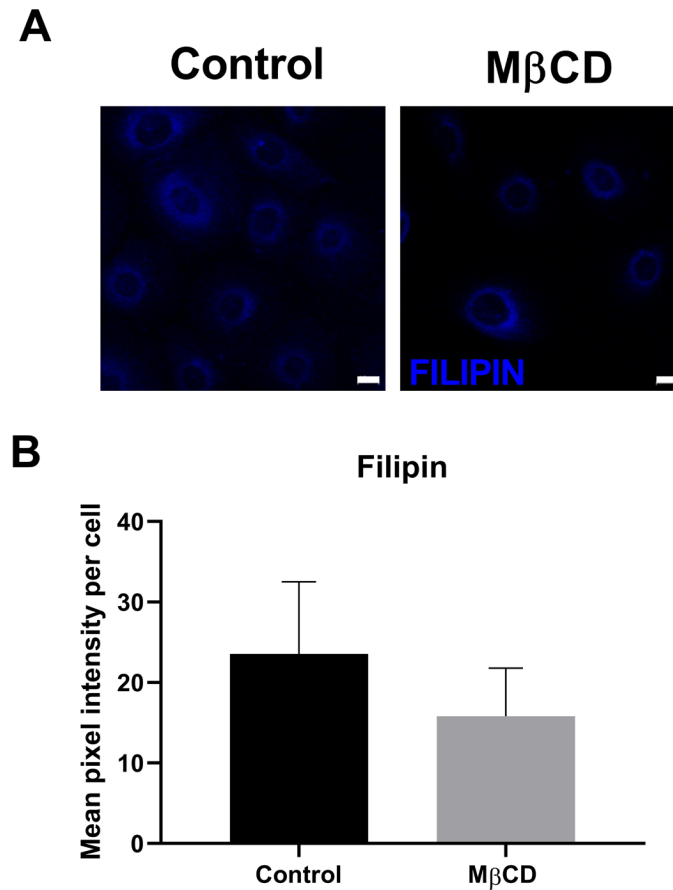
Figure 4.2 Filipin staining in outer root sheath keratinocytes with cholesterol depletion. Filipin staining (blue) in ORS keratinocytes treated with 1 mM MβCD for 1-hour + 23-hours recovery (A). Scale bars represent 10 μm. Image analysis for mean pixel intensity (a.u.) per cell (B). Data are mean ± SEM for n=3

To detect changes in membrane cholesterol, cholera toxin conjugated to the fluorescent FITC tag (CTX-FITC) was employed, allowing a measurement of ganglioside receptor-rich (and cholesterol-rich) lipid rafts (Figure 4.3). FC loading showed no change in CTX-FITC-labelled lipid rafts at either 24 or 72-hour treatments. However, a small non-significant increase (1.3-fold) was detected following 1-hour MβCD treatment.
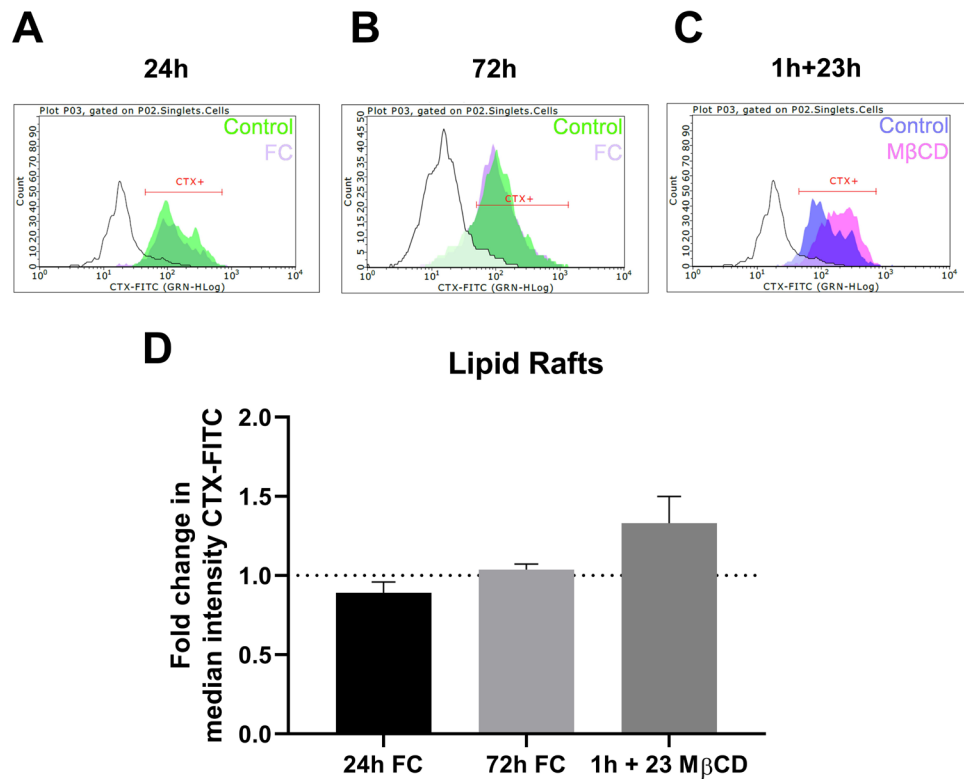
Figure 4.3 Cholesterol depletion disrupts lipid rafts. CTX-FITC flow cytometry plots in ORS keratinocytes treated with 25 µM FC (lilac) for 24-hours (A) or 72-hours (B), or 1 mM MβCD (pink) for 1-hour + 23-hours recovery (C) detected by flow cytometry. Negative control (clear), vehicle control for FC (green) control (blue). (D) Analysis is fold change of median values in comparison to control, data are mean ± SEM for n=3.

4.2.2 Cholesterol depletion reduces cell density but does not alter cellular proliferation

Next, to determine changes in cell viability, MTT assays were performed in ORS keratinocytes treated with 25 µM FC or 5 µM T0901317 for 72-hours, and MβCD for 1-hour with a 23-hour recovery. No changes in viability were detected following FC or T0901317 treatment, however a significant reduction was detected following cholesterol depletion by MβCD. (Figure 4.4A).

To examine whether changes in proliferation result from these treatments, EdU incorporation was employed for 3-hours prior to the end of treatment times. FC loading did not alter cell numbers or the percentage of proliferative cells (Figure 4.4C). MβCD revealed a small, non-significant increase in the percentage of proliferative cells (Figure 4.4D), however a significant reduction (P=0.046) in the total cell number was seen (Figure 4.4E). This corresponds with the MTT results suggesting reduced viability following cholesterol depletion.
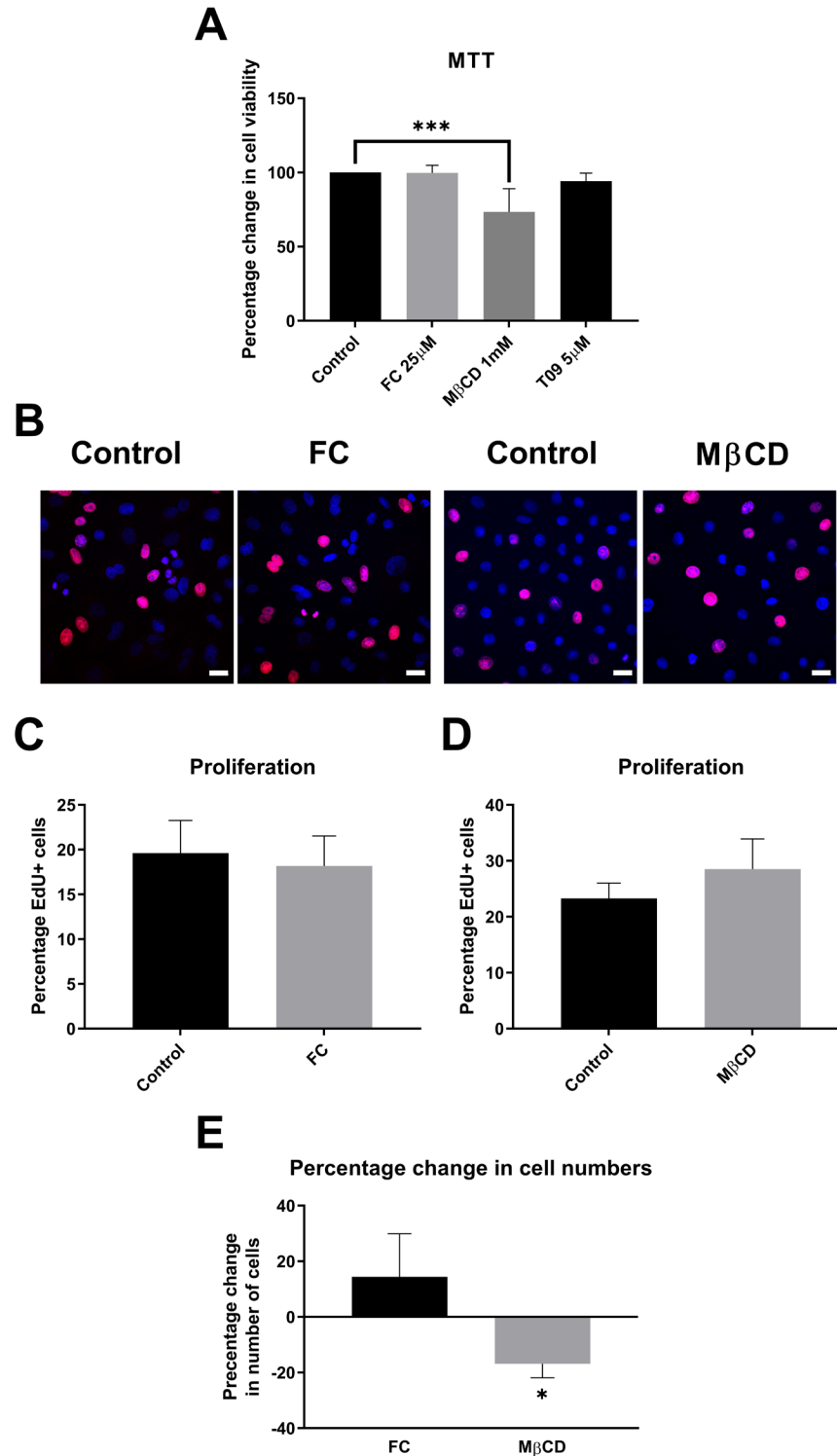
Figure 4.4 Effects of cholesterol loading and depletion on proliferation. (A) Percentage change in cellular viability represented by MTT assay in ORS keratinocytes cells loaded with 25 µM FC for 72-hour or 1 mM MβCD for 1-hour + 23-hour recovery. (B) EdU (red) incorporation 4-hours to the end following 72-hour FC loading or 1 mM MβCD treatment for 1-hour + 23-hour recovery. Scale bars represent 10 µm, DAPI (blue). Percentage of EdU+ cells (C+D), percentage change in total number of cells compared to control (E). Data are mean ± SEM for n=3/4. One-sample t-test performed; significance denoted by * P≤0.05 *** P≤0.001.

4.2.3   Cholesterol depletion induces apoptosis of senescent cells

In order to detect changes in cellular senescence, β-gal activity was detected using chromogenic X-gal staining (Dimri *et al.*, 1995, Debacq-Chainiaux *et al.*, 2009). Addition of 25 µM FC for 72-hours did not alter senescence levels with a fold change of 0.92 (Figure 4.5A). Following a 23-hour recovery period, 1-hour MβCD treatment resulted in a significant reduction in β-gal staining, with a fold change of 0.39 (P=0.047) at passage 2-3 (Figure 4.5B). ORS keratinocytes undergoing two more round of subculture (passage 5) displayed a smaller reduction in β-gal staining (0.75-fold change; P=0.031). Given that senescence in primary cells increases with each round of subculture, it may be that a greater proportion of senescent cells were present in the untreated passage-5 cells, lowering the capacity to measure changes following cholesterol depletion (Figure 4.5C).
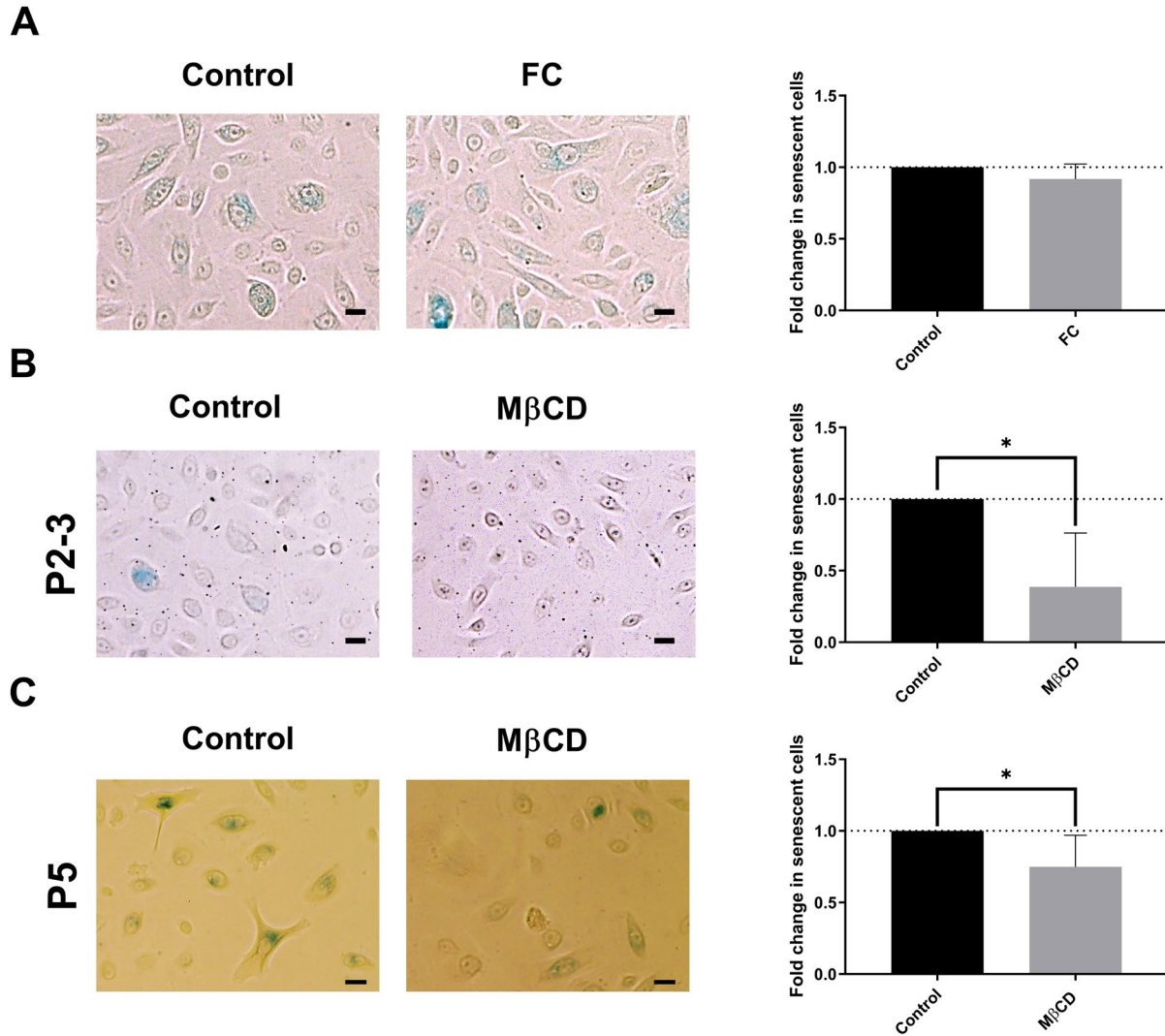
Figure 4.5 Effects of cholesterol loading and depletion on senescence. β-gal staining (blue) in ORS keratinocytes treated with 25 µM FC for 72-hours (A) or 1 mM MβCD for 1-hour + 23-hours recovery at passage 2-3 (P2-3) (B) or passage 5 (P5) (C). Scale bars represent 10 µm. Percentage of β-gal+ cells. Data are mean ± SEM for n=3. One-sample t-test performed; significance denoted by * P≤0.05

A reduction in senescence following cholesterol depletion might suggest that cellular proliferation would be higher, however EdU experiments (Figure 4B) showed that this was not the case. To investigate this finding further, caspase 3/7 assays were employed to determine whether changes in apoptosis were apparent. Figure 4.6A shows a small, non-significant increase in caspase 3/7 activity with both 1-hour MβCD treatment and prolonged exposure to MβCD over a period of 24-hours. Next, to determine if apoptosis was higher in senescent ORS keratinocytes, experiments were repeated at passage 5. Figure 4.6B shows an increase in apoptosis in 24-hour MβCD-treated cells, whereas cells treated for 1-hour with MβCD prior to the assay reagent being added showed a reduction in apoptosis, albeit the preliminary data (n=2) shows substantial inter-assay variability.

To further investigate apoptosis, annexin and propidium iodide uptake were measured using flow cytometry. A very low percentage of cells were detected in the live (unstained) group of cells for both control and MβCD treated passage 5 ORS cells. A greater number of live cells were detected in treatments with MβCD in correlation to the reduction in caspase 3/7 activity in 1-hour treated cells after a 23-hour recovery period (n=2) (Figure 4.6C). It should be noted that these results are preliminary as well and further repeats are needed.
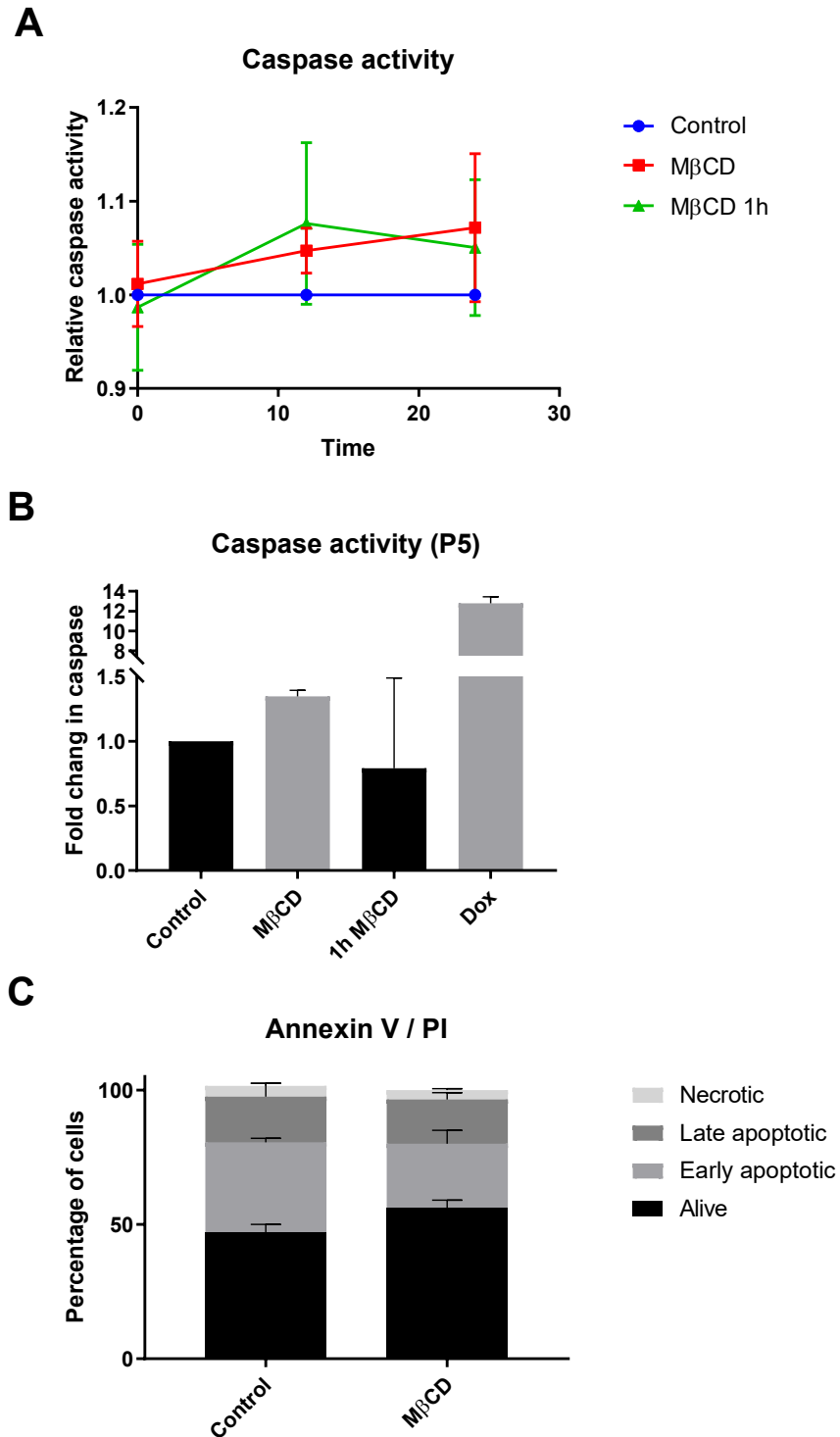
Figure 4.6 Effects of cholesterol on depletion apoptosis. Caspase 3/7 activity in ORS keratinocytes with 1 mM MβCD 1-hour pre-treatment (green) or throughout assay (red). (A) time course readings in passage 2-3 ORS keratinocytes (B) 24-hour endpoint reading in passage 5 (P5) ORS keratinocytes. (C) annexin/propidium iodide (PI) staining measured by flow cytometry in ORS keratinocytes 1 mM MβCD for 1-hour + 23-hours recovery (passage 5). Data are mean ± SEM for n=3 (A) n=2 (B,C).

4.2.4 Cholesterol loading and depletion does not alter anagen to catagen transition after 24-hours

Next, to investigate the effects of cholesterol loading and depletion in human HF, organ-cultured follicles were treated with 25 µM FC for 24-hours. Furthermore, to enhance cholesterol depletion, a higher concentration of 5 mM MβCD treatment was examined for 1-hour, followed by a 23-hour recovery period. This was within the range of MβCD treatments previously performed in keratinocytes (Jans *et al.*, 2004, Spörl *et al.*, 2010, Mathay *et al.*, 2011). Following FC loading, a small non-significant increase in the proportion of anagen follicles was observed (60% versus 57% in treated and control cells, respectively); however, this varied between donors (Figure 4.7). In Figure 4.8 cholesterol depletion resulted in a slight increase in the percentage of early catagen follicles (65.1% versus 51.2%). The large fluctuations in inter-donor variability was detected for both treatments, including ~ 35% spontaneous catagen transition following 24-hour cultures, this could therefore account for any changes in the proportion of anagen HFs.
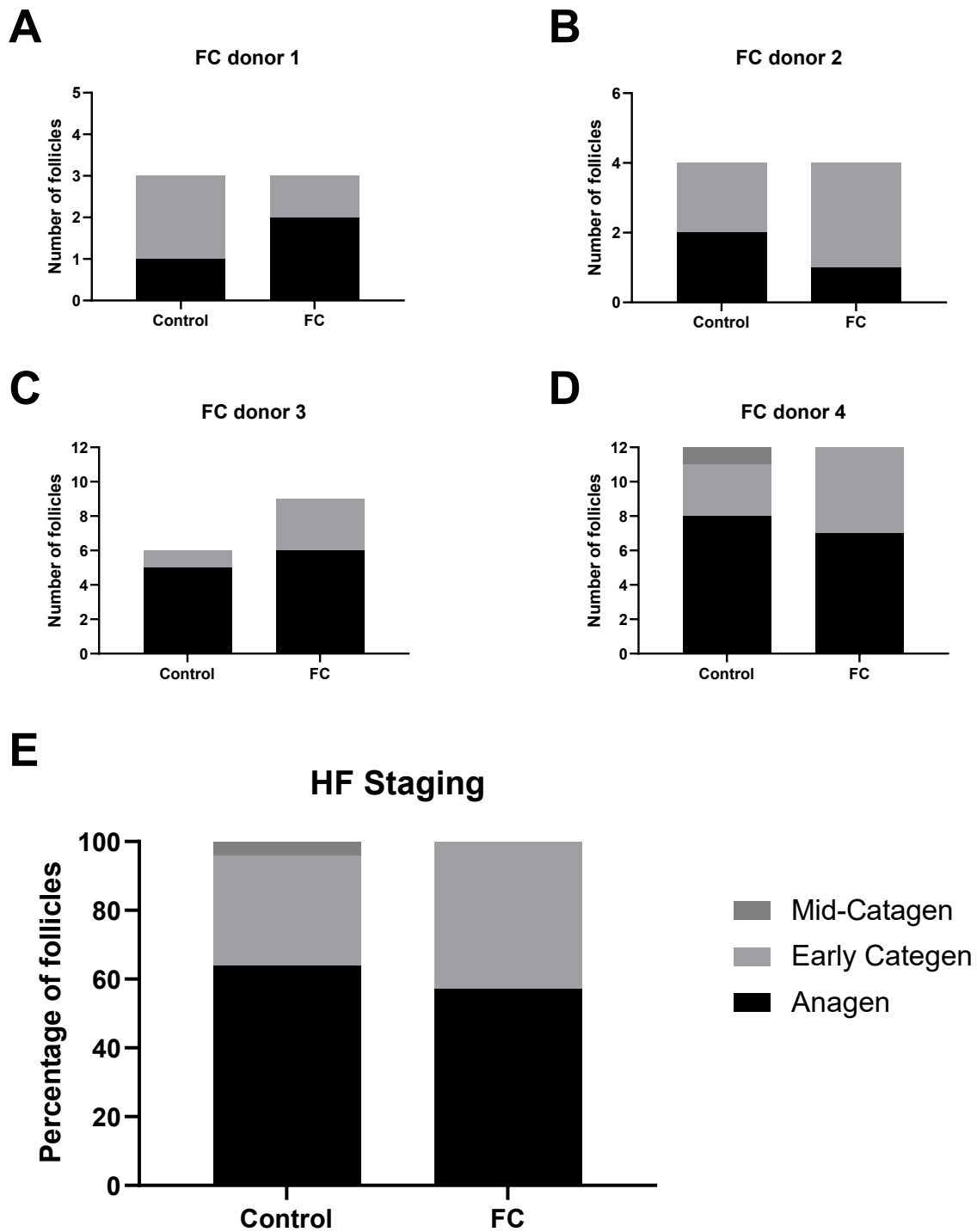
Figure 4.7 Proportion of anagen and catagen hair follicles with cholesterol loading. Anagen VI to catagen like transition analysis of HFs cultured with 25 µM FC for 24-hours. Data are mean ± SEM for (A) n=3, (B) n=4, (C) n=6 (Control) /9 (FC), (D) n=8 (control) /9 (FC) and(E) n=21 (control) /25 (FC) HFs pooled from 4 donors.
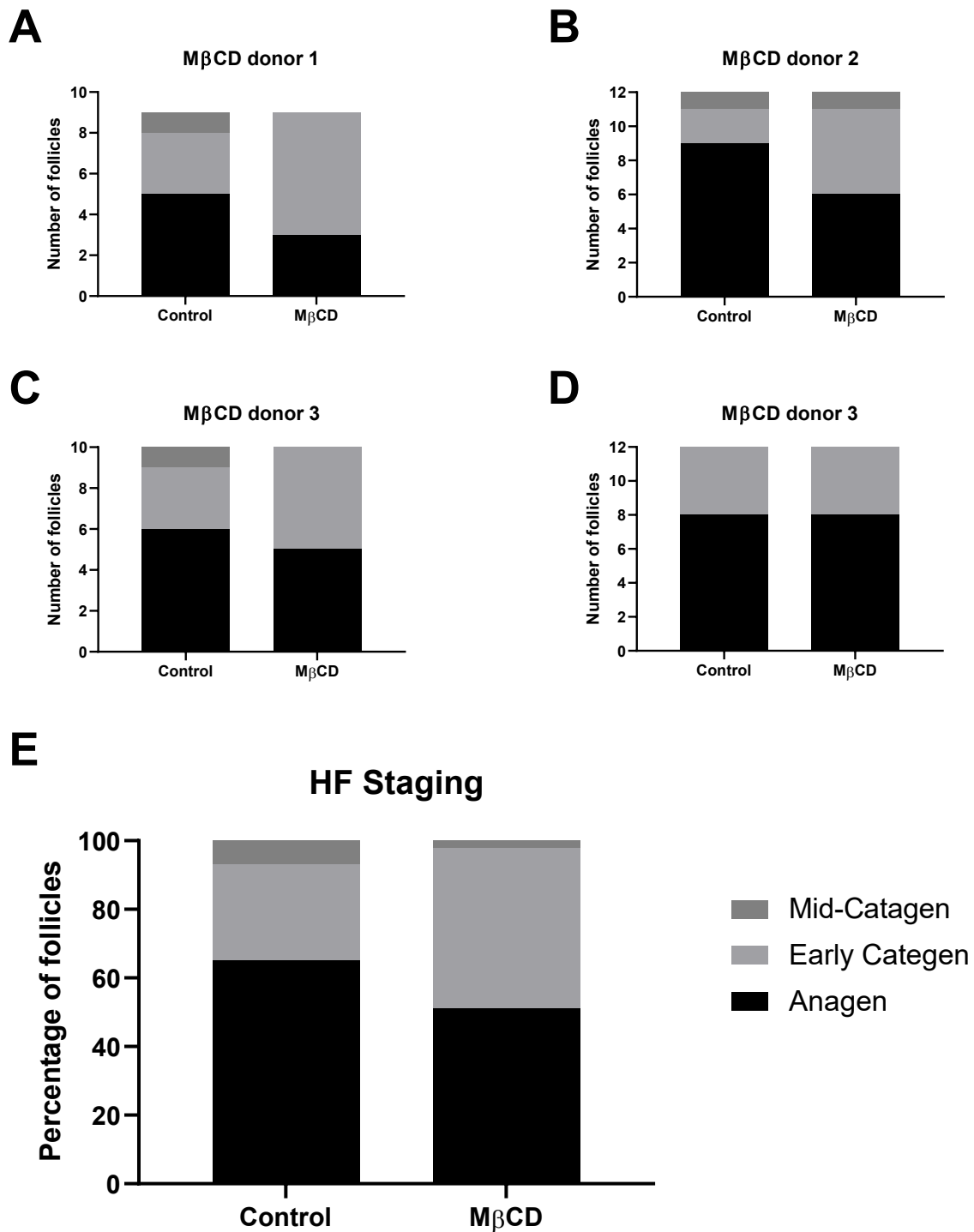
Figure 4.8 Proportion of anagen and catagen hair follicles with cholesterol depletion. Anagen VI to catagen like transition analysis of HFs cultured with 5 mM methyl-β-cyclodextrin (MβCD) for 1-hour + 23-hours recovery Data are mean ± SEM for (A) n=9, (C) n=10, (B,D) n=12, (E) n=43 HFs pooled from 4 donors.

4.2.5   Pigmentation in hair follicles following loading & depletion

To determine if cholesterol loading or depletion alters pigmentation, Masson Fontana staining was performed on HF tissue sections. Neither FC loading nor cholesterol depletion were found to alter pigmentation (Figure 4.9D and Figure 4.10D). A slight increase in the number of melanin clumps was detected in FC treated follicles (Figure 4.9B,E; mean=7.45 versus 6, P=0.059). Ectopic melanin was detected in the DP and DP stalk, however no differences were found between follicles treated with vehicle control or FC (Figure 4.9F). Analysis of melanin clumping revealed no significant differences in the number of clumps per follicle for MβCD treatment (Figure 4.10E), along with no change in the percentage of follicles with ectopic melanin in the DP stalk. No control follicles had ectopic melanin present in the DP, whereas 10% of MβCD HFs displayed ectopic melanin in this area (Figure 4.10F).
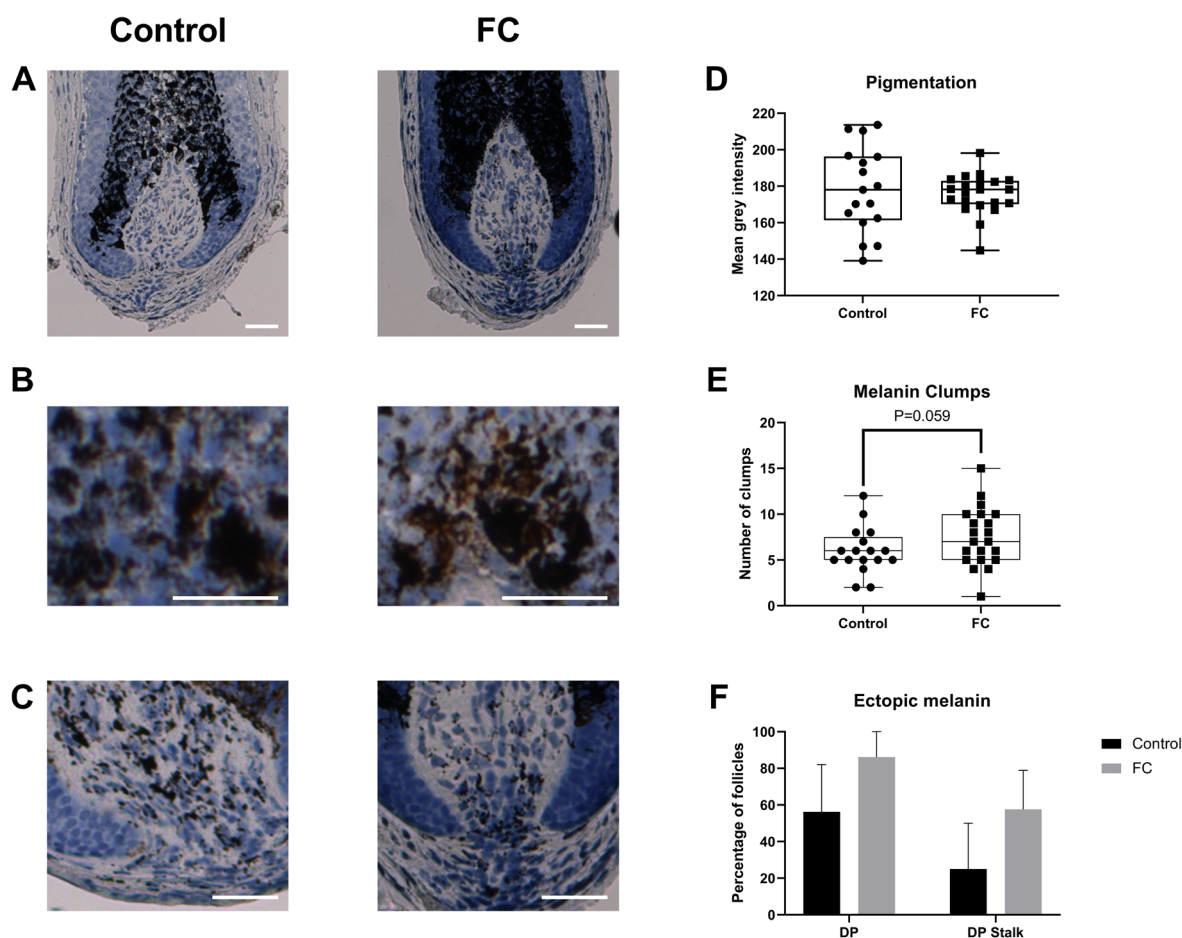
Figure 4.9 Pigmentation analysis in hair follicles with cholesterol loading. Masson Fontana staining in HFs treated with 25 μM FC for 24-hours. Representative images of bulb (A), melanin clumping (B) ectopic melanin (C). Mean pixel intensity of epithelial region of the bulb (a.u.) (D). Number of melanin clumps (E). Data are individual follicles ± SEM for n=18 (Control) /21 (FC) HFs pooled from 4 donors . Percentage of follicles with ectopic melanin (F), Data are mean ± SEM for n=4 donors. Scale bars represent 50 μm. Unpaired t-test performed.

Figure 4.10 Pigmentation analysis in hair follicles with cholesterol depletion. Masson Fontana staining in HFs treated with 5 mM MβCD for 1-hour with 23-hour recovery. Representative images of bulb (A), melanin clumping (B) ectopic melanin (C). Mean pixel intensity (a.u.) of epithelial region of the bulb (D). Number of melanin clumps (E). Data are individual follicles ± SEM for n=14 (control) /12 (MβCD) HFs pooled from 2 donors. Percentage of follicles with ectopic melanin (F), Data are mean ± SEM for n=2 donors. Scale bars represent 50 μm.

4.2.6 Proliferation and apoptosis in hair follicles following loading & depletion

To detect alterations in proliferation and apoptosis in the hair bulb, dual Ki67 and TUNEL immunofluorescence staining was performed (Figure 4.11, Figure 4.13). Analysis revealed no change in Ki67+ matrix keratinocytes below Auber's line with FC loading (Figure 4.12A). Mean number of TUNEL+ bulb cells with FC loading was greater than control treated follicles (21.9% versus 6.5%), although a large range is detected, and median values are 1.9% (0-50%) and 2.4% (0-100%) respectively Figure 4.12B). Likewise, no significant differences were detected for TUNEL+ cells in the DP or DP stalk with FC loading (Figure 4.12C,D). The number of DAPI+ nuclei within the Bulb, DP and DP stalk remain unchanged following FC loading (Figure 4.12F-H). A slight increase in the average number of DAPI+ nuclei below Auber's line is detected with FC treatment (100.6 versus 117.6), however this change is not significant (P=0.32) (Figure 4.12E).

Control　　　　　　　　　　　　**FC**
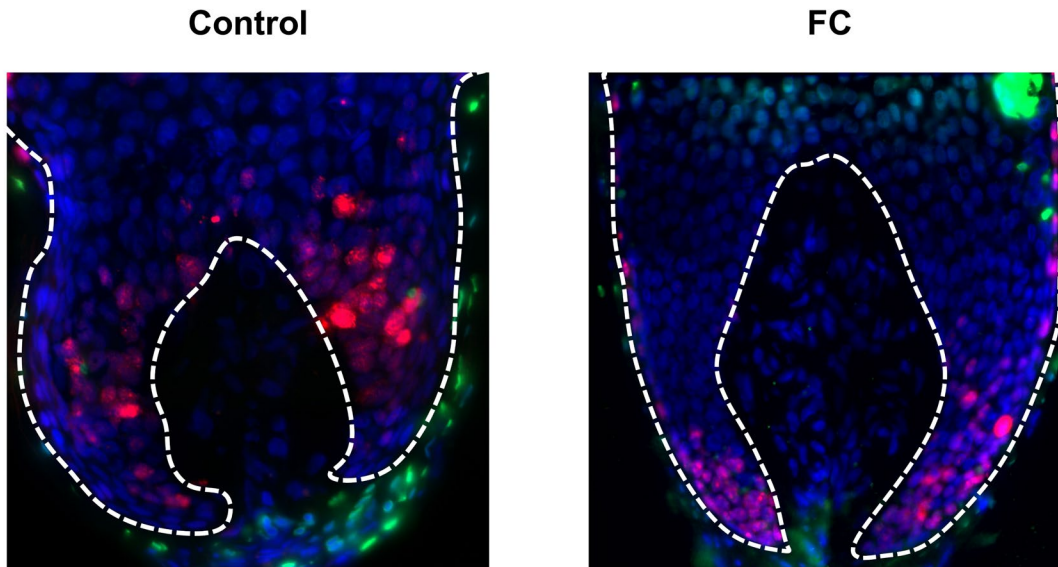
Figure 4.11 Proliferation and apoptosis analysis in hair follicles with cholesterol loading. Ki67 and TUNEL dual immunofluorescence staining in HF treated with 25 µM FC for 24-hours.
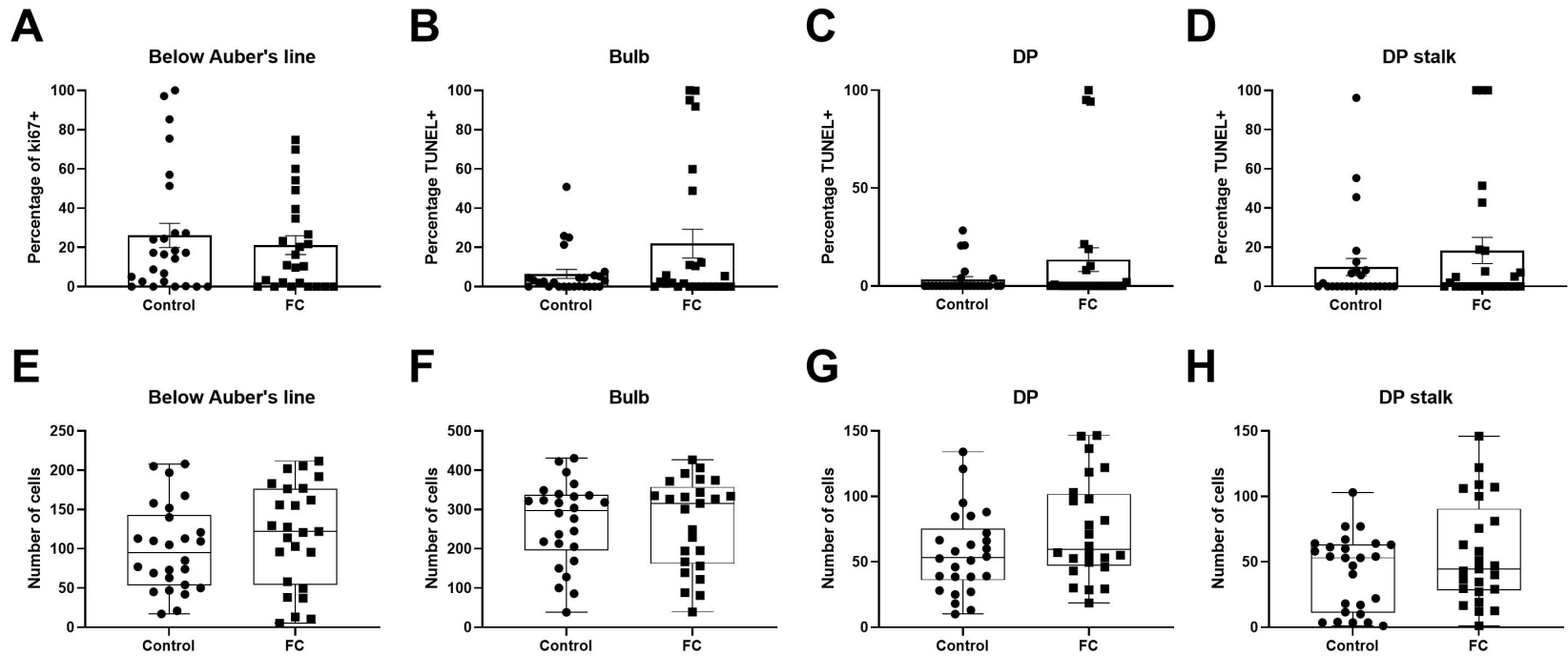
Figure 4.12 Analysis of ki67/TUNEL staining in hair follicles with cholesterol loading. Percentage of Ki67+ cells below Auber's line (A), Percentage of TUNEL+ cells in bulb (B), DP (C), DP stalk (D), number of nuclei below Auber's line (E), blub (F), DP (G), DP stalk (H). Data are individual follicles ± SEM for n=26 (control) /25 (FC) HFs pooled from 3 donors.

MβCD treatment revealed no changes in the number of Ki67+ matrix cells below Auber's line (Figure 4.14A). A slight reduction in the number of TUNEL+ cells was detected in the bulb (P=0.27) (Figure 4.14B). There was no change in the median value of TUNEL+ DP cells, however the mean values are 40.44% and 28.23% for Control and MβCD treatment respectively (Figure 4.14C). No significant differences are detected for the number of TUNEL+ DP stalk cells (Figure 4.14D). The number of nuclei detected below Auber's line (Figure 4.14E), within the bulb (Figure 4.14F) and within the DP stalk (Figure 4.14G) did not change with cholesterol depletion. A non-significant (P=0.174) reduction in the number of nuclei detected in the DP with cholesterol depletion was also seen (44.4 versus 38.9) (Figure 4.14H).
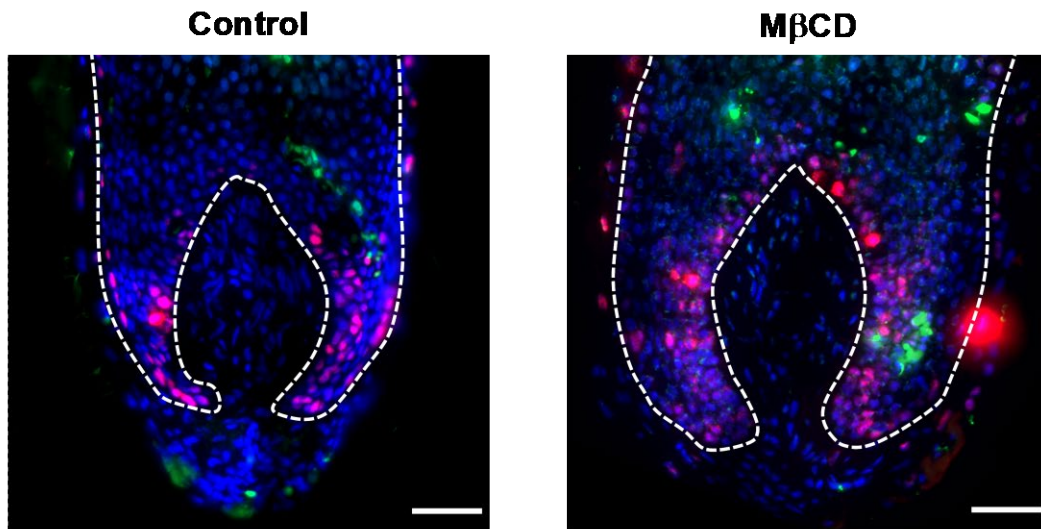
Figure 4.13 Proliferation and apoptosis analysis in hair follicles with cholesterol depletion. Ki67 and TUNEL dual immunofluorescence staining in HF treated with 5 mM MβCD for 1-hour with 23-hour recovery.
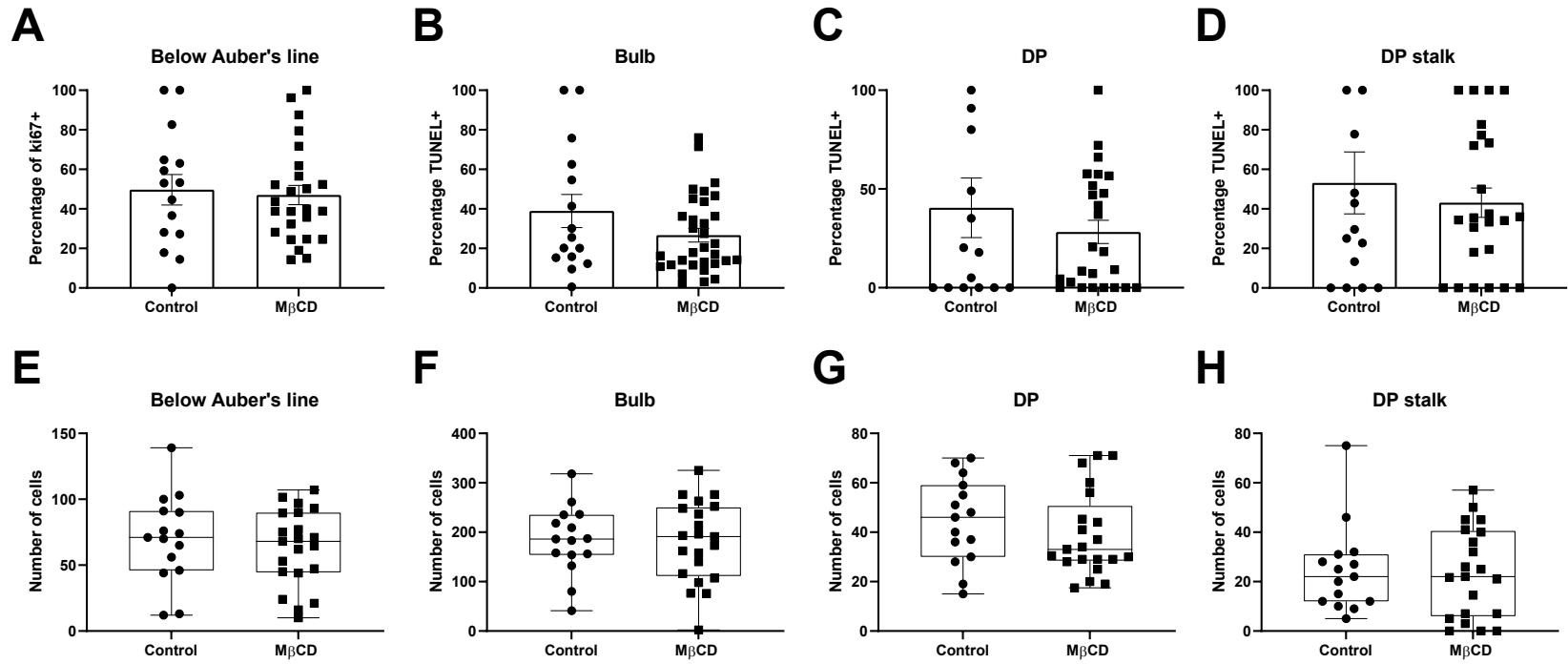
Figure 4.14 Analysis of ki67/TUNEL staining in hair follicles with cholesterol depletion. Percentage of Ki67+ cells below Auber's line (A), Percentage of TUNEL+ cells in bulb (B), DP (C), DP stalk (D), number of nuclei below Auber's line (E), blub (F), DP (G), DP stalk (H). Data are individual follicles ± SEM for n=15 (control)/21 (MβCD) from 2 donors.

4.2.7   Cholesterol loading and depletion alters Wnt signalling

Given previous evidence suggesting a role for cholesterol in the modulation of signalling pathways, Wnt signalling was examined by measurement of downstream target gene expression (*via* qPCR). ORS keratinocytes and HFs were treated with 25 µM FC for 24 or 72-hours (ORS keratinocytes) and either 1 mM or 5 mM (HFs) MβCD for 1-hour with a 23-hour recovery period. Downstream Wnt/β-catenin targets *LEF1* (lymphoid enhancer binding factor 1) and *AXIN2* (only detected in HFs) were measured by qPCR. Figure 4.15A demonstrates that 72-hour FC loading increased *LEF1* gene expression (P=0.016), whereas cholesterol depletion significantly reduced *LEF1* expression in ORS keratinocytes (P=0.023). Likewise, in the HFs FC loading showed an increase in both *LEF1* (P=0.019) and *AXIN2* (P=0.071), whereas MβCD treatment resulted in no change in *LEF1* and only a non-significant decrease in *AXIN2* levels (Figure 4.15B,C).
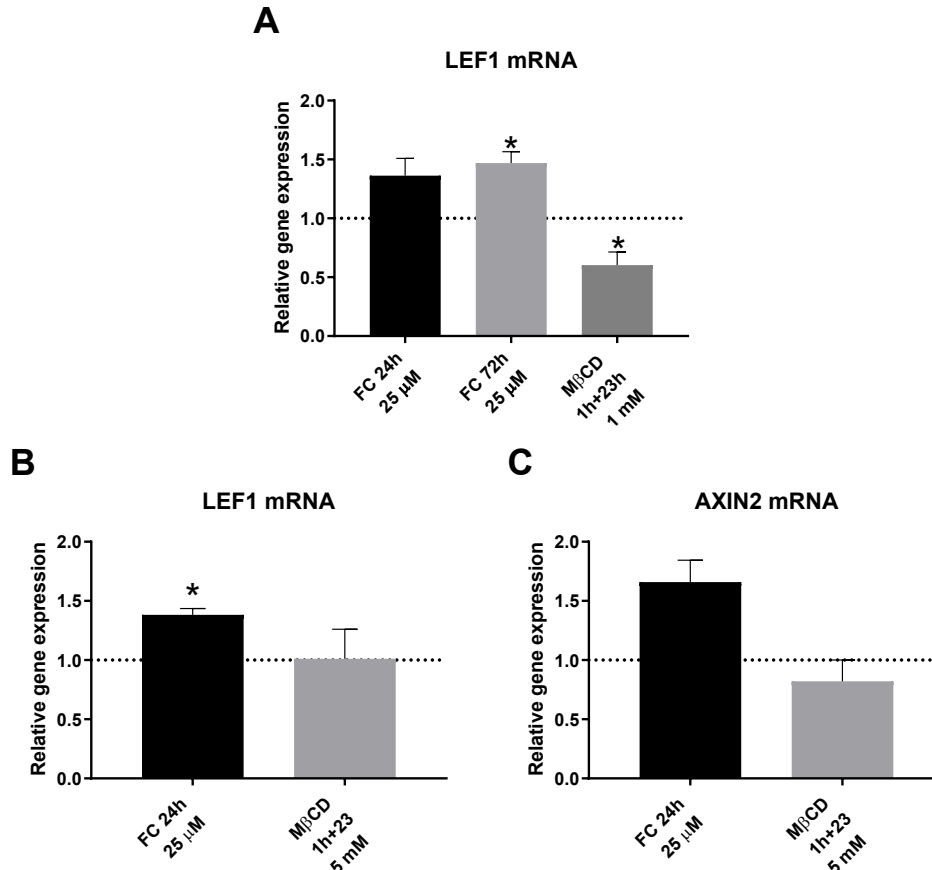
Figure 4.15 Wnt signalling with cholesterol loading and depletion. Gene expression changes in ORS keratinocytes treated with 25 µM FC for 24-hours, 72-hours or 1 mM MβCD for 1-hour + 23-hours recovery of *LEF1* (A) or HFs treated with 25 µM FC for 24-hours or 5 mM MβCD for 1-hour + 23-hours recovery for *LEF1* (B), *AXIN2* (C). Gene expression reported relative to vehicle control and normalised to *PPIA*. Data are mean ± SEM for n=5 or 6 donors (ORS keratinocytes) n=3 (HFs). One-sample t-test performed; significance denoted by * P≤0.05

4.3 Discussion

Previous studies in epidermal keratinocytes have shown that modulating cholesterol levels can impact keratinocyte growth, differentiation and apoptosis (Jans *et al.*, 2004, Mathay *et al.*, 2011, Spörl *et al.*, 2010). Yet this effect has not been directly explored within the HF. Therefore, this chapter provides the first evidence of the impact of cholesterol loading and depletion in both HF-derived ORS keratinocytes and human HFs in organ culture.

The data presented here confirms that intracellular cholesterol levels can be modulated in ORS keratinocytes through exogenous FC loading and MβCD-mediated depletion. Notably, FC loading resulted in a clear redistribution of cholesterol to the nuclear periphery of ORS keratinocytes, as shown with the filipin staining (Figure 4.1). Co-localisation with endo-lysosomal marker LAMP1 suggests accumulation of the exogenous cholesterol within endo-lysosomal compartments, as has been shown previously in macrophages (Cox *et al.*, 2007) and keratinocytes isolated from patients with a form of congenital hypertrichosis (DeStefano *et al.*, 2014). Consistent with the data in this chapter Spörl *et al.* (2010) detected a 50% reduction in filipin intensity following 0.125% MβCD treatment at both 2 and 24-hours in epidermal keratinocytes.

FC loading did not alter lipid rafts in ORS keratinocytes at 24 or 72-hours, as shown by the lack of change in CTX-FITC labelling. Alternative cholesterol delivery methods include complexing the lipid with MβCD, which can be used to facilitate more rapid uptake of cholesterol to the plasma membrane (Holtta-Vuori *et al.*, 2008). Addition of a 0.0125% MβCD : 20 µg/ml cholesterol complex to epidermal keratinocytes shows a clear increase in plasma membrane cholesterol and results in a 200% increase in cholesterol levels when measured *via* thin layer chromatography (Spörl *et al.*, 2010). As the delivery method used here involved dissolution of cholesterol in an organic solvent, delivery may not have been rapid enough, or sufficient to alter membrane cholesterol to a level that would disrupt lipids rafts.

Cholesterol depletion studies were consistent with previous studies in epidermal keratinocytes, where 7.5 mM MβCD treatment for 1-hour showed a reduction in both total and plasma membrane cholesterol (Jans *et al.*, 2004). Although a lower concentration was used in this study alterations to filipin staining were detected. The increase in lipid raft intensity with cholesterol depletion detected is consistent with previous results in HaCaT cells with 1% MβCD, which was thought to be cholesterol repletion following disruption of lipid rafts (Bang *et al.*, 2005).

Having observed changes in cholesterol content and localisation in response to cholesterol loading and depletion, the impact this may have on cell viability was investigated. MβCD depletion in ORS keratinocytes is consistent with previous results in epidermal keratinocytes (Spörl *et al.*, 2010). Whereas Spörl *et al.* (2010) showed increases in proliferation with FC treatment, these experiments did not reproduce this. A higher concentration of FC along with FC complexed with MβCD was used by Spörl *et al.* (2010). In fact, FC-MβCD complex showed a greater increase in proliferation than FC presented on its own (Spörl *et al.*, 2010). Concentrations of 5 µg/ml FC-MβCD were sufficient to significantly increase proliferation in bone marrow derived mesenchymal stem cells with 48-hours loading (Li *et al.*, 2013).

Persistently high concentrations of oxysterols are known to initiate apoptosis through reactive oxygen species and calcium influx induced BCL2 associated agonist of cell death (BAD) phosphorylation (Vejux *et al.*, 2008). 25-hydroxycholesterol has been shown to significantly reduce cell viability in HaCaT cells at concentrations above 5 µM (Olivier *et al.*, 2017). One mechanism cells utilise to lower cholesterol levels is through metabolism into oxysterols, which subsequently activates LXR and SREBP2 (Bovenga *et al.*, 2015). Furthermore, LXR agonism has been shown to reduce proliferation of epidermal keratinocytes (Russell *et al.*, 2007), however Russell *et al.* (2007) reported changes at two and five days post treatment. As no changes in viability or proliferation were detected with FC loading, it could be presumed that short time-course treatments at this concentration do not induce a significant change in cellular oxysterols to induce apoptosis.

As was observed in the ORS keratinocytes, exogenous cholesterol loading in HF organ cultures altered neither proliferation nor apoptosis. This may indicate that the HFs capacity to maintain growth in response to exposure to this physiological concentration of excess cholesterol is not exceeded. Further studies with increased concentrations of FC would be needed to investigate the effects of supra-physiological cholesterol loading on HF keratinocyte proliferation. Furthermore, although a 5-fold higher concentration of MβCD was used in HF organ culture treatments compared with the ORS keratinocytes, this concentration revealed no effect on proliferation or apoptosis. This result contrasts with the slight increase in preliminary apoptosis results and reduction in cell numbers *in vitro* (Figure 4.6). Longer treatment times may be needed to succeed in depleting cholesterol levels within the densely packed mini organ.

As with the proliferation studies, addition of FC did not alter cellular senescence levels in ORS keratinocytes, however cholesterol depletion significantly reduced β-gal staining. Although the investigations into the role of cholesterol on senescence are sparse, a reduction in cellular

senescence with cholesterol loading in bone marrow was detected (Zhang *et al.*, 2016b), opposing to the results shown in this chapter. In the data presented here for ORS keratinocytes, one could hypothesise that the decrease in cell viability following cholesterol depletion was due to the preferential apoptosis of senescent cells, leading to reduced β-gal staining and apparently lower levels of senescence. This was further investigated through use of the caspase 3/7 assay to look at changes to apoptosis.

Investigation of apoptosis in senescent ORS keratinocytes revealed a trend of increased caspase apoptosis with continuous MβCD treatment for 24-hours. However, in comparison when media was changed following 1-hour cholesterol depletion, annexin/PI results showed an increase in the percentage of live cells, and a variable response was detected with caspase 3/7 assay. Previous studies have shown injections of MβCD treatment in aged mice result in a reduction of caveolin 1, a marker of senescence, and an increase in collagen 1 (Lee *et al.*, 2015). Atorvastatin treatment (which would reduce cellular cholesterol content) reversed the effects of angiotensin-induced senescence in human umbilical vein endothelial cells (Dang *et al.*, 2018). 27-hydroxylcholesterol treatment induces senescence markers p51, p21 and p16 along with β-gal positive cells in both human lung fibroblasts and adult bronchial endothelial cells (Hashimoto *et al.*, 2016). Taken together with the reduction of senescent P2-3 and P5 ORS keratinocytes with cholesterol depletion, these data suggest that depletion of cholesterol promotes the survival of basal keratinocytes and apoptosis of senescent cells. One could hypothesise that removal of the MβCD treatment to allow for a recovery period, additionally removes detached senescent cells leading to the increase in percentage of alive cells as detected by annexin/PI results. Reversal of senesce has been shown with cholesterol loading in bone marrow mesenchymal stem cells (Zhang *et al.*, 2016b), therefore it could also be hypothesised that in this cell type cholesterol depletion drives senescent reversal. However, these results were preliminary and additional replicates would be needed in higher-passage ORS keratinocytes to confirm this, in addition to investigating changes in additional senescent markers.

The hair cycle is a tightly regulated process, initiated by signalling pathways (such as the Wnt/β-catenin pathway) as detailed in Chapter 1: Section 1.2.1. Lipid modifications of signalling proteins have been shown to be vital to plasma membrane localisation of signalling molecules, enabling initiation of signalling cascades. Specifically, modification *via* cholesterol is important in the selectivity of the Wnt/β-catenin pathway (Sheng *et al.*, 2014). 1-hour 1 mM MβCD treatment in Hela cells has been shown to reduce the binding of dishevelled 2 to the frizzled receptor (Sheng *et al.*, 2014). The data presented here in ORS keratinocytes reflects this with significant reduction

of downstream Wnt/β-catenin signalling target *LEF1* expression with cholesterol depletion, in addition to FC loading significantly increasing *LEF1* in both ORS keratinocytes and the HF. In contrast, 30-minutes treatment with 5 mM MβCD in xenopus embryos showed an increase in Wnt/β-catenin signalling, however this was thought to be tissue specific and disruption of cholesterol-rich microdomains can also potentiate the spread of Wnt inhibitor DKK1 (Reis *et al.*, 2016). Furthermore, cholesterol depletion through HMGCR inhibitor simvastatin increases expression of *LEF1* in spinal cord neurones (Gao *et al.*, 2016), whereas atorvastatin treatment results in reduced DKK1 expression in human umbilical vein endothelial cells (Pontremoli *et al.*, 2018). This further cements the theory of tissue specific cholesterol modifications of Wnt/β-catenin signalling by Reis *et al.* (2016), and the data here promotes cholesterol modifications to the role of enhancement of Wnt/β-catenin signalling within the HF. Although cholesterol loading and depletion studies *ex vivo* at 24-hours showed no changes in hair cycle stage, the small alterations to Wnt signalling demonstrate a potential to further investigate the effects of cholesterol in hair cycling with both longer time points and increases in concentrations.

Schallreuter *et al.* (2009) showed an increase in melanin content with increasing cholesterol concentrations in epidermal melanocytes. Higher cholesterol levels were found in melanosomes of early melanocytes in comparison to pigmented cells, which the authors suggested that cholesterol may be important for the stability of early melanosomes (Schallreuter *et al.*, 2009). Although the data presented in this chapter showed no alterations in pigmentation with the addition of cholesterol, significant increases in melanin content were only detected at 20 μg/ml (Schallreuter *et al.*, 2009) which is double the concentration of FC used in this study, therefore further experiments with higher concentrations of cholesterol should be used to detect changes in melanogenesis.

Furthermore, MβCD treatment has been shown to reduce melanogenesis through increased ERK phosphorylation in both human melanocytes and breast skin (Jin *et al.*, 2008). As a large proportion of the HFs were in catagen, the cycle stage which is characterised by a reduction in pigmentation and apoptosis of mature melanocytes (Tobin *et al.*, 1998, Slominski *et al.*, 2005), this may explain the variation in pigmentation observed across the treatment groups. The increase in melanin clumping with FC loading could be an indication of melanocyte apoptosis. Further research with additional concentrations and time points, along with dual immunofluorescence staining of pre-melanosome protein (GP100) with TUNEL to detect melanocyte apoptosis would be necessary to confirm this.

The work in this chapter demonstrates the HFs capacity to buffer small increases in cellular cholesterol levels following addition of a physiological concentration of FC. Cholesterol depletion studies revealed no changes in cellular proliferation, however a reduction in cellular senescence and a small increase in caspase-mediated apoptosis was found. Cholesterol loading altered cholesterol compartmentalisation increasing endo-lysosomal accumulation, however lipid rafts in the plasma membrane remained unchanged. Small increases in Wnt signalling were suggested by increased expression of downstream targets in both ORS keratinocytes and human HFs, which may be indicative of cholesterol modification of Wnt signalling proteins. The functional significance of these alterations in HF growth and cycling requires further investigation.

Chapter 5: Localisation of cholesterol transporters in the human hair follicle: mapping changes across the hair cycle

5.1 Introduction

As previously outlined in Chapter 1, cholesterol modification of signalling molecules such as Hh and Wnt are vital for transduction of signalling cascades (Incardona and Eaton, 2000); both of these pathways are fundamental in the control of HF cycling (Lee and Tumbar, 2012). Chapter 3 established the expression, localisation and dynamic regulation of cholesterol transporters using a primary cell model for the HF epithelium (ORS keratinocytes). Chapter 4 then demonstrated the capacity of human HFs to buffer changes in cholesterol status (response to exogenous delivery and MβCD-mediated depletion). Furthermore, small changes in the expression of downstream Wnt targets suggested an influence of cholesterol levels on this vital pathway in the control of hair cycling.

Given that the movement of cholesterol within aqueous environments is essential for its involvement in different biological processes, this chapter explores the expression and localisation of cholesterol transport proteins in the HF. Furthermore, the expression of these transporters across the hair cycle is examined. This may provide some insight into the importance of cholesterol transport in different cellular compartments within the HF and the changing requirements for cholesterol transport during different phases of hair growth. In addition, pilot experiments examine the changes in cholesterol homeostatic genes in response to LXR activation in human HFs.

The specific aims of this chapter are to:

- Determine the localisation of cholesterol transport proteins ABCA1, ABCA5, ABCG1 and SCARB1, along with the rate-limiting enzyme of cholesterol synthesis HMGCR, in human HFs
- Understand the distribution of FC in human HFs utilising filipin staining
- Investigate the expression of cholesterol transporters across the hair cycle and in response to LXR agonism

5.2 Results

5.2.1 The cholesterol efflux transporter ABCA1 is highly expressed in the human hair follicle

The distribution of the ubiquitous cholesterol efflux transporter, ABCA1, was examined across the hair cycle. Anagen HFs displayed a distinct staining pattern, showing higher expression in the epithelial compartment compared with the mesenchymal CTS (Figure 5.1A,B,C). Within the CTS and the DP, staining was predominantly cytoplasmic, with some indication of increased staining in the DP at the nuclear periphery (Figure 5.1C). The elongated staining pattern within the mesenchymal compartment suggested possible expression in the endothelium. The ORS of the isthmus displayed the highest staining intensity (Figure 5.1A), with polarised expression in the basal ORS (Figure 5.1D). Membrane staining was apparent in the PCM and matrix keratinocytes (Figure 5.1C). Whilst staining was indistinct within the IRS, plasma membrane localisation was apparent in the HC (Figure 5.1B).

Similar staining patterns were observed in early catagen, with distinct membrane staining in the matrix and PCM (Figure 5.1G,H). The CTS and DP (Figure 5.1G) showed a lower intensity of staining, compared with the suprabulbar ORS (Figure 5.1F). Membrane staining was observed throughout the ORS and IRS. In mid-catagen, higher expression was found in the developing club hair (Figure 5.1K), with staining at the nuclear periphery (Figure 5.1M), and no expression was present in the CTS or DP (Figure 5.1L). Examining the club hair of plucked telogen follicles (Figure 5.1N,O), high expression was only found within the inner bulge layers, with a predominantly localisation at the nuclear periphery (Figure 5.1O).
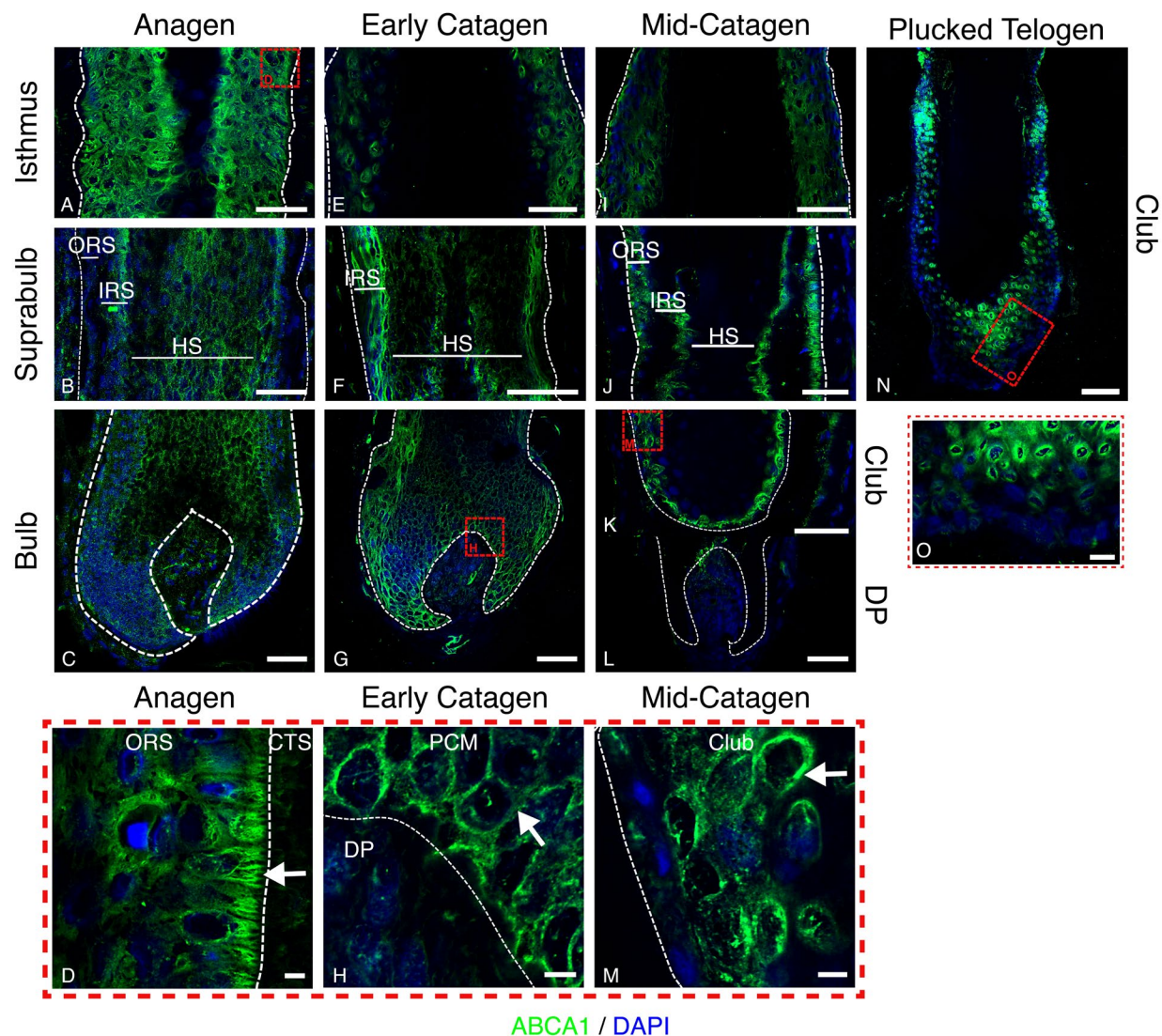
Figure 5.1 ABCA1 immunofluorescence staining the hair cycle. Localisation of ABCA1 (green) immunofluorescence staining in human anagen (A,B,C,D), early catagen (E,F,G,H) mid-catagen (I,J,K,L,M) and plucked telogen (N,O) HFs with DAPI counterstaining (blue). Dashed white lines showing epithelial components, scale bars 50 μm. Red dashed box delineates magnified images, scale bar represents 5 μm. White arrows show: polar staining (D), membrane staining (H) and staining at the nuclear periphery (M). ORS, outer root sheath; IRS, inner root sheath; HS, hair shaft; CTS, connective tissue sheath; PCM, pre-cortical matrix; DP, dermal papilla. Representative images from n=3 donors, with imaging performed in 2-3 follicles per donor (except mid-catagen, n=2 donors, with 2 follicles per donor imaged).

5.2.2　ABCG1 is highly expressed in the sebaceous gland

In addition to ABCA1 the physiologically important cholesterol transporter ABCG1 was examined (Figure 5.2) (Engel *et al.*, 2007, Phillips, 2014). Immunofluorescence detection of ABCG1 was found to be low throughout the HF (Figure 5.2D), however considerably higher staining levels were seen in the SG (Figure 5.2 ABCG1 immunofluorescence staining in the pilosebaceous unit. H).

The highest levels of ABCG1 staining in anagen HFs was seen within the ORS (Figure 5.2A,B), a pattern also observed during early catagen (Figure 5.2E,F). Little expression was seen within the matrix keratinocytes, PCM and ORS (Figure 5.2C) in anagen.

Mid-catagen HFs showed a broadly comparable staining pattern (Figure 5.2I.J), however staining intensity increased in the IRS proximal to the club hair, with the club hair itself showing more intense staining (Figure 5.2K). Low levels of ABCG1 were found within the mesenchymal compartments of the HF across the hair cycle (Figure 5.2). Within the plucked telogen HF staining was largely indistinct, although notably, a higher intensity of staining at the tip of the club hair was observed consistently across HFs from three individual donors (Figure 5.2M).

Anagen **Early Catagen** **Mid-Catagen** **Plucked Telogen**

Isthmus

Suprabulb

ORS
IRS
HS

Bulb

Club

DP

ABCG1

Merge

Anagen **Anagen**

SG

ABCG1 / CD200 / DAPI
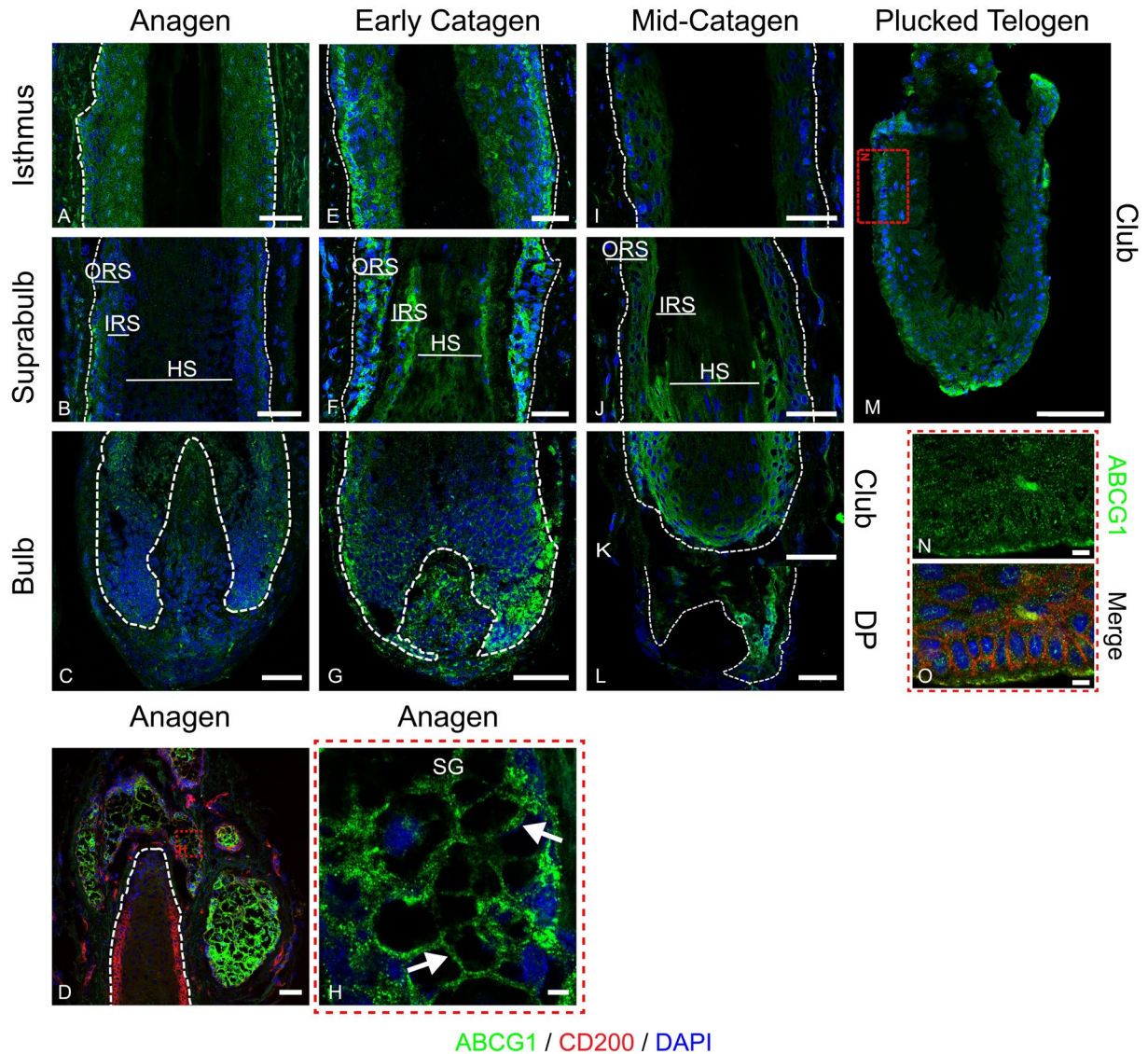
Figure 5.2 ABCG1 immunofluorescence staining in the pilosebaceous unit. ABCG1 immunofluorescence (green) staining in anagen (A,B,C,D,H), early catagen (E,F,G), mid-catagen (I,J,K,L) and plucked telogen (N,O,P) HFs with DAPI counterstaining (blue). Dashed white lines showing epithelial components, scale bars 50 μm, red dashed box delineates magnified images, scale bar 5 μm. CD200 dual immunofluorescence staining (red) in bulge region of the anagen HF (D) and telogen (O). Membrane staining in the sebaceous gland as shown in magnified image by white arrows (L). HF images intensity adjusted to represent the localisation patterns of the weekly expressed ABCG1. ORS; outer root sheath, IRS; inner root sheath, HS; hair shaft, SG; sebaceous gland. Representative images from n=3 donors, with imaging performed in 2-3 follicles per donor (except mid-catagen, n=2 donors, with 2 follicles per donor imaged). *Telogen red dashed box is representative field of view for magnified image and not actual image.

5.2.3   ABCA5 is highly expressed in the inner root sheath and membranous in the hair shaft cuticle

Next, expression and localisation of the putative cholesterol transporter ABCA5 was examined across the hair cycle (Figure 5.3). As previously reported (DeStefano *et al.*, 2014), expression was high in both the ORS and IRS of anagen follicles (Figure 5.3A,B,C), with the suprabulbar ORS showing lower expression than the ORS of the isthmus (Figure 5.3). In the mesenchymal regions of the HF expression was high in the DP, yet substantially lower in the CTS (Figure 5.3C). Both the matrix and PCM (Figure 5.3H) displayed high-intensity ABCA5 staining. Within anagen HFs, sub-cellular expression was predominately cytoplasmic, however membrane staining is apparent within the HC (Figure 5.3K). The highest intensity staining was shown in the Cu, with the IRS and the companion layer showing the greatest intensity ABCA5 staining in suprabulbar regions (Figure 5.3D).

ABCA5 staining patterns in early catagen were largely consistent with that of anagen HFs, though staining intensity within the matrix and ORS was somewhat lower (Figure 5.3H).

By contrast, mid-catagen HFs showed much lower levels of ABCA5 (Figure 5.3I,J,K,L). Staining intensity in the IRS was extremely low and was undetectable in the HS (Figure 5.3J). In opposition to this, high-intensity staining was apparent in the DP and the CTS in proximity to this area (Figure 5.3J). Staining was polarised to the basal layer of the ORS (Figure 5.3L) of the isthmus.

Within plucked telogen follicles (Figure 5.3N,O,P), staining polarity showed higher expression levels in the ORS cells adjacent to the basement membrane, with a largely cytoplasmic pattern (Figure 5.3O).
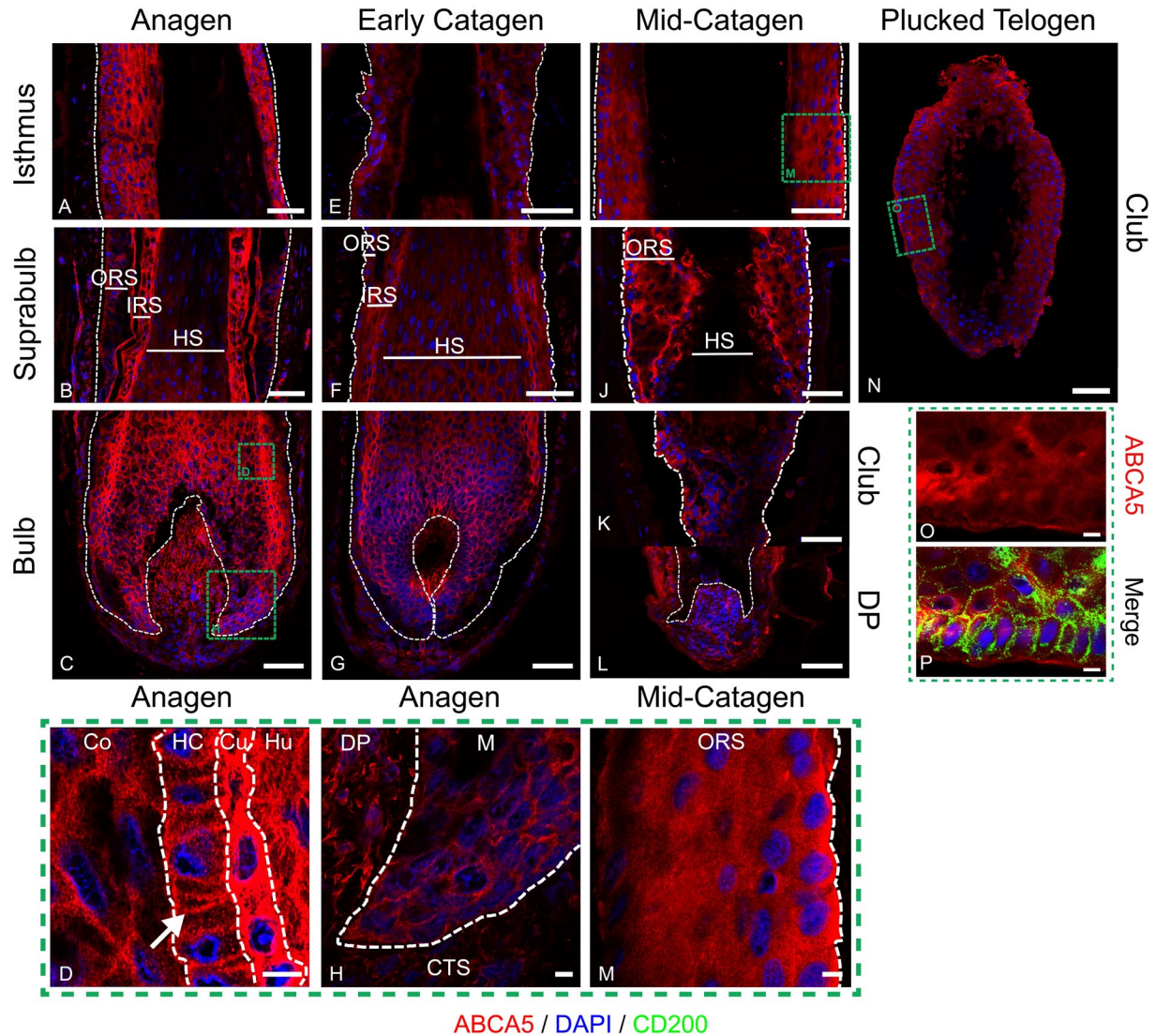
Figure 5.3 ABCA5 immunolocalisation in the hair cycle . ABCA5 (Red) immunofluorescence staining in anagen (A,B,C,D,H), early catagen (E,F,G), mid-catagen (I,J,K,L,M) and plucked telogen (N,O,P) HFs with DAPI counterstaining (Blue). Dashed white lines showing epithelial components. Scale bars 50 µm, magnified images represented by green dashed box, scale bar 5 µm. Membrane staining in the HS cuticle demonstrated by white arrow (D). Polar staining towards the basal membrane (M). ORS; outer root sheath, IRS; inner root sheath, HS; hair shaft, CTS; connective tissue sheath, DP; dermal papilla, M; matrix, Co; cortex, HC; hair cuticle, Cu; cuticle, Hu; Huxley's layer, SG; sebaceous gland. Representative images from n=3 donors, with imaging performed in 2-3 follicles per donor (except mid-catagen, n=2 donors, with 2 follicles per donor imaged). *Telogen green dashed box is representative field of view for magnified image and not actual image.

5.2.4 Distinct SCARB1 staining is found in the dermal papilla basement membrane

In addition to the ABC transporters examined above, the expression pattern of the bi-directional HDL transporter SCARB1 was investigated (Figure 5.4), given documented evidence describing its influence on cholesterol homeostasis in numerous tissues (Shen *et al.*, 2018b, Sticozzi *et al.*, 2012, Shen *et al.*, 2018a). Staining intensity in anagen HFs was high within the bulb, with membrane staining apparent throughout (Figure 5.4C). Mesenchymal immunofluorescence was low, with some higher intensity elongated staining patterns that could indicate expression in the HF vasculature.

To investigate the distinctive halo of SCARB1 expression observed surrounding the DP, dual staining with the basement membrane marker laminin-332, was performed. As shown in Figure 5.4D, a clear co-localisation of SCARB1 with laminin-332 was seen. The antibody used to detect SCARB1 recognises the extracellular domain, which would face the DP basement membrane (Shen *et al.*, 2018b). This may suggest a role for SCARB1 in facilitating movement of cholesterol between the DP and matrix keratinocytes.

In the early catagen HFs, membrane staining was present in He of the IRS (Figure 5.4H). Membrane staining continues in the suprabulbar ORS (Figure 5.4F). As seen with ABCG1, SCARB1 expression was lower in mid-catagen follicles (Figure 5.4I,J,K,L) in comparison with early catagen or anagen.

During telogen, distinct membrane staining was found (Figure 5.4M-O), with some co-localisation to the CD200 expressing stem cells found in the basal and lateral membranes (Figure 5.4O).
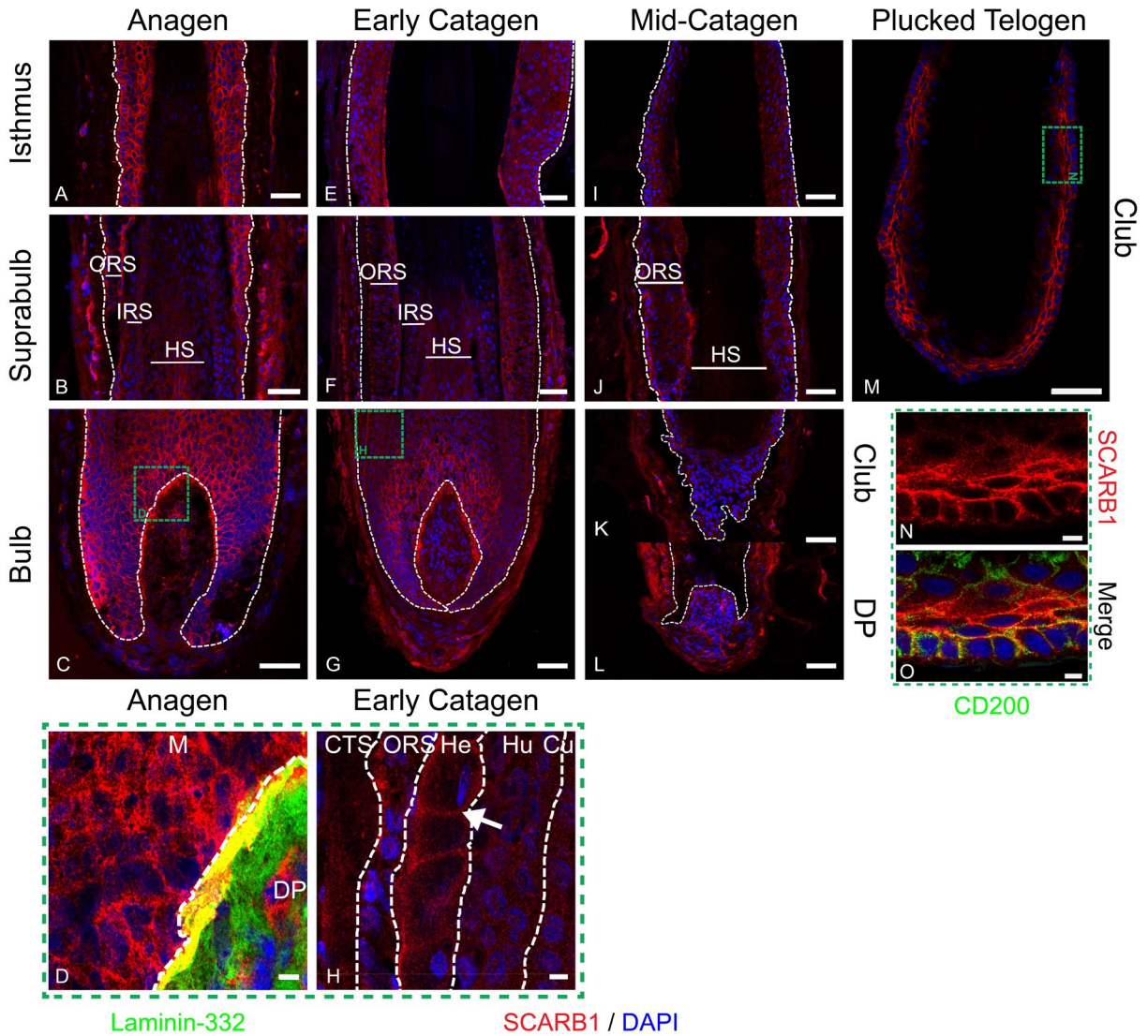
Figure 5.4 SCARB1 is present in the dermal papilla basement membrane. SCARB1 immunofluorescence staining (red) in anagen (A,B,C,D), early catagen (E,F,G,H), mid-catagen (I,J,K,L) and plucked telogen (M,N,O) HFs with DAPI counterstain (blue). Dashed white lines showing epithelial components, scale bars 50 µm. Green dashed box delineates magnified images, scale bar 5 µm. Magnified image of DP co-stained with laminin-332 (green) showing co-localisation of SCARB1 to laminin-332 (D). Membrane staining shown by white arrow (L). Telogen bulge marker CD200 (green) (O). ORS; outer root sheath, IRS; inner root sheath, HS; hair shaft, DP; dermal papilla, M; matrix, Cu; cuticle, Hu; Huxley's layer, He; Henle's layer. Representative images from n=3 donors, with imaging performed in 2-3 follicles per donor (except mid-catagen, n=2 donors, with 2 follicles per donor imaged).

5.2.5 Cholesterol synthesis enzyme, HMGCR, is highly expressed throughout the hair cycle

Further to the expression of cholesterol transporters, cholesterol handling in the HF was investigated by examining the expression and localisation of HMGCR, the enzyme responsible for the rate-limiting step in the biosynthetic pathway (Figure 5.5). During anagen (Figure 5.5A,B,C), intense staining was found in the matrix, DP, and ORS (being highest within the isthmus) with lower levels in the IRS and HS. Staining in the CTS was low to absent. During early catagen (Figure 5.5D,E,F) the intensity of HMGCR staining in the epithelial HF was lower than in anagen, though remained high in the DP. During mid-catagen, high expression was seen in the epithelial strand and developing club hair (Figure 5.5I,J), as well as the ORS of the isthmus (Figure 5.5G). Within the plucked telogen follicle (Figure 5.5K,L,M) the highest intensity of staining was found within the medial layers of the inner bulge. The widespread expression of HMGCR across the hair cycle points to the HFs capability for *de novo* cholesterol synthesis.

HMGCR was expressed throughout the epidermis (Figure 5.6A) with a higher level shown in the basal layer, including staining at the nuclear periphery, but at a lower level than the HF. Likewise, within the CTS extremely low HMGCR staining intensity was found. In contrast, high expression was found in the SG (Figure 5.6B).
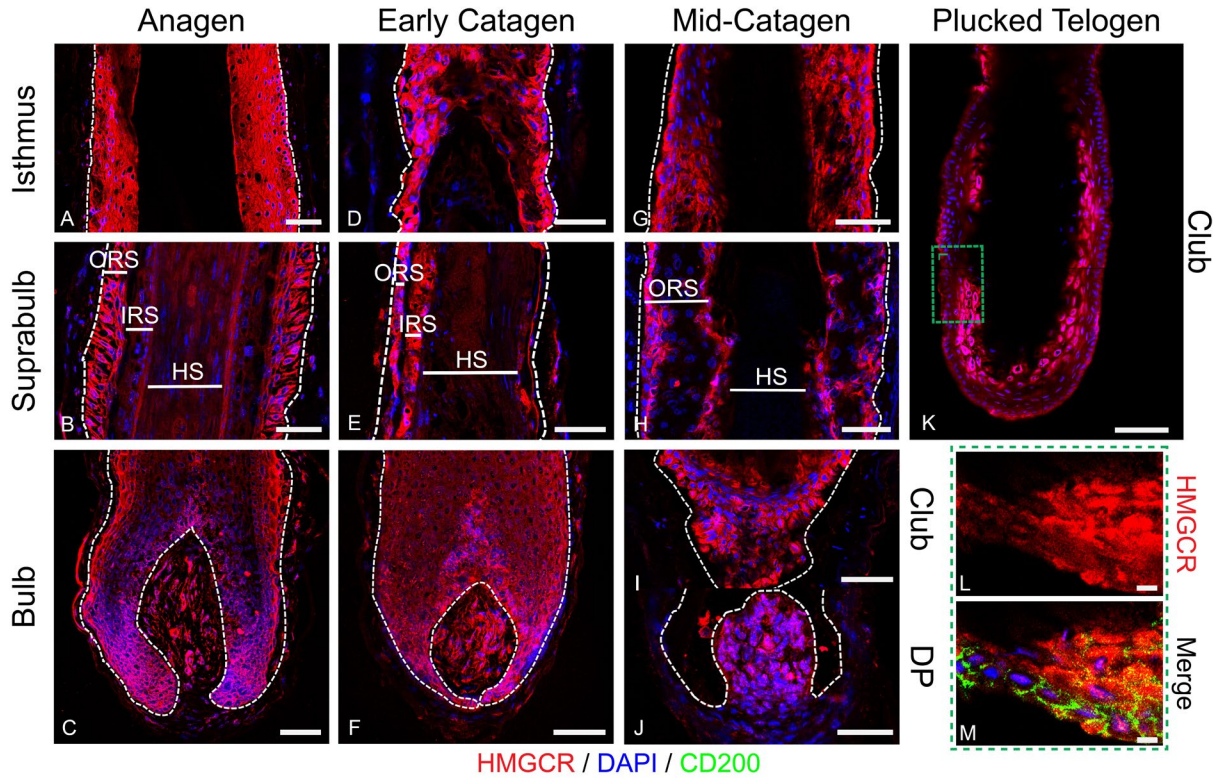
Figure 5.5 HMGCR is expressed in the outer root sheath and dermal papilla throughout the hair cycle. HMGCR immunofluorescence staining (red) in anagen (A,D,G), early catagen (B,E,H) and mid-catagen (C,F,I,J) HFs with DAPI counterstaining (blue). Dashed white lines showing epithelial components. Scale bars 50 μm. Green dashed box delineates magnified images, scale bar 5 μm. Telogen bulge marker CD200 (green) (M). ORS; outer root sheath, IRS; inner root sheath, HS; hair shaft. Representative images from n=3 donors, with imaging performed in 2-3 follicles per donor (except mid-catagen, n=2 donors, with 2 follicles per donor imaged).*Telogen green dashed box is representative field of view for magnified image and not actual image.
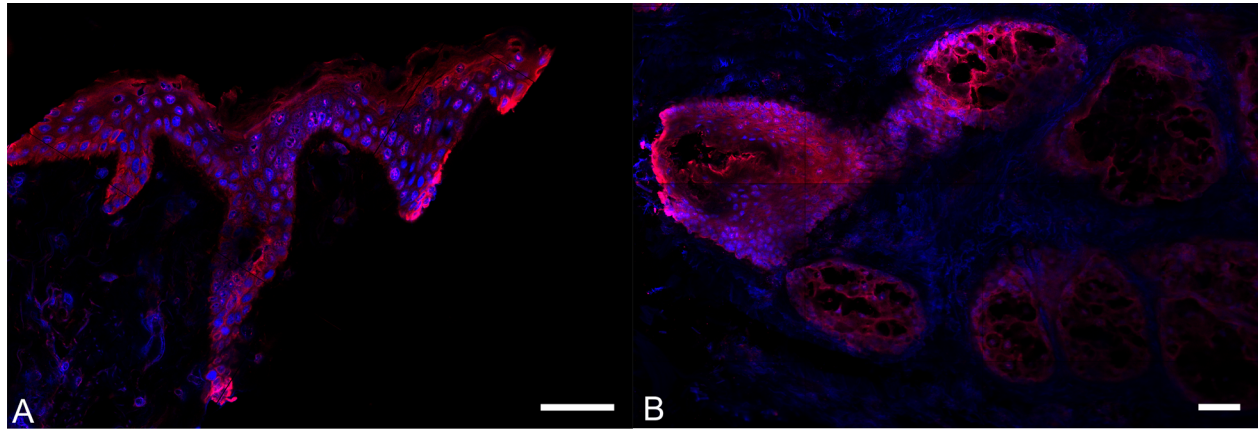
HMGCR / DAPI

Figure 5.6 HMGCR immunolocalisation in the pilosebaceous unit. HMGCR immunofluorescence staining (red) in the epidermis and sebaceous glands, counterstaining DAPI (Blue), scale bar 50 μm.

5.2.6 Filipin staining identifies distinct membrane cholesterol staining across the hair cycle with striations present in the basement membrane

Beyond examining the expression and localisation of proteins involved in cholesterol homeostasis, changes in FC distribution were investigated using filipin staining (Figure 5.7). During anagen, mesenchymal filipin staining was somewhat diffuse compared with the distinct membrane staining pattern seen in the HF keratinocytes (Figure 5.7A,B,C). Striations in filipin staining were present in the basement membrane of the ORS and CTS from the level of the suprabulbar region and continues into the isthmus but not the bulb (Figure 5.8).

To further investigate these striations, immunofluorescence staining of basement membrane protein laminin-332 was performed along with filipin staining. Images (Figure 5.8Aiii,Biii,) reveal that these cholesterol striations were present within the laminin-332 region, and increase in both volume and length in the epithelial strand of mid-catagen (Figure 5.8D,E). This is in contrast with the basement membrane of the epidermis, where no filipin-stained striations were observed in the laminin-332 region (Figure 5.8C), suggesting that this pattern of cholesterol is distinct to the basement membrane distal HF bulb.

Within the ORS both membrane and cytoplasmic filipin staining could be observed (Figure 5.7A). The greatest intensity membrane staining was found within the IRS (Figure 5.7D), particularly in the Cu and Hu. Within the HS, both the HC and Co had distinctive membrane staining. FC was present throughout the CTS, particularly within the DP stalk Figure 5.7 C).

A similar pattern of filipin staining was observed during early catagen (Figure 5.7E,F,G). Notably, filipin staining within the matrix keratinocytes (Figure 5.7G) was of higher intensity than observed in the anagen HFs. During mid-catagen filipin levels in the ORS remained high (Figure 5.7H). At the level of the club hair, filipin staining is notably lower and more diffuse (Figure 5.7J).

Filipin staining in plucked telogen HFs showed that both layers of the bulge had a highly membranous staining pattern (Figure 5.7L,M).
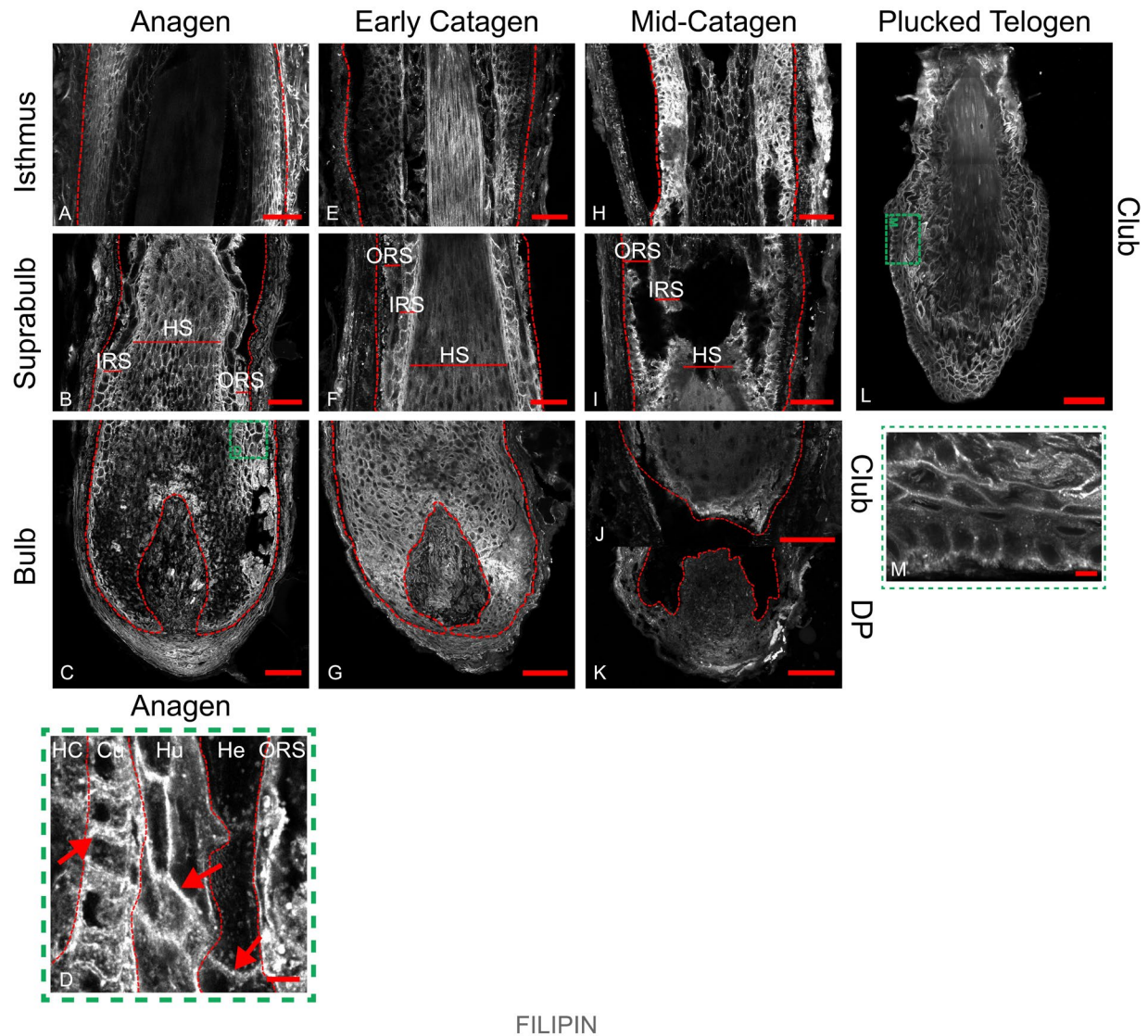
Figure 5.7 Differential expression of cholesterol throughout the hair cycle. Filipin immunofluorescence staining (grey scale) in HF tissue sections of anagen (A,B,C,D,H), early catagen (E,F,G), mid-catagen (I,J,K,L,M), plucked telogen (N,O) HFs, and epidermis (P). Red dashed lines showing epithelial components, scale bars 50 µm. Magnified images represented by the green dashed box, scale bars 5 µm. Membrane staining indicated by the red arrows (D). ORS; outer root sheath, IRS; inner root sheath, HS; hair shaft, HC; hair cuticle, Cu; cuticle, Hu; Huxley's layer, He; Henle's layer, Representative images from n=3 donors, with imaging performed in 2-3 follicles per donor (except mid-catagen, n=2 donors, with 2 follicles per donor imaged).
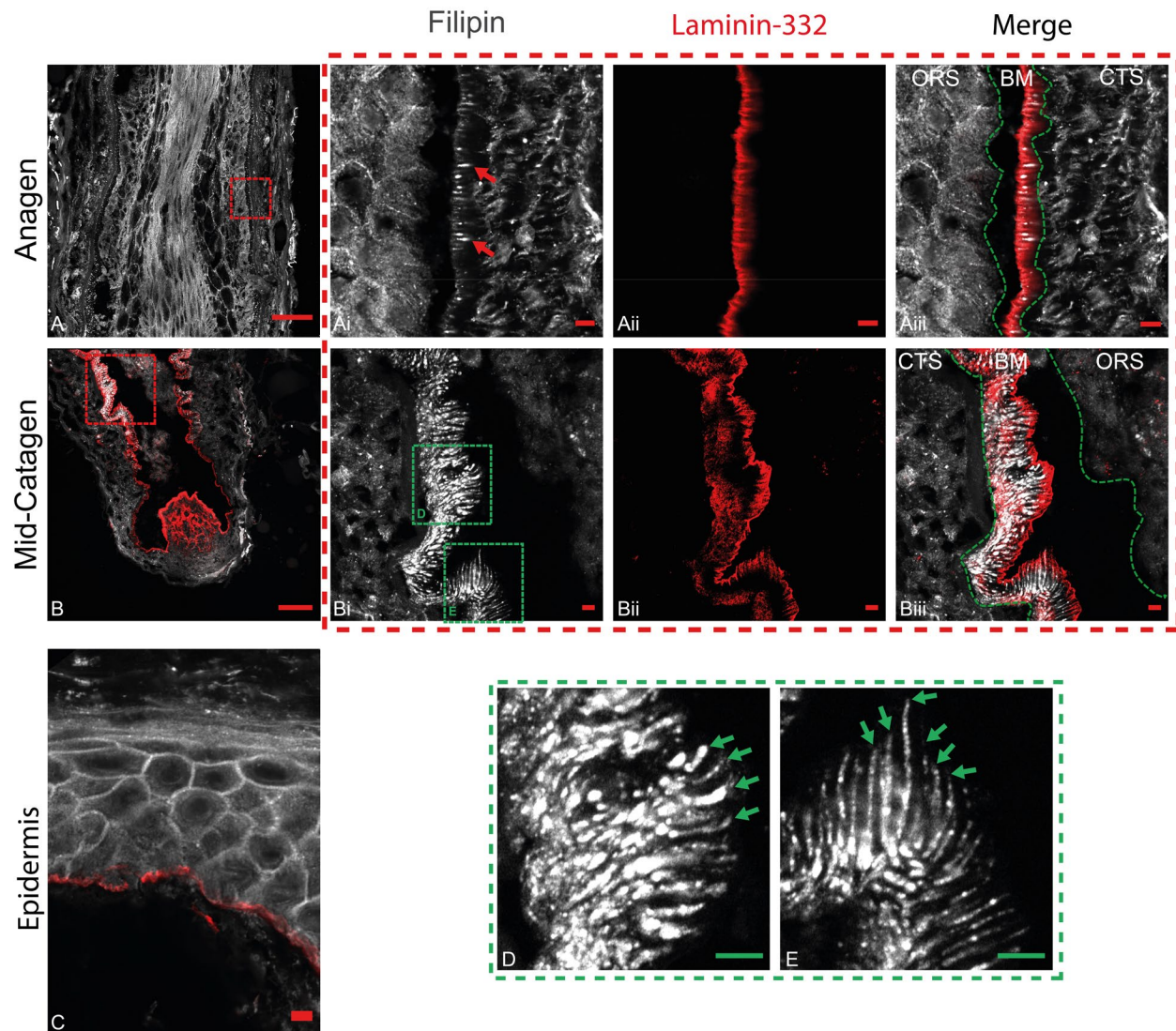
Figure 5.8 Cholesterol striations are unique to the basement membrane of hair follicles. Freshly isolated anagen (A), mid-catagen (B,D,E) and epidermis (C), co-localisation of Filipin (grey) with Laminin-332 (red). Basement membrane outlined with green dashed line. (C) Epidermis shows cholesterol staining within the membranes of the epidermis, whereas epidermal basement membrane as shown by laminin-332 staining does not contain striations of cholesterol. Striations of cholesterol within the basement membrane of (Ai) anagen (red arrows) and (D,E) mid-catagen (green arrows). Scale bar 50 μm or dashed box delineates magnified area, scale bars 5 μm, green dashed box delineates magnified area from mid-catagen. *Anagen is representative field of view for magnified image of upper suprabulbar area (A) and not actual image. Representative images from 3 donors (anagen), 2 donors (mid-catagen) and 3 donors (epidermis), with imaging performed in 2-3 follicles per donor.

5.2.7 Cholesterol transporters are dynamically regulated by activation of liver X receptor in human hair follicles

Beyond determining changes in the distribution of proteins involved in cholesterol transport and synthesis in the HF, changes in the expression of these cholesterol homeostatic genes were examined. Their regulation by LXR, an important transcription factor in the control of cholesterol homeostasis, was determined in HFs following a 24-hour incubation with the LXR agonist T0901317.

The expression of *ABCA1* and *ABCG1* increased in response to LXR activation in HFs, whereas *SCARB1* was reduced (Figure 5.9A). Next HFs were cultured with 25 µM FC for 24-hours. Uncharacteristically, a significant reduction in *ABCA1* was detected. Large variations were found across donors in the expression of *ABCA5, ABCG1, SCARB1* and *HMGCR* in response to exogenous cholesterol loading (Figure 5.9B).

The effects of cholesterol depletion on cholesterol transporters in the HFs were next examined by addition of 5 mM MβCD for 1-hour, followed by a 23-hour recovery period. In Figure 5.9C, a large variation in expression levels was seen between donors, however consistent increases in gene expression were detected for cholesterol biosynthesis enzyme *HMGCR*. This suggests that HFs are capable of *de novo* cholesterol synthesis during period of cholesterol starvation.
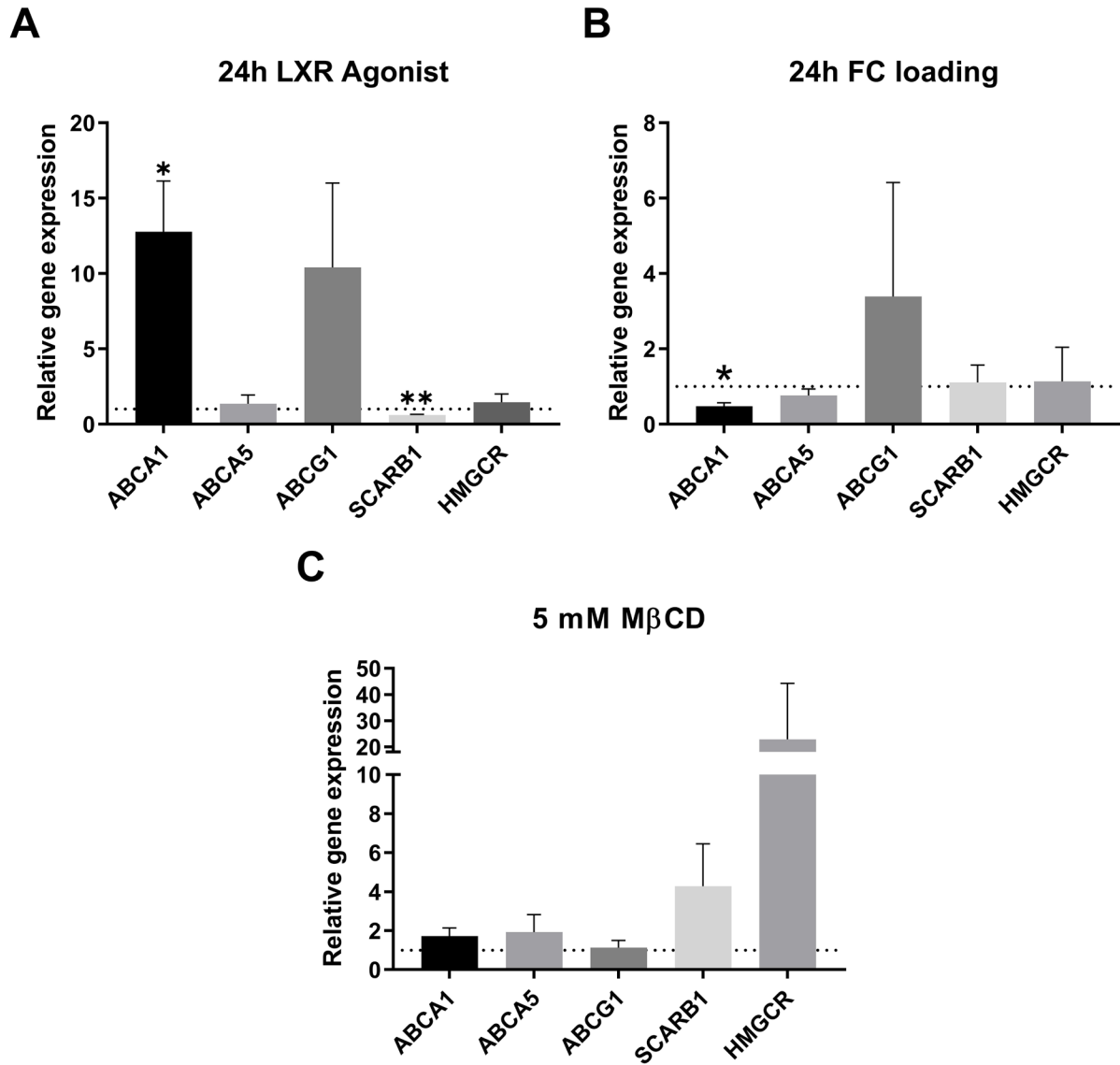
Figure 5.9 Cholesterol transporters are differentially expressed in the hair follicle with liver X receptor activation. Gene expression changes in HFs treated with (A) 5 µM T0901317, (B) 25 µM FC for 24-hours, (C) 1 mM MβCD for 1-hour + 23-hours recovery. Gene expression reported relative to vehicle control and normalised to *PPIA*. Data are mean ± SEM for n=4 donors. One sample t test performed; significance denoted by * p≤0.05, ** P<0.01.

5.3 Discussion

This chapter describes the expression, localisation and regulation of transport proteins involved in cholesterol homeostasis across the human hair cycle. ABCA1 and ABCG1, two highly characterised proteins involved in modulating intracellular cholesterol levels, displayed both membranous and intracellular staining patterns as previously described (Neufeld *et al.*, 2001). ABCA5, a putative cholesterol transporter implicated in a form of heritable hypertrichosis (DeStefano *et al.*, 2014, Hayashi *et al.*, 2017) also localised to both the plasma membrane and intracellular compartments. The bi-directional cholesterol transporter SCARB1 was highly expressed in the DP basement membrane, suggesting a possible role in modulating movement of sterols between the DP and matrix keratinocytes. HMGCR was highly expressed in keratinocytes throughout the hair cycle, indicating *de novo* cholesterol synthesis capacity is maintained from anagen through to telogen. Variations in expression of these proteins across the hair cycle suggest that cholesterol transport and homeostasis is dynamically regulated, changing to meet cellular needs during different hair cycle phases. Furthermore, these data suggest that LXR activity plays a role in regulating cholesterol transporter expression and activity in HF cell populations.

Whereas the expression of ABCA1 in anagen HFs has been described previously (Haslam *et al.*, 2015), the data shown here expands on this analysis to include catagen and telogen follicles. Cellular localisation of ABCA1 is dependent on both HF region and hair cycle stage, with matrix keratinocytes of anagen and early catagen HFs showing plasma membrane staining, whereas expression at the nuclear periphery is apparent within the isthmus of catagen HFs and telogen club hairs. These changes in the subcellular localisation of ABCA1 would be expected to alter cholesterol efflux capacity. Although ABCA1 is understood to shuttle between endosomal compartments and the plasma membrane, loss of membrane staining would reduce the efflux of FC to APOA1 (Phillips, 2014). As such, the upper permanent regions of the HF and the telogen follicle may have a reduced need for cholesterol efflux when compared to the lower cycling portions.

Indeed, this is supported by the observation that the expression of ABCG1 and SCARB1 are reduced as the HF moves through catagen and into telogen. Whilst expression of HMGCR remains high, this does not necessarily reflect high levels of cholesterol synthesis activity, which would need to be confirmed using biochemical assays (Zhang *et al.*, 2015).

Translocation of ABCA1 to the Golgi, and therefore the plasma membrane, is inhibited *via* an interaction of ABCA1 with serine palmitoyltransferase 1 (SPTCL1), a key enzyme in sphingolipid biosynthesis (Kardassis *et al.*, 2015). The ABCA1-SPTCL1 complex is speculated to play a role in enhancing both cholesterol and phospholipid biosynthesis, along with the inhibition of cholesterol efflux (Tamehiro *et al.*, 2008). Furthermore, from a HF perspective, sphingolipid treatment results in earlier telogen to anagen transition (Park *et al.*, 2017), and knockdown of sphingolipid synthesis in *Fa2h⁻/⁻* mice (fatty acid 2-hydroxylase) resulted in hair loss during telogen (Maier *et al.*, 2011). In addition, inhibition of sphingolipid enzymes results in an early second telogen to anagen transition in both alkaline ceramidase 1 (*Acer1⁻/⁻*) (Lin *et al.*, 2017) and ceramide synthase 4 (*Cers4⁻/⁻*) mice (Peters *et al.*, 2015), which are associated with a reduction in BMP and increase in Wnt/β-catenin signalling. Therefore, the expression of ABCA1 at the periphery of the nucleus in club hairs may indicate a role for ABCA1 in sphingolipid synthesis and transport during this hair cycle stage.

ABCG1 gene expression has previously been identified in anagen HFs (Haslam *et al.*, 2015), with protein expression noted in keratinocytes and murine epidermis (Jiang *et al.*, 2010, Marko *et al.*, 2012). The human protein atlas suggests low expression within the epidermis and ORS of the infundibulum, absence from the dermal fibroblasts and a moderate level within the SG (Uhlen *et al.*, 2015). In agreement with this, ABCG1 expression is not detected in the CTS, however low levels are found within the DP and DP stalk. Jiang *et al.* (2010) demonstrate ABCG1 expression in the more differentiated layers of murine epidermis, SG and at the isthmus of the HF.

In addition to cholesterol, ABCG1 mediates the transport of oxysterols (Engel *et al.*, 2007) and intermediates of cholesterol biosynthesis (Wang *et al.*, 2008), which are thought to play a role in preventing oxysterol induced apoptosis (Aye *et al.*, 2010, Engel *et al.*, 2007). The accumulation of cholesterol intermediates in the HF results in hair loss and cycling disorders (Evers *et al.*, 2010, Zhang *et al.*, 2017, Karnik *et al.*, 2009) (as discussed further in Chapter 1 and Palmer *et al.* (2020)), yet this study detects only low levels of ABCG1. This may indicate some functional redundancy, with other transport proteins contributing to oxysterol efflux in the HF or suggest the presence of relatively low levels of oxysterols.

ABCA5 is a less well studied ABC transporter, yet its impact on HF biology has been uncovered following identification of mutations that result in a congenital hypertrichosis (DeStefano *et al.*, 2014). Although the specific allocrite remains to be identified, overexpression of this protein is linked to enhanced cholesterol efflux to APOE (Fu *et al.*, 2015), and knockout of *Abca5* in murine macrophages lowers HDL efflux (Ye *et al.*, 2010). Within the HF, ABCA5 expression is

predominantly cytoplasmic, with the exception of the HC. Murine studies have indicated localisation to lysosomes and late endosomes (Kubo *et al.*, 2005), and cholesterol has been observed to accumulate within the lysosomes of keratinocytes derived from congenital hypertrichosis patients carrying ABCA5 mutations (DeStefano *et al.*, 2014). Chapter 3 confirmed the intracellular localisation of ABCA5 in ORS keratinocytes, with co-localisation to endo-lysosomes, ER and mitochondria. The cytoplasmic localisation of ABCA5 identified here could suggest an involvement in intracellular cholesterol transport within human HFs, as described in other cell types.

Unlike ABC transporters the unique bi-directional transporter SCARB1 facilitates diffusional cholesterol movement (Shen *et al.*, 2018b). Predominantly responsible for the uptake of CE from HDL, SCARB1 can also participate in the efflux of FC to HDL (Shen *et al.*, 2018b). The protein has several additional functions, including bacterial detection (Guo *et al.*, 2014), and transport of carotenoids (Shyam *et al.*, 2017) and vitamins (Reboul *et al.*, 2011, Reboul *et al.*, 2006). As pharmacological inhibition of SCARB1 reduced cholesterol efflux, as shown in Chapter 3, a role in cholesterol transport in the HF seems likely. SCARB1 expression in skin has been previously shown, along with the SG, where the expression was cytoplasmic with a higher level in the basal layer (Crivellari *et al.*, 2017, Sticozzi *et al.*, 2012). This chapter observed membrane staining in the ORS and the He of the bulb, whereas other cellular layers have less defined cytoplasmic staining. Uptake of cholesterol *via* SCARB1 occurs *via* internalisation of the receptor and bound HDL particles (Marques *et al.*, 2019), leading to lysosomal distribution.

SCARB1 plays a vital role in the facilitation of cholesterol for steroidogenesis (Gordon *et al.*, 2019) and the influence of steroid hormones on HF behaviours has been previously described (Cattet *et al.*, 2017, Randall, 2008, Sawaya, 1991, Schweikert and Wilson, 1974). Yet it remains unclear if steroidogenesis occurs within the HF, or if circulating steroid hormones regulate HF biology. Although the HF appears capable of steroidogenesis, the relative influence of *de novo* synthesis versus uptake of circulating steroid hormones remains to be defined (Slominski *et al.*, 2013, Palmer *et al.*, 2020).

In keratinocytes, FC is predominantly distributed in the plasma membrane (Lange, 1991, Liscum and Underwood, 1995, Jans *et al.*, 2004), maintaining membrane fluidity and coordinating lipid rafts (McGuinn and Mahoney, 2014). Intracellular cholesterol often undergoes oxidation, esterification or is metabolised to steroid hormones. Whereas the IRS and HS keratinocytes show prominent filipin membrane staining throughout the hair cycle, the ORS shows mixed

membrane/cytoplasmic filipin staining. These unique patterns of FC distribution may indicate differing requirements for cholesterol across HF compartments.

Strikingly, when examining filipin staining patterns, cholesterol striations were observed within the basement membrane of suprabulbar and isthmus regions, but not the bulb (Figure 5.8). The extracellular matrix separating the epithelial and mesenchymal compartments of the HF is predominantly composed of collagen IV and laminin (Chermnykh *et al.*, 2018). Previous studies in macrophages have shown that both ABCA1 and ABCG1 can deposit cholesterol within the extracellular matrix (Jin *et al.*, 2015, Jin *et al.*, 2016). These cholesterol deposits have been described as both needles and plates ranging from 4 to 50 µm in size (Suhalim *et al.*, 2012b).

Movement of HDL but not LDL has been noted within the basement membranes of the testis (Fofana *et al.*, 1996). Where circulating lipoproteins are rich in CE, FC resides within lipoprotein membranes and is associated with discoidal APO leading to nascent HDL (Clay and Barter, 1996). Moreover treatment of astrocytes with MβCD resulted in a decrease in laminin (Freire *et al.*, 2004). Whereas treatment of CS results in the degradation of laminin-332 (Yamamoto *et al.*, 2010), knockdown of the α3 chain of laminin-332 leads to the increase in cholesterol biosynthesis genes in keratinocytes, in addition a disruption of cholesterol trafficking to the plasma membrane was observed (Jones *et al.*, 2019, Jones *et al.*, 2018). The cholesterol striations identified in the HF basement membrane may represent an interaction of cholesterol with laminin-332 during cholesterol movement from CTS to ORS, or deposits of excess cholesterol monohydrate needles, however additional experiments are required to confirm this.

Within the HF, *de novo* cholesterol synthesis appears to primarily occur within the ORS and the DP, given the presence of a rich immunofluorescence staining for HMGCR. Uptake of cholesterol from circulating lipoproteins (LDL) may furnish capillary network in these regions (Yen and Braverman, 1976, Braverman and Yen, 1977). Indeed, the LDLR was previously found to be present in various regions of the HF, yet it was suggested to be non-functional given the lack of regulatory response to addition of LDL in *ex vivo* HF cultures, nor were any changes detected in subjects with hypercholesterolemia (Brannan *et al.*, 1975).

Chapter 4 demonstrated alterations to Wnt signalling with cholesterol loading and depletion. Lipid modifications of Shh are required for sufficient downstream signalling (Porter *et al.*, 1996). With the localisation of membranous ABCA1 and SCARB1 in the ORS, along with polarity of ABCA1 to the basal layer of the ORS of the isthmus, it would appear that cholesterol synthesised within

the ORS may be effluxed into the basement membrane. Here it could play a role in modifying Shh activity, a pathway integral to the maintenance of the bulge stem cell niche (Rittie *et al.*, 2009).

Regulation of cholesterol efflux by LXR agonism is well established (Wang *et al.*, 2006, Zanotti *et al.*, 2008). The data in this chapter shows that T0901317 agonism of LXR increased *ABCA1/ABCG1* expression, as previously reported (Jiang *et al.*, 2006, Jiang *et al.*, 2010). Cholesterol efflux from ABCG1 to HDL is well documented (Zanotti *et al.*, 2008) and the transcriptional changes observed correlate with this function in the HF. There is some evidence for LXR activation of SCARB1, however regulation in steroidogenic tissues is achieved through trophic hormones (Komaromy *et al.*, 1996, Rigotti *et al.*, 1996, Shen *et al.*, 2018b). Chapter 3 demonstrated that neither gene nor protein expression of SCARB1 in ORS keratinocytes responded to LXR agonism. This is yet to be established in the HF, which has its own, comparatively limited capacity for steroidogenesis (Slominski *et al.*, 2013).

Uncharacteristically 24-hour treatment with 25 µM FC significantly reduced *ABCA1* gene expression in HF organ culture. Given that, during early catagen, no expression of cholesterol transporters was detected and *HMGCR* gene expression was reduced, these changes may be due to hair cycle changes, as opposed to being directly related to FC loading. As a caveat, it should be noted that these data is preliminary and requires further investigation.

The differential patterns of cholesterol transporter expression identified in this chapter suggest dynamic changes in cholesterol requirements across the hair cycle. Furthermore, preliminary functional data indicate a role for LXR activity in modulating cholesterol transport activity. Future studies focusing on regulation of cholesterol transport during the hair cycle are needed to shed more light on the role of cholesterol homeostasis in hair growth.

Chapter 6: Cholesterol homeostasis in hair follicle keratinocytes is disrupted by impaired ABCA5 activity

6.1 Introduction

ABCA5 has yet to be assigned a conclusive function and specific allocrites remain unknown. Of the evidence currently available, there has been some suggestion that this membrane protein plays a role in cholesterol transport and/or trafficking, which enables it to influence both the efflux of cholesterol across the plasma membrane (Fu *et al.*, 2015, Ye *et al.*, 2010) as well as intracellular accumulation within cytosolic compartments (Kubo *et al.*, 2005). Recently, mutations in *ABCA5* were also associated with a form of congenital hypertrichosis (DeStefano *et al.*, 2014, Hayashi *et al.*, 2017) with the suggestion that the observed phenotypic hair overgrowth was related to altered accumulation of FC within HF keratinocytes (DeStefano *et al.*, 2014).

Chapter 5 detailed ABCA5 expression and localisation in human HFs; ABCA5 staining was detected in both the epithelial and mesenchymal regions of the HF. Expression was noted in the matrix keratinocytes and ORS, being strongest in the IRS. ABCA5 immunofluorescence was also detected in the DP and sporadically in the CTS. The pattern of expression largely matches that reported by DeStefano *et al.* (2014). As such, a role for ABCA5 in HF-derived ORS keratinocytes was examined.

This chapter aims to determine the impact of loss of ABCA5 activity on ORS keratinocytes with a view to generating insights into:

1.   The role of ABCA5 in cholesterol homeostasis in the HF

2.   Potential mechanisms relating to hypertrichosis through ABCA5 loss-of-function mutation.

6.2 Results

6.2.1 ABCA5 siRNA reduces half transporter

Firstly, a model for reduced ABCA5 activity was established in ORS keratinocytes using siRNA-mediated knockdown. A 79.1% reduction in mRNA was achieved after 24-hours (Figure 6.1B). Immunofluorescence staining (Figure 6.1A) was utilised to detect overall changes in protein expression, which revealed a 21.8% reduction in mean ABCA5 immunofluorescence pixel intensity (Figure 6.1C). Western blotting (Figure 6.1D) showed a 69.9% reduction in the 99 kDa ABCA5 protein (Figure 6.1E). Additionally, the oligomeric 400 kDa ABCA5 protein shows a 49.7% reduction (P=0.062).

Following successful knockdown of ABCA5 expression, it was examined whether this influenced cellular response to exogenous cholesterol loading.
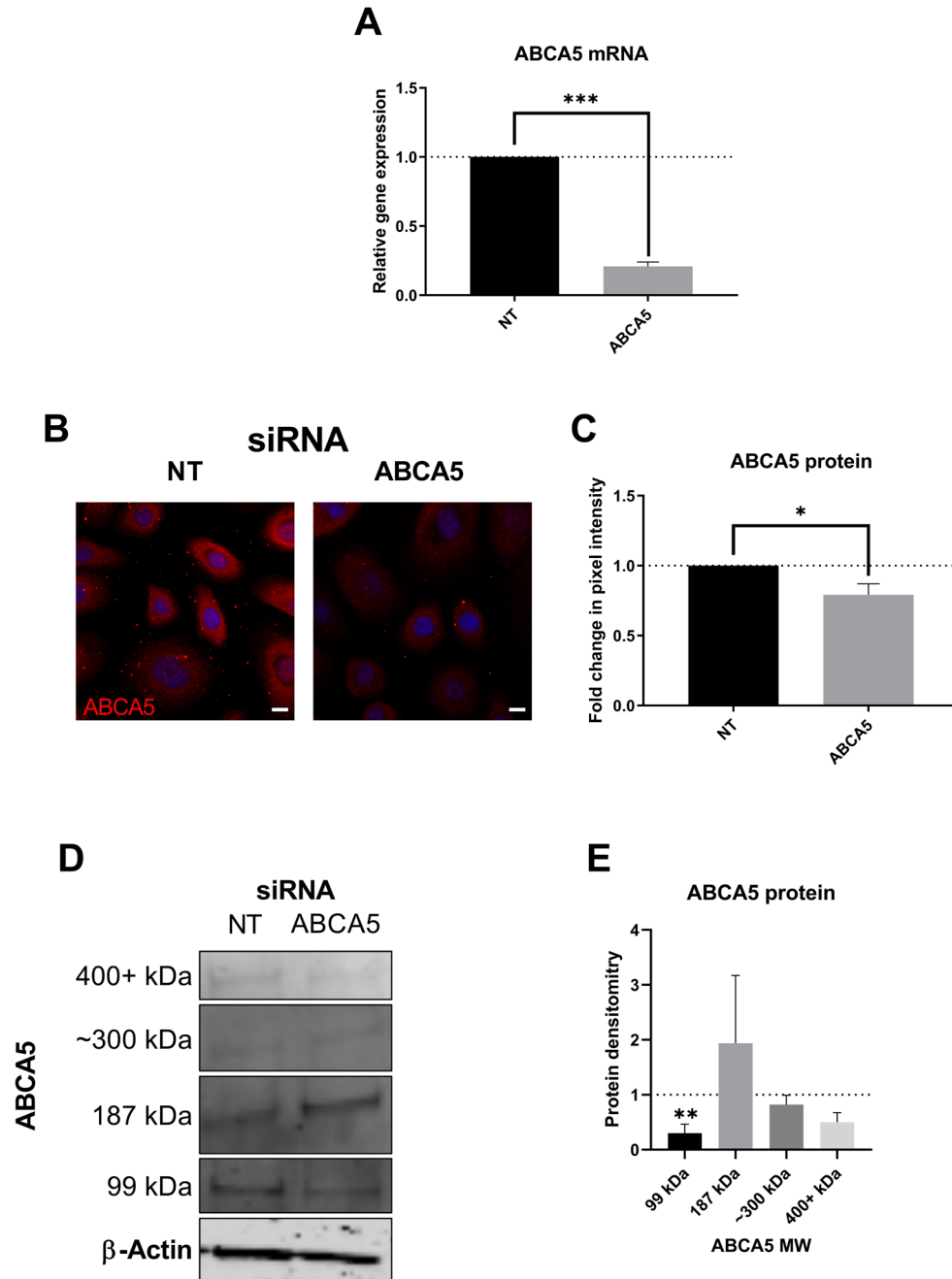
Figure 6.1 ABCA5 mRNA and protein levels are significantly reduced with siRNA. **(**A) ABCA5 immunocytochemistry staining (red) in ORS keratinocytes transfected with NT control or *ABCA5* siRNA for 72-hours. Scale bars 10 µm, counterstained with DAPI (blue) for nuclei. (B) *ABCA5* gene expression changes in ORS keratinocytes transfected with NT or *ABCA5* siRNA for 24-hours show a significant reduction in mRNA. Gene expression relative to NT and normalised to *PPIA*. (C) Fold change in mean pixel intensity per cell of ABCA5 immunocytochemistry staining. (D) Western blot for ABCA5 in ORS keratinocytes transfected with NT or ABCA5 siRNA for 72-hours. (E) Protein densitometry values relative to NT and normalised to reference protein β-Actin. Data are mean ± SEM for n=4 donors. One sample t-test performed; significance denoted by * P<0.05, ** P<0.01, *** P<0.005.

6.2.2 ABCA5 knockdown alters cholesterol distribution following exogenous loading

ORS keratinocytes were exposed to a physiological level (25 µM) of FC (Shiigi *et al.*, 2008) in the presence or absence of *ABCA5* siRNA. Changes in distribution of FC were determined by filipin staining (Figure 6.2) and CTX-FITC flow cytometry (Figure 6.4), to detect total FC and membrane cholesterol levels, respectively.

FC loading in ORS keratinocytes led to a significant increase in total (Figure 6.3D) and endo-lysosomal cholesterol (Figure 6.3A), as shown *via* co-localisation with LAMP1 (Figure 6.2A). Knockdown of ABCA5 alone did not alter FC distribution in the absence of exogenous cholesterol loading. In ORS keratinocytes in which ABCA5 expression was reduced, exogenous cholesterol did not result in a significant increase in total cholesterol, with significantly lower filipin staining than NT control cells exposed to the same concentration of cholesterol (Figure 6.3D). Endo-lysosomal accumulation of cholesterol was also reduced (P=0.062 Figure 6.2A, Figure 6.3A). This suggested that loss of ABCA5 activity could reduce intracellular cholesterol trafficking to endo-lysosomes.

Furthermore, changes to ER cholesterol with FC loading were measured through co-localisation to PDI (Figure 6.2B). Small fluctuations of ER cholesterol levels were detected following exogenous cholesterol loading, however ABCA5 knockdown had no impact (Figure 6.3B). Next, mitochondrial cholesterol levels were measured through co-localisation with ATPB (Figure 6.2C). Mitochondria cholesterol levels were significantly reduced with the addition of FC, with no impact of *ABCA5* siRNA observed (Figure 6.3C).

CTX-FITC binds to the ganglioside receptor (GM1) within lipid rafts and was used as a method to quantify membrane cholesterol (Gniadecki *et al.*, 2002). Flow cytometry analysis (Figure 6.4) showed no change in membrane cholesterol following ABCA5 knockdown or exogenous cholesterol loading.
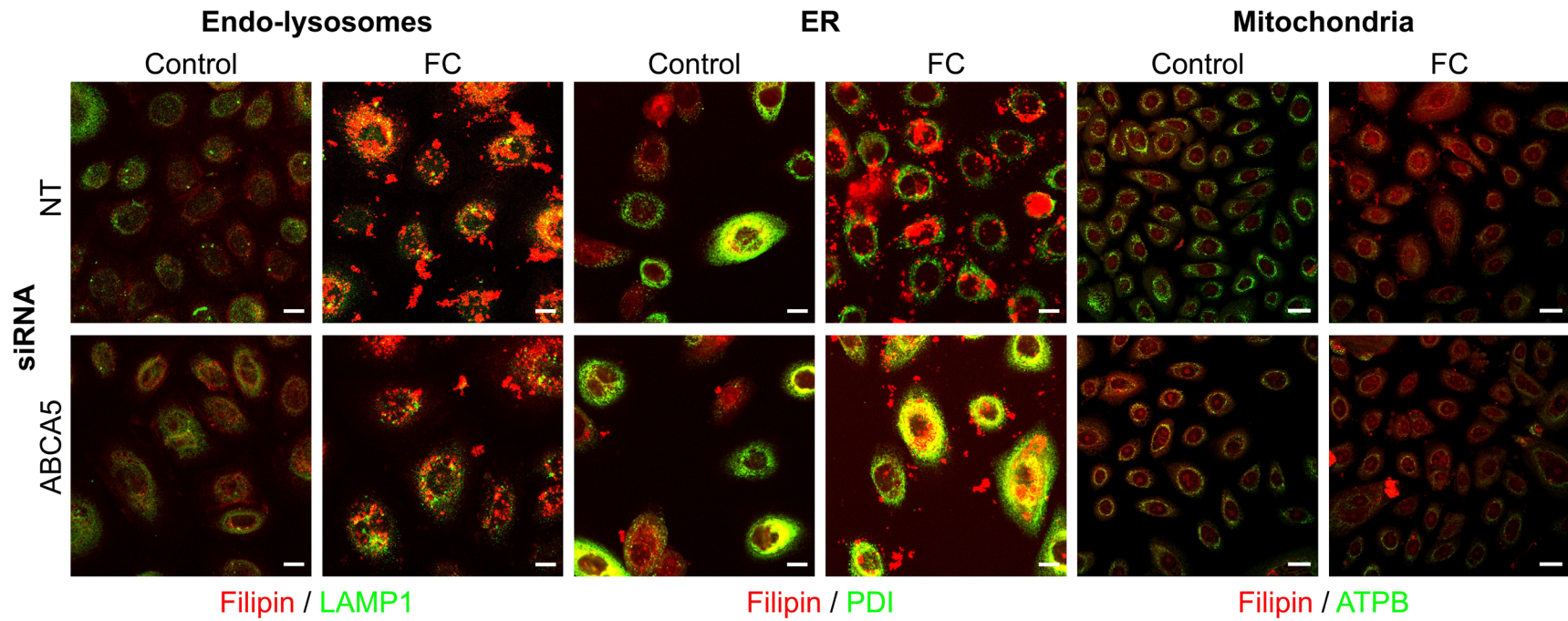
Figure 6.2 Filipin staining with ABCA5 knockdown. Filipin staining in ORS keratinocytes cells transfected with NT or *ABCA5* siRNA for 48-hours, with the addition of 25 µM FC for 24-hours. Dual immunocytochemistry staining was performed with antibodies for LAMP1 (A), PDI (B) and ATPB (C).
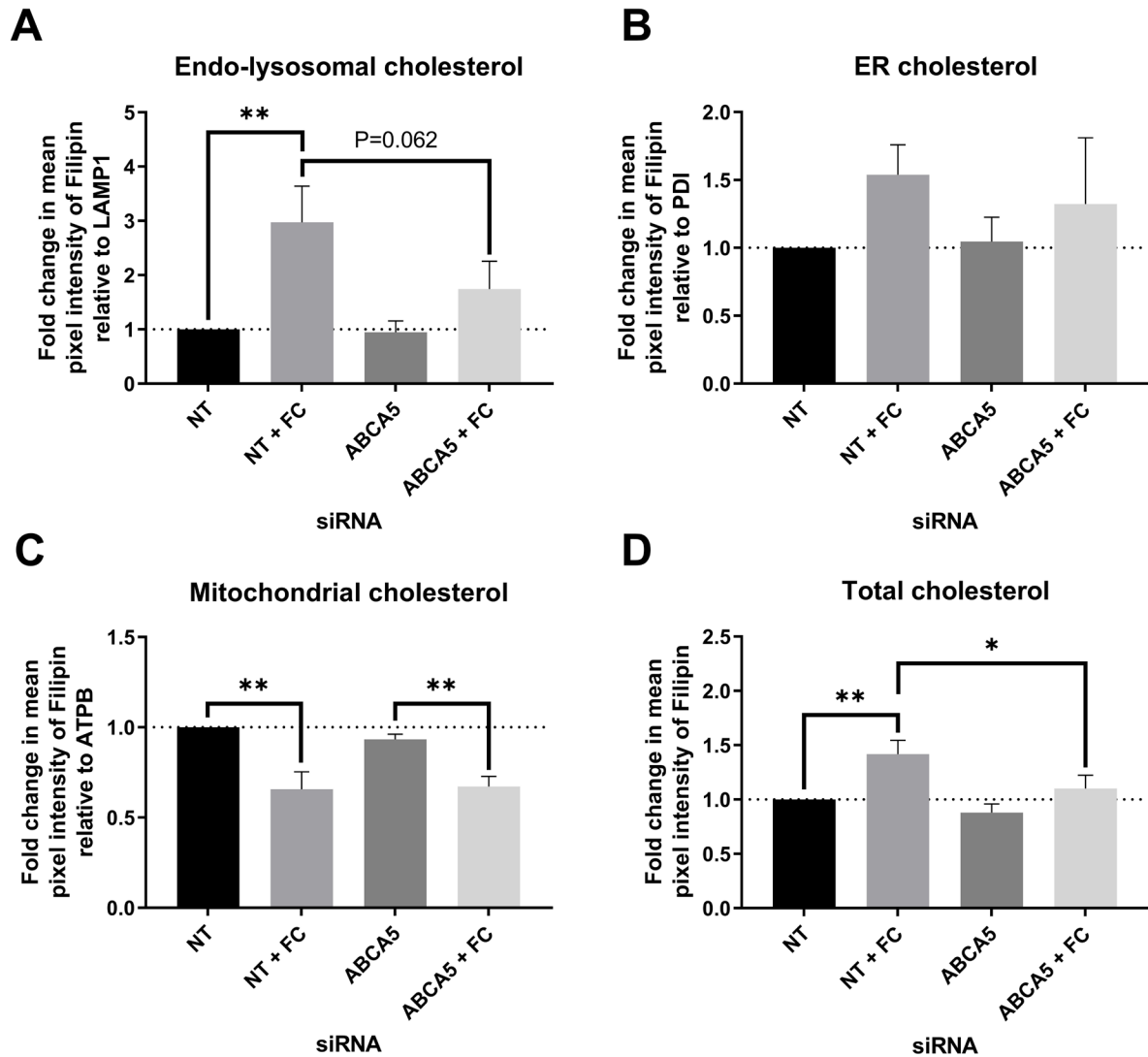
Figure 6.3 ABCA5 knockdown alters endo-lysosomal cholesterol. Analysis of filipin staining of fold change in mean pixel intensity masked to organelle marker (A-C) or total pixel intensity per cell (D). Data are mean ± SEM for n=4/5 donors, total n=13. One-way ANOVA were performed with Fisher's multiple comparisons test; significance denoted by * P≤0.05, ** P≤0.01, *** P≤0.005
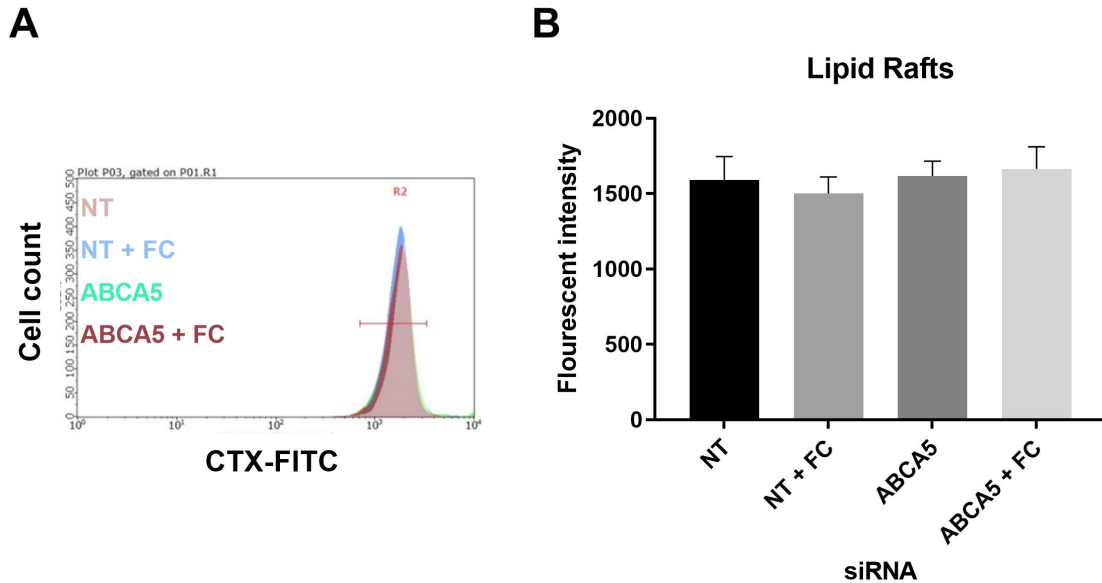
Figure 6.4 Lipid rafts remain unchanged with ABCA5 knockdown. (A) Flow cytometry plot of CTX-FITC stained ORS keratinocytes transfected with NT (pink) or *ABCA5* (green) siRNA for 48-hours, with the addition of 25 µM FC for 24-hours (A) (blue or maroon). (B) Analysis of median peek values, data are mean ± SEM n=4 donors.

Next live cell imaging using fluorescently-tagged cholesterol (BODIPY cholesterol) was utilised to determine cellular cholesterol distribution following exogenous loading. 25 µM BODIPY cholesterol was complexed 1:10 with MβCD to enable a rapid uptake of cholesterol for live cell tracking, as previously reported by Holtta-Vuori *et al.* (2016). Figure 6.5-Figure 6.7 show a time-lapse of 150-minutes with 30-minute intervals. Cholesterol first enters the plasma membrane and accumulates intracellularly, increasing in intensity over time. Additionally, cells were stained with organelle trackers for endo-lysosomes (Figure 6.5), ER (Figure 6.6) and mitochondria (Figure 6.7). Quantification of mean peak intensity values were obtained. A significant increase in cholesterol accumulation overtime was observed in all three compartments. Endo-lysosomal accumulation was significantly reduced by ABCA5 knockdown (Figure 6.8A), confirming changes detected with filipin staining (Figure 6.2D). Furthermore, significant reductions were detected between NT and *ABCA5* siRNA for the time points of 30, 90, 120 and 150-minutes (P=0.035, 0.044, 0.034, 0.048, respectively). No changes were observed in accumulation within the ER (Figure 6.8B). There was a small but non-significant decrease in mitochondrial cholesterol accumulation (Figure 6.8C). *ABCA5* siRNA knockdown had no impact on the total accumulation of BODIPY-cholesterol (Figure 6.8D).

Time (mins)
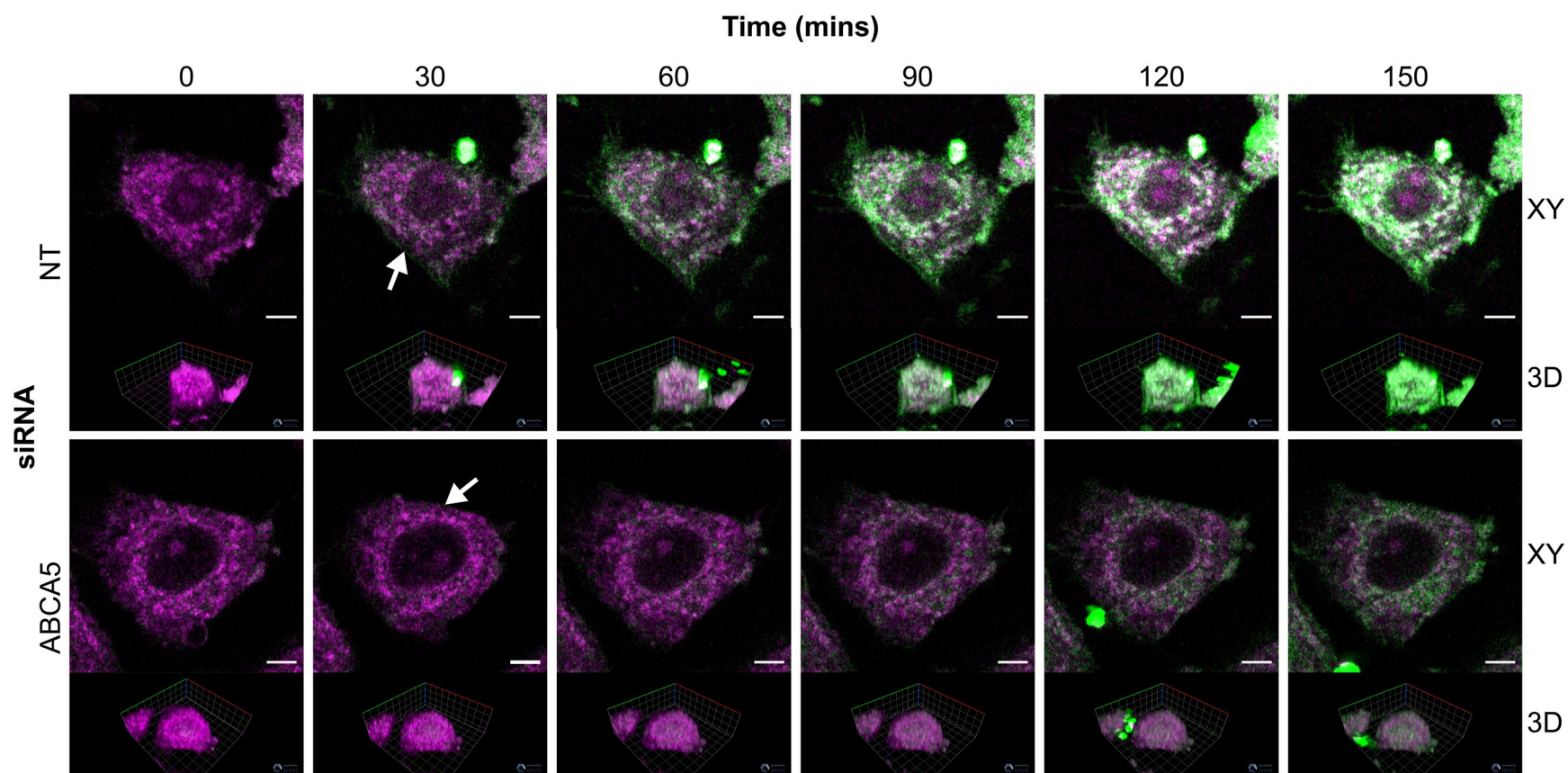
LysoTracker / BODIPY Cholesterol

Figure 6.5 Endo-lysosomal cholesterol accumulation is significantly reduced in ABCA5 knockdown outer root sheath keratinocytes. ORS keratinocytes cells transfected with NT or *ABCA5* siRNA for 48-hours incubated with 25 µM of BODIPY cholesterol (green) and LysoTracker (magenta). Time-lapse images taken at 30-minute intervals for 150-minutes. 3D images show total distribution of BODIPY within the cell. BODIPY in plasma membrane represented by white arrows. Scale bars 5 µm.

Time (mins)

| 0 | 30 | 60 | 90 | 120 | 150 |

ER Cytopainter / BODIPY Cholesterol
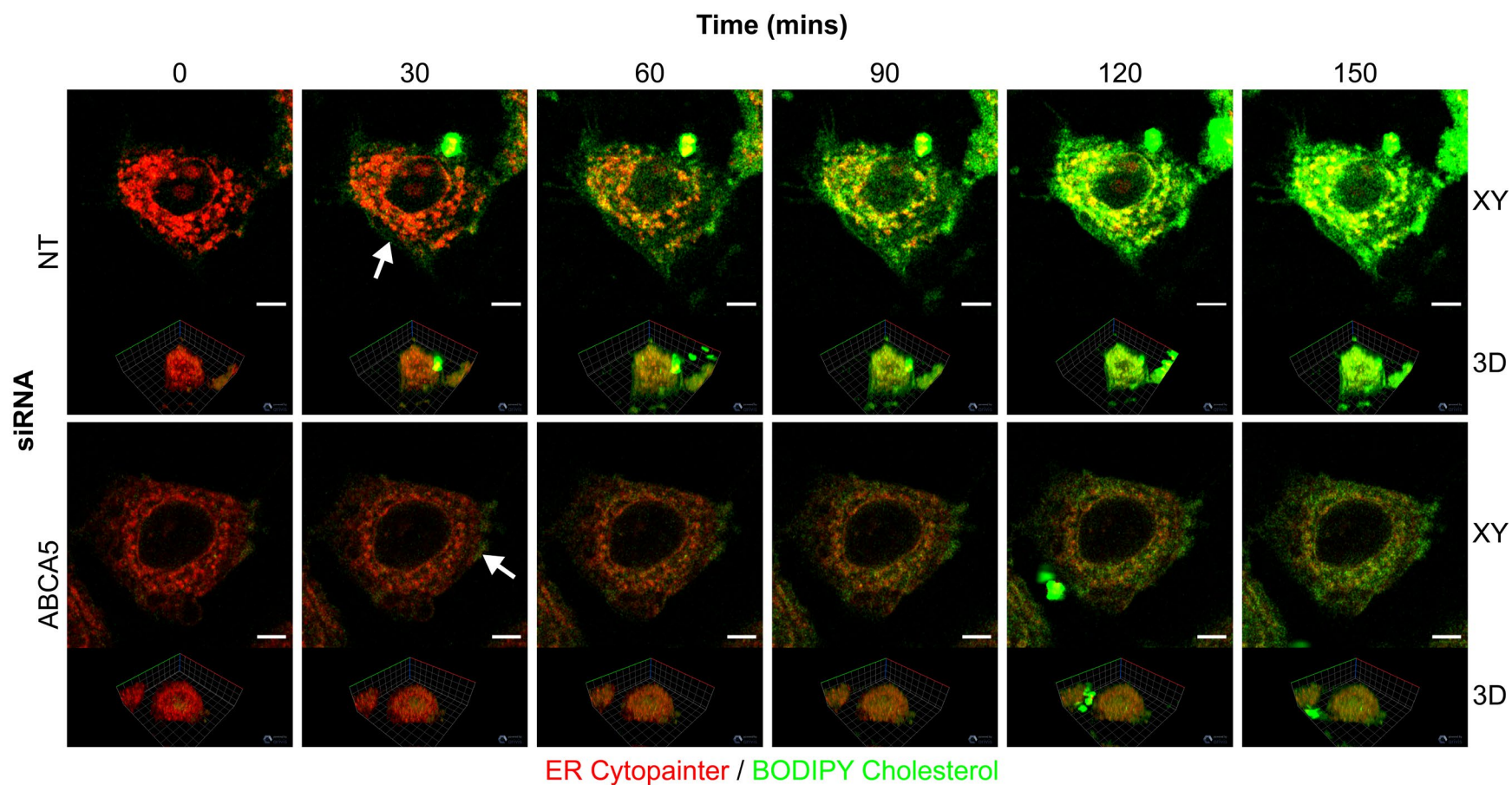
Figure 6.6 Endoplasmic reticulum cholesterol accumulation in ABCA5 knockdown outer root sheath keratinocytes. ORS keratinocytes cells transfected with NT or *ABCA5* siRNA for 48-hours incubated with 25 µM of BODIPY cholesterol (green) and ER Cytopainter (red). Time-lapse images taken at 30-minute intervals for 150-minutes. 3D images show total distribution of BODIPY within the cell. BODIPY in plasma membrane represented by white arrows. Scale bars 5 µm.

169
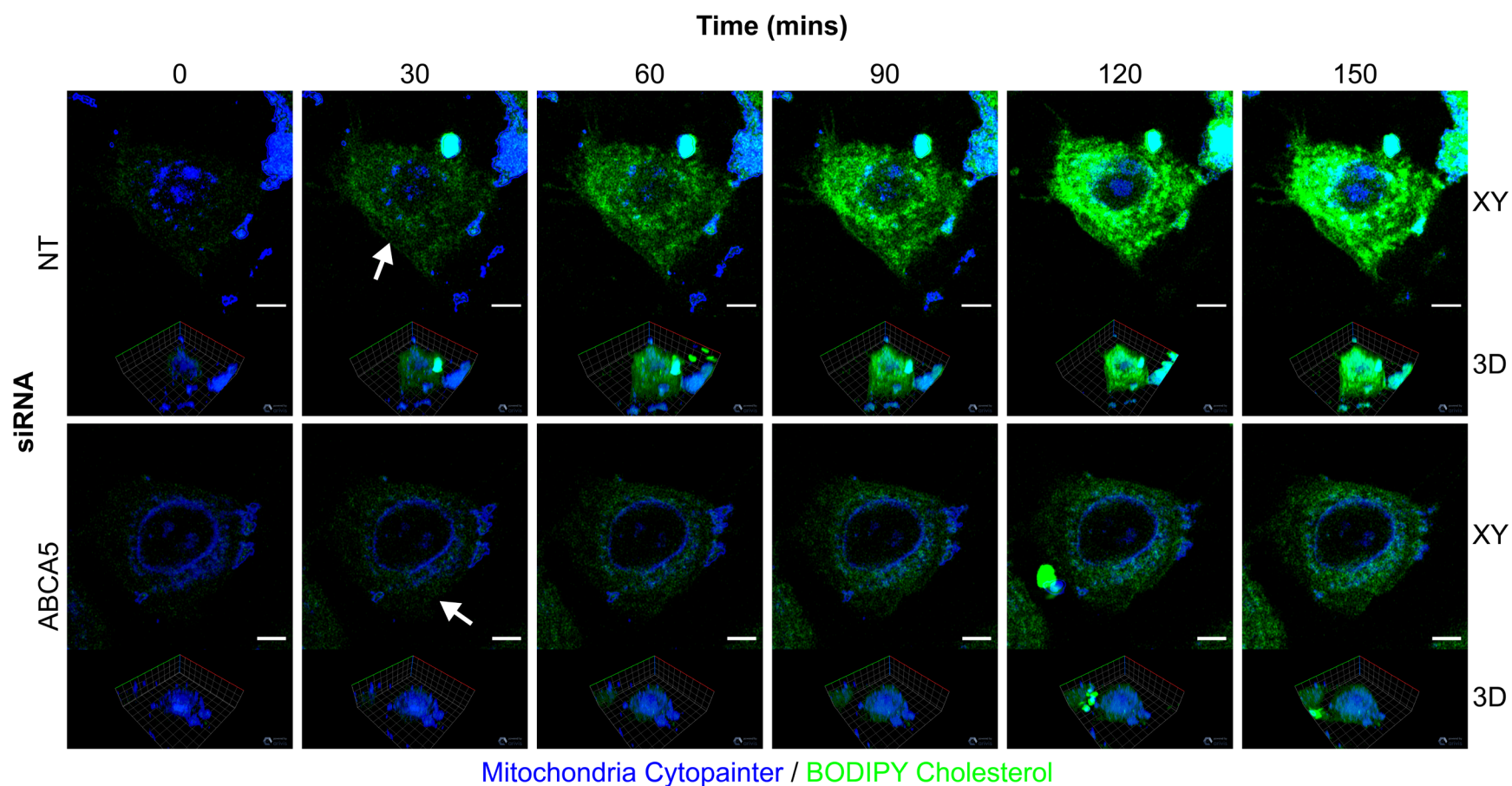
Figure 6.7 Mitochondria cholesterol accumulation in ABCA5 knockdown outer root sheath keratinocytes. ORS keratinocytes cells transfected with NT or *ABCA5* siRNA for 48-hours incubated with 25 μM of BODIPY cholesterol (green) and Mitochondria Cytopainter (blue). Time-lapse images taken at 30-minute intervals for 150-minutes. 3D images show total distribution of BODIPY within the cell. BODIPY in plasma membrane represented by white arrows. Scale bars 5 μm.
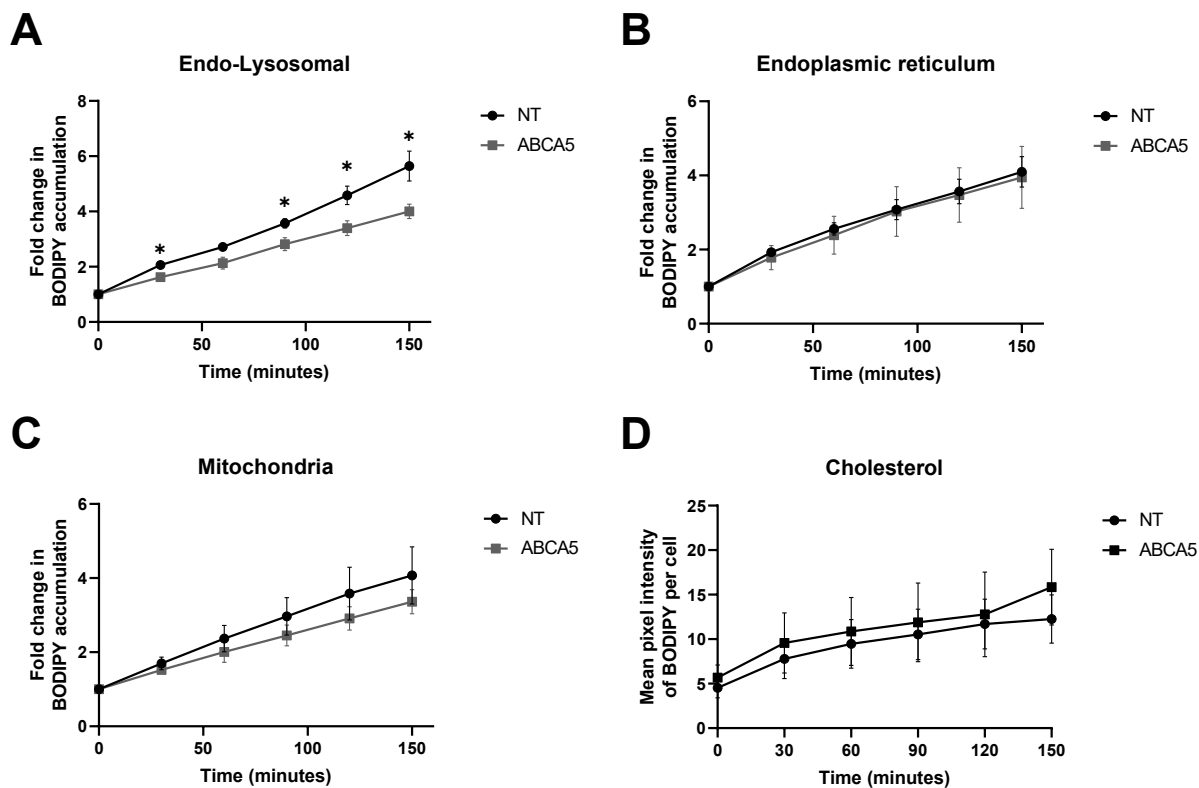
Figure 6.8 Quantification of live cholesterol imaging. Quantification of mean peak intensities of BODIPY cholesterol masked to organelle marker (A-C) or total (D) per cell. Data are mean ± SEM n=4 donors. Two-way ANOVA performed with Fisher's multiple comparisons test; significance denoted by * P≤0.05.

To investigate the influence of ABCA5 activity on plasma membrane cholesterol efflux activity, BODIPY-cholesterol efflux assays were performed following ABCA5 knockdown. The two primary pathways for cholesterol efflux are ABCA1 and ABCG1, both of which are expressed in the skin and HF (Haslam *et al.*, 2015, Jiang *et al.*, 2006, Jiang *et al.*, 2010). ABCA1 and ABCG1 move cholesterol to the acceptor molecules APOA1 and HDL, respectively (Wang *et al.*, 2008, Wang *et al.*, 2000). Efflux to HDL was found to be greater (~13%) than to APOA1 (~8%) in the NT control cells. Following ABCA5 knockdown, no change in efflux to HDL was observed (Figure 6.9D). Conversely, a significant drop in ABCA1-mediated efflux to APOA1 was seen (Figure 6.9C). As ABCA5 was not found to be localised to the plasma membrane (Figure 3.9), this suggests it may not directly efflux FC to APOA1. Instead, reducing ABCA5 activity might impair delivery of FC to the plasma membrane for ABCA1-mediated efflux.

To investigate the reduction in cholesterol efflux to APOA1, western blot analysis was performed for ABCA1, ABCG1 and SCARB1 to understand whether reduction of the expression of cholesterol efflux proteins occurred as a result of ABCA5 knockdown (Figure 6.9A-B). No significant changes were detected for ABCG1 and SCARB1, however a trend towards loss of ABCA1 protein was observed (Figure 6.9A,B) (P=0.055).
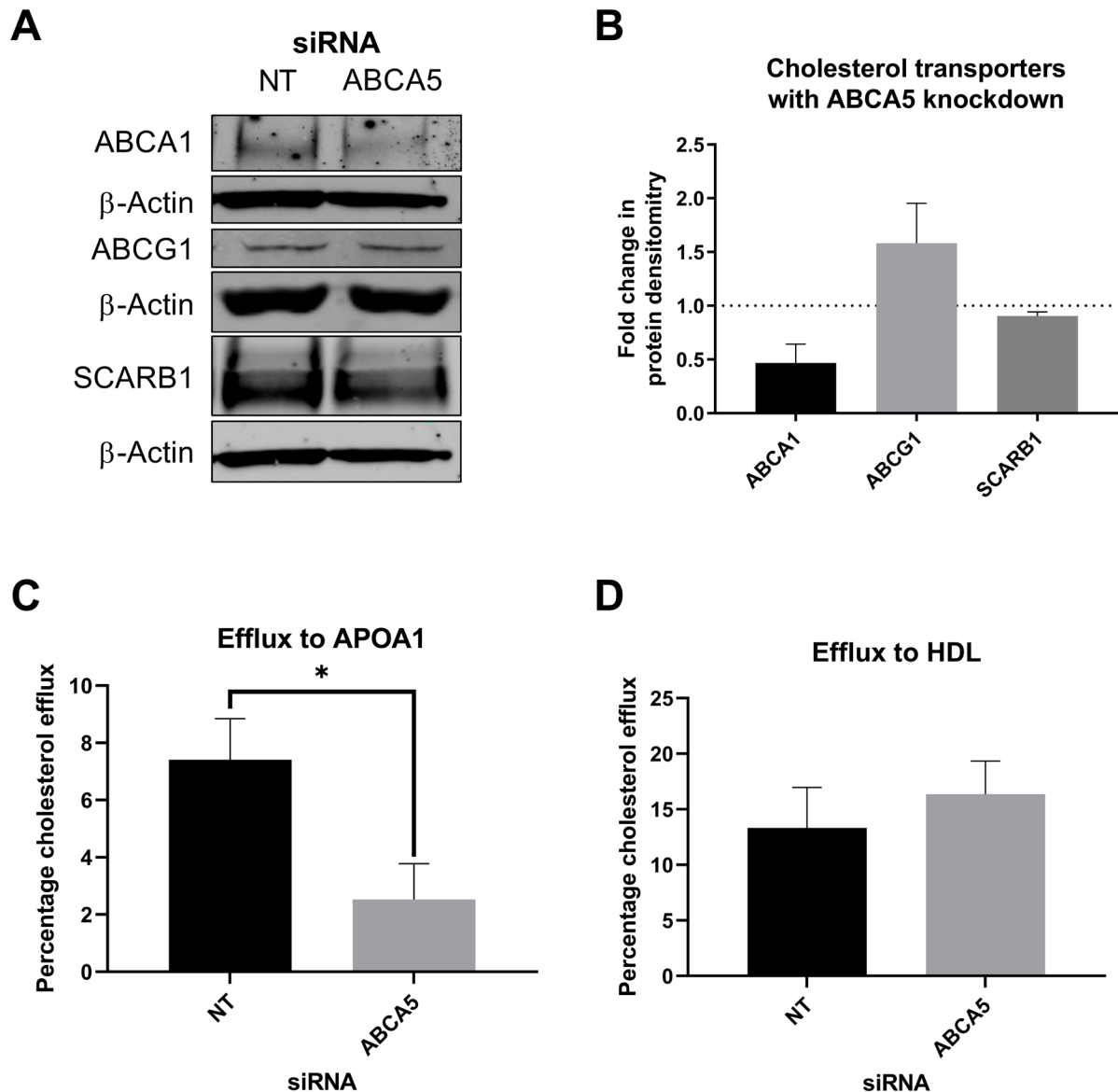
Figure 6.9 ABCA5 knockdown reduced cholesterol efflux to APOA1. (A) Protein expression of ABCA1, ABCG1 and SCARB1 in ORS keratinocytes cells transfected with NT or *ABCA5* siRNA for 72-hours. Protein densitometry values relative to reference protein β-Actin. Data are mean ± SEM for n=4 donors. BODIPY cholesterol efflux in ORS keratinocytes cells transfected with NT or *ABCA5* siRNA for 72-hours. Efflux to APOA1 (C) or HDL (D). Data are mean percentage change in efflux ± SEM n=6 (C) n=3 (D) donors. Unpaired t-test performed; significance denoted by * P≤0.05.

These results prompted the investigation of other cholesterol homeostatic pathways that may be disrupted by ABCA5 knockdown.

6.2.3 ABCA5 knockdown disrupts the homeostatic response to exogenous cholesterol in outer root sheath keratinocytes

Delivery of exogenous cholesterol elicits a cellular homeostatic response, generally through the activation of lipid sensitive transcription factors LXR and SREBP2. Cellular cholesterol accumulation results in increased sterol efflux and a reduction in *de novo* biosynthesis (Adams *et al.*, 2004b, Phillips, 2014).

Addition of 25 µM exogenous cholesterol to ORS keratinocytes resulted in an increase in the expression of genes responsible for cholesterol efflux (*ABCA1*, *ABCG1* and *SCARB1*) but no change in *ABCA5* (Figure 6.10). *HMGCR*, the gene encoding the rate-limiting enzyme in cholesterol biosynthesis, was reduced (Figure 6.11). siRNA-mediated knockdown of ABCA5 did not significantly alter the expression of *ABCA1*, *ABCG1*, *SCARB1* or *HMGCR*. Strikingly, the ABCA5 knockdown truncated the FC-mediated increases in *ABCA1* and *ABCG1* (Figure 6.10B,C). Furthermore, *HMCGR* was downregulated to a much greater degree following addition of FC to the ABCA5 knockdown ORS keratinocytes (Figure 6.11A).

These data suggest that the normal homeostatic response to FC loading was altered, which could indicate changes in LXR-mediated signalling processes. To determine whether LXR activity was impaired in ABCA5 knockdown cells, ORS keratinocytes were treated with the LXR agonist T0901317. In the absence of *ABCA5* siRNA, LXR activation significantly increased *ABCA1* and *ABCG1* expression (Figure 6.10F,G), with a small reduction in *HMGCR* (Figure 6.11B). As HMGCR is primarily regulated by activation of SREBP2, a significant reduction in expression may not be expected following LXR activation. Importantly, T0901317 addition to ABCA5 knockdown ORS keratinocytes continued to elicit the typical LXR response, namely *ABCA1* and *ABCG1* were increased in comparison to ABCA5 knockdown alone, and no significant differences to the control were apparent (Figure 6.10F,G). This is in sharp contrast to the addition of FC, which did not induce *ABCA1* and *ABCG1* expression in the ABCA5 knockdown cells.
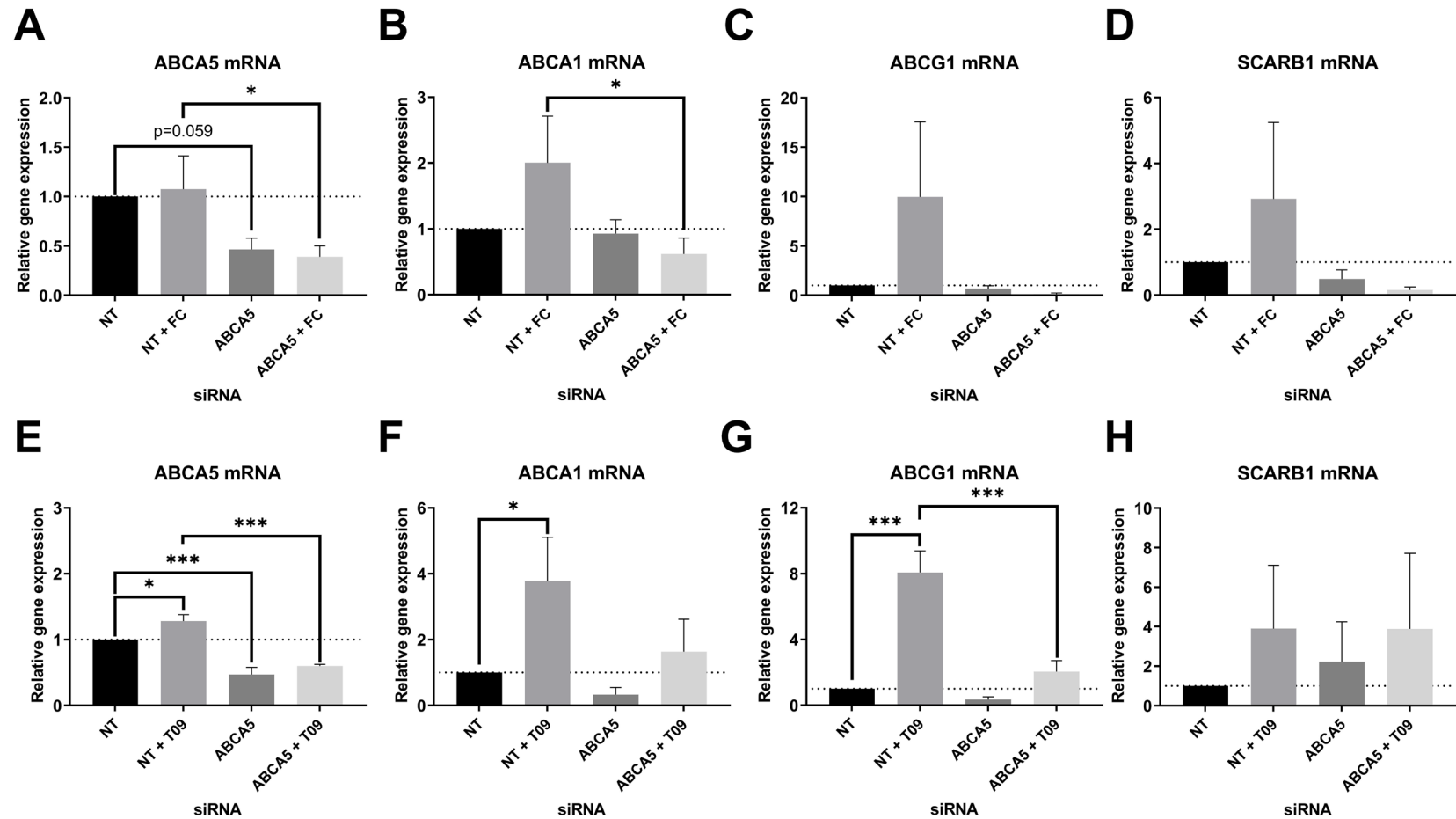
Figure 6.10 ABCA5 knockdown disrupts cholesterol transport. Gene expression changes in ORS keratinocytes transfected with NT or *ABCA5* siRNA for 48-hours, with or without 25 μM FC (A-D) or 5 μM T0901317 (E-H) for a further 24-hours. Gene expression reported relative to vehicle control and normalised to *PPIA*. Data are mean ± SEM for n=5/n=3 (FC/T0901317). One-way ANOVA were performed with Fisher's multiple comparisons test; significance denoted by * P≤0.05, ** P≤0.01, *** P≤0.005.

Further analysis demonstrated that SREBP2 transcription was significantly reduced by 22.1% with ABCA5 knockdown (Figure 6.11E). Additional FC loading results with a typical response in lowering *SREBP2* transcripts, which was further reduced in ABCA5 knockdown ORS keratinocytes with FC loading (Figure 6.11C). This may account for the extreme reduction in *HMGCR* mRNA levels detected in FC-loaded ABCA5 knockdown ORS keratinocytes.

Furthermore, although there are no changes to either the total or intracellular cholesterol levels with knockdown of ABCA5 a reduction in the transcription of *HMGCR* was shown. This can be explained in terms of the reduction in SREBP2 transcriptional activity (Figure 6.11E), however it remains unclear as to why *SREBP2* mRNA and activity would be repressed.
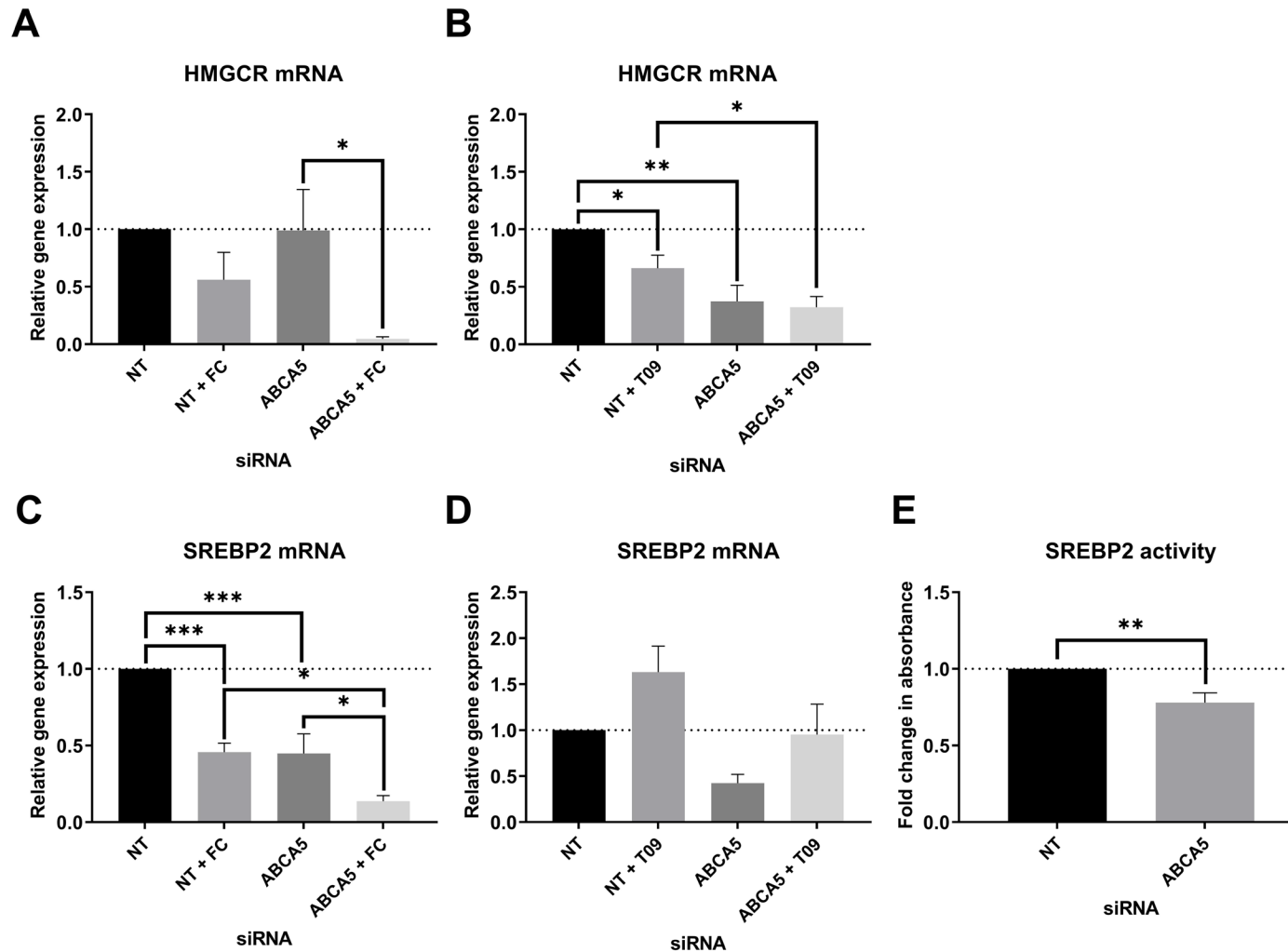
Figure 6.11 ABCA5 knockdown reduces cholesterol synthesis. Gene expression changes in ORS keratinocytes transfected with NT or *ABCA5* siRNA for 48-hours, with or without 25 µM FC (A,C) or 5 µM T0901317 (B,D) for a further 24-hours. Gene expression reported relative to vehicle control and normalised to *PPIA*. Data are mean ± SEM for n=5/n=3 donors (FC/T0901317). One-way ANOVA were performed with Fisher's multiple comparisons test; significance denoted by * P≤0.05, ** P≤0.01, *** P≤0.005. (E) Transcriptional activity of SREBP2 in ORS keratinocytes transfected with NT or *ABCA5* siRNA for 72-hours. Data are mean ± SEM for n=4 donors. Unpaired t-test performed; significance denoted by ** P≤0.01.

6.2.4 Sterol profile in free cholesterol-loaded outer root sheath keratinocytes

Next lipidomic analysis was performed to determine whether ABCA5 knockdown impacted on the sterol profile (FC, oxysterols) in ORS keratinocytes. Oxysterols can activate transcription factors such as LXR and SREBP2, and are an important component of the homeostatic control of the cellular sterol status (Olkkonen *et al.*, 2012).

As with filipin staining, lipidomic analysis showed significant increases in the concentration of cellular FC (Table 6.1) in cells treated with FC for 24-hours, however this was significant for both NT and ABCA5 knockdown ORS keratinocytes (Table 6.1). Concentrations of individual oxysterols are displayed in Table 6.1, whereas Figure 6.12 demonstrates fold change normalised to NT control treatment. The most abundant oxysterols were 27-hydroxycholesterol, 4β-hydroxycholesterol, 7-ketochonesterol and 7β-hydroxycholesterol.

7-α, 25-Dihydroxycholesterol significantly increased with FC loading, and was not altered by ABCA5 knockdown. A significant increase was detected in fold change of 7-β-hydroxycholesterol in *ABCA5* siRNA-treated keratinocytes with exogenous FC loading (Figure 6.12). 25-hydroxycholesterol significantly increased in fold change in *ABCA5* siRNA keratinocytes with exogenous FC loading, which is significantly different than FC loaded NT siRNA keratinocytes (Figure 6.12). 27-hydroxycholesterol significantly reduced in both NT and *ABCA5* siRNA-treated keratinocytes.

Table 6.1 Concentration of lipids in ABCA5 knockdown keratinocytes

Lipid (nM)	NT	NT + FC	ABCA5	ABCA5 + FC
Cholesterol	2550 ± 354	3716 ± 359.1 *	2419 ± 386.7	3712 ± 281.7 †
27-Hydroxycholesterol	67.02 ± 9.21	51.90 ± 67.38	67.38 ± 9.74	51.84 ± 4.66
24-Hydroxycholesterol	2.86 ± 0.71	1.90 ± 0.81	2.39 ± 0.01	2.54 ± 0.54
4-β-Hydroxycholesterol	95.81 ± 24.85	94.36 ± 19.94	73.71 ± 19.86	82.20 ± 18.80
25-Hydroxycholesterol	6.50 ± 1.49	7.83 ± 1.82	6.64 ± 1.20	11.87 ± 2.58
7-α,25-Dihyroxycholesterol	3.27 ± 0.20	19.05 ± 3.25 *	3.31 ± 0.23	17.47 ± 2.75 †
7-Ketocholesterol	56.82 ± 22.56	45.20 ± 14.89	57.38 ± 23.33	48.48 ± 17.76
7-β-Hydroxycholesterol	48.52 ± 16.20	81.67 ± 28.70	50.72 ± 18.43	103.78 ± 35.89
5,6-Epoxycholesterol	3.87 ± 0.12	4.17 ± 0.25	3.96 ± 0.24	4.40 ± 0.25

Concentrations of cholesterol and oxysterols (nM) determined *via* mass spectrometry ORS keratinocytes cells were transfected with siRNA for 48-hours and subsequently exposed to 25 µM FC for 24-hours. Data are mean ± SEM of n=6 except for 4β-hydroxycholesterol, 7α,25-hydroxycholesterol, 5,6-epoxycholesterol (n=4) and 24-hydroxycholesterol (n=2). One-way ANOVA or Kruskal Wallis tests were performed, significance denoted by * P≤0.05 for NT to NT + FC, † P≤0.05 for ABCA5 to ABCA5 + FC.
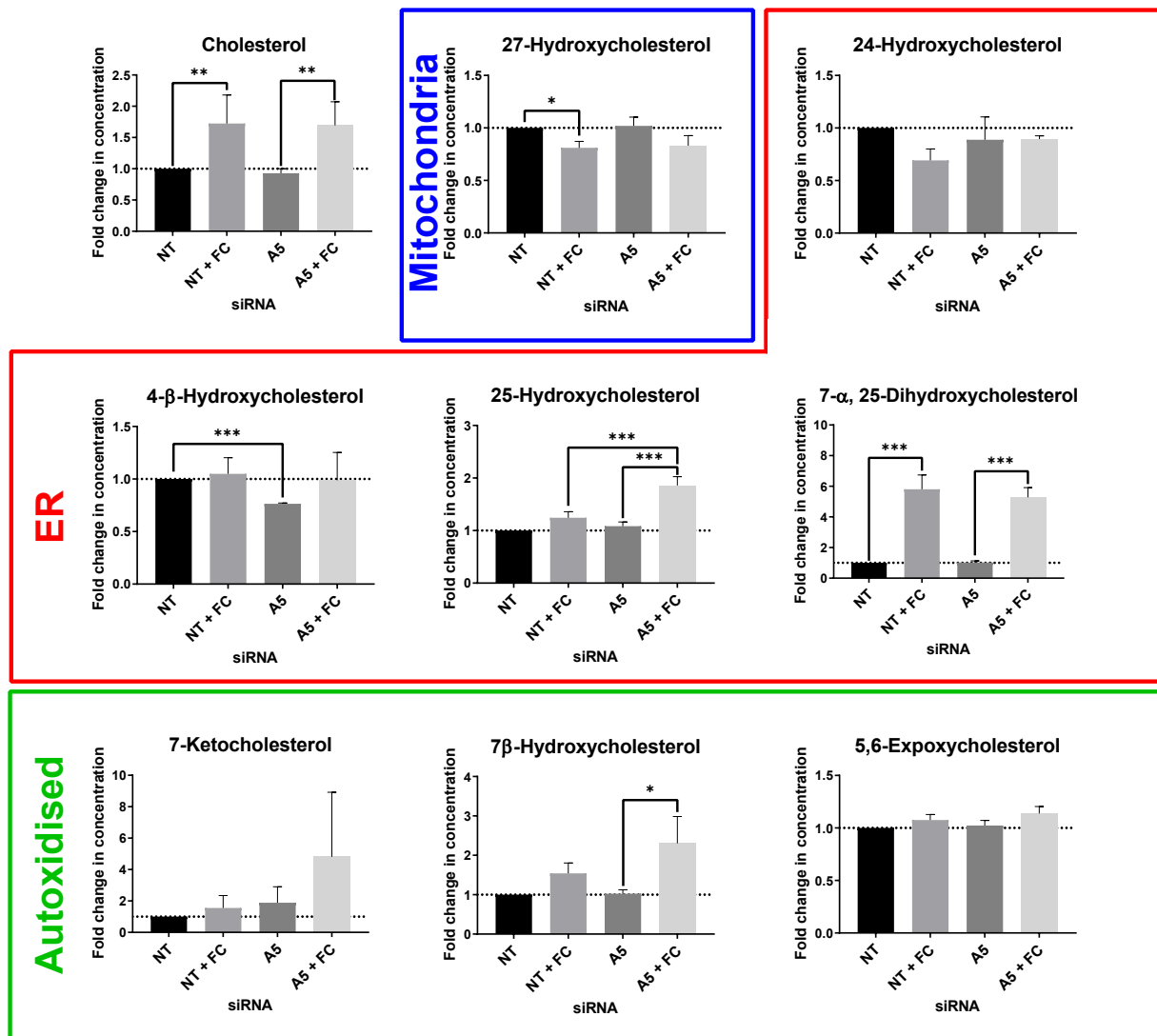
Figure 6.12 Lipidomic analysis of cholesterol-loaded outer root sheath keratinocytes with ABCA5 knockdown. Mass spectrometry analysis of ORS keratinocytes transfected with siRNA for 48-hours and subsequently exposed to 25 µM FC for 24-hours. Blue box donates mitochondrial derived oxysterols, red box for ER derived oxysterols and green box for autoxidised oxysterols. Data are mean ± SEM of n=6 donors, except for 4β-hydroxycholesterol, 7α,25-hydroxycholesterol, 5,6-epoxycholesterol (n=4) and 24-hydroxycholesterol (n=2). One-way ANOVA or Kruskal Wallis tests were performed; significance denoted by * P≤0.05, *** P≤0.005.

6.3 Discussion

This chapter aimed to provide a deeper understanding for the role ABCA5 might play in cholesterol transport processes in ORS keratinocytes. Chapter 3 revealed that ABCA5 protein expression can be modulated by changes in cellular cholesterol levels, which also alters intracellular co-localisation to endo-lysosomes, ER and mitochondria. Here, siRNA silencing showed that ABCA5 is implicated in the maintenance of cholesterol homeostatic pathways. Furthermore, endo-lysosomal cholesterol trafficking was also found to be influenced by ABCA5 levels. Additional siRNA experiments were performed in *ex vivo* HF cultures, however limited samples were available, and of the two cultures performed the majority of follicles had spontaneously entered catagen. Therefore, this *ex vivo* HF data was not included in this chapter, and the focus on *in vitro* ABCA5 siRNA experiments in ORS keratinocytes was made instead to provide insight into the role of ABCA5 in the HF.

Although ABCA5 has not previously been reported in the plasma membrane, it could be hypothesised that like ABCA1 (Neufeld *et al.*, 2001), ABCA5 shuttles between endo-lysosomes and the plasma membrane. ABCA1-mediated cholesterol efflux to APOA1 is well characterised (Quazi and Molday, 2011), however binding and efflux to APOE has also been documented (Krimbou *et al.*, 2004). Furthermore, a high expression *Apoe* is documented in murine HF cells *via* single cell RNA-sequencing (Joost, 2020, Joost *et al.*, 2020), suggesting the HFs capability to generate APOE lipoproteins for cholesterol efflux. In fact, ABCA5-induced neuroblastoma cells showed an increase in efflux to APOE, to the same level as ABCA1 upregulated cells (Fu *et al.*, 2015). As it was shown here that *ABCA1* mRNA and protein abundance were reduced following ABCA5 knockdown in ORS keratinocytes, it could be postulated that the reduction in APOA1 stimulated efflux is due to the loss of ABCA1 rather than ABCA5 itself functioning in plasma-membrane cholesterol efflux. Indeed, no change in HDL efflux was detected, which is consistent with the lack of change in ABCG1 or SCARB1 proteins, both of which utilise HDL as an acceptor for cholesterol efflux. Notably, this conflicts with data seen in mouse derived *Abca5*^{-/-} macrophages, where the loss of cholesterol efflux to HDL and not ABCA1-mediated efflux was observed (Ye *et al.*, 2010).

What is more, Chapter 5 reported comparatively low-level expression of ABCG1 in the HF when compared to both ABCA1 and ABCA5, which might suggest lower ABCG1-mediated efflux activity. Another important contrast with the murine *Abca5*^{-/-} data reported by Ye *et al.* (2010) is that here, ABCA5 knockdown resulted in reduced Abca1 expression, whereas the murine *Abca5*^{-/-}

resulted in an increase in Abca1. Which may explain the differences in cholesterol efflux observed between the current study, and Ye *et al.* (2010). There may also be tissue-specific differences in the predominant routes for cholesterol transport, as different expression patterns of ABC transporters in peripheral tissues have been previously described (Zhou *et al.*, 2015, Quazi and Molday, 2011).

In addition to reduced cholesterol efflux to APOA1, a dysregulation in the accumulation of endo-lysosomal cholesterol with ABCA5 knockdown was confirmed by both filipin and live BODIPY cholesterol fluorescence imaging. As suggested by the data in Chapter 3 (Figure 3.9), ABCA5 may be involved in endo-lysosomal cholesterol transport. The presence of ABCA5 within ER and mitochondria could also suggest that the ABCA5-mediated cholesterol transport occurs within these organelles too. However, as changes in cholesterol accumulation were only detected in endo-lysosomes, transport activity in other organelles cannot be confirmed in ORS keratinocytes. It does however appear likely that within ORS keratinocytes, ABCA5 is an intracellular cholesterol transporter, which is supported by its previous co-localisation with endo-lysosomes (Kubo *et al.*, 2005) and Golgi (Petry *et al.*, 2006) in mouse and rat, respectively.

Knockdown of ABCA5 reveals a disruption in the regulatory pathways controlling cholesterol homeostasis; these findings present both a loss of *SRBEP2* gene expression and transcriptional activity with ABCA5 knockdown, along with dysregulation of the normal homeostatic response of LXR target genes in response to cholesterol loading. As co-localisation of ABCA5 to intracellular organelles increases with cholesterol loading, it is hypothesised that ABCA5 is an integral component of intracellular cholesterol movement. Thus, a loss of ABCA5 following siRNA treatment resulted in the impaired movement of excess cholesterol, which would otherwise be effluxed or converted into oxysterols to initiate an LXR response. However, no change was detected in 27-hydroxycholesterol whereas the autoxidised variants 7-ketocholesterol and 7β-hydroxycholesterol were both increased in ABCA5 knockdown cells following cholesterol loading, compared to NT controls. Also, of note is the increase in 25-hydroxycholesterol, synthesised through CH25H within the ER (Olkkonen *et al.*, 2012). As detailed in Chapter 1 (Figure 1.4), in cholesterol-rich environments the binding of 25-hydroxycholesterol to INSIG and FC to SCAP prevents the movement of SREBP2 to the Golgi for proteolytic processing, and therefore prevents the protein translocation to the nucleus to initiate transcription. The greater increase in 25-hydroxycholesterol within FC-loaded ABCA5 knockdown cells could be used to explain the greater differences in both *HMGCR* and *SREBP2* levels. However, a likewise effect of an increase in transcription of LXR targets would be expected.

Whereas live BODIPY cholesterol imaging showed an accumulation of cholesterol to the mitochondria over a 150-minute period, a reduction in filipin staining was detected at 24-hours post FC loading in comparison to unloaded cells. Furthermore, synthesis of 27-hydroxycholesteol occurs in mitochondria *via* CYP27A1 (Olkkonen *et al.*, 2012). In correlation with the reduction in mitochondrial cholesterol with exogenous cholesterol loading detected with filipin staining, a reduction in 27-hydroxycholesterol is also detected. That said, no change in mitochondrial cholesterol accumulation is detected between NT and ABCA5 knockdown in both live BODIPY imaging and filipin staining.

This may however provide some insight into how alterations in cholesterol levels in the HF could affect hair growth and cycling. As cholesterol is shown to accumulate within the mitochondria over a comparatively short time-period during loading, yet is reduced at 24-hours post loading, it could be hypothesised that enzymatic metabolism of cholesterol occurs between 2.5 and 24-hours post-loading. The drop in 27-hydroxycholesterol, suggests that oxysterol production by CYP27A1 (Olkkonen *et al.*, 2012) is not the dominant route for mitochondrial cholesterol metabolism.

In addition, mitochondria are the site of initial steroid hormone synthesis, in which cholesterol is converted into pregnenolone *via* CYP11A1 (Li *et al.*, 2014). Indeed steroidogenesis enzymes have been detected within the HF (Slominski *et al.*, 2013), however the expression of CYP11A1 has yet to be identified, although skin, sebocyte and adipocyte expression are known (Li *et al.*, 2014, Slominski *et al.*, 1996). Therefore, the exogenous cholesterol in the mitochondria may be synthesised into pregnenolone, however both the expression of CYP11A1 and pregnenolone levels would need to be measured to confirm this. As discussed in Section 1.4, if indeed excess cholesterol leads to the synthesis of steroid hormones in the HF, this could lead to alterations in hair cycling through AR-mediated Wnt/β-catenin signalling (Kretzschmar *et al.*, 2015), along with the onset of AGA through DHT (Inui and Itami, 2013, Sawaya, 1991).

The half-life of oxysterols is very short in comparison to cholesterol (Olkkonen *et al.*, 2012) (a few hours versus ranges reported from days in lipoproteins (Daniels *et al.*, 2009) to years in brain tissue (Zhang and Liu, 2015)), and it could be suggested that at a different time point an increase in 27-hydroxycholesterol would be detected. However, 27-hydroxycholesterol is well documented in LXR agonism (Fu *et al.*, 2001, Olkkonen *et al.*, 2012) and therefore transcriptional responses in correlation to this would be expected to match. As one of the more abundant oxysterols detected within ORS keratinocytes, the functionality of CYP27A1 is clear. Furthermore 27-hydroxycholesterol has been noted as a selective oestrogen receptor modulator (DuSell *et al.*, 2008). Treatment of cancers with SERMs is associated with alopecia (Saggar *et al.*, 2013), and

oestrogen has been associated with hair growth and cycling *via* oestrogen receptor-mediated signalling (Ohnemus *et al.*, 2006). Although only slight decreases in 27-hydroxycholesterol were detected, alterations due to excess cholesterol levels may lead to changes in cycling *via* changes to oestrogen receptor signalling.

Keratinocyte differentiation has previously been shown to increase with 25-hydroxycholesterol treatment (Olivier *et al.*, 2017, Hanley *et al.*, 2000). The mechanisms by which 25-hydroxycholesterol-mediated differentiation occur are not fully understood, however they have been linked with an increases in Activator protein 1 (Hanley *et al.*, 2000), autophagy and intracellular calcium levels (Olivier *et al.*, 2017). Hanley *et al.* (2000) speculate this is mediated by LXR and not SREBP2, but as the results here suggest a reduction in LXR activation following ABCA5 knockdown, any potential increases in differentiation would not be through this mechanism. Furthermore, the concentrations used in these studies exceeded 10 µM 25-hydroxycholesterol, an almost 1000-fold higher concentration than that detected in ORS keratinocytes following ABCA5 knockdown with exogenous cholesterol loading. However, this result may indicate an alteration in how the loss of ABCA5 effects cholesterol handling. Synthesis of 25-hydroxycholesterol from cholesterol is achieved by CH25H in the ER (Olkkonen *et al.*, 2012). Although no changes in ER cholesterol staining or accumulation was detected with ABCA5 knockdown, *de novo* cholesterol synthesis occurs in the ER (Ikonen, 2008) and a reduction to *HMGCR* and *SREBP2* is noted, suggesting a reduction in cholesterol synthesis following ABCA5 knockdown. 25-Hydroxycholesterol is well documented in binding to INSIG and aiding in the reduction of SREBP2 processing *via* inhibition of SCAP transport to the Golgi, and therefore transcription of HMGCR (Adams *et al.*, 2004a, Yang *et al.*, 2002). Thus, an expected response has been detected in SREBP2-mediated cholesterol homeostasis following exogenous cholesterol loading.

Moreover, 25-hydroxycholesterol has been shown to activate Shh signalling, which is thought to be through interactions with smoothened (Corcoran and Scott, 2006). Given the importance of Shh signalling in HF morphogenesis, and smoothened integral in maintenance of the dermal cup (Woo *et al.*, 2012), loss of ABCA5 in congenital hypertrichosis patients may lead to increased oxysterol activation of Shh signalling, and therefore induce excessive hair growth and vellus to terminal hair formation. Furthermore, additional oxysterols have been shown to bind to smoothened including 7-keto-25-hydroxycholesterol (Myers *et al.*, 2013, Nedelcu *et al.*, 2013), which demonstrates the need to further analyse additional oxysterols with the loss of ABCA5 in conjunction with Shh signalling.

Transcription control of ABCA1 is most commonly associated with LXR activation, however SREBP2 has been shown to positively regulate *ABCA1* transcription through subsequent synthesis of ligands for LXR activation (Wong *et al.*, 2006). ABCA5 knockdown results in the decrease of SREBP2 activity and mRNA expression, along with a further reduction in mRNA following cholesterol loading. Furthermore, addition of LXR agonist T0901317 recovered the transcriptional activity of LXR targets, suggesting ABCA5 knockdown causes a dysregulation in LXR ligand formation. With both pathways downregulated that control transcription of *ABCA1*, this may explain the subsequent loss of protein and function, with lowered cholesterol efflux to APOA1.

LXRs have been shown to down regulate keratinocyte proliferation, and inhibit hair growth *in vitro* (Russell *et al.*, 2007). Although no changes in proliferation were detected (data not shown), there is a reduced transcriptional response in genes that are understood to be under the control of LXR. When applying the findings from cellular based ABCA5 knockdown, one could hypothesise that circulatory cholesterol levels may not induce the same level of LXR activity in HFs of ABCA5 loss-of-function individuals, thus producing excessive hair growth. The proliferation and senescence rate of ORS keratinocytes may be a limiting factor in the detection of changes to proliferation. Whereas rapidly proliferating matrix keratinocytes, which were shown to have a high expression of ABCA5, could have been a more relevant model to investigate, the isolation and culture of sufficient numbers of keratinocytes are more easily achieved from ORS than the matrix.

One notion to explain the lack of LXR response may be due to *ABCA5* being a PPAR target (Mak, 2014). Some evidence suggests that activation of PPARα can have a competitive inhibitory effect on LXR/RXR binding to the LXRE (Yoshikawa *et al.*, 2003). Although PPARs have been known to induce ABCA1 expression (Ogata *et al.*, 2009), PPARγ has been shown to increase mRNA and reduce protein expression in HepG2 cells (Mogilenko *et al.*, 2010). ABCA1 knockdown in bone marrow-derived macrophages resulted in a downregulation of protein and mRNA of both PPARγ and LXRα (Kim *et al.*, 2018). Furthermore, it was noted that PPARγ expression was essential for apoptosis-mediated upregulation of ABCA1 and LXRα (Kim *et al.*, 2018).

Indeed, PPARs are known to be important regulators for HF growth and cycling. Optimal concentrations of PPARα agonist clofibrate can promote HF survival and growth (Billoni *et al.*, 2000), whereas high concentrations can induce alopecia (Tosti and Pazzaglia, 2007). PPARβ/δ is important for HF morphogenesis (Di-Poi *et al.*, 2004, Icre *et al.*, 2006). A balance in PPARγ signalling is needed, co-activator (PPARGC1α) is upregulated in HFs of patients with AGA (Ho *et*

al., 2019), whereas treatment with PPAR agonist rosiglitazone causes a reduction in hirsutism (Yilmaz *et al.*, 2005).

Maintaining an optimal balance in signalling is required for normal functioning of HF growth and cycling. In congenital hypertrichosis, patients phenotypically present with excessive hair growth including vellus to terminal hair formation throughout the body. If indeed loss of ABCA5 protein causes alterations to PPAR levels and/or signalling, this may explain the hair pathology. Further analysis to investigate the expression levels of nuclear receptors along with investigations through luciferase reporter assays could be used to determine if the loss of ABCA5 causes a competitive based PPAR inhibition of LXR activity, or results in a downregulation of both PPAR and LXR pathways.

Another mechanism to consider could be that impaired intracellular trafficking of cholesterol and a reduction in APOA1-mediated cholesterol efflux over time, may lead to increased endo-lysosomal accumulation of cholesterol noted in keratinocytes derived from congenital hypertrichosis patients (DeStefano *et al.*, 2014). As these data has shown a reduction in cholesterol efflux, excess cholesterol may be utilised in other ways. Cholesterol is associated with many signalling pathways associated with HF growth and cycling (Incardona and Eaton, 2000, Palmer *et al.*, 2020, Stenn and Karnik, 2010). Although this chapter showed conflicting evidence with that reported by DeStefano *et al.* (2014) where increased endo-lysosomal cholesterol accumulation was described with ABCA5 mutations, the authors did not perform any quantification, and the conclusions drawn from the qualitative analysis of the filipin/LAMP1 staining is therefore not objective.

Inhibition of the JAK/STAT pathway has been shown to induce hair growth (Harel *et al.*, 2015), and interactions of ABCA1 with APOA1 have been shown to activate the JAK/STAT pathway (Tang *et al.*, 2009, Kim *et al.*, 2018, Zhao *et al.*, 2012). Specifically binding of APOA1 to ABCA1 initiates the phosphorylation of JAK, leading to the cascade of STAT phosphorylation and signalling. Furthermore, pharmacological inhibition of JAK/STAT has been shown to induce Wnt/β-catenin signalling and supress DKK1 in murine HFs, leading to the inductivity of the DP and re-entry into anagen (Harel *et al.*, 2015, Kim *et al.*, 2020). Treatment of AA patients with JAK/STAT inhibitors resulted in initial vellus hair formation and subsequent vellus to terminal hair growth (Chiang *et al.*, 2018, Shivanna *et al.*, 2018). The reduction in both ABCA1 expression and cholesterol efflux to APOA1 therefore may be a link in congenital hypertrichosis through promotion of anagen, and vellus to terminal hair formation by inhibition of JAK/STAT signalling. However

further experiments utilising patient derived-keratinocytes would be needed to confirm this, along with analysis of JAK/STAT signalling.

To conclude, these data has shown that ABCA5 knockdown induces a dysregulation of cholesterol homeostasis and reduction of APOA1 cholesterol efflux. It suggests that ABCA5 plays a role in maintaining cellular cholesterol levels, leading to the hypothesis that ABCA5 functions as an intracellular cholesterol transporter, in particular through shuttling cholesterol *via* endo-lysosomal transport. These data also provided insight in potential mechanisms by which loss of ABCA5 causes excessive hair growth, specifically, potential modulation of signalling pathways such as Shh, PPAR or JAK/STAT, along with increase in differentiation. A need for further research in these pathways in both patient and murine ABCA5 models could help determine new therapies for hair growth and hair loss disorders.

Chapter 7:   Conclusions and future perspectives

7.1 Conclusions

Determining the routes of cholesterol transport in the HF provides insight into the mechanisms in which cholesterol may influence hair growth. Cholesterol is an integral component of all cells, and dysregulation of cholesterol homeostasis results in hair disorders (Romano *et al.*, 2018, DeStefano *et al.*, 2014, Hayashi *et al.*, 2017, Panicker *et al.*, 2012, Palmer *et al.*, 2020). Furthermore, cholesterol can modulate certain signalling pathways associated with hair cycling, along with altered keratinocyte behaviour, and is a precursor for androgen synthesis. Together this suggests an important role for cholesterol in HF biology, leading to the hypothesis that altered cholesterol homeostasis can disrupt human hair growth and cycling. Therefore, the preliminary emphasis of this thesis was to characterise the routes of cholesterol transport within the HF and the effects of modulation of cholesterol levels on hair growth and cycling.

Firstly, this project aimed to determine the expression and activity of cholesterol transport proteins in human HF keratinocytes, with a particular focus on the ABC transporter superfamily. Previous research by Haslam et al. (2015) had demonstrated the expression of ABC transporters in the HF, some of which have been characterised as cholesterol transporters. Two ubiquitously expressed cholesterol transporters, ABCA1 and ABCG1, along with putative cholesterol transporter ABCA5, which is implicated in congenital hypertrichosis (Dereure, 2014, Hayashi *et al.*, 2017), and bi-directional cholesterol transporter SCARB1, were selected to be investigated in this project. Chapter 3 revealed the HFs capability to regulate cholesterol homeostasis through LXR-mediated transcription of ABCA1 and ABCG1 (Figure 3.4). Functionality of these transporters was determined through a cholesterol efflux assay revealing efflux by ABCA1 and ABCG1 to acceptors APOA1 and HDL, respectively. Furthermore, the ability of SCARB1 in cholesterol efflux to HDL was determined using the specific inhibitor BLT-1 (Figure 3.4). Immunocytochemistry analysis revealed an increase in co-localisation of ABCA5 following cholesterol loading (Figure 3.9). Oligomeric isoforms of ABCA5 were detected *via* western blotting (Figure 3.3).

The next aim was to investigate how modulation of cholesterol level impacts on HF biology, using human HF keratinocytes and organ-cultured human HFs. Exogenous cholesterol loading with FC along with cholesterol depletion by MβCD revealed the HFs to be proficient in handling physiologically relevant changes in cholesterol levels. Cholesterol loading revealed endo-lysosomal accumulation (Figure 4.1) but no changes to membrane cholesterol (Figure 4.3). Neither cholesterol loading nor depletion resulted in changes in proliferation, pigmentation, cycling

or apoptosis in cultured HFs (Chapter 4). However, Chapter 4 indicates that cholesterol depletion may lead to the selective apoptosis of senescent ORS keratinocytes. Small fluctuations in Wnt/β-catenin target genes *LEF1* and *AXIN2* were detected following changes in cholesterol levels, suggesting the potential for cholesterol status to influence this important signalling pathway in human HFs (Figure 4.15).

Chapter 5 followed with the aim to determine the expression of cholesterol transport proteins and compartmentalisation of cholesterol across the hair cycle. Differential expression of cholesterol transporters in HF tissue sections from anagen, early catagen, mid-catagen and plucked telogen were detected. ABCA1 showed a mixture of membranous staining within the matrix, and expression pattern at the nuclear periphery within club hairs (Figure 5.1). Expression of ABCG1 was high in the SG (Figure 5.2), and although transcriptionally active in ORS keratinocytes (Figure 3.1) and HFs (Figure 5.9) following LXR agonism, a low level of protein expression was found *via* immunofluorescence staining. SCARB1 was highly expressed in the DP basement membrane suggesting a role in facilitating movement between the DP and matrix keratinocytes (Figure 5.4). ABCA5 was highly expressed in the IRS, matrix and DP (Figure 5.5). HMGCR, the rate-limiting enzyme for cholesterol synthesis, was highly expressed throughout the hair cycle. Throughout the hair cycle, both membrane and cytoplasmic staining patters of cholesterol were detected. Furthermore, striations of cholesterol were present in the basement membrane of the HF at the suprabulb and isthmus but not the bulb (Figure 5.8).

The final aim of this thesis was to investigate how modulation of ABCA5 impacts on HF biology, using primary HF keratinocytes to give insight into potential mechanisms of hypertrichosis. This was achieved using siRNA-mediated knockdown of ABCA5 in ORS keratinocytes. Loss of ABCA5 demonstrated a dysregulation of intracellular cholesterol transport, with a reduction in endo-lysosomal cholesterol following exogenous FC loading (Figure 6.2, Figure 6.5). Furthermore, a disruption in the normal homeostatic response of LXR-mediated transcription following exogenous cholesterol loading was detected. Alterations to oxysterol production with exogenous cholesterol loading were revealed with ABCA5 knockdown. The binding of APOA1 to ABCA1 is important in the phosphorylation of JAK, and therefore initiation of JAK/STAT signalling (Tang *et al.*, 2009, Kim *et al.*, 2018, Zhao *et al.*, 2012). A reduction to ABCA1 expression and APOA1 efflux was detected (Figure 6.9) leading to the hypothesis that reduced JAK/STAT signalling with the loss of ABCA5 may lead to increased hair growth through inhibition of catagen entry.

7.2   Future perspectives

Chapter 3 demonstrated the capacity for ORS keratinocytes to alter transcription of cholesterol transporters in response to FC loading, whereas LXR agonism induced mRNA, protein expression and activity of cholesterol transporters. Previous studies in keratinocytes have predominantly used oxysterols to induce protein expression of ABCA1 and ABCG1 (Jiang *et al.*, 2006, Jiang *et al.*, 2010), whereas FC loading has been used in other cell types (Choi *et al.*, 2003, Hsieh *et al.*, 2014, Seeree *et al.*, 2019, Spann *et al.*, 2012). These studies have used a range of FC concentrations (from 10 μg/ml to 30 μg/ml) and detected increases in protein expression of ABCA1 and ABCG1 (Seeree *et al.*, 2019, Spann *et al.*, 2012, Choi *et al.*, 2003). Therefore, additional studies should include a dose response component to determine the concentrations of sterols capable of modulating the expression of cholesterol transporters and other cholesterol homeostatic proteins. Furthermore, alterations into cholesterol packaging should be explored through mass spectrometry imaging, utilising secondary ion mass spectrometry imaging to detect plasma membrane cholesterol, and matrix-assisted laser desorption/ionization for CE (Cologna, 2019) in both HF tissue sections and cell cultures.

The effects of different ways to modulate cholesterol levels should also be examined, and the use of statins is a particularly interesting area to investigate. As outlined in Chapter 1: Section 1.7.1 some evidence suggests statin treatment induces hair loss (Mohammad-Ali *et al.*, 2015, Segal, 2002), along with statin treatment inducing hair regrowth in AA (Lattouf *et al.*, 2015). Experiments outlining changes in proliferation/apoptosis, along with alterations to signalling should be explored. In particular the JAK/STAT pathway, which has previously been shown to be inhibited by statin treatments (Jougasaki *et al.*, 2010) should be further investigated. Reduction of intrafollicular sterols through HMGCR inhibition may lead to a reduction of cholesterol efflux from ABCA1 to APOA1, which has previously been shown to be important in the phosphorylation of JAK (Tang *et al.*, 2009, Zhao *et al.*, 2012). Obtaining patient samples prior and after statin treatment from either scalp biopsy or more likely plucked hairs could be utilised to determine if statin treatment induces changes in expression of cholesterol transporters, lipid profile and signalling. A statin treated mouse model could be utilised to mimic human oral treatments in order to investigate whether HMGCR inhibition alters hair cycling or cholesterol levels within the HF.

In Chapter 5 exploration of cholesterol transporters during the hair cycle exhibited some limitations, namely detection in protein quantification. In the human scalp HFs are predominantly in anagen VI (Oh *et al.*, 2016) and due to sample sizes, a limited number of follicles were obtained

at other cycle stages. Proficient studies should profile HFs derived from the same patient at different cycle points, as this would be unlikely, protein quantification should be performed in mice. Membrane fractionation should be utilised to improve quantification of protein expression *via* western blotting. Moreover, liquid chromatography high resolution mass spectrometry should be utilised for a more accurate method of protein quantification (Jacqueroux *et al.*, 2020). Furthermore, gene expression changes were taken from whole follicles, therefore the use of *in situ* hybridisation or laser capture microdissection could be an interesting tool to detect changes in RNA levels between different layers of the HF.

As antibodies for HMGCR will also detect degraded forms of the enzyme, it cannot be fully used to determine activity of cholesterol synthesis, therefore activity assays should be performed to fully determine this. Investigations into expression of the final enzymatic steps of the cholesterol biosynthesis pathway (DHCR7 and DHCR24) should also be performed, in addition to enzyme activity which could be measured using labelled desmosterol of 7-DHC to quantify the conversion rate into cholesterol within cellular models (Luu *et al.*, 2014).

Cholesterol efflux was measured in Chapter 3 and Chapter 6 using APOA1 and HDL to detect changes in ABCA1 and ABCG1 or SCARB1-mediated efflux, respectively. However previous studies in ABCA5 overexpressing cells found cholesterol efflux to APOE to be of a similar level compared to that of ABCA1 overexpressing cells (Fu *et al.*, 2015). Interestingly, Joost (2020) demonstrated a high expression of *Apoe* in mouse HFs (Joost *et al.*, 2020). This expression was detected throughout the telogen follicle and specifically within the upper companion layer and DP (which was double in the DP for anagen versus telogen), correlating with the highest regions of ABCA5 expression. Additionally, a low expression level of *Apoe* is detected within the ORS and IRS. Although *APOA1* expression is low in comparisons to *Apoe*, it can be detected throughout the mouse HF keratinocytes, but not fibroblasts. Nascent HDL can be formed in peripheral tissues though both APOA1 and APOE (Getz and Reardon, 2009). Thus, perhaps APOE lipoprotein is a dominant route for cholesterol efflux in the HF. Further analysis into localisation of APO in human HFs through antibody staining along with efflux assays using APOE as an acceptor in cell cultures derived from different HF populations (e.g. ORS, DP, matrix) should be investigated.

STAR proteins are understood to function as intracellular cholesterol transport proteins, moving cholesterol from the inner to the outer membrane of mitochondria, endosomes to ER and from lipid droplets to the plasma membrane (Jefcoate and Lee, 2018). Further analysis of this family of proteins could give insight into mitochondrial cholesterol trafficking in the HF. In particular, cholesterol in the mitochondria is first converted into pregnenolone before further enzymatic

reactions in the ER for steroid hormone synthesis take place (Hu *et al.*, 2010). Steroidogenic enzyme has been previously detected within the pilosebaceous unit (Slominski *et al.*, 2013). Yet it remains unclear if steroid hormones within the HF are up-taken from circulation or generated through *de novo* synthesis. Experiments into the activity of steroidogenesis should examine if modulating cholesterol levels effects steroid hormone synthesis, with insights into AGA.

Chapter 6 explored the role of ABCA5 in ORS keratinocytes, where this study provided a foundation for understanding how ABCA5 and cholesterol may affect hair growth, though further research is needed. The use of primary ORS keratinocytes provided a relevant cell culture model in which to perform siRNA experiments. Further work should focus on the use of a longer-term model in which to inhibit ABCA5 expression. One way in which to do this would be to use *Abca5* knockout mice, examining HF morphogenesis during embryogenesis to detect the pathways associated with vellus to terminal hair formation. Data from investigating alterations into hair cycling, cholesterol packaging and cholesterol transporter expression, in particular if there is a change in ABCA1 expression is needed. Along with investigations into changes in signalling pathways that could be associated with changes to cholesterol, i.e. Wnt/β-catenin, Shh, BMPs and JAK/STAT.

Another avenue to explore in human cell culture would be using either patient-derived keratinocytes or generating a HF keratinocyte derived immortalised cell line. The latter would allow the development of a permanent deletion of ABCA5 through the use of CRISPR. Currently HF-derived keratinocytes are limited through passage numbers, and single cell colony formation would not be possible in this model. In addition, ABCA5 is highly expressed in the DP, and therefore this cell type should also be investigated. Further research in cell culture can allow for cholesterol efflux studies.

Uptake of cholesterol from circulating lipoproteins is likely to occur within the mesenchymal portions of the HF, which contain the HF vasculature (Ellis and Moretti, 1959). Furthermore, the DP is the signalling centre of the HF, and alterations to cholesterol levels within this region could be more indicative of changes in HF cycling through cholesterol modification of signalling proteins. Exploring DP cells in culture presents its own limitations, the inductive properties of DP are lost with 2D cell culture (Higgins *et al.*, 2010). Either spheroid culture would provide a better mechanism in studying cholesterol within the DP, or whole HF organ culture could be used. Mouse studies using high-cholesterol diet or statin treatments may be able to detect the effect of circulating lipoproteins on HF growth and cycling. Furthermore, *ex vivo* culture of whole

pilosebaceous units may also provide another avenue to explore, investigating the potential sources of cholesterol to the HF from the sebaceous gland and adipocytes.

The presence of a unique staining pattern of cholesterol in the laminin-332 region of the basement membrane was detected in Chapter 5. Furthermore, the striations of cholesterol increase in density during the catagen of the hair cycle. These striations were hypothesised to be either deposits of excess cholesterol as cholesterol mono-hydrate needles or a mechanism for transport of cholesterol between the ORS and CTS. The use of polarised or electron microscopy would determine the presence of cholesterol crystals (Suhalim *et al.*, 2012a). Furthermore, the development of an *in vitro* model of the basement membrane with co-culture of ORS keratinocytes and CTS fibroblasts could be used to track cholesterol movement *via* live BODIPY cholesterol imaging.

To conclude, loss of ABCA5 in siRNA knockdown ORS keratinocytes revealed a dysregulation in cholesterol homeostasis and intracellular cholesterol transport. Future work should focus on the role of ABCA5 and subsequently cholesterol transport in modulating signalling pathways associated with HF morphogenesis and cycling.

References

Image available from v19.3.proteinatlas.org [Online]. Available: https://www.proteinatlas.org/ENSG00000160179-ABCG1/tissue/skin#img [Accessed 20/04/2020].

AARON, J. S., TAYLOR, A. B. & CHEW, T.-L. 2018. Image co-localization – co-occurrence versus correlation. *Journal of Cell Science,* 131**,** jcs211847.

AASEN, T. & IZPISUA BELMONTE, J. C. 2010. Isolation and cultivation of human keratinocytes from skin or plucked hair for the generation of induced pluripotent stem cells. *Nat Protoc,* 5**,** 371-82.

ACIBUCU, F., KAYATAS, M. & CANDAN, F. 2010. The association of insulin resistance and metabolic syndrome in early androgenetic alopecia. *Singapore Med J,* 51**,** 931-6.

ADAMS, C. M., REITZ, J., DE BRABANDER, J. K., FERAMISCO, J. D., LI, L., BROWN, M. S. & GOLDSTEIN, J. L. 2004a. Cholesterol and 25-Hydroxycholesterol Inhibit Activation of SREBPs by Different Mechanisms, Both Involving SCAP and Insigs. *Journal of Biological Chemistry,* 279**,** 52772-52780.

ADAMS, C. M., REITZ, J., DE BRABANDER, J. K., FERAMISCO, J. D., LI, L., BROWN, M. S. & GOLDSTEIN, J. L. 2004b. Cholesterol and 25-hydroxycholesterol inhibit activation of SREBPs by different mechanisms, both involving SCAP and Insigs. *J Biol Chem,* 279**,** 52772-80.

AGAMIA, N. F., ABOU YOUSSIF, T., EL-HADIDY, A. & EL-ABD, A. 2016. Benign prostatic hyperplasia, metabolic syndrome and androgenic alopecia: Is there a possible relationship? *Arab J Urol,* 14**,** 157-62.

AHMED, H. & O'TOOLE, E. A. 2014. Recent Advances in the Genetics and Management of Harlequin Ichthyosis. *Pediatric Dermatology,* 31**,** 539-546.

ALI, A. & MARTIN, J. M. T. 2010. Hair growth in patients alopecia areata totalis after treatment with simvastatin and ezetimibe. *J Drugs Dermatol,* 9**,** 62-4.

ANNILO, T., CHEN, Z. Q., SHULENIN, S. & DEAN, M. 2003. Evolutionary analysis of a cluster of ATP-binding cassette (ABC) genes. *Mamm Genome,* 14**,** 7-20.

ARAUJO, C., GONCALVES-ROCHA, M., RESENDE, C., VIEIRA, A. P. & BRITO, C. 2015. A Case of IFAP Syndrome with Severe Atopic Dermatitis. *Case Rep Med,* 2015**,** 450937.

ARIAS-SANTIAGO, S., GUTIERREZ-SALMERON, M. T., BUENDIA-EISMAN, A., GIRON-PRIETO, M. S. & NARANJO-SINTES, R. 2010a. A comparative study of dyslipidaemia in men and woman with androgenic alopecia. *Acta Derm Venereol,* 90**,** 485-7.

ARIAS-SANTIAGO, S., GUTIERREZ-SALMERON, M. T., CASTELLOTE-CABALLERO, L., BUENDIA-EISMAN, A. & NARANJO-SINTES, R. 2010b. [Male androgenetic alopecia and cardiovascular risk factors: A case-control study]. *Actas Dermosifiliogr,* 101**,** 248-56.

ATEN, E., BRASZ, L. C., BORNHOLDT, D., HOOIJKAAS, I. B., PORTEOUS, M. E., SYBERT, V. P., VERMEER, M. H., VOSSEN, R. H., VAN DER WIELEN, M. J., BAKKER, E., BREUNING, M. H., GRZESCHIK, K. H., OOSTERWIJK, J. C. & DEN DUNNEN, J. T. 2010. Keratosis Follicularis Spinulosa Decalvans is caused by mutations in MBTPS2. *Hum Mutat,* 31**,** 1125-33.

AYE, I. L., SINGH, A. T. & KEELAN, J. A. 2009. Transport of lipids by ABC proteins: interactions and implications for cellular toxicity, viability and function. *Chem Biol Interact,* 180**,** 327-39.

AYE, I. L., WADDELL, B. J., MARK, P. J. & KEELAN, J. A. 2010. Placental ABCA1 and ABCG1 transporters efflux cholesterol and protect trophoblasts from oxysterol induced toxicity. *Biochim Biophys Acta,* 1801**,** 1013-24.

BAKRY, O. A., EL FARARGY, S. M., GHANAYEM, N. & SOLIMAN, A. 2015. Atherogenic index of plasma in non-obese women with androgenetic alopecia. *Int J Dermatol,* 54**,** e339-44.

BANG, B., GNIADECKI, R. & GAJKOWSKA, B. 2005. Disruption of lipid rafts causes apoptotic cell death in HaCaT keratinocytes. *Exp Dermatol,* 14**,** 266-72.

BANGER, H. S., MALHOTRA, S. K., SINGH, S. & MAHAJAN, M. 2015. Is Early Onset Androgenic Alopecia a Marker of Metabolic Syndrome and Carotid Artery Atherosclerosis in Young Indian Male Patients? *Int J Trichology,* 7**,** 141-7.

BASEL-VANAGAITE, L., ATTIA, R., ISHIDA-YAMAMOTO, A., RAINSHTEIN, L., BEN AMITAI, D., LURIE, R., PASMANIK-CHOR, M., INDELMAN, M., ZVULUNOV, A., SABAN, S., MAGAL, N., SPRECHER, E. & SHOHAT, M. 2007. Autosomal recessive ichthyosis with hypotrichosis caused by a mutation in ST14, encoding type II transmembrane serine protease matriptase. *Am J Hum Genet,* 80**,** 467-77.

BEIU, C., MIHAI, M., POPA, L. G., TEBEICA, T. & GIURCANEANU, C. 2019. Epidermolysis Bullosa Acquisita: A Case Report of a Rare Clinical Phenotype and a Review of Literature. *Cureus,* 11**,** e6386.

BERG, S., KUTRA, D., KROEGER, T., STRAEHLE, C. N., KAUSLER, B. X., HAUBOLD, C., SCHIEGG, M., ALES, J., BEIER, T., RUDY, M., EREN, K., CERVANTES, J. I., XU, B., BEUTTENMUELLER, F., WOLNY, A., ZHANG, C., KOETHE, U., HAMPRECHT, F. A. & KRESHUK, A. 2019. ilastik: interactive machine learning for (bio)image analysis. *Nat Methods,* 16**,** 1226-1232.

BILLONI, N., BUAN, B., GAUTIER, B., COLLIN, C., GAILLARD, O., MAHE, Y. F. & BERNARD, B. A. 2000. Expression of peroxisome proliferator activated receptors (PPARs) in human hair follicles and PPAR alpha involvement in hair growth. *Acta Derm Venereol,* 80**,** 329-34.

BJÖRKHEM, I. 2002. Do oxysterols control cholesterol homeostasis? *Journal of Clinical Investigation,* 110**,** 725-730.

BLOCH, K. 1992. Sterol molecule: structure, biosynthesis, and function. *Steroids,* 57**,** 378-383.

BODO, E., BIRO, T., TELEK, A., CZIFRA, G., GRIGER, Z., TOTH, B. I., MESCALCHIN, A., ITO, T., BETTERMANN, A., KOVACS, L. & PAUS, R. 2005. A hot new twist to hair biology: involvement of vanilloid receptor-1 (VR1/TRPV1) signaling in human hair growth control. *Am J Pathol,* 166**,** 985-98.

BORNHOLDT, D., ATKINSON, T. P., BOUADJAR, B., CATTEAU, B., COX, H., DE SILVA, D., FISCHER, J., GUNASEKERA, C. N., HADJ-RABIA, S., HAPPLE, R., HOLDER-ESPINASSE, M., KAMINSKI, E., KONIG, A., MEGARBANE, A., MEGARBANE, H., NEIDEL, U., OEFFNER, F., OJI, V., THEOS, A., TRAUPE, H., VAHLQUIST, A., VAN BON, B. W., VIRTANEN, M. & GRZESCHIK, K. H. 2013. Genotype-phenotype correlations emerging from the identification of missense mutations in MBTPS2. *Hum Mutat,* 34**,** 587-94.

BOVENGA, F., SABBÀ, C. & MOSCHETTA, A. 2015. Uncoupling Nuclear Receptor LXR and Cholesterol Metabolism in Cancer. *Cell Metabolism,* 21**,** 517-526.

BRANNAN, P. G., GOLDSTEIN, J. L. & BROWN, M. S. 1975. 3-hydroxy-3-methylglutaryl coenzyme A reductase activity in human hair roots. *J Lipid Res,* 16**,** 7-11.

BRAVERMAN, I. M. & YEN, A. 1977. ULTRASTRUCTURE OF THE HUMAN DERMAL MICROCIRCULATION. 68**,** 44-52.

BRAVERMAN, N., LIN, P., MOEBIUS, F. F., OBIE, C., MOSER, A., GLOSSMANN, H., WILCOX, W. R., RIMOIN, D. L., SMITH, M., KRATZ, L., KELLEY, R. I. & VALLE, D. 1999. Mutations in the gene encoding 3 beta-hydroxysteroid-delta 8, delta 7-isomerase cause X-linked dominant Conradi-Hunermann syndrome. *Nat Genet,* 22**,** 291-4.

BROSCHE, T., DRESSLER, S. & PLATT, D. 2001. Age-associated changes in integral cholesterol and cholesterol sulfate concentrations in human scalp hair and finger nail clippings. *Aging (Milano),* 13**,** 131-8.

BRUNNER, M. A. T., JAGANNATHAN, V., WALUK, D. P., ROOSJE, P., LINEK, M., PANAKOVA, L., LEEB, T., WIENER, D. J. & WELLE, M. M. 2017. Novel insights into the pathways regulating the canine hair cycle and their deregulation in alopecia X. *PLOS ONE,* 12**,** e0186469.

BURKE, R., NELLEN, D., BELLOTTO, M., HAFEN, E., SENTI, K. A., DICKSON, B. J. & BASLER, K. 1999. Dispatched, a novel sterol-sensing domain protein dedicated to the release of cholesterol-modified hedgehog from signaling cells. *Cell,* 99**,** 803-15.

CAO, G., GARCIA, C. K., WYNE, K. L., SCHULTZ, R. A., PARKER, K. L. & HOBBS, H. H. 1997. Structure and localization of the human gene encoding SR-BI/CLA-1. Evidence for transcriptional control by steroidogenic factor 1. *J Biol Chem,* 272**,** 33068-76.

CATTET, M., STENHOUSE, G. B., JANZ, D. M., KAPRONCZAI, L., ANNE ERLENBACH, J., JANSEN, H. T., NELSON, O. L., ROBBINS, C. T. & BOULANGER, J. 2017. The quantification of reproductive hormones in the hair of captive adult brown bears and their application as indicators of sex and reproductive state. *Conserv Physiol,* 5**,** cox032.

CECCANTI, M., CAMBIERI, C., FRASCA, V., ONESTI, E., BIASIOTTA, A., GIORDANO, C., BRUNO, S. M., TESTINO, G., LUCARELLI, M., ARCA, M. & INGHILLERI, M. 2016. A Novel Mutation in ABCA1 Gene Causing Tangier Disease in an Italian Family with Uncommon Neurological Presentation. *Frontiers in Neurology,* 7**,** 185.

CERVANTES, J., JIMENEZ, J. J., DELCANTO, G. M. & TOSTI, A. 2018. Treatment of Alopecia Areata with Simvastatin/Ezetimibe. *J Investig Dermatol Symp Proc,* 19**,** S25-S31.

CHAKRABARTY, S., HARIHARAN, R., GOWDA, D. & SURESH, H. 2014. Association of premature androgenetic alopecia and metabolic syndrome in a young Indian population. *Int J Trichology,* 6**,** 50-3.

CHERMNYKH, E., KALABUSHEVA, E. & VOROTELYAK, E. 2018. Extracellular Matrix as a Regulator of Epidermal Stem Cell Fate. *Int J Mol Sci,* 19**,** 1003.

CHIANG, A., ORTENZIO, F., JUHASZ, M. L. W., YU, V. & MESINKOVSKA, N. A. 2018. Balance of tofacitinib efficacy and disease flare in the treatment of alopecia universalis: A case report and review of the literature. *JAAD case reports,* 4**,** 733-736.

CHIANG, C., SWAN, R. Z., GRACHTCHOUK, M., BOLINGER, M., LITINGTUNG, Y., ROBERTSON, E. K., COOPER, M. K., GAFFIELD, W., WESTPHAL, H., BEACHY, P. A. & DLUGOSZ, A. A. 1999. Essential Role forSonic hedgehogduring Hair Follicle Morphogenesis. *Developmental Biology,* 205**,** 1-9.

CHIANG, J. Y. 1998. Regulation of bile acid synthesis. *Front Biosci,* 3**,** d176-93.

CHOI, H. Y., KARTEN, B., CHAN, T., VANCE, J. E., GREER, W. L., HEIDENREICH, R. A., GARVER, W. S. & FRANCIS, G. A. 2003. Impaired ABCA1-dependent lipid efflux and hypoalphalipoproteinemia in human Niemann-Pick type C disease. *J Biol Chem,* 278**,** 32569-77.

CLAY, M. A. & BARTER, P. J. 1996. Formation of new HDL particles from lipid-free apolipoprotein A-I. *J Lipid Res,* 37**,** 1722-32.

CODERCH, L., MENDEZ, S., BARBA, C., PONS, R., MARTI, M. & PARRA, J. L. 2008. Lamellar rearrangement of internal lipids from human hair. *Chem Phys Lipids,* 155**,** 1-6.

COISNE, C., HALLIER-VANUXEEM, D., BOUCAU, M. C., HACHANI, J., TILLOY, S., BRICOUT, H., MONFLIER, E., WILS, D., SERPELLONI, M., PARISSAUX, X., FENART, L. & GOSSELET, F. 2016. beta-Cyclodextrins Decrease Cholesterol Release and ABC-Associated Transporter Expression in Smooth Muscle Cells and Aortic Endothelial Cells. *Front Physiol,* 7**,** 185.

COLOGNA, S. M. 2019. Mass Spectrometry Imaging of Cholesterol. *In:* ROSENHOUSE-DANTSKER, A. & BUKIYA, A. N. (eds.) *Cholesterol Modulation of Protein Function: Sterol Specificity and Indirect Mechanisms.* Cham: Springer International Publishing.

COOPER, M. K., WASSIF, C. A., KRAKOWIAK, P. A., TAIPALE, J., GONG, R., KELLEY, R. I., PORTER, F. D. & BEACHY, P. A. 2003. A defective response to Hedgehog signaling in disorders of cholesterol biosynthesis. *Nat Genet,* 33**,** 508-13.

CORCORAN, R. B. & SCOTT, M. P. 2006. Oxysterols stimulate Sonic hedgehog signal transduction and proliferation of medulloblastoma cells. *Proceedings of the National Academy of Sciences,* 103**,** 8408-8413.

CORTES, V. A., BUSSO, D., MAIZ, A., ARTEAGA, A., NERVI, F. & RIGOTTI, A. 2014. Physiological and pathological implications of cholesterol. *Front Biosci (Landmark Ed),* 19**,** 416-28.

COTSARELIS, G., SUN, T. T. & LAVKER, R. M. 1990. Label-retaining cells reside in the bulge area of pilosebaceous unit: implications for follicular stem cells, hair cycle, and skin carcinogenesis. *Cell,* 61**,** 1329-37.

COUCHMAN, J. R. & GIBSON, W. T. 1985. Expression of basement membrane components through morphological changes in the hair growth cycle. *Dev Biol,* 108**,** 290-8.

COX, B. E., GRIFFIN, E. E., ULLERY, J. C. & JEROME, W. G. 2007. Effects of cellular cholesterol loading on macrophage foam cell lysosome acidification. *J Lipid Res,* 48**,** 1012-21.

CRIVELLARI, I., STICOZZI, C., BELMONTE, G., MURESAN, X. M., CERVELLATI, F., PECORELLI, A., CAVICCHIO, C., MAIOLI, E., ZOUBOULIS, C. C., BENEDUSI, M., CERVELLATI, C. & VALACCHI, G. 2017. SRB1 as a new redox target of cigarette smoke in human sebocytes. *Free Radic Biol Med,* 102**,** 47-56.

CRUZ, C. F., FERNANDES, M. M., GOMES, A. C., CODERCH, L., MARTI, M., MENDEZ, S., GALES, L., AZOIA, N. G., SHIMANOVICH, U. & CAVACO-PAULO, A. 2013. Keratins and lipids in ethnic hair. *Int J Cosmet Sci,* 35**,** 244-9.

CZUBA, L. C., HILLGREN, K. M. & SWAAN, P. W. 2018. Post-translational modifications of transporters. *Pharmacol Ther,* 192**,** 88-99.

DAFFU, G., SHEN, X., SENATUS, L., THIAGARAJAN, D., ABEDINI, A., HURTADO DEL POZO, C., ROSARIO, R., SONG, F., FRIEDMAN, R. A., RAMASAMY, R. & SCHMIDT, A. M. 2015. RAGE Suppresses ABCG1-Mediated Macrophage Cholesterol Efflux in Diabetes. *Diabetes,* 64**,** 4046-60.

DANG, H., SONG, B., DONG, R. & ZHANG, H. 2018. Atorvastatin reverses the dysfunction of human umbilical vein endothelial cells induced by angiotensin II. *Experimental and Therapeutic Medicine,* 16**,** 5286-5297.

DANIELS, T. F., KILLINGER, K. M., MICHAL, J. J., WRIGHT, R. W., JR. & JIANG, Z. 2009. Lipoproteins, cholesterol homeostasis and cardiac health. *Int J Biol Sci,* 5**,** 474-88.

DAVIES, J. P., SCOTT, C., OISHI, K., LIAPIS, A. & IOANNOU, Y. A. 2005. Inactivation of NPC1L1 Causes Multiple Lipid Transport Defects and Protects against Diet-induced Hypercholesterolemia. *Journal of Biological Chemistry,* 280**,** 12710-12720.

DE LA LLERA-MOYA, M., ROTHBLAT, G. H., CONNELLY, M. A., KELLNER-WEIBEL, G., SAKR, S. W., PHILLIPS, M. C. & WILLIAMS, D. L. 1999. Scavenger receptor BI (SR-BI) mediates free cholesterol flux independently of HDL tethering to the cell surface. *J Lipid Res,* 40**,** 575-80.

DEBACQ-CHAINIAUX, F., ERUSALIMSKY, J. D., CAMPISI, J. & TOUSSAINT, O. 2009. Protocols to detect senescence-associated beta-galactosidase (SA-betagal) activity, a biomarker of senescent cells in culture and in vivo. *Nat Protoc,* 4**,** 1798-806.

DENG, Y., OHGAMI, N., IIDA, M., TAZAKI, A., INTOH, A., KONDO-IDA, L., LU, R., TSUZUKI, T., YOKOYAMA, S. & KATO, M. 2019. Histological analysis of the skin of Abca1-deleted mice: A potential model for dry skin. *Eur J Dermatol,* 29**,** 549-551.

DENIS, M., HAIDAR, B., MARCIL, M., BOUVIER, M., KRIMBOU, L. & GENEST, J. 2004a. Characterization of oligomeric human ATP binding cassette transporter A1. Potential implications for determining the structure of nascent high density lipoprotein particles. *J Biol Chem,* 279**,** 41529-36.

DENIS, M., HAIDAR, B., MARCIL, M., BOUVIER, M., KRIMBOU, L. & GENEST, J. 2004b. Molecular and Cellular Physiology of Apolipoprotein A-I Lipidation by the ATP-binding Cassette Transporter A1 (ABCA1). *Journal of Biological Chemistry,* 279**,** 7384-7394.

DEREURE, O. 2014. [Of genes and hair]. *Ann Dermatol Venereol,* 141**,** 648-9.

DESTEFANO, G. M., KURBAN, M., ANYANE-YEBOA, K., DALL'ARMI, C., DI PAOLO, G., FEENSTRA, H., SILVERBERG, N., ROHENA, L., LOPEZ-CEPEDA, L. D., JOBANPUTRA, V., FANTAUZZO, K. A., KIURU, M., TADIN-STRAPPS, M., SOBRINO, A., VITEBSKY, A., WARBURTON, D., LEVY, B., SALAS-ALANIS, J. C. & CHRISTIANO, A. M. 2014. Mutations in the cholesterol transporter gene ABCA5 are associated with excessive hair overgrowth. *PLoS Genet,* 10**,** e1004333.

DI-POI, N., MICHALIK, L., DESVERGNE, B. & WAHLI, W. 2004. Functions of peroxisome proliferator-activated receptors (PPAR) in skin homeostasis. *Lipids,* 39**,** 1093-9.

DIAS, I. H. K., MILIC, I., DEVITT, A., SPICKETT, C. M., PITT, A. R. & GRIFFITHS, H. R. 2016. Mass spectrometry based method for measurement of oxysterols. *Free Radical Biology and Medicine,* 96**,** S27.

DIMRI, G. P., LEE, X., BASILE, G., ACOSTA, M., SCOTT, G., ROSKELLEY, C., MEDRANO, E. E., LINSKENS, M., RUBELJ, I., PEREIRA-SMITH, O. & ET AL. 1995. A biomarker that identifies senescent human cells in culture and in aging skin in vivo. *Proc Natl Acad Sci U S A,* 92**,** 9363-7.

DUCHATELET, S. & HOVNANIAN, A. 2015. Olmsted syndrome: clinical, molecular and therapeutic aspects. *Orphanet Journal of Rare Diseases,* 10**,** 33.

DUSELL, C. D., UMETANI, M., SHAUL, P. W., MANGELSDORF, D. J. & MCDONNELL, D. P. 2008. 27-hydroxycholesterol is an endogenous selective estrogen receptor modulator. *Mol Endocrinol,* 22**,** 65-77.

EL SAYED, M. H., ABDALLAH, M. A., ALY, D. G. & KHATER, N. H. 2016. Association of metabolic syndrome with female pattern hair loss in women: A case-control study. *Int J Dermatol,* 55**,** 1131-7.

ELBADAWY, H. M., BORTHWICK, F., WRIGHT, C., MARTIN, P. E. & GRAHAM, A. 2011. Cytosolic StAR-related lipid transfer domain 4 (STARD4) protein influences keratinocyte lipid phenotype and differentiation status. *Br J Dermatol,* 164**,** 628-32.

ELIAS, P. M., WILLIAMS, M. L., CHOI, E. H. & FEINGOLD, K. R. 2014. Role of cholesterol sulfate in epidermal structure and function: lessons from X-linked ichthyosis. *Biochim Biophys Acta,* 1841**,** 353-61.

ELIAS, P. M., WILLIAMS, M. L., HOLLERAN, W. M., JIANG, Y. J. & SCHMUTH, M. 2008. Pathogenesis of permeability barrier abnormalities in the ichthyoses: inherited disorders of lipid metabolism. *J Lipid Res,* 49**,** 697-714.

ELLIS, J. A., STEBBING, M. & HARRAP, S. B. 2001. Male pattern baldness is not associated with established cardiovascular risk factors in the general population. *Clin Sci (Lond),* 100**,** 401-4.

ELLIS, R. A. & MORETTI, G. 1959. Vascular patterns associated with categen hair follicles in the human scalp. *Ann N Y Acad Sci,* 83**,** 448-57.

ENGEL, T., KANNENBERG, F., FOBKER, M., NOFER, J. R., BODE, G., LUEKEN, A., ASSMANN, G. & SEEDORF, U. 2007. Expression of ATP binding cassette-transporter ABCG1 prevents cell death by transporting cytotoxic 7beta-hydroxycholesterol. *FEBS Lett,* 581**,** 1673-80.

ENGLISH, R. S., JR. 2018. A hypothetical pathogenesis model for androgenic alopecia: clarifying the dihydrotestosterone paradox and rate-limiting recovery factors. *Med Hypotheses,* 111**,** 73-81.

EVERS, B. M., FAROOQI, M. S., SHELTON, J. M., RICHARDSON, J. A., GOLDSTEIN, J. L., BROWN, M. S. & LIANG, G. 2010. Hair growth defects in Insig-deficient mice caused by cholesterol precursor accumulation and reversed by simvastatin. *J Invest Dermatol,* 130**,** 1237-48.

FECHER, L. A. & SHARFMAN, W. H. 2015. Advanced basal cell carcinoma, the hedgehog pathway, and treatment options - role of smoothened inhibitors. *Biologics : targets & therapy,* 9**,** 129-140.

FEINGOLD, K. R. 2009. The outer frontier: the importance of lipid metabolism in the skin. *J Lipid Res,* 50 Suppl**,** S417-22.

FEINGOLD, K. R., BROWN, B. E., LEAR, S. R., MOSER, A. H. & ELIAS, P. M. 1983. Localization of de novo sterologenesis in mammalian skin. *J Invest Dermatol,* 81**,** 365-9.

FEINGOLD, K. R. & ELIAS, P. M. 2014. Role of lipids in the formation and maintenance of the cutaneous permeability barrier. *Biochim Biophys Acta,* 1841**,** 280-94.

FEINGOLD, K. R. & JIANG, Y. J. 2011. The mechanisms by which lipids coordinately regulate the formation of the protein and lipid domains of the stratum corneum: Role of fatty acids, oxysterols, cholesterol sulfate and ceramides as signaling molecules. *Dermatoendocrinol,* 3**,** 113-8.

FENG, J., GAO, J., LI, Y., YANG, Y., DANG, L., YE, Y., DENG, J. & LI, A. 2014. BMP4 enhances foam cell formation by BMPR-2/Smad1/5/8 signaling. *Int J Mol Sci,* 15**,** 5536-52.

FOFANA, M., MABOUNDOU, J. C., BOCQUET, J. & LE GOFF, D. 1996. Transfer of cholesterol between high density lipoproteins and cultured rat Sertoli cells. *Biochem Cell Biol,* 74**,** 681-6.

FONG, K., TAKEICHI, T., LIU, L., PRAMANIK, R., LEE, J., AKIYAMA, M. & MCGRATH, J. A. 2015. Ichthyosis follicularis, atrichia, and photophobia syndrome associated with a new mutation in MBTPS2. *Clin Exp Dermatol,* 40**,** 529-32.

FONG, K., WEDGEWORTH, E. K., LAI-CHEONG, J. E., TOSI, I., MELLERIO, J. E., POWELL, A. M. & MCGRATH, J. A. 2012. MBTPS2 mutation in a British pedigree with keratosis follicularis spinulosa decalvans. *Clin Exp Dermatol,* 37**,** 631-4.

FREIRE, E., GOMES, F. C., JOTHA-MATTOS, T., NETO, V. M., SILVA FILHO, F. C. & COELHO-SAMPAIO, T. 2004. Sialic acid residues on astrocytes regulate neuritogenesis by controlling the assembly of laminin matrices. *J Cell Sci,* 117**,** 4067-76.

FREITAS GOUVEIA, M. & TRUEB, R. M. 2017. Unsuccessful Treatment of Alopecia Areata with Simvastatin/Ezetimibe: Experience in 12 Patients. *Skin Appendage Disord,* 3**,** 156-160.

FU, X., MENKE, J. G., CHEN, Y., ZHOU, G., MACNAUL, K. L., WRIGHT, S. D., SPARROW, C. P. & LUND, E. G. 2001. 27-hydroxycholesterol is an endogenous ligand for liver X receptor in cholesterol-loaded cells. *J Biol Chem,* 276**,** 38378-87.

FU, Y., HSIAO, J. H., PAXINOS, G., HALLIDAY, G. M. & KIM, W. S. 2015. ABCA5 regulates amyloid-beta peptide production and is associated with Alzheimer's disease neuropathology. *J Alzheimers Dis,* 43**,** 857-69.

FU, Y., MUKHAMEDOVA, N., IP, S., D'SOUZA, W., HENLEY, K. J., DITOMMASO, T., KESANI, R., DITIATKOVSKI, M., JONES, L., LANE, R. M., JENNINGS, G., SMYTH, I. M., KILE, B. T. & SVIRIDOV, D. 2013. ABCA12 regulates ABCA1-dependent cholesterol efflux from macrophages and the development of atherosclerosis. *Cell Metab,* 18**,** 225-38.

GAO, J., DEROUEN, M. C., CHEN, C.-H., NGUYEN, M., NGUYEN, N. T., IDO, H., HARADA, K., SEKIGUCHI, K., MORGAN, B. A., MINER, J. H., ORO, A. E. & MARINKOVICH, M. P. 2008. Laminin-511 is an epithelial message promoting dermal papilla development and function during early hair morphogenesis. *Genes & development,* 22**,** 2111-2124.

GAO, K., SHEN, Z., YUAN, Y., HAN, D., SONG, C., GUO, Y. & MEI, X. 2016. Simvastatin inhibits neural cell apoptosis and promotes locomotor recovery via activation of Wnt/beta-catenin signaling pathway after spinal cord injury. *J Neurochem,* 138**,** 139-49.

GAO, Y., LI, W., LIU, X., GAO, F. & ZHAO, X. 2015. Reversing effect and mechanism of soluble resistance-related calcium-binding protein on multidrug resistance in human lung cancer A549/DDP cells. *Mol Med Rep,* 11**,** 2118-24.

GASPAR, N. K. 2016. DHEA and frontal fibrosing alopecia: molecular and physiopathological mechanisms. *Anais brasileiros de dermatologia,* 91**,** 776-780.

GEILLON, F., GONDCAILLE, C., RAAS, Q., DIAS, A. M. M., PECQUEUR, D., TRUNTZER, C., LUCCHI, G., DUCOROY, P., FALSON, P., SAVARY, S. & TROMPIER, D. 2017. Peroxisomal ATP-binding cassette transporters form mainly tetramers. *J Biol Chem,* 292**,** 6965-6977.

GETZ, G. S. & REARDON, C. A. 2009. Apoprotein E as a lipid transport and signaling protein in the blood, liver, and artery wall. *J Lipid Res,* 50 Suppl**,** S156-61.

GEYFMAN, M., PLIKUS, M. V., TREFFEISEN, E., ANDERSEN, B. & PAUS, R. 2015. Resting no more: re-defining telogen, the maintenance stage of the hair growth cycle. *Biological Reviews,* 90**,** 1179-1196.

GNIADECKI, R., CHRISTOFFERSEN, N. & WULF, H. C. 2002. Cholesterol-rich plasma membrane domains (lipid rafts) in keratinocytes: importance in the baseline and UVA-induced generation of reactive oxygen species. *J Invest Dermatol,* 118**,** 582-8.

GOLA, M., CZAJKOWSKI, R., BAJEK, A., DURA, A. & DREWA, T. 2012. Melanocyte stem cells: biology and current aspects. *Medical science monitor : international medical journal of experimental and clinical research,* 18**,** RA155-RA159.

GOLDSTEIN, J. L. & BROWN, M. S. 1990. Regulation of the mevalonate pathway. *Nature,* 343**,** 425-430.

GORDON, J. A., NOBLE, J. W., MIDHA, A., DERAKHSHAN, F., WANG, G., ADOMAT, H. H., TOMLINSON GUNS, E. S., LIN, Y. Y., REN, S., COLLINS, C. C., NELSON, P. S., MORRISSEY, C., WASAN, K. M. & COX, M. E. 2019. Upregulation of Scavenger Receptor B1 Is Required for Steroidogenic and Nonsteroidogenic Cholesterol Metabolism in Prostate Cancer. *Cancer Res,* 79**,** 3320-3331.

GU, H.-M., LI, G., GAO, X., BERTHIAUME, L. G. & ZHANG, D.-W. 2013. Characterization of palmitoylation of ATP binding cassette transporter G1: Effect on protein trafficking and function. *Biochimica et Biophysica Acta (BBA) - Molecular and Cell Biology of Lipids,* 1831**,** 1067-1078.

GU, H. F., LI, H. Z., TANG, Y. L., TANG, X. Q., ZHENG, X. L. & LIAO, D. F. 2016. Nicotinate-Curcumin Impedes Foam Cell Formation from THP-1 Cells through Restoring Autophagy Flux. *PLoS One,* 11**,** e0154820.

GUHA, U., MECKLENBURG, L., COWIN, P., KAN, L., O'GUIN, W. M., D'VIZIO, D., PESTELL, R. G., PAUS, R. & KESSLER, J. A. 2004. Bone morphogenetic protein signaling regulates postnatal hair follicle differentiation and cycling. *Am J Pathol,* 165**,** 729-40.

GUO, L., ZHENG, Z., AI, J., HUANG, B. & LI, X. A. 2014. Hepatic scavenger receptor BI protects against polymicrobial-induced sepsis through promoting LPS clearance in mice. *J Biol Chem,* 289**,** 14666-73.

GUPTA, M., MAHAJAN, V. K., MEHTA, K. S., CHAUHAN, P. S. & RAWAT, R. 2015. Peroxisome proliferator-activated receptors (PPARs) and PPAR agonists: the 'future' in dermatology therapeutics? *Archives of Dermatological Research,* 307**,** 767-780.

GUZZO, C. A., MARGOLIS, D. J. & JOHNSON, J. 1996. Lipid profiles, alopecia, and coronary disease: any relationship? *Dermatol Surg,* 22**,** 481.

HAGHIGHI, A., SCOTT, C. A., POON, D. S., YAGHOOBI, R., SALEH-GOHARI, N., PLAGNOL, V. & KELSELL, D. P. 2013. A missense mutation in the MBTPS2 gene underlies the X-linked form of Olmsted syndrome. *J Invest Dermatol,* 133**,** 571-3.

HAIDAR, B., DENIS, M., KRIMBOU, L., MARCIL, M. & GENEST, J., JR. 2002. cAMP induces ABCA1 phosphorylation activity and promotes cholesterol efflux from fibroblasts. *J Lipid Res,* 43**,** 2087-94.

HAMILTON, J. B. 1960. EFFECT OF CASTRATION IN ADOLESCENT AND YOUNG ADULT MALES UPON FURTHER CHANGES IN THE PROPORTIONS OF BARE AND HAIRY SCALP*. *The Journal of Clinical Endocrinology & Metabolism,* 20**,** 1309-1318.

HANLEY, K., NG, D. C., HE, S. S., LAU, P., MIN, K., ELIAS, P. M., BIKLE, D. D., MANGELSDORF, D. J., WILLIAMS, M. L. & FEINGOLD, K. R. 2000. Oxysterols induce differentiation in human keratinocytes and increase Ap-1-dependent involucrin transcription. *J Invest Dermatol,* 114**,** 545-53.

HANLEY, K., WOOD, L., NG, D. C., HE, S. S., LAU, P., MOSER, A., ELIAS, P. M., BIKLE, D. D., WILLIAMS, M. L. & FEINGOLD, K. R. 2001. Cholesterol sulfate stimulates involucrin transcription in keratinocytes by increasing Fra-1, Fra-2, and Jun D. *J Lipid Res,* 42**,** 390-8.

HANNEN, R. F., MICHAEL, A. E., JAULIM, A., BHOGAL, R., BURRIN, J. M. & PHILPOTT, M. P. 2011. Steroid synthesis by primary human keratinocytes; implications for skin disease. *Biochem Biophys Res Commun,* 404**,** 62-7.

HANYU, O., NAKAE, H., MIIDA, T., HIGASHI, Y., FUDA, H., ENDO, M., KOHJITANI, A., SONE, H. & STROTT, C. A. 2012. Cholesterol sulfate induces expression of the skin barrier protein filaggrin in normal human epidermal keratinocytes through induction of RORalpha. *Biochem Biophys Res Commun,* 428**,** 99-104.

HARDY, L., FRISDAL, E. & LE GOFF, W. 2017. Critical Role of the Human ATP-Binding Cassette G1 Transporter in Cardiometabolic Diseases. *International Journal of Molecular Sciences,* 18**,** 1892.

HAREL, S., HIGGINS, C. A., CERISE, J. E., DAI, Z., CHEN, J. C., CLYNES, R. & CHRISTIANO, A. M. 2015. Pharmacologic inhibition of JAK-STAT signaling promotes hair growth. *Sci Adv,* 1**,** e1500973.

HARLAND, D. P. & PLOWMAN, J. E. 2018. Development of Hair Fibres. *In:* PLOWMAN, J. E., HARLAND, D. P. & DEB-CHOUDHURY, S. (eds.) *The Hair Fibre: Proteins, Structure and Development.* Singapore: Springer Singapore.

HARNCHOOWONG, S. & SUCHONWANIT, P. 2017. PPAR-γ Agonists and Their Role in Primary Cicatricial Alopecia %J PPAR Research. *PPAR Res,* 2017**,** 12.

HARRIES, M. J., JIMENEZ, F., IZETA, A., HARDMAN, J., PANICKER, S. P., POBLET, E. & PAUS, R. 2018. Lichen Planopilaris and Frontal Fibrosing Alopecia as Model Epithelial Stem Cell Diseases. *Trends Mol Med,* 24**,** 435-448.

HARRIS, I. R., HOPPNER, H., SIEFKEN, W., FARRELL, A. M. & WITTERN, K. P. 2000. Regulation of HMG-CoA synthase and HMG-CoA reductase by insulin and epidermal growth factor in HaCaT keratinocytes. *J Invest Dermatol,* 114**,** 83-7.

HAS, C., BRUCKNER-TUDERMAN, L., MÜLLER, D., FLOETH, M., FOLKERS, E., DONNAI, D. & TRAUPE, H. 2000. The Conradi–Hünermann–Happle syndrome (CDPX2) and emopamil binding protein: novel mutations, and somatic and gonadal mosaicism. *Human Molecular Genetics,* 9**,** 1951-1955.

HASHIMOTO, K. 1988. The structure of human hair. *Clinics in Dermatology,* 6**,** 7-21.

HASHIMOTO, Y., SUGIURA, H., TOGO, S., KOARAI, A., ABE, K., YAMADA, M., ICHIKAWA, T., KIKUCHI, T., NUMAKURA, T., ONODERA, K., TANAKA, R., SATO, K., YANAGISAWA, S., OKAZAKI, T., TAMADA, T., KIKUCHI, T., HOSHIKAWA, Y., OKADA, Y. & ICHINOSE, M. 2016. 27-Hydroxycholesterol accelerates cellular senescence in human lung resident cells. *Am J Physiol Lung Cell Mol Physiol,* 310**,** L1028-L1041.

HASLAM, I. S., EL-CHAMI, C., FARUQI, H., SHAHMALAK, A., O'NEILL, C. A. & PAUS, R. 2015. Differential expression and functionality of ATP-binding cassette transporters in the human hair follicle. *Br J Dermatol,* 172**,** 1562-1572.

HASLAM, I. S., JADKAUSKAITE, L., SZABO, I. L., STAEGE, S., HESEBECK-BRINCKMANN, J., JENKINS, G., BHOGAL, R. K., LIM, F. L., FARJO, N., FARJO, B., BIRO, T., SCHAFER, M. & PAUS, R. 2017. Oxidative Damage Control in a Human (Mini-) Organ: Nrf2 Activation Protects against Oxidative Stress-Induced Hair Growth Inhibition. *J Invest Dermatol,* 137**,** 295-304.

HAWKSHAW, N. J., HARDMAN, J. A., ALAM, M., JIMENEZ, F. & PAUS, R. 2020. Deciphering the molecular morphology of the human hair cycle: Wnt signalling during the telogen–anagen transformation. *British Journal of Dermatology,* 182**,** 1184-1193.

HAYASHI, R., YOSHIDA, K., ABE, R., NIIZEKI, H. & SHIMOMURA, Y. 2017. First Japanese case of congenital generalized hypertrichosis with a copy number variation on chromosome 17q24. *J Dermatol Sci,* 85**,** 63-65.

HEDDITCH, E. L., GAO, B., RUSSELL, A. J., LU, Y., EMMANUEL, C., BEESLEY, J., JOHNATTY, S. E., CHEN, X., HARNETT, P., GEORGE, J., WILLIAMS, R. T., FLEMMING, C., LAMBRECHTS, D., DESPIERRE, E., LAMBRECHTS, S., VERGOTE, I., KARLAN, B., LESTER, J., ORSULIC, S., WALSH, C., FASCHING, P., BECKMANN, M. W., EKICI, A. B., HEIN, A., MATSUO, K., HOSONO, S., NAKANISHI, T., YATABE, Y., PEJOVIC, T., BEAN, Y., HEITZ, F., HARTER, P., DU BOIS, A., SCHWAAB, I., HOGDALL, E., KJAER, S. K., JENSEN, A., HOGDALL, C., LUNDVALL, L., ENGELHOLM, S. A., BROWN, B., FLANAGAN, J., METCALF, M. D., SIDDIQUI, N., SELLERS, T., FRIDLEY, B., CUNNINGHAM, J., SCHILDKRAUT, J., IVERSEN, E., WEBER, R. P., BERCHUCK, A., GOODE, E., BOWTELL, D. D., CHENEVIX-TRENCH, G., DEFAZIO, A., NORRIS, M. D., MACGREGOR, S., HABER, M. & HENDERSON, M. J. 2014. ABCA transporter gene expression and poor outcome in epithelial ovarian cancer. *J Natl Cancer Inst,* 106**,** dju149.

HEGYI, Z. & HOMOLYA, L. 2016. Functional Cooperativity between ABCG4 and ABCG1 Isoforms. *PLoS One,* 11**,** e0156516.

HEINZ, L., KIM, G. J., MARRAKCHI, S., CHRISTIANSEN, J., TURKI, H., RAUSCHENDORF, M. A., LATHROP, M., HAUSSER, I., ZIMMER, A. D. & FISCHER, J. 2017. Mutations in SULT2B1 Cause Autosomal-Recessive Congenital Ichthyosis in Humans. *Am J Hum Genet,* 100**,** 926-939.

HIBINO, T. & NISHIYAMA, T. 2004. Role of TGF-β2 in the human hair cycle. *Journal of Dermatological Science,* 35**,** 9-18.

HIGGINS, C. A., RICHARDSON, G. D., FERDINANDO, D., WESTGATE, G. E. & JAHODA, C. A. B. 2010. Modelling the hair follicle dermal papilla using spheroid cell cultures. *Experimental Dermatology,* 19**,** 546-548.

HLAVÁČ, V., BRYNYCHOVÁ, V., VÁCLAVÍKOVÁ, R., EHRLICHOVÁ, M., VRÁNA, D., PECHA, V., KOŽEVNIKOVOVÁ, R., TRNKOVÁ, M., GATĚK, J., KOPPEROVÁ, D., GUT, I. & SOUČEK, P. 2013. The expression profile of ATP-binding cassette transporter genes in breast carcinoma. *Pharmacogenomics,* 14**,** 515-29.

HO, B. S., VAZ, C., RAMASAMY, S., CHEW, E. G. Y., MOHAMED, J. S., JAFFAR, H., HILLMER, A., TANAVDE, V., BIGLIARDI-QI, M. & BIGLIARDI, P. L. 2019. Progressive expression of PPARGC1alpha is associated with hair miniaturization in androgenetic alopecia. *Sci Rep,* 9**,** 8771.

HOLTTA-VUORI, M., SEZGIN, E., EGGELING, C. & IKONEN, E. 2016. Use of BODIPY-Cholesterol (TF-Chol) for Visualizing Lysosomal Cholesterol Accumulation. *Traffic,* 17**,** 1054-7.

HOLTTA-VUORI, M., URONEN, R. L., REPAKOVA, J., SALONEN, E., VATTULAINEN, I., PANULA, P., LI, Z., BITTMAN, R. & IKONEN, E. 2008. BODIPY-cholesterol: a new tool to visualize sterol trafficking in living cells and organisms. *Traffic,* 9**,** 1839-49.

HOZOJI, M., KIMURA, Y., KIOKA, N. & UEDA, K. 2009. Formation of Two Intramolecular Disulfide Bonds Is Necessary for ApoA-I-dependent Cholesterol Efflux Mediated by ABCA1. *Journal of Biological Chemistry,* 284**,** 11293-11300.

HSIEH, V., KIM, M. J., GELISSEN, I. C., BROWN, A. J., SANDOVAL, C., HALLAB, J. C., KOCKX, M., TRAINI, M., JESSUP, W. & KRITHARIDES, L. 2014. Cellular cholesterol regulates ubiquitination and degradation of the cholesterol export proteins ABCA1 and ABCG1. *J Biol Chem,* 289**,** 7524-36.

HSU, Y.-C., PASOLLI, H. A. & FUCHS, E. 2011. Dynamics between stem cells, niche, and progeny in the hair follicle. *Cell,* 144**,** 92-105.

HSU, Y. C., LI, L. & FUCHS, E. 2014. Transit-amplifying cells orchestrate stem cell activity and tissue regeneration. *Cell,* 157**,** 935-49.

HU, J., ZHANG, Z., SHEN, W.-J., AZHAR, S. J. N. & METABOLISM 2010. Cellular cholesterol delivery, intracellular processing and utilization for biosynthesis of steroid hormones. *Nutr Metab (Lond),* 7**,** 47.

HU, Y., WANG, M., VEVERKA, K., GARCIA, F. U. & STEARNS, M. E. 2007. The ABCA5 Protein: A Urine Diagnostic Marker for Prostatic Intraepithelial Neoplasia. *Clin Cancer Res,* 13**,** 929-938.

HUANG, P., NEDELCU, D., WATANABE, M., JAO, C., KIM, Y., LIU, J. & SALIC, A. 2016. Cellular Cholesterol Directly Activates Smoothened in Hedgehog Signaling. *Cell,* 166**,** 1176-1187.e14.

HUANG, W. Y., LIN, E. T. Y., HSU, Y. C. & LIN, S. J. 2019a. Anagen hair follicle repair: Timely regenerative attempts from plastic extra-bulge epithelial cells. *Experimental Dermatology,* 28**,** 406-412.

HUANG, X., LIU, D., ZHANG, R. & SHI, X. 2019b. Transcriptional Responses in Defense-Related Genes of Sitobion avenae (Hemiptera: Aphididae) Feeding on Wheat and Barley. *J Econ Entomol,* 112**,** 382-395.

HUBLER, Z., ALLIMUTHU, D., BEDERMAN, I., ELITT, M. S., MADHAVAN, M., ALLAN, K. C., SHICK, H. E., GARRISON, E., T. KARL, M., FACTOR, D. C., NEVIN, Z. S., SAX, J. L., THOMPSON, M. A., FEDOROV, Y., JIN, J., WILSON, W. K., GIERA, M., BRACHER, F., MILLER, R. H., TESAR, P. J. & ADAMS, D. J. 2018. Accumulation of 8,9-unsaturated sterols drives oligodendrocyte formation and remyelination. *Nature,* 560**,** 372-376.

ICRE, G., WAHLI, W. & MICHALIK, L. 2006. Functions of the peroxisome proliferator-activated receptor (PPAR) alpha and beta in skin homeostasis, epithelial repair, and morphogenesis. *J Investig Dermatol Symp Proc,* 11**,** 30-5.

IKEGAWA, S., OHASHI, H., OGATA, T., HONDA, A., TSUKAHARA, M., KUBO, T., KIMIZUKA, M., SHIMODE, M., HASEGAWA, T., NISHIMURA, G. & NAKAMURA, Y. 2000. Novel and recurrent EBP mutations in X-linked dominant chondrodysplasia punctata. *Am J Med Genet,* 94**,** 300-5.

IKONEN, E. 2008. Cellular cholesterol trafficking and compartmentalization. *Nat Rev Mol Cell Biol,* 9**,** 125-38.

IMANISHI, H., ANSELL, D. M., CHERET, J., HARRIES, M., BERTOLINI, M., SEPP, N., BIRO, T., POBLET, E., JIMENEZ, F., HARDMAN, J., PANICKER, S. P., WARD, C. M. & PAUS, R. 2018. Epithelial-to-Mesenchymal Stem Cell Transition in a Human Organ: Lessons from Lichen Planopilaris. *J Invest Dermatol,* 138**,** 511-519.

IMANISHI, H., TSURUTA, D., TATEISHI, C., SUGAWARA, K., PAUS, R., TSUJI, T., ISHII, M., IKEDA, K., KUNIMOTO, H., NAKAJIMA, K., JONES, J. C. R. & KOBAYASHI, H. 2010. Laminin-

511, inducer of hair growth, is down-regulated and its suppressor in hair growth, laminin-332 up-regulated in chemotherapy-induced alopecia. *Journal of dermatological science,* 58**,** 43-54.

INCARDONA, J. P. & EATON, S. 2000. Cholesterol in signal transduction. *Current Opinion in Cell Biology,* 12**,** 193-203.

INOUE, T., MIKI, Y., ABE, K., HATORI, M., HOSAKA, M., KARIYA, Y., KAKUO, S., FUJIMURA, T., HACHIYA, A., HONMA, S., AIBA, S. & SASANO, H. 2012. Sex steroid synthesis in human skin in situ: the roles of aromatase and steroidogenic acute regulatory protein in the homeostasis of human skin. *Mol Cell Endocrinol,* 362**,** 19-28.

INUI, S. & ITAMI, S. 2013. Androgen actions on the human hair follicle: perspectives. *Exp Dermatol,* 22**,** 168-71.

IZUMI, K., WILKENS, A., TREAT, J. R., PRIDE, H. B. & KRANTZ, I. D. 2013. Novel MBTPS2 missense mutation in the N-terminus transmembrane domain in a patient with ichthyosis follicularis, alopecia, and photophobia syndrome. *Pediatr Dermatol,* 30**,** e263-4.

JACQUEROUX, E., HODIN, S., SAIB, S., HE, Z., BIN, V., DELÉZAY, O. & DELAVENNE, X. 2020. Value of quantifying ABC transporters by mass spectrometry and impact on in vitro-to-in vivo prediction of transporter-mediated drug-drug interactions of rivaroxaban. *European Journal of Pharmaceutics and Biopharmaceutics,* 148**,** 27-37.

JANS, R., ATANASOVA, G., JADOT, M. & POUMAY, Y. 2004. Cholesterol depletion upregulates involucrin expression in epidermal keratinocytes through activation of p38. *J Invest Dermatol,* 123**,** 564-73.

JANS, R., MOTTRAM, L., JOHNSON, D. L., BROWN, A. M., SIKKINK, S., ROSS, K. & REYNOLDS, N. J. 2013. Lysophosphatidic acid promotes cell migration through STIM1- and Orai1-mediated Ca2+(i) mobilization and NFAT2 activation. *The Journal of investigative dermatology,* 133**,** 793-802.

JEFCOATE, C. R. & LEE, J. 2018. Cholesterol signaling in single cells: lessons from STAR and sm-FISH. *Journal of molecular endocrinology,* 60**,** R213-R235.

JIANG, Y. J., KIM, P., ELIAS, P. M. & FEINGOLD, K. R. 2005. LXR and PPAR activators stimulate cholesterol sulfotransferase type 2 isoform 1b in human keratinocytes. *J Lipid Res,* 46**,** 2657-66.

JIANG, Y. J., LU, B., KIM, P., ELIAS, P. M. & FEINGOLD, K. R. 2006. Regulation of ABCA1 expression in human keratinocytes and murine epidermis. *J Lipid Res,* 47**,** 2248-58.

JIANG, Y. J., LU, B., TARLING, E. J., KIM, P., MAN, M. Q., CRUMRINE, D., EDWARDS, P. A., ELIAS, P. M. & FEINGOLD, K. R. 2010. Regulation of ABCG1 expression in human keratinocytes and murine epidermis. *J Lipid Res,* 51**,** 3185-95.

JIN, S. H., LEE, Y. Y. & KANG, H. Y. 2008. Methyl-β-cyclodextrin, a specific cholesterol-binding agent, inhibits melanogenesis in human melanocytes through activation of ERK. *Archives of Dermatological Research,* 300**,** 451-454.

JIN, X., FREEMAN, S. R., VAISMAN, B., LIU, Y., CHANG, J., VARSANO, N., ADDADI, L., REMALEY, A. & KRUTH, H. S. 2015. ABCA1 contributes to macrophage deposition of extracellular cholesterol. *J Lipid Res,* 56**,** 1720-6.

JIN, X., SVIRIDOV, D., LIU, Y., VAISMAN, B., ADDADI, L., REMALEY, A. T. & KRUTH, H. S. 2016. ABCA1 (ATP-Binding Cassette Transporter A1) Mediates ApoA-I (Apolipoprotein A-I) and ApoA-I Mimetic Peptide Mobilization of Extracellular Cholesterol Microdomains Deposited by Macrophages. *Arterioscler Thromb Vasc Biol,* 36**,** 2283-2291.

JOHN, E., WIENECKE-BALDACCHINO, A., LIIVRAND, M., HEINÄNIEMI, M., CARLBERG, C. & SINKKONEN, L. 2012. Dataset integration identifies transcriptional regulation of microRNA genes by PPARγ in differentiating mouse 3T3-L1 adipocytes. *Nucleic Acids Research,* 40**,** 4446-4460.

JONES, E., MARSH, S., O'SHAUGHNESSY, R., AUMAILLEY, M., O'TOOLE, E. A. & CALEY, M. P. 2018. 680 A role for the basement membrane in skin lipid trafficking. *Journal of Investigative Dermatology,* 138**,** S116.

JONES, E. M., MARSH, S., O'SHAUGHNESSY, R. F., CAMERA, E., PICARDO, M., AUMAILLEY, M., O'TOOLE, E. & CALEY, M. 2019. 274 Junctional Epidermolysis Bullosa: Bottom Up Control Of The Skin Barrier? *Journal of Investigative Dermatology,* 139**,** S261.

JOOST, S., ANNUSVER, K., JACOB, T., SUN, X., DALESSANDRI, T., SIVAN, U., SEQUEIRA, I., SANDBERG, R. & KASPER, M. 2020. The Molecular Anatomy of Mouse Skin during Hair Growth and Rest. *Cell Stem Cell,* 26**,** 441-457.e7.

JOOST, S., ANNUSVER, K.*, JACOB, T., SUN, X., SIVAN, U., DALESSANDRI T., SEQUEIRA, I., SANDBERG, R. AND KASPER M. 2020. *The molecular anatomy of mouse skin during hair growth and rest: data portal* [Online]. Available: http://kasperlab.org/mouseskin [Accessed 26/02/2020 2020].

JOSHI, R. S. 2011. The Inner Root Sheath and the Men Associated with it Eponymically. *International journal of trichology,* 3**,** 57-62.

JOUBEH, S., MORI, O., OWARIBE, K. & HASHIMOTO, T. 2003. Immunofluorescence analysis of the basement membrane zone components in human anagen hair follicles. *Experimental Dermatology,* 12**,** 365-370.

JOUGASAKI, M., ICHIKI, T., TAKENOSHITA, Y. & SETOGUCHI, M. 2010. Statins suppress interleukin-6-induced monocyte chemo-attractant protein-1 by inhibiting Janus kinase/signal

transducers and activators of transcription pathways in human vascular endothelial cells. *British journal of pharmacology,* 159**,** 1294-1303.

KADAJA, M., KEYES, B. E., LIN, M., PASOLLI, H. A., GENANDER, M., POLAK, L., STOKES, N., ZHENG, D. & FUCHS, E. 2014. SOX9: a stem cell transcriptional regulator of secreted niche signaling factors. *Genes & development,* 28**,** 328-341.

KANDUTSCH, A. A. & RUSSELL, A. E. 1960. Preputial gland tumor sterols. 3. A metabolic pathway from lanosterol to cholesterol. *J Biol Chem,* 235**,** 2256-61.

KARATAS, O. F., GUZEL, E., DUZ, M. B., ITTMANN, M. & OZEN, M. 2016. The role of ATP-binding cassette transporter genes in the progression of prostate cancer. *Prostate,* 76**,** 434-444.

KARDASSIS, D., GAFENCU, A., ZANNIS, V. I. & DAVALOS, A. 2015. Regulation of HDL genes: transcriptional, posttranscriptional, and posttranslational. *Handb Exp Pharmacol,* 224**,** 113-79.

KARNIK, P., TEKESTE, Z., MCCORMICK, T. S., GILLIAM, A. C., PRICE, V. H., COOPER, K. D. & MIRMIRANI, P. 2009. Hair follicle stem cell-specific PPARγ deletion causes scarring alopecia. *J Invest Dermatol,* 129**,** 1243-57.

KELLIE, S., PATEL, B., PIERCE, E. J. & CRITCHLEY, D. R. 1983. Capping of cholera toxin-ganglioside GM1 complexes on mouse lymphocytes is accompanied by co-capping of alpha-actinin. *J Cell Biol,* 97**,** 447-54.

KIELAR, D., KAMINSKI, W. E., LIEBISCH, G., PIEHLER, A., WENZEL, J. J., MOHLE, C., HEIMERL, S., LANGMANN, T., FRIEDRICH, S. O., BOTTCHER, A., BARLAGE, S., DROBNIK, W. & SCHMITZ, G. 2003. Adenosine triphosphate binding cassette (ABC) transporters are expressed and regulated during terminal keratinocyte differentiation: a potential role for ABCA7 in epidermal lipid reorganization. *J Invest Dermatol,* 121**,** 465-74.

KIM, J. E., LEE, Y. J., PARK, H. R., LEE, D. G., JEONG, K. H. & KANG, H. 2020. The Effect of JAK Inhibitor on the Survival, Anagen Re-Entry, and Hair Follicle Immune Privilege Restoration in Human Dermal Papilla Cells. *International Journal of Molecular Sciences,* 21**,** 5137.

KIM, M. J., LEE, Y. J., YOON, Y. S., KIM, M., CHOI, J. H., KIM, H. S. & KANG, J. L. 2018. Apoptotic cells trigger the ABCA1/STAT6 pathway leading to PPAR-gamma expression and activation in macrophages. *J Leukoc Biol,* 103**,** 885-895.

KIM, M. W., SHIN, I. S., YOON, H. S., CHO, S. & PARK, H. S. 2017. Lipid profile in patients with androgenetic alopecia: a meta-analysis. *J Eur Acad Dermatol Venereol,* 31**,** 942-951.

KIM, W. S. & HALLIDAY, G. M. 2012. Changes in sphingomyelin level affect alpha-synuclein and ABCA5 expression. *J Parkinsons Dis,* 2**,** 41-6.

KIPP, H., PICHETSHOTE, N. & ARIAS, I. M. 2001. Transporters on demand: intrahepatic pools of canalicular ATP binding cassette transporters in rat liver. *J Biol Chem,* 276**,** 7218-24.

KLAPPE, K., HUMMEL, I., HOEKSTRA, D. & KOK, J. W. 2009. Lipid dependence of ABC transporter localization and function. *Chem Phys Lipids,* 161**,** 57-64.

KLOEPPER, J. E., SUGAWARA, K., AL-NUAIMI, Y., GASPAR, E., VAN BEEK, N. & PAUS, R. 2010. Methods in hair research: how to objectively distinguish between anagen and catagen in human hair follicle organ culture. *Exp Dermatol,* 19**,** 305-12.

KOMAROMY, M., AZHAR, S. & COOPER, A. D. 1996. Chinese hamster ovary cells expressing a cell surface-anchored form of hepatic lipase. Characterization of low density lipoprotein and chylomicron remnant uptake and selective uptake of high density lipoprotein-cholesteryl ester. *J Biol Chem,* 271**,** 16906-14.

KRETZSCHMAR, K., COTTLE, D. L., SCHWEIGER, P. J. & WATT, F. M. 2015. The Androgen Receptor Antagonizes Wnt/β-Catenin Signaling in Epidermal Stem Cells. *The Journal of investigative dermatology,* 135**,** 2753-2763.

KRIMBOU, L., DENIS, M., HAIDAR, B., CARRIER, M., MARCIL, M. & GENEST, J. 2004. Molecular interactions between apoE and ABCA1. *Journal of Lipid Research,* 45**,** 839-848.

KRISANS, S. K. 1992. The role of peroxisomes in cholesterol metabolism. *Am J Respir Cell Mol Biol,* 7**,** 358-64.

KUBO, Y., SEKIYA, S., OHIGASHI, M., TAKENAKA, C., TAMURA, K., NADA, S., NISHI, T., YAMAMOTO, A. & YAMAGUCHI, A. 2005. ABCA5 resides in lysosomes, and ABCA5 knockout mice develop lysosomal disease-like symptoms. *Mol Cell Biol,* 25**,** 4138-49.

KWACK, M. H., KIM, M. K., KIM, J. C. & SUNG, Y. K. 2012. Dickkopf 1 promotes regression of hair follicles. *J Invest Dermatol,* 132**,** 1554-60.

LAMBRECHT, C., WOUTERS, C., VAN ESCH, H., MOENS, P., CASTEELS, I. & MORREN, M. A. 2014. Conradi-Hunermann-Happle syndrome: a novel heterozygous missense mutation, c.204G>T (p.W68C). *Pediatr Dermatol,* 31**,** 493-6.

LANDSCHULZ, K. T., PATHAK, R. K., RIGOTTI, A., KRIEGER, M. & HOBBS, H. H. 1996. Regulation of scavenger receptor, class B, type I, a high density lipoprotein receptor, in liver and steroidogenic tissues of the rat. *J Clin Invest,* 98**,** 984-95.

LANGAN, E. A., PHILPOTT, M. P., KLOEPPER, J. E. & PAUS, R. 2015. Human hair follicle organ culture: theory, application and perspectives. *Exp Dermatol,* 24**,** 903-11.

LANGE, Y. 1991. Disposition of intracellular cholesterol in human fibroblasts. *J Lipid Res,* 32**,** 329-39.

LATTOUF, C., JIMENEZ, J. J., TOSTI, A., MITEVA, M., WIKRAMANAYAKE, T. C., KITTLES, C., HERSKOVITZ, I., HANDLER, M. Z., FABBROCINI, G. & SCHACHNER, L. A. 2015. Treatment of alopecia areata with simvastatin/ezetimibe. *J Am Acad Dermatol,* 72**,** 359-61.

LEE, J.-A., CHOI, D.-I., CHOI, J.-Y., KIM, S.-O., CHO, K.-A., LEE, J.-B., YUN, S.-J. & LEE, S.-C. 2015. Methyl-β-cyclodextrin up-regulates collagen I expression in chronologically-aged skin via its anti-caveolin-1 activity. *Oncotarget,* 6**,** 1942-1953.

LEE, J. & TUMBAR, T. 2012. Hairy tale of signaling in hair follicle development and cycling. *Semin Cell Dev Biol,* 23**,** 906-16.

LEE, J. S., SEPPANEN, E., PATEL, J., RODERO, M. P. & KHOSROTEHRANI, K. 2016. ST2 receptor invalidation maintains wound inflammation, delays healing and increases fibrosis. *Exp Dermatol,* 25**,** 71-4.

LEE, T. H. 2000. By the way, doctor... My hair has been thinning out for the past decade or so, but since my doctor started me on Lipitor (atorvastatin) a few months ago for high cholesterol, I swear it's been falling out much faster. My doctor discounts the possibility, but I looked in the Physicians' desk reference (PDR) and alopecia is listed under "adverse reactions." What do you think? *Harv Health Lett,* 25**,** 8.

LEE, W. S. 2011. Integral hair lipid in human hair follicle. *J Dermatol Sci,* 64**,** 153-8.

LEI, M., YANG, L. & CHUONG, C.-M. 2017. Getting to the Core of the Dermal Papilla. *Journal of Investigative Dermatology,* 137**,** 2250-2253.

LI, H., GUO, H. & LI, H. 2013. Cholesterol loading affects osteoblastic differentiation in mouse mesenchymal stem cells. *Steroids,* 78**,** 426-433.

LI, J., DALY, E., CAMPIOLI, E., WABITSCH, M. & PAPADOPOULOS, V. 2014. De novo synthesis of steroids and oxysterols in adipocytes. *J Biol Chem,* 289**,** 747-64.

LIM, Y. Y., KIM, S. Y., KIM, H. M., LI, K. S., KIM, M. N., PARK, K. C. & KIM, B. J. 2014. Potential relationship between the canonical Wnt signalling pathway and expression of the vitamin D receptor in alopecia. *Clin Exp Dermatol,* 39**,** 368-75.

LIMAT, A. & NOSER, F. K. 1986. Serial cultivation of single keratinocytes from the outer root sheath of human scalp hair follicles. *J Invest Dermatol,* 87**,** 485-8.

LIN, C. L., XU, R., YI, J. K., LI, F., CHEN, J., JONES, E. C., SLUTSKY, J. B., HUANG, L., RIGAS, B., CAO, J., ZHONG, X., SNIDER, A. J., OBEID, L. M., HANNUN, Y. A. & MAO, C. 2017. Alkaline Ceramidase 1 Protects Mice from Premature Hair Loss by Maintaining the Homeostasis of Hair Follicle Stem Cells. *Stem Cell Reports,* 9**,** 1488-1500.

LISCUM, L. & UNDERWOOD, K. W. 1995. Intracellular cholesterol transport and compartmentation. *J Biol Chem,* 270**,** 15443-6.

LOI, C., STARACE, M. & PIRACCINI, B. M. 2016. Alopecia areata (AA) and treatment with simvastatin/ezetimibe: Experience of 20 patients. *J Am Acad Dermatol,* 74**,** e99-e100.

LOPEZ, D., SANDHOFF, T. W. & MCLEAN, M. P. 1999. Steroidogenic factor-1 mediates cyclic 3',5'-adenosine monophosphate regulation of the high density lipoprotein receptor. *Endocrinology,* 140**,** 3034-44.

LORDAN, S., MACKRILL, J. J. & O'BRIEN, N. M. 2009. Oxysterols and mechanisms of apoptotic signaling: implications in the pathology of degenerative diseases☆. *The Journal of Nutritional Biochemistry,* 20**,** 321-336.

LORKOWSKI, S., KRATZ, M., WENNER, C., SCHMIDT, R., WEITKAMP, B., FOBKER, M., REINHARDT, J., RAUTERBERG, J., GALINSKI, E. A. & CULLEN, P. 2001. Expression of the ATP-Binding Cassette Transporter Gene ABCG1 (ABC8) in Tangier Disease. *Biochemical and Biophysical Research Communications,* 283**,** 821-830.

LU, G. Q., WU, Z. B., CHU, X. Y., BI, Z. G. & FAN, W. X. 2016. An investigation of crosstalk between Wnt/beta-catenin and transforming growth factor-beta signaling in androgenetic alopecia. *Medicine (Baltimore),* 95**,** e4297.

LUNDBY, A., LAGE, K., WEINERT, B. T., BEKKER-JENSEN, D. B., SECHER, A., SKOVGAARD, T., KELSTRUP, C. D., DMYTRIYEV, A., CHOUDHARY, C., LUNDBY, C. & OLSEN, J. V. 2012. Proteomic analysis of lysine acetylation sites in rat tissues reveals organ specificity and subcellular patterns. *Cell Rep,* 2**,** 419-31.

LUO, D. X., CAO, D. L., XIONG, Y., PENG, X. H. & LIAO, D. F. 2010. A novel model of cholesterol efflux from lipid-loaded cells. *Acta Pharmacol Sin,* 31**,** 1243-57.

LUU, W., ZERENTURK, E. J., KRISTIANA, I., BUCKNALL, M. P., SHARPE, L. J. & BROWN, A. J. 2014. Signaling regulates activity of DHCR24, the final enzyme in cholesterol synthesis. *Journal of lipid research,* 55**,** 410-420.

LYLE, S., CHRISTOFIDOU-SOLOMIDOU, M., LIU, Y., ELDER, D. E., ALBELDA, S. & COTSARELIS, G. 1998. The C8/144B monoclonal antibody recognizes cytokeratin 15 and defines the location of human hair follicle stem cells. *Journal of Cell Science,* 111**,** 3179-3188.

MACK, J. T., TOWNSEND, D. M., BELJANSKI, V. & TEW, K. D. 2007. The ABCA2 transporter: intracellular roles in trafficking and metabolism of LDL-derived cholesterol and sterol-related compounds. *Curr Drug Metab,* 8**,** 47-57.

MAIER, H., MEIXNER, M., HARTMANN, D., SANDHOFF, R., WANG-ECKHARDT, L., ZOLLER, I., GIESELMANN, V. & ECKHARDT, M. 2011. Normal fur development and sebum production depends on fatty acid 2-hydroxylase expression in sebaceous glands. *J Biol Chem,* 286**,** 25922-34.

MAK, L. 2014. *Role of ABCA5 in the Pathogenesis of Parkinson's disease.* Masters by Research, University of New South Wales.

MALERØD, L., JUVET, L. K., HANSSEN-BAUER, A., ESKILD, W. & BERG, T. 2002. Oxysterol-activated LXRα/RXR induces hSR-BI-promoter activity in hepatoma cells and preadipocytes. *Biochemical and Biophysical Research Communications,* 299**,** 916-923.

MANDARD, S., ZANDBERGEN, F., TAN, N. S., ESCHER, P., PATSOURIS, D., KOENIG, W., KLEEMANN, R., BAKKER, A., VEENMAN, F., WAHLI, W., MULLER, M. & KERSTEN, S. 2004. The direct peroxisome proliferator-activated receptor target fasting-induced adipose factor (FIAF/PGAR/ANGPTL4) is present in blood plasma as a truncated protein that is increased by fenofibrate treatment. *J Biol Chem,* 279**,** 34411-20.

MARKO, L., PARAGH, G., UGOCSAI, P., BOETTCHER, A., VOGT, T., SCHLING, P., BALOGH, A., TARABIN, V., ORSO, E., WIKONKAL, N., MANDL, J., REMENYIK, E. & SCHMITZ, G. 2012. Keratinocyte ATP binding cassette transporter expression is regulated by ultraviolet light. *J Photochem Photobiol B,* 116**,** 79-88.

MARQUES, P. E., NYEGAARD, S., COLLINS, R. F., TROISE, F., FREEMAN, S. A., TRIMBLE, W. S. & GRINSTEIN, S. 2019. Multimerization and Retention of the Scavenger Receptor SR-B1 in the Plasma Membrane. *Dev Cell,* 50**,** 283-295 e5.

MARTANOVA, H., KREPELOVA, A., BAXOVA, A., HANSIKOVA, H., CANSKY, Z., KVAPIL, M., GREGOR, V., MAGNER, M. & ZEMAN, J. 2007. X-linked dominant chondrodysplasia punctata (CDPX2): multisystemic impact of the defect in cholesterol biosynthesis. *Prague Med Rep,* 108**,** 263-9.

MASCALCHI, P. & CORDELIÈRES, F. P. 2019. Which Elements to Build Co-localization Workflows? From Metrology to Analysis. *In:* REBOLLO, E. & BOSCH, M. (eds.) *Computer Optimized Microscopy: Methods and Protocols.* New York, NY: Springer New York.

MASUKAWA, Y., NARITA, H. & IMOKAWA, G. 2005. Characterization of the lipid composition at the proximal root regions of human hair. *J Cosmet Sci,* 56**,** 1-16.

MATHAY, C., PIERRE, M., PITTELKOW, M. R., DEPIEREUX, E., NIKKELS, A. F., COLIGE, A. & POUMAY, Y. 2011. Transcriptional profiling after lipid raft disruption in keratinocytes identifies critical mediators of atopic dermatitis pathways. *J Invest Dermatol,* 131**,** 46-58.

MAXFIELD, F. R. & WÜSTNER, D. 2012. Analysis of Cholesterol Trafficking with Fluorescent Probes. Elsevier.

MCGUINN, K. P. & MAHONEY, M. G. 2014. Lipid rafts and detergent-resistant membranes in epithelial keratinocytes. *Methods Mol Biol,* 1195**,** 133-44.

MEGARBANE, H. & MEGARBANE, A. 2011. Ichthyosis follicularis, alopecia, and photophobia (IFAP) syndrome. *Orphanet J Rare Dis,* 6**,** 29.

MESINKOVSKA, N. A., TELLEZ, A., DAWES, D., PILIANG, M. & BERGFELD, W. 2015. The use of oral pioglitazone in the treatment of lichen planopilaris. *Journal of the American Academy of Dermatology,* 72**,** 355-356.

MING, A., HAPPLE, R., GRZESCHIK, K. H. & FISCHER, G. 2009. Ichthyosis follicularis, alopecia, and photophobia (IFAP) syndrome due to mutation of the gene MBTPS2 in a large Australian kindred. *Pediatr Dermatol,* 26**,** 427-31.

MIRZA, R., QIAO, S., MURATA, Y. & SEO, H. 2009. Requirement of DHCR24 for postnatal development of epidermis and hair follicles in mice. *Am J Dermatopathol,* 31**,** 446-52.

MITSCHE, M. A., MCDONALD, J. G., HOBBS, H. H. & COHEN, J. C. 2015. Flux analysis of cholesterol biosynthesis in vivo reveals multiple tissue and cell-type specific pathways. *eLife,* 4**,** e07999.

MOGILENKO, D. A., SHAVVA, V. S., DIZHE, E. B., ORLOV, S. V. & PEREVOZCHIKOV, A. P. 2010. PPARgamma activates ABCA1 gene transcription but reduces the level of ABCA1 protein in HepG2 cells. *Biochem Biophys Res Commun,* 402**,** 477-82.

MOHAMMAD-ALI, Y. A., PREETHI, R., KENNETH, K., HEINZ, K., KORTZ, A. & ANDREW, C. J. 2015. Circumscribed cicatricial alopecia due to localized sarcoidal granulomas and single-organ granulomatous arteritis: a case report and systematic review of sarcoidal vasculitis. *Journal of Cutaneous Pathology,* 42**,** 746-756.

MORICE-PICARD, F., KOSTRZEWA, E., WOLF, C., BENLIAN, P., TAIEB, A. & LACOMBE, D. 2011. Evidence of postzygotic mosaicism in a transmitted form of Conradi-Hunermann-Happle syndrome associated with a novel EBP mutation. *Arch Dermatol,* 147**,** 1073-6.

MURESAN, X. M., NARZT, M.-S., WOODBY, B., FERRARA, F., GRUBER, F. & VALACCHI, G. 2019. Involvement of cutaneous SR-B1 in skin lipid homeostasis. *Archives of Biochemistry and Biophysics,* 666**,** 1-7.

MURESAN, X. M., STICOZZI, C., BELMONTE, G., SAVELLI, V., EVELSON, P. & VALACCHI, G. 2018. Modulation of cutaneous scavenger receptor B1 levels by exogenous stressors impairs "in vitro" wound closure. *Mech Ageing Dev,* 172**,** 78-85.

MYERS, B. R., SEVER, N., CHONG, Y. C., KIM, J., BELANI, J. D., RYCHNOVSKY, S., BAZAN, J. F. & BEACHY, P. A. 2013. Hedgehog pathway modulation by multiple lipid binding sites on the smoothened effector of signal response. *Developmental cell,* 26**,** 346-357.

NAKAMURA, K., KENNEDY, M. A., BALDAN, A., BOJANIC, D. D., LYONS, K. & EDWARDS, P. A. 2004. Expression and regulation of multiple murine ATP-binding cassette transporter G1 mRNAs/isoforms that stimulate cellular cholesterol efflux to high density lipoprotein. *J Biol Chem,* 279**,** 45980-9.

NASSIR, F., WILSON, B., HAN, X., GROSS, R. W. & ABUMRAD, N. A. 2007. CD36 is important for fatty acid and cholesterol uptake by the proximal but not distal intestine. *J Biol Chem,* 282**,** 19493-501.

NEDELCU, D., LIU, J., XU, Y., JAO, C. & SALIC, A. 2013. Oxysterol binding to the extracellular domain of Smoothened in Hedgehog signaling. *Nature chemical biology,* 9**,** 557-564.

NEMAZANNIKOVA, N., BLATCH, G. L., DASS, C. R., SINCLAIR, R. & APOSTOLOPOULOS, V. 2019. Vitamin D enzymes (CYP27A1, CYP27B1, and CYP24A1) and receptor expression in non-melanoma skin cancer. *Acta Biochimica et Biophysica Sinica,* 51**,** 444-447.

NEMER, G., SAFI, R., KREIDIEH, F., USTA, J., BERGQVIST, C., BALLOUT, F., BTADINI, W., HAMZEH, N., ABBAS, O., KIBBI, A. G., SHIMOMURA, Y. & KURBAN, M. 2017. Understanding the phenotypic similarities between IFAP and Olmsted syndrome from a molecular perspective: the interaction of MBTPS2 and TRPV3. *Arch Dermatol Res,* 309**,** 637-643.

NEUFELD, E. B., REMALEY, A. T., DEMOSKY, S. J., STONIK, J. A., COONEY, A. M., COMLY, M., DWYER, N. K., ZHANG, M., BLANCHETTE-MACKIE, J., SANTAMARINA-FOJO, S. & BREWER, H. B., JR. 2001. Cellular localization and trafficking of the human ABCA1 transporter. *J Biol Chem,* 276**,** 27584-90.

NICU, C., HARDMAN, J. A., POPLE, J. & PAUS, R. 2019. Do human dermal adipocytes switch from lipogenesis in anagen to lipophagy and lipolysis during catagen in the human hair cycle? *Exp Dermatol,* 28**,** 432-435.

NIKLES, D. & TAMPE, R. 2007. Targeted degradation of ABC transporters in health and disease. *J Bioenerg Biomembr,* 39**,** 489-97.

NIKOLAKIS, G., STRATAKIS, C. A., KANAKI, T., SLOMINSKI, A. & ZOUBOULIS, C. C. 2016. Skin steroidogenesis in health and disease. *Rev Endocr Metab Disord,* 17**,** 247-258.

NIU, P., YAO, B., WEI, L., ZHU, H., FANG, C. & ZHAO, Y. 2019. Construction of prognostic risk prediction model based on high-throuput sequencing expression profile data in childhood acute myeloid leukemia. *Blood Cells Mol Dis,* 77**,** 43-50.

OEFFNER, F., FISCHER, G., HAPPLE, R., KONIG, A., BETZ, R. C., BORNHOLDT, D., NEIDEL, U., BOENTE MDEL, C., REDLER, S., ROMERO-GOMEZ, J., SALHI, A., VERA-CASANO, A., WEIRICH, C. & GRZESCHIK, K. H. 2009. IFAP syndrome is caused by deficiency in MBTPS2, an intramembrane zinc metalloprotease essential for cholesterol homeostasis and ER stress response. *Am J Hum Genet,* 84**,** 459-67.

OGATA, M., TSUJITA, M., HOSSAIN, M. A., AKITA, N., GONZALEZ, F. J., STAELS, B., SUZUKI, S., FUKUTOMI, T., KIMURA, G. & YOKOYAMA, S. 2009. On the mechanism for PPAR agonists to enhance ABCA1 gene expression. *Atherosclerosis,* 205**,** 413-9.

OH, J. W., KLOEPPER, J., LANGAN, E. A., KIM, Y., YEO, J., KIM, M. J., HSI, T. C., ROSE, C., YOON, G. S., LEE, S. J., SEYKORA, J., KIM, J. C., SUNG, Y. K., KIM, M., PAUS, R. & PLIKUS, M. V. 2016. A Guide to Studying Human Hair Follicle Cycling In Vivo. *J Invest Dermatol,* 136**,** 34-44.

OHNEMUS, U., UENALAN, M., INZUNZA, J., GUSTAFSSON, J.-A. K. & PAUS, R. 2006. The Hair Follicle as an Estrogen Target and Source. *Endocrine Reviews,* 27**,** 677-706.

OHTSUKI, S., KAMOI, M., WATANABE, Y., SUZUKI, H., HORI, S. & TERASAKI, T. 2007. Correlation of induction of ATP binding cassette transporter A5 (ABCA5) and ABCB1 mRNAs with differentiation state of human colon tumor. *Biol Pharm Bull,* 30**,** 1144-6.

OHVO-REKILÄ, H., RAMSTEDT, B., LEPPIMÄKI, P. & PETER SLOTTE, J. 2002. Cholesterol interactions with phospholipids in membranes. *Progress in Lipid Research,* 41**,** 66-97.

OLIVIER, E., DUTOT, M., REGAZZETTI, A., DARGERE, D., AUZEIL, N., LAPREVOTE, O. & RAT, P. 2017. Lipid deregulation in UV irradiated skin cells: Role of 25-hydroxycholesterol in keratinocyte differentiation during photoaging. *J Steroid Biochem Mol Biol,* 169**,** 189-197.

OLKKONEN, V. M., BEASLAS, O. & NISSILA, E. 2012. Oxysterols and their cellular effectors. *Biomolecules,* 2**,** 76-103.

OSHIMA, H., ROCHAT, A., KEDZIA, C., KOBAYASHI, K. & BARRANDON, Y. 2001. Morphogenesis and Renewal of Hair Follicles from Adult Multipotent Stem Cells. *Cell,* 104**,** 233-245.

PALMER, M. A., BLAKEBOROUGH, L., HARRIES, M. & HASLAM, I. S. 2020. Cholesterol homeostasis: Links to hair follicle biology and hair disorders. *Exp Dermatol,* 29**,** 299-311.

PANDZIC, E., GELISSEN, I. C., WHAN, R., BARTER, P. J., SVIRIDOV, D., GAUS, K., RYE, K.-A. & COCHRAN, B. J. 2017. The ATP binding cassette transporter, ABCG1, localizes to cortical actin filaments. *Scientific Reports,* 7**,** 42025.

PANICKER, S. P., GANGULY, T., CONSOLO, M., PRICE, V., MIRMIRANI, P., HONDA, K. & KARNIK, P. 2012. Sterol intermediates of cholesterol biosynthesis inhibit hair growth and trigger an innate immune response in cicatricial alopecia. *PLoS One,* 7**,** e38449.

PARK, B. M., BAK, S. S., SHIN, K. O., KIM, M., KIM, D., JUNG, S. H., JEONG, S., SUNG, Y. K. & KIM, H. J. 2017. Promotion of hair growth by newly synthesized ceramide mimetic compound. *Biochem Biophys Res Commun,* 491**,** 173-177.

PARK, E., HYPHEN & KYUNG 2009. Cholesterol depletion induces anoikis-like apoptosis via FAK down-regulation and caveolae internalization. *The Journal of pathology,* 218**,** 337-349.

PATEL, M. V., MCKAY, I. A. & BURRIN, J. M. 2001. Transcriptional regulators of steroidogenesis, DAX-1 and SF-1, are expressed in human skin. *J Invest Dermatol,* 117**,** 1559-65.

PAYNE, A. H. & HALES, D. B. 2004. Overview of steroidogenic enzymes in the pathway from cholesterol to active steroid hormones. *Endocr Rev,* 25**,** 947-70.

PETERS, F., VORHAGEN, S., BRODESSER, S., JAKOBSHAGEN, K., BRUNING, J. C., NIESSEN, C. M. & KRONKE, M. 2015. Ceramide synthase 4 regulates stem cell homeostasis and hair follicle cycling. *J Invest Dermatol,* 135**,** 1501-1509.

PETRY, F., KOTTHAUS, A. & HIRSCH-ERNST, K. I. 2003. Cloning of human and rat ABCA5/Abca5 and detection of a human splice variant. *Biochem Biophys Res Commun,* 300**,** 343-50.

PETRY, F., RITZ, V., MEINEKE, C., MIDDEL, P., KIETZMANN, T., SCHMITZ-SALUE, C. & HIRSCH-ERNST, K. I. 2006. Subcellular localization of rat Abca5, a rat ATP-binding-cassette transporter expressed in Leydig cells, and characterization of its splice variant apparently encoding a half-transporter. *Biochem J,* 393**,** 79-87.

PHILLIPS, M. C. 2014. Molecular mechanisms of cellular cholesterol efflux. *J Biol Chem,* 289**,** 24020-9.

PHILPOTT, M., GREEN, M. R. & KEALEY, T. 1989. Studies on the biochemistry and morphology of freshly isolated and maintained rat hair follicles. *J Cell Sci,* 93 (Pt 3)**,** 409-18.

PHILPOTT, M. P. 2018. Culture of the human pilosebaceous unit, hair follicle and sebaceous gland. *Exp Dermatol,* 27**,** 571-577.

PICARDO, M., OTTAVIANI, M., CAMERA, E. & MASTROFRANCESCO, A. 2009. Sebaceous gland lipids. *Dermato-endocrinology,* 1**,** 68-71.

PLIKUS, M. V., MAYER, J. A., DE LA CRUZ, D., BAKER, R. E., MAINI, P. K., MAXSON, R. & CHUONG, C. M. 2008. Cyclic dermal BMP signalling regulates stem cell activation during hair regeneration. *Nature,* 451**,** 340-4.

PONEC, M., HAVEKES, L., KEMPENAAR, J., LAVRIJSEN, S., WIJSMAN, M., BOONSTRA, J. & VERMEER, B. J. 1985. Calcium-mediated regulation of the low density lipoprotein receptor and intracellular cholesterol synthesis in human epidermal keratinocytes. *J Cell Physiol,* 125**,** 98-106.

PONEC, M., KEMPENAAR, J. & BOONSTRA, J. 1987. Regulation of lipid synthesis in relation to keratinocyte differentiation capacity. *Biochim Biophys Acta,* 921**,** 512-21.

PONTREMOLI, M., BRIOSCHI, M., BAETTA, R., GHILARDI, S. & BANFI, C. 2018. Identification of DKK-1 as a novel mediator of statin effects in human endothelial cells. *Sci Rep,* 8**,** 16671.

PORTER, J. A., YOUNG, K. E. & BEACHY, P. A. 1996. Cholesterol modification of hedgehog signaling proteins in animal development. *Science,* 274**,** 255-9.

PUHVEL, S. M., REISNER, R. M. & SAKAMOTO, M. 1975. Analysis of lipid composition of isolated human sebaceous gland homogenates after incubation with cutaneous bacteria. Thin-layer chromatography. *J Invest Dermatol,* 64**,** 406-11.

PURBA, T. S., HASLAM, I. S., POBLET, E., JIMÉNEZ, F., GANDARILLAS, A., IZETA, A. & PAUS, R. 2014. Human epithelial hair follicle stem cells and their progeny: Current state of knowledge, the widening gap in translational research and future challenges. *BioEssays,* 36**,** 513-525.

PURBA, T. S., HASLAM, I. S., SHAHMALAK, A., BHOGAL, R. K. & PAUS, R. 2015. Mapping the expression of epithelial hair follicle stem cell-related transcription factors LHX2 and SOX9 in the human hair follicle. *Experimental Dermatology,* 24**,** 462-467.

PURBA, T. S., PEAKE, M., FARJO, B., FARJO, N., BHOGAL, R. K., JENKINS, G. & PAUS, R. 2017. Divergent proliferation patterns of distinct human hair follicle epithelial progenitor niches in situ and their differential responsiveness to prostaglandin D2. *Scientific Reports,* 7**,** 15197.

QUAZI, F. & MOLDAY, R. S. 2011. Lipid transport by mammalian ABC proteins. *Essays Biochem,* 50**,** 265-90.

QUEZADA, C. A., GARRIDO, W. X., GONZÁLEZ-OYARZÚN, M. A., RAUCH, M. C., SALAS, M. R., SAN MARTÍN, R. E., CLAUDE, A. A., YAÑEZ, A. J., SLEBE, J. C. & CÁRCAMO, J. G. 2008. Effect of tacrolimus on activity and expression of P-glycoprotein and ATP-binding cassette transporter A5 (ABCA5) proteins in hematoencephalic barrier cells. *Biol Pharm Bull,* 31**,** 1911-6.

RALDUA, D. & BABIN, P. J. 2007. BLT-1, a specific inhibitor of the HDL receptor SR-BI, induces a copper-dependent phenotype during zebrafish development. *Toxicol Lett,* 175**,** 1-7.

RAMOT, Y., MASTROFRANCESCO, A., CAMERA, E., DESREUMAUX, P., PAUS, R. & PICARDO, M. 2015. The role of PPARgamma-mediated signalling in skin biology and pathology: new targets and opportunities for clinical dermatology. *Exp Dermatol,* 24**,** 245-51.

RANDALL, V. A. 2008. The Endocrine Control of the Hair Follicle. *In:* BLUME-PEYTAVI, U., TOSTI, A. & TRÜEB, R. M. (eds.) *Hair Growth and Disorders.* Berlin, Heidelberg: Springer Berlin Heidelberg.

REBOUL, E., GONCALVES, A., COMERA, C., BOTT, R., NOWICKI, M., LANDRIER, J. F., JOURDHEUIL-RAHMANI, D., DUFOUR, C., COLLET, X. & BOREL, P. 2011. Vitamin D intestinal absorption is not a simple passive diffusion: evidences for involvement of cholesterol transporters. *Mol Nutr Food Res,* 55**,** 691-702.

REBOUL, E., KLEIN, A., BIETRIX, F., GLEIZE, B., MALEZET-DESMOULINS, C., SCHNEIDER, M., MARGOTAT, A., LAGROST, L., COLLET, X. & BOREL, P. 2006. Scavenger receptor class B type I (SR-BI) is involved in vitamin E transport across the enterocyte. *J Biol Chem,* 281**,** 4739-45.

REIS, A. H., MORENO, M. M., MAIA, L. A., OLIVEIRA, F. P., SANTOS, A. S. & ABREU, J. G. 2016. Cholesterol-rich membrane microdomains modulate Wnt/β-catenin morphogen gradient during Xenopus development. *Mech Dev,* 142**,** 30-39.

REKA, A. K., KURAPATI, H., NARALA, V. R., BOMMER, G., CHEN, J., STANDIFORD, T. J. & KESHAMOUNI, V. G. 2010. Peroxisome proliferator-activated receptor-gamma activation inhibits tumor metastasis by antagonizing Smad3-mediated epithelial-mesenchymal transition. *Mol Cancer Ther,* 9**,** 3221-32.

REN, S., KIM, J. K., KAKIYAMA, G., RODRIGUEZ-AGUDO, D., PANDAK, W. M., MIN, H.-K. & NING, Y. 2014. Identification of Novel Regulatory Cholesterol Metabolite, 5-Cholesten, 3β,25-Diol, Disulfate. *PLoS ONE,* 9**,** e103621.

RHAINDS, D. & BRISSETTE, L. 2004. The role of scavenger receptor class B type I (SR-BI) in lipid trafficking. defining the rules for lipid traders. *Int J Biochem Cell Biol,* 36**,** 39-77.

RIGOTTI, A., EDELMAN, E. R., SEIFERT, P., IQBAL, S. N., DEMATTOS, R. B., TEMEL, R. E., KRIEGER, M. & WILLIAMS, D. L. 1996. Regulation by adrenocorticotropic hormone of the in vivo expression of scavenger receptor class B type I (SR-BI), a high density lipoprotein receptor, in steroidogenic cells of the murine adrenal gland. *J Biol Chem,* 271**,** 33545-9.

RITTIE, L., STOLL, S. W., KANG, S., VOORHEES, J. J. & FISHER, G. J. 2009. Hedgehog signaling maintains hair follicle stem cell phenotype in young and aged human skin. *Aging Cell,* 8**,** 738-51.

ROBB-NICHOLSON, C. 1998. Recently, I heard on a TV show that anticholesterol drugs can cause hair loss. I've been taking Zocor for about 18 months now, and in the past 6 months I've noticed hair loss from the top and sides of my head. Is this common? Will my hair regrow once I stop taking the drug? *Harv Womens Health Watch,* 5**,** 8.

ROBINS, D. N. 2007. Case reports: alopecia universalis: hair growth following initiation of simvastatin and ezetimibe therapy. *J Drugs Dermatol,* 6**,** 946-7.

ROMANO, M. T., TAFAZZOLI, A., MATTERN, M., SIVALINGAM, S., WOLF, S., RUPP, A., THIELE, H., ALTMULLER, J., NURNBERG, P., ELLWANGER, J., GAMBON, R., BAUMER, A., KOHLSCHMIDT, N., METZE, D., HOLDENRIEDER, S., PAUS, R., LUTJOHANN, D., FRANK, J., GEYER, M., BERTOLINI, M., KOKORDELIS, P. & BETZ, R. C. 2018. Bi-allelic Mutations in LSS, Encoding Lanosterol Synthase, Cause Autosomal-Recessive Hypotrichosis Simplex. *Am J Hum Genet,* 103**,** 777-785.

RUSSELL, L. E., HARRISON, W. J., BAHTA, A. W., ZOUBOULIS, C. C., BURRIN, J. M. & PHILPOTT, M. P. 2007. Characterization of liver X receptor expression and function in human skin and the pilosebaceous unit. *Exp Dermatol,* 16**,** 844-52.

SAGGAR, V., WU, S., DICKLER, M. N. & LACOUTURE, M. E. 2013. Alopecia with endocrine therapies in patients with cancer. *Oncologist,* 18**,** 1126-34.

SAHOO, D., PENG, Y., SMITH, J. R., DARLINGTON, Y. F. & CONNELLY, M. A. 2007. Scavenger receptor class B, type I (SR-BI) homo-dimerizes via its C-terminal region: fluorescence resonance energy transfer analysis. *Biochim Biophys Acta,* 1771**,** 818-29.

SÁNCHEZ, P., SERRANO-FALCÓN, C., TORRES, J., SERRANO, S. & ORTEGA, E. J. A. O. D. R. 2018. 5α-Reductase isozymes and aromatase mRNA levels in plucked hair from young women with female pattern hair loss. *Arch Dermatol Res,* 310**,** 77-83.

SANTAMARINA-FOJO, S., REMALEY, A. T., NEUFELD, E. B. & BREWER, H. B., JR. 2001. Regulation and intracellular trafficking of the ABCA1 transporter. *J Lipid Res,* 42**,** 1339-45.

SASMAZ, S., SENOL, M., OZCAN, A., DOGAN, G., TUNCER, C., AKYOL, O. & SENER, S. 1999. The risk of coronary heart disease in men with androgenetic alopecia. *J Eur Acad Dermatol Venereol,* 12**,** 123-5.

SAWAYA, M. E. 1991. Steroid chemistry and hormone controls during the hair follicle cycle. *Ann N Y Acad Sci,* 642**,** 376-83; discussion 383-4.

SCHALLREUTER, K. U., HASSE, S., ROKOS, H., CHAVAN, B., SHALBAF, M., SPENCER, J. D. & WOOD, J. M. 2009. Cholesterol regulates melanogenesis in human epidermal melanocytes and melanoma cells. *Exp Dermatol,* 18**,** 680-8.

SCHINDELIN, J., ARGANDA-CARRERAS, I., FRISE, E., KAYNIG, V., LONGAIR, M., PIETZSCH, T., PREIBISCH, S., RUEDEN, C., SAALFELD, S., SCHMID, B., TINEVEZ, J. Y., WHITE, D. J., HARTENSTEIN, V., ELICEIRI, K., TOMANCAK, P. & CARDONA, A. 2012. Fiji: an open-source platform for biological-image analysis. *Nat Methods,* 9**,** 676-82.

SCHMUTH, M., ELIAS, P. M., HANLEY, K., LAU, P., MOSER, A., WILLSON, T. M., BIKLE, D. D. & FEINGOLD, K. R. 2004. The effect of LXR activators on AP-1 proteins in keratinocytes. *J Invest Dermatol,* 123**,** 41-8.

SCHNEIDER, M. R., SCHMIDT-ULLRICH, R. & PAUS, R. 2009. The hair follicle as a dynamic miniorgan. *Curr Biol,* 19**,** R132-42.

SCHRODER, B., WROCKLAGE, C., PAN, C., JAGER, R., KOSTERS, B., SCHAFER, H., ELSASSER, H. P., MANN, M. & HASILIK, A. 2007. Integral and associated lysosomal membrane proteins. *Traffic,* 8**,** 1676-86.

SCHWEIKERT, H. U. & WILSON, J. D. 1974. Regulation of human hair growth by steroid hormones. I. Testerone metabolism in isolated hairs. *J Clin Endocrinol Metab,* 38**,** 811-9.

SEEREE, P., JANVILISRI, T., KANGSAMAKSIN, T., TOHTONG, R. & KUMKATE, S. 2019. Downregulation of ABCA1 and ABCG1 transporters by simvastatin in cholangiocarcinoma cells. *Oncol Lett,* 18**,** 5173-5184.

SEGAL, A. S. 2002. Alopecia associated with atorvastatin. *Am J Med,* 113**,** 171.

SERRA, M., MATABOSCH, X., YING, L., WATSON, G. & SHACKLETON, C. 2010. Hair and skin sterols in normal mice and those with deficient dehydrosterol reductase (DHCR7), the enzyme associated with Smith-Lemli-Opitz syndrome. *The Journal of steroid biochemistry and molecular biology,* 122**,** 318-325.

SEVER, N., YANG, T., BROWN, M. S., GOLDSTEIN, J. L. & DEBOSE-BOYD, R. A. 2003. Accelerated Degradation of HMG CoA Reductase Mediated by Binding of Insig-1 to Its Sterol-Sensing Domain. *Molecular Cell,* 11**,** 25-33.

SHARMA, K. H. & JINDAL, A. 2014. Association between androgenetic alopecia and coronary artery disease in young male patients. *Int J Trichology,* 6**,** 5-7.

SHARMA, L., DUBEY, A., GUPTA, P. R. & AGRAWAL, A. 2013. Androgenetic alopecia and risk of coronary artery disease. *Indian Dermatol Online J,* 4**,** 283-7.

SHARPE, L. J. & BROWN, A. J. 2013. Controlling cholesterol synthesis beyond 3-hydroxy-3-methylglutaryl-CoA reductase (HMGCR). *J Biol Chem,* 288**,** 18707-15.

SHEN, W.-J., ASTHANA, S., KRAEMER, F. B. & AZHAR, S. 2018a. Scavenger receptor B type 1 : Expression, Molecular Regulation, and Cholesterol Transport Function. *Journal of Lipid Research,* 59**,** 1114-1131.

SHEN, W. J., AZHAR, S. & KRAEMER, F. B. 2018b. SR-B1: A Unique Multifunctional Receptor for Cholesterol Influx and Efflux. *Annu Rev Physiol,* 80**,** 95-116.

SHENG, R., KIM, H., LEE, H., XIN, Y., CHEN, Y., TIAN, W., CUI, Y., CHOI, J. C., DOH, J., HAN, J. K. & CHO, W. 2014. Cholesterol selectively activates canonical Wnt signalling over non-canonical Wnt signalling. *Nat Commun,* 5**,** 4393.

SHIIGI, H., MATSUMOTO, H., OTA, I. & NAGAOKA, T. 2008. Detection of skin cholesterol by a molecularly imprinted electrode. *Journal of Flow Injection Analysis,* 25**,** 81.

SHIMANO, H. & SATO, R. 2017. SREBP-regulated lipid metabolism: convergent physiology — divergent pathophysiology. *Nature Reviews Endocrinology,* 13**,** 710-730.

SHIMOMURA, Y., AGALLIU, D., VONICA, A., LURIA, V., WAJID, M., BAUMER, A., BELLI, S., PETUKHOVA, L., SCHINZEL, A., BRIVANLOU, A. H., BARRES, B. A. & CHRISTIANO, A. M. 2010. APCDD1 is a novel Wnt inhibitor mutated in hereditary hypotrichosis simplex. *Nature,* 464**,** 1043-7.

SHIVANNA, C. B., SHENOY, C. & PRIYA, R. A. 2018. Tofacitinib (Selective Janus Kinase Inhibitor 1 and 3): A Promising Therapy for the Treatment of Alopecia Areata: A Case Report of Six Patients. *International journal of trichology,* 10**,** 103-107.

SHUKLA, A., HILLEGASS, J. M., MACPHERSON, M. B., BEUSCHEL, S. L., VACEK, P. M., PASS, H. I., CARBONE, M., TESTA, J. R. & MOSSMAN, B. T. 2010. Blocking of ERK1 and ERK2 sensitizes human mesothelioma cells to doxorubicin. *Mol Cancer,* 9**,** 314.

SHYAM, R., VACHALI, P., GORUSUPUDI, A., NELSON, K. & BERNSTEIN, P. S. 2017. All three human scavenger receptor class B proteins can bind and transport all three macular xanthophyll carotenoids. *Arch Biochem Biophys,* 634**,** 21-28.

SIEFKEN, W., HOPPNER, H. & HARRIS, I. R. 2000. Regulation of cholesterol synthesis by oleic and palmitic acid in keratinocytes. *Exp Dermatol,* 9**,** 138-45.

SINGARAJA, R. R., KANG, M. H., VAID, K., SANDERS, S. S., VILAS, G. L., ARSTIKAITIS, P., COUTINHO, J., DRISDEL, R. C., EL-HUSSEINI AEL, D., GREEN, W. N., BERTHIAUME, L. & HAYDEN, M. R. 2009. Palmitoylation of ATP-binding cassette transporter A1 is essential for its trafficking and function. *Circ Res,* 105**,** 138-47.

SLOMINSKI, A., ERMAK, G. & MIHM, M. 1996. ACTH receptor, CYP11A1, CYP17 and CYP21A2 genes are expressed in skin. *J Clin Endocrinol Metab,* 81**,** 2746-9.

SLOMINSKI, A., WORTSMAN, J., PLONKA, P. M., SCHALLREUTER, K. U., PAUS, R. & TOBIN, D. J. 2005. Hair follicle pigmentation. *The Journal of investigative dermatology,* 124**,** 13-21.

SLOMINSKI, A., ZBYTEK, B., NIKOLAKIS, G., MANNA, P. R., SKOBOWIAT, C., ZMIJEWSKI, M., LI, W., JANJETOVIC, Z., POSTLETHWAITE, A., ZOUBOULIS, C. C. & TUCKEY, R. C. 2013. Steroidogenesis in the skin: implications for local immune functions. *J Steroid Biochem Mol Biol,* 137**,** 107-23.

SMEETH, L., DOUGLAS, I., HALL, A. J., HUBBARD, R. & EVANS, S. 2009. Effect of statins on a wide range of health outcomes: a cohort study validated by comparison with randomized trials. *Br J Clin Pharmacol,* 67**,** 99-109.

SMYTHE, C. D. W., GREENALL, M. & KEALEY, T. 1998. The Activity of HMG-CoA Reductase and Acetyl-CoA Carboxylase in Human Apocrine Sweat Glands, Sebaceous Glands, and Hair Follicles Is Regulated by Phosphorylation and by Exogenous Cholesterol. *Journal of Investigative Dermatology,* 111**,** 139-148.

SOCCIO, R. E. & BRESLOW, J. L. 2004. Intracellular cholesterol transport. *Arterioscler Thromb Vasc Biol,* 24**,** 1150-60.

SPANN, N. J., GARMIRE, L. X., MCDONALD, J. G., MYERS, D. S., MILNE, S. B., SHIBATA, N., REICHART, D., FOX, J. N., SHAKED, I., HEUDOBLER, D., RAETZ, C. R., WANG, E. W., KELLY,

S. L., SULLARDS, M. C., MURPHY, R. C., MERRILL, A. H., JR., BROWN, H. A., DENNIS, E. A., LI, A. C., LEY, K., TSIMIKAS, S., FAHY, E., SUBRAMANIAM, S., QUEHENBERGER, O., RUSSELL, D. W. & GLASS, C. K. 2012. Regulated accumulation of desmosterol integrates macrophage lipid metabolism and inflammatory responses. *Cell,* 151**,** 138-52.

SPÖRL, F., WUNDERSKIRCHNER, M., ULLRICH, O., BOMKE, G., BREITENBACH, U., BLATT, T., WENCK, H., WITTERN, K. P. & SCHRADER, A. 2010. Real-time monitoring of membrane cholesterol reveals new insights into epidermal differentiation. *J Invest Dermatol,* 130**,** 1268-78.

STEIJLEN, P. M., VAN GEEL, M., VREEBURG, M., MARCUS-SOEKARMAN, D., SPAAPEN, L. J., CASTELIJNS, F. C., WILLEMSEN, M. & VAN STEENSEL, M. A. 2007. Novel EBP gene mutations in Conradi-Hunermann-Happle syndrome. *Br J Dermatol,* 157**,** 1225-9.

STENN, K. S. & KARNIK, P. 2010. Lipids to the top of hair biology. *J Invest Dermatol,* 130**,** 1205-7.

STENN, K. S. & PAUS, R. 2001. Controls of Hair Follicle Cycling. *Physiological Reviews,* 81**,** 449-494.

STICOZZI, C., BELMONTE, G., PECORELLI, A., AREZZINI, B., GARDI, C., MAIOLI, E., MIRACCO, C., TOSCANO, M., FORMAN, H. J. & VALACCHI, G. 2012. Cigarette smoke affects keratinocytes SRB1 expression and localization via H2O2 production and HNE protein adducts formation. *PLoS One,* 7**,** e33592.

STICOZZI, C., PECORELLI, A., BELMONTE, G. & VALACCHI, G. 2010. Cigarette Smoke Affects ABCAI Expression via Liver X Receptor Nuclear Translocation in Human Keratinocytes. *Int J Mol Sci,* 11**,** 3375-3386.

STRAUS, D. S. & GLASS, C. K. 2007. Anti-inflammatory actions of PPAR ligands: new insights on cellular and molecular mechanisms. *Trends Immunol,* 28**,** 551-8.

STROTT, C. A. & HIGASHI, Y. 2003. Cholesterol sulfate in human physiology: what's it all about? *J Lipid Res,* 44**,** 1268-78.

SUGAWARA, K., TSURUTA, D., KOBAYASHI, H., IKEDA, K., HOPKINSON, S. B., JONES, J. C. R. & ISHII, M. 2007. Spatial and temporal control of laminin-332 (5) and -511 (10) expression during induction of anagen hair growth. *The journal of histochemistry and cytochemistry : official journal of the Histochemistry Society,* 55**,** 43-55.

SUHALIM, J. L., CHUNG, C.-Y., LILLEDAHL, M. B., LIM, R. S., LEVI, M., TROMBERG, B. J. & POTMA, E. O. 2012a. Characterization of cholesterol crystals in atherosclerotic plaques using stimulated Raman scattering and second-harmonic generation microscopy. *Biophysical journal,* 102**,** 1988-1995.

SUHALIM, J. L., CHUNG, C. Y., LILLEDAHL, M. B., LIM, R. S., LEVI, M., TROMBERG, B. J. & POTMA, E. O. 2012b. Characterization of cholesterol crystals in atherosclerotic plaques using stimulated Raman scattering and second-harmonic generation microscopy. *Biophys J,* 102**,** 1988-95.

SUZUKI, S., OTA, Y., OZAWA, K. & IMAMURA, T. 2000. Dual-Mode Regulation of Hair Growth Cycle by Two Fgf-5 Gene Products. *Journal of Investigative Dermatology,* 114**,** 456-463.

TABAS, I. 2002. Consequences of cellular cholesterol accumulation: basic concepts and physiological implications. *Journal of Clinical Investigation,* 110**,** 905-911.

TACHIKAWA, M., TOKI, H., WATANABE, M., TOMI, M., HOSOYA, K. I. & TERASAKI, T. 2018. Gene expression of A6-like subgroup of ATP-binding cassette transporters in mouse brain parenchyma and microvessels. *Anat Sci Int,* 93**,** 456-463.

TAKENAKA, S., ITOH, T. & FUJIWARA, R. 2013. Expression pattern of human ATP-binding cassette transporters in skin. *Pharmacol Res Perspect,* 1**,** e00005.

TAMEHIRO, N., ZHOU, S., OKUHIRA, K., BENITA, Y., BROWN, C. E., ZHUANG, D. Z., LATZ, E., HORNEMANN, T., VON ECKARDSTEIN, A., XAVIER, R. J., FREEMAN, M. W. & FITZGERALD, M. L. 2008. SPTLC1 binds ABCA1 to negatively regulate trafficking and cholesterol efflux activity of the transporter. *Biochemistry,* 47**,** 6138-47.

TANG, C., LIU, Y., KESSLER, P. S., VAUGHAN, A. M. & ORAM, J. F. 2009. The macrophage cholesterol exporter ABCA1 functions as an anti-inflammatory receptor. *J Biol Chem,* 284**,** 32336-43.

TANG, J. Y., SO, P. L. & EPSTEIN, E. H., JR. 2007. Novel Hedgehog pathway targets against basal cell carcinoma. *Toxicol Appl Pharmacol,* 224**,** 257-64.

TARLING, E. J., DE AGUIAR VALLIM, T. Q. & EDWARDS, P. A. 2013. Role of ABC transporters in lipid transport and human disease. *Trends Endocrinol Metab,* 24**,** 342-50.

TARLING, E. J. & EDWARDS, P. A. 2011. ATP binding cassette transporter G1 (ABCG1) is an intracellular sterol transporter. *Proc Natl Acad Sci U S A,* 108**,** 19719-24.

TAVES, M. D., GOMEZ-SANCHEZ, C. E. & SOMA, K. K. 2011. Extra-adrenal glucocorticoids and mineralocorticoids: evidence for local synthesis, regulation, and function. *American journal of physiology. Endocrinology and metabolism,* 301**,** E11-E24.

THAKARE, S. A. S., A. 2016. Early-onset Male Androgenetic Alopecia and Metabolic Syndrome: Are They Associated? *International Journal of Recent Surgical & Medical Science,* 2**,** 5-9.

THIBOUTOT, D., JABARA, S., MCALLISTER, J. M., SIVARAJAH, A., GILLILAND, K., CONG, Z. & CLAWSON, G. 2003. Human skin is a steroidogenic tissue: steroidogenic enzymes and

cofactors are expressed in epidermis, normal sebocytes, and an immortalized sebocyte cell line (SEB-1). *J Invest Dermatol,* 120**,** 905-14.

THOMAS, A. C., CULLUP, T., NORGETT, E. E., HILL, T., BARTON, S., DALE, B. A., SPRECHER, E., SHERIDAN, E., TAYLOR, A. E., WILROY, R. S., DELOZIER, C., BURROWS, N., GOODYEAR, H., FLECKMAN, P., STEPHENS, K. G., MEHTA, L., WATSON, R. M., GRAHAM, R., WOLF, R., SLAVOTINEK, A., MARTIN, M., BOURN, D., MEIN, C. A., O'TOOLE, E. A. & KELSELL, D. P. 2006. ABCA12 is the major harlequin ichthyosis gene. *J Invest Dermatol,* 126**,** 2408-13.

THOMPSON, S. L. & KRISANS, S. K. 1990. Rat liver peroxisomes catalyze the initial step in cholesterol synthesis. The condensation of acetyl-CoA units into acetoacetyl-CoA. *J Biol Chem,* 265**,** 5731-5.

TOBIN, D. J. 2011. The cell biology of human hair follicle pigmentation. *Pigment Cell & Melanoma Research,* 24**,** 75-88.

TOBIN, D. J., HAGEN, E., BOTCHKAREV, V. A. & PAUS, R. 1998. Do Hair Bulb Melanocytes Undergo Apotosis During Hair Follicle Regression (Catagen)? *Journal of Investigative Dermatology,* 111**,** 941-947.

TOSTI, A. & PAZZAGLIA, M. 2007. Drug reactions affecting hair: diagnosis. *Dermatol Clin,* 25**,** 223-31, vii.

TREVISAN, M., FARINARO, E., KROGH, V., JOSSA, F., GIUMETTI, D., FUSCO, G., PANICO, S., MELLONE, C., FRASCATORE, S., SCOTTONI, A. & ET AL. 1993. Baldness and coronary heart disease risk factors. *J Clin Epidemiol,* 46**,** 1213-8.

TROMPIER, D., ALIBERT, M., DAVANTURE, S., HAMON, Y., PIERRES, M. & CHIMINI, G. 2006. Transition from dimers to higher oligomeric forms occurs during the ATPase cycle of the ABCA1 transporter. *J Biol Chem,* 281**,** 20283-90.

TSURUOKA, H., KHOVIDHUNKIT, W., BROWN, B. E., FLUHR, J. W., ELIAS, P. M. & FEINGOLD, K. R. 2002. Scavenger receptor class B type I is expressed in cultured keratinocytes and epidermis. Regulation in response to changes in cholesterol homeostasis and barrier requirements. *J Biol Chem,* 277**,** 2916-22.

TZIOTZIOS, C., STEFANATO, C. M., FENTON, D. A., SIMPSON, M. A. & MCGRATH, J. A. 2016. Frontal fibrosing alopecia: reflections and hypotheses on aetiology and pathogenesis. *Exp Dermatol,* 25**,** 847-852.

UHLEN, M., FAGERBERG, L., HALLSTROM, B. M., LINDSKOG, C., OKSVOLD, P., MARDINOGLU, A., SIVERTSSON, A., KAMPF, C., SJOSTEDT, E., ASPLUND, A., OLSSON, I., EDLUND, K., LUNDBERG, E., NAVANI, S., SZIGYARTO, C. A., ODEBERG, J., DJUREINOVIC,

D., TAKANEN, J. O., HOBER, S., ALM, T., EDQVIST, P. H., BERLING, H., TEGEL, H., MULDER, J., ROCKBERG, J., NILSSON, P., SCHWENK, J. M., HAMSTEN, M., VON FEILITZEN, K., FORSBERG, M., PERSSON, L., JOHANSSON, F., ZWAHLEN, M., VON HEIJNE, G., NIELSEN, J. & PONTEN, F. 2015. Proteomics. Tissue-based map of the human proteome. *Science,* 347**,** 1260419.

URYSIAK-CZUBATKA, I., KMIEĆ, M. L. & BRONIARCZYK-DYŁA, G. 2014. Assessment of the usefulness of dihydrotestosterone in the diagnostics of patients with androgenetic alopecia. *Postepy dermatologii i alergologii,* 31**,** 207-215.

VARATHARAJAN, S., ABRAHAM, A., KARATHEDATH, S., GANESAN, S., LAKSHMI, K. M., ARTHUR, N., SRIVASTAVA, V. M., GEORGE, B., SRIVASTAVA, A., MATHEWS, V. & BALASUBRAMANIAN, P. 2017. ATP-binding casette transporter expression in acute myeloid leukemia: association with in vitro cytotoxicity and prognostic markers. *Pharmacogenomics,* 18**,** 235-244.

VEJUX, A., MALVITTE, L. & LIZARD, G. 2008. Side effects of oxysterols: cytotoxicity, oxidation, inflammation, and phospholipidosis. *Braz J Med Biol Res,* 41**,** 545-56.

WANG, H., LIU, Y., ZHU, L., WANG, W., WAN, Z., CHEN, F., WU, Y., ZHOU, J. & YUAN, Z. 2014a. 17beta-estradiol promotes cholesterol efflux from vascular smooth muscle cells through a liver X receptor alpha-dependent pathway. *Int J Mol Med,* 33**,** 550-8.

WANG, H. J., TANG, Z. L., LIN, Z. M., DAI, L. L., CHEN, Q. & YANG, Y. 2014b. Recurrent splice-site mutation in MBTPS2 underlying IFAP syndrome with Olmsted syndrome-like features in a Chinese patient. *Clin Exp Dermatol,* 39**,** 158-61.

WANG, N., RANALLETTA, M., MATSUURA, F., PENG, F. & TALL, A. R. 2006. LXR-induced redistribution of ABCG1 to plasma membrane in macrophages enhances cholesterol mass efflux to HDL. *Arterioscler Thromb Vasc Biol,* 26**,** 1310-6.

WANG, N., SILVER, D. L., COSTET, P. & TALL, A. R. 2000. Specific binding of ApoA-I, enhanced cholesterol efflux, and altered plasma membrane morphology in cells expressing ABC1. *J Biol Chem,* 275**,** 33053-8.

WANG, N., YVAN-CHARVET, L., LUTJOHANN, D., MULDER, M., VANMIERLO, T., KIM, T. W. & TALL, A. R. 2008. ATP-binding cassette transporters G1 and G4 mediate cholesterol and desmosterol efflux to HDL and regulate sterol accumulation in the brain. *FASEB J,* 22**,** 1073-82.

WANG, Z., WONG, P., LANGBEIN, L., SCHWEIZER, J. & COULOMBE, P. A. 2003. Type II Epithelial Keratin 6hf (K6hf) Is Expressed in the Companion Layer, Matrix, and Medulla in Anagen-Stage Hair Follicles. 121**,** 1276-1282.

WATANABE, T., KIOKA, N., UEDA, K. & MATSUO, M. 2019. Phosphorylation by protein kinase C stabilizes ABCG1 and increases cholesterol efflux. *J Biochem,* 166**,** 309-314.

WECHSLER, A., BRAFMAN, A., SHAFIR, M., HEVERIN, M., GOTTLIEB, H., DAMARI, G., GOZLAN-KELNER, S., SPIVAK, I., MOSHKIN, O., FRIDMAN, E., BECKER, Y., SKALITER, R., EINAT, P., FAERMAN, A., BJORKHEM, I. & FEINSTEIN, E. 2003. Generation of viable cholesterol-free mice. *Science,* 302**,** 2087.

WERTZ, P. W. 2000. Lipids and barrier function of the skin. *Acta Derm Venereol Suppl (Stockh),* 208**,** 7-11.

WERTZ, P. W. & DOWNING, D. T. 1988. Integral lipids of human hair. *Lipids,* 23**,** 878-81.

WESTERGAARD, M., HENNINGSEN, J., KRATCHMAROVA, I., KRISTIANSEN, K., SVENDSEN, M. L., JOHANSEN, C., JENSEN, U. B., SCHRØDER, H. D., BERGE, R. K., IVERSEN, L., BOLUND, L. & KRAGBALLE, K. 2001. Modulation of Keratinocyte Gene Expression and Differentiation by PPAR-Selective Ligands and Tetradecylthioacetic Acid. *Journal of Investigative Dermatology,* 116**,** 702-712.

WINTER, H., JACOBS, M., ROGERS, M. A., SCHWEIZER, J., LANGBEIN, L., PRAETZEL, S., LEIGH, I. M. & TIDMAN, N. 1998. A Novel Human Type II Cytokeratin, K6hf, Specifically Expressed in the Companion Layer of the Hair Follicle. *Journal of Investigative Dermatology,* 111**,** 955-962.

WONG, J., QUINN, C. M. & BROWN, A. J. 2006. SREBP-2 positively regulates transcription of the cholesterol efflux gene, ABCA1, by generating oxysterol ligands for LXR. *The Biochemical journal,* 400**,** 485-491.

WOO, W.-M., ZHEN, H. H. & ORO, A. E. 2012. Shh maintains dermal papilla identity and hair morphogenesis via a Noggin-Shh regulatory loop. *Genes & development,* 26**,** 1235-1246.

WU, H. H., CAO, H., WANG, Y. Z., WANG, D. X., LIN, H. R., QIN, Y. Z., CHANG, Y., HAO, L., LI, L. D., LI, J. L., RUAN, G. R., HUANG, X. J. & LIU, Y. R. 2009. [Expression of 5 genes in CD7 positive acute myeloid leukemia stem/progenitor cells from bone marrow]. *Zhongguo Shi Yan Xue Ye Xue Za Zhi,* 17**,** 298-303.

WUSTNER, D. & SOLANKO, K. 2015. How cholesterol interacts with proteins and lipids during its intracellular transport. *Biochim Biophys Acta,* 1848**,** 1908-26.

WWW.GENECARDS.ORG, D. A. F. G. 2020. *ABCA5 genecards* [Online]. Available: https://www.genecards.org/cgi-bin/carddisp.pl?gene=ABCA5 [Accessed 07/05/2020 2020].

WWW.UNIPROT.ORG, D. A. F. 2020. *ABCA5 uniprot* [Online]. Available: https://www.uniprot.org/uniprot/Q8WWZ7 [Accessed 08/07/2020 2020].

XIE, Q., ENGEL, T., SCHNOOR, M., NIEHAUS, J., HOFNAGEL, O., BUERS, I., CULLEN, P., SEEDORF, U., ASSMANN, G. & LORKOWSKI, S. 2006. Cell surface localization of ABCG1 does not require LXR activation. *Arterioscler Thromb Vasc Biol,* 26**,** e143-4; author reply e145.

XU, J., LIU, Y., YANG, Y., BATES, S. & ZHANG, J. T. 2004. Characterization of oligomeric human half-ABC transporter ATP-binding cassette G2. *J Biol Chem,* 279**,** 19781-9.

YAMAMOTO, K., MIYAZAKI, K. & HIGASHI, S. 2010. Cholesterol sulfate alters substrate preference of matrix metalloproteinase-7 and promotes degradations of pericellular laminin-332 and fibronectin. *J Biol Chem,* 285**,** 28862-73.

YAMANE, T., MURAMATSU, A., SHIMURA, M., KOBAYASHI-HATTORI, K. & OISHI, Y. 2016. Transforming growth factor-β1 induces cholesterol synthesis by increasing HMG-CoA reductase mRNA expression in keratinocytes. *Biosci Biotechnol Biochem,* 80**,** 1379-1381.

YANG, T., ESPENSHADE, P. J., WRIGHT, M. E., YABE, D., GONG, Y., AEBERSOLD, R., GOLDSTEIN, J. L. & BROWN, M. S. 2002. Crucial Step in Cholesterol Homeostasis: Sterols Promote Binding of SCAP to INSIG-1, a Membrane Protein that Facilitates Retention of SREBPs in ER. *Cell,* 110**,** 489-500.

YAO, P. M. & TABAS, I. 2000. Free Cholesterol Loading of Macrophages Induces Apoptosis Involving the Fas Pathway. *J Biol Chem,* 275**,** 23807-23813.

YE, D., HOEKSTRA, M., OUT, R., MEURS, I., KRUIJT, J. K., HILDEBRAND, R. B., VAN BERKEL, T. J. & VAN ECK, M. 2008. Hepatic cell-specific ATP-binding cassette (ABC) transporter profiling identifies putative novel candidates for lipid homeostasis in mice. *Atherosclerosis,* 196**,** 650-8.

YE, D., MEURS, I., OHIGASHI, M., CALPE-BERDIEL, L., HABETS, K. L., ZHAO, Y., KUBO, Y., YAMAGUCHI, A., VAN BERKEL, T. J., NISHI, T. & VAN ECK, M. 2010. Macrophage ABCA5 deficiency influences cellular cholesterol efflux and increases susceptibility to atherosclerosis in female LDLr knockout mice. *Biochem Biophys Res Commun,* 395**,** 387-94.

YEN, A. & BRAVERMAN, I. M. 1976. Ultrastructure of the human dermal microcirculation: the horizontal plexus of the papillary dermis. *J Invest Dermatol,* 66**,** 131-42.

YILMAZ, M., KARAKOC, A., TORUNER, F. B., CAKIR, N., TIRAS, B., AYVAZ, G. & ARSLAN, M. 2005. The effects of rosiglitazone and metformin on menstrual cyclicity and hirsutism in polycystic ovary syndrome. *Gynecol Endocrinol,* 21**,** 154-60.

YOSHIKAWA, T., IDE, T., SHIMANO, H., YAHAGI, N., AMEMIYA-KUDO, M., MATSUZAKA, T., YATOH, S., KITAMINE, T., OKAZAKI, H., TAMURA, Y., SEKIYA, M., TAKAHASHI, A., HASTY, A. H., SATO, R., SONE, H., OSUGA, J.-I., ISHIBASHI, S. & YAMADA, N. 2003. Cross-Talk between Peroxisome Proliferator-Activated Receptor (PPAR) α and Liver X Receptor (LXR) in

Nutritional Regulation of Fatty Acid Metabolism. I. PPARs Suppress Sterol Regulatory Element Binding Protein-1c Promoter through Inhibition of LXR Signali. *Molecular Endocrinology,* 17**,** 1240-1254.

ZANOTTI, I., POTI, F., PEDRELLI, M., FAVARI, E., MOLERI, E., FRANCESCHINI, G., CALABRESI, L. & BERNINI, F. 2008. The LXR agonist T0901317 promotes the reverse cholesterol transport from macrophages by increasing plasma efflux potential. *J Lipid Res,* 49**,** 954-60.

ZHANG, D., TOMISATO, W., SU, L., SUN, L., CHOI, J. H., ZHANG, Z., WANG, K. W., ZHAN, X., CHOI, M., LI, X., TANG, M., CASTRO-PEREZ, J. M., HILDEBRAND, S., MURRAY, A. R., MORESCO, E. M. Y. & BEUTLER, B. 2017. Skin-specific regulation of SREBP processing and lipid biosynthesis by glycerol kinase 5. *Proc Natl Acad Sci U S A,* 114**,** E5197-E5206.

ZHANG, J. & LIU, Q. 2015. Cholesterol metabolism and homeostasis in the brain. *Protein Cell,* 6**,** 254-64.

ZHANG, J., WANG, Y., CHENG, R., NI, C., LIANG, J., LI, M. & YAO, Z. 2016a. Novel MBTPS2 missense mutation causes a keratosis follicularis spinulosa decalvans phenotype: mutation update and review of the literature. *Clin Exp Dermatol,* 41**,** 757-60.

ZHANG, M., DU, Y., LU, R., SHU, Y., ZHAO, W., LI, Z., ZHANG, Y., LIU, R., YANG, T., LUO, S., GAO, M., ZHANG, Y., ZHANG, G., LIU, J. & LU, Y. 2016b. Cholesterol Retards Senescence in Bone Marrow Mesenchymal Stem Cells by Modulating Autophagy and ROS/p53/p21(Cip1/Waf1) Pathway. *Oxidative Medicine and Cellular Longevity,* 2016**,** 7524308.

ZHANG, X., SONG, Y., FENG, M., ZHOU, X., LU, Y., GAO, L., YU, C., JIANG, X. & ZHAO, J. 2015. Thyroid-stimulating hormone decreases HMG-CoA reductase phosphorylation via AMP-activated protein kinase in the liver. *Journal of Lipid Research,* 56**,** 963-971.

ZHANG, Y., XU, J., JING, J., WU, X. & LV, Z. 2018. Serum Levels of Androgen-Associated Hormones Are Correlated with Curative Effect in Androgenic Alopecia in Young Men. *Med Sci Monit,* 24**,** 7770-7777.

ZHAO, C. & DAHLMAN-WRIGHT, K. 2010. Liver X receptor in cholesterol metabolism. *J Endocrinol,* 204**,** 233-40.

ZHAO, G. J., YIN, K., FU, Y. C. & TANG, C. K. 2012. The interaction of ApoA-I and ABCA1 triggers signal transduction pathways to mediate efflux of cellular lipids. *Mol Med,* 18**,** 149-58.

ZHAO, T., LI, X., SUN, D. & ZHANG, Z. 2019. Oxidative stress: One potential factor for arsenite-induced increase of N(6)-methyladenosine in human keratinocytes. *Environ Toxicol Pharmacol,* 69**,** 95-103.

ZHOU, L., JING, J., WANG, H., WU, X. & LU, Z. 2018. Decorin promotes proliferation and migration of ORS keratinocytes and maintains hair anagen in mice. *Exp Dermatol,* 27**,** 1237-1244.

ZHOU, L., LI, C., GAO, L. & WANG, A. 2015. High-density lipoprotein synthesis and metabolism (Review). *Molecular Medicine Reports,* 12**,** 4015-4021.

ZOUBOULIS, C. C. 2009. The skin as an endocrine organ. *Dermato-endocrinology,* 1**,** 250-252.

ZOUBOULIS, C. C., CHEN, W. C., THORNTON, M. J., QIN, K. & ROSENFIELD, R. 2007. Sexual hormones in human skin. *Horm Metab Res,* 39**,** 85-95.

Appendix 1   Review paper

Experimental Dermatology **WILEY**

Cholesterol homeostasis: Links to hair follicle biology and hair disorders

Megan A. Palmer[1] | Liam Blakeborough[1] | Matthew Harries[2,3] | Iain S. Haslam[1] (iD)

[1]School of Applied Sciences, Department of Biological and Geographical Sciences, University of Huddersfield, Huddersfield, UK

[2]Salford Royal NHS Foundation Trust, Manchester Academic Health Science Centre, Manchester, UK

[3]Musculoskeletal and Dermatological Sciences, School of Biological Sciences, Faculty of Biology, Medicine and Health, University of Manchester, Manchester, UK

Correspondence
Iain Haslam, School of Applied Sciences, Department of Biological and Geographical Sciences, University of Huddersfield, Huddersfield, UK.
Email: i.haslam@hud.ac.uk

Funding information
University of Huddersfield

Abstract

Lipids and lipid metabolism are critical factors in hair follicle (HF) biology, and cholesterol has long been suspected of influencing hair growth. Altered cholesterol homeostasis is involved in the pathogenesis of primary cicatricial alopecia, mutations in a cholesterol transporter are associated with congenital hypertrichosis, and dyslipidaemia has been linked to androgenic alopecia. The underlying molecular mechanisms by which cholesterol influences pathways involved in proliferation and differentiation within HF cell populations remain largely unknown. As such, expanding our knowledge of the role for cholesterol in regulating these processes is likely to provide new leads in the development of treatments for disorders of hair growth and cycling. This review describes the current state of knowledge with respect to cholesterol homeostasis in the HF along with known and putative links to hair pathologies.

KEYWORDS

alopecia, cholesterol, hair follicle, hypertrichosis, transporters

1 | INTRODUCTION

Cholesterol is vital to the normal function of all animal cells and has particular importance in cutaneous tissues. In addition to forming an important component of cell membranes, partitioning into the phospholipid bilayer to regulate membrane fluidity,[1] cholesterol also regulates cell signalling via, for example, modulation of hedgehog protein (Hh) biogenesis and activation of the canonical Wnt pathway.[2,3] Cholesterol performs tissue-specific functions including in the maintenance of the skin permeability barrier[4,5] and acts as a precursor for steroid hormone synthesis.[6,7]

The importance of cholesterol is underscored by the capacity of vertebrate cells for *de novo* biosynthesis.[8] Furthermore, cells can receive cholesterol from circulating lipoproteins (ie, low-density lipoprotein, LDL-; or high-density lipoprotein, HDL), with removal of excess cholesterol facilitated by membrane efflux pumps, such as ATP-binding cassette transporter (ABC) A1 and ABCG1. As cellular cholesterol balance must be maintained within a relatively narrow concentration range, physiological feedback loops exist to control the rates of biosynthesis, uptake and efflux that form such a crucial part of cellular cholesterol metabolism.

The roles for cholesterol in peripheral tissues have been previously described. In the skin, cholesterol is a protagonist in the development of the epidermal permeability barrier,[4,5] is a precursor for the synthesis of local steroid hormones,[7,9] and influences keratinocyte differentiation,[10-12] corneocyte desquamation,[11] barrier repair[13] and melanogenesis.[14,15] Yet there remains one important skin appendage in which the role of cholesterol is yet to be fully explored, namely the hair follicle (HF). Whereas lipids are understood to impact on HF biology, not least through the HF association with the lipid-rich sebaceous gland, the specific functions modulated by cholesterol are less well understood. Associations have been made between sterol levels and certain hair disorders, and lipid-modulatory drug therapies have been reported to cause both hair loss and hair growth.[16-21]

A greater understanding of the control of cellular cholesterol in the HF and the potential impact on the hair cycle may identify novel targets for regulating hair growth and the treatment of hair disorders linked to disordered sterol homeostasis or sterol-sensitive signalling pathways.[22-24]

1

2 | CHOLESTEROL HOMEOSTASIS: A CELLULAR OVERVIEW

Cellular cholesterol metabolism has been covered in detail in many previous reviews.[2,25–28] This section is therefore restricted to providing a generic summary of cellular cholesterol homeostasis.

De novo cholesterol synthesis accounts for approximately 70% of the total body cholesterol. Primarily, this occurs through a series of defined reactions in the endoplasmic reticulum, with the acetyl CoA precursor ultimately metabolised to cholesterol, with 3-hydroxy-3-methylglutaryl-CoA reductase (HMGCR) catalysing the rate-limiting step.[2,26] The pathway is summarised in Figure 1A.

Uptake in the peripheral tissues occurs primarily through the binding of LDL to the LDL receptor (LDLR) followed by receptor-mediated endocytosis.[26] An additional route for cholesterol uptake exists via the scavenger receptor class B member 1 (SRB1) receptor, which mediates uptake of free cholesterol and cholesterol esters from circulating HDL.[29]

ABC transporters play an important role in the transport of lipids; in particular, the ABCA family is involved in both cholesterol efflux and intracellular transport. ABCA1 is a well-characterised cholesterol transporter and is ubiquitously expressed. It mediates the efflux of excess cholesterol from cells to apolipoproteins (apo), in particular apoA1, for the formation of HDL for reverse cholesterol transport.[27,28]

Intracellular trafficking of cholesterol can occur via vesicular and non-vesicular movement. Vesicular transport involves ATP-dependent movement along the cellular cytoskeleton. Non-vesicular transport occurs through hydrophobic cavity transporter proteins, such as steroidogenic acute regulatory protein (StAR) and through spontaneous resorption which is thought to be processed through as yet unidentified specialist proteins.[30]

Numerous transcription factors including sterol regulatory binding protein (SREBP2) (Figure 1A), liver X receptor (LXR) and peroxisome proliferator-activated receptors (PPAR) have primary roles in regulating the expression of genes involved in maintaining cholesterol homeostasis.

The roles of cholesterol in keratinocytes and the HF specifically are detailed in the following sections, with reference to the homeostatic mechanisms outlined above.

3 | CHOLESTEROL FUNCTION IN KERATINOCYTE CELL BIOLOGY PROVIDES LINKS TO HF SIGNALLING PATHWAYS

The HF is a regenerating, hair shaft producing mini-organ that undergoes cyclical periods of growth (anagen) (Figure 2), regression (catagen) and relative quiescence (telogen).[31] The direct impact of cholesterol metabolism on distinct HF cell populations is unclear, yet it is likely to play an important role. Although differentiation of
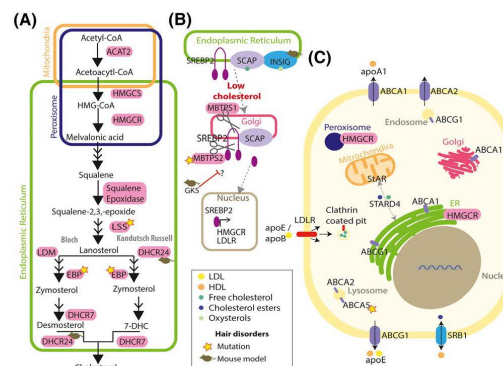
FIGURE 1 Cholesterol homeostasis in the hair follicle: identification of known mutations and knockout mouse models associated with hair disorders. A, Cholesterol biosynthetic pathways. A summary of cholesterol biosynthesis,[26,104] including known mutations associated with hair disorders (as indicated by stars). Mutation to LSS has been associated with autosomal-recessive hypotrichosis simplex presenting with sparse scalp hair.[103] Mutations to EBP in Conradi–Hünermann syndrome are associated with Follicular atrophoderma and patchy scarring alopecia.[130–132] DHCR24 knockout mouse present with fewer hair follicles and thickening of the epidermis.[50] B, SREBP2 mediated cholesterol regulation. In a sterol-rich environment, SREBP2-mediated transcription is downregulated through insulin-induced gene 1 protein (INSIG) and SREBP2 cleavage-activating protein (SCAP). This is initiated through the binding of free cholesterol to SCAP and hydroxycholesterols to INSIG. SREBP2 transport is blocked and expression of downstream targets inhibited. Sterol regulatory element-binding protein 2 (SREBP2) is activated in cholesterol poor environments and regulates gene transcription to increase cellular cholesterol levels. The binding of SCAP to SREBP2 results in transport to the Golgi for processing via MBTPS1 and then MBTPS2. The proteolytic fragmented SREBP2 is produced, which moves to the nucleus, initiating the transcription of HMGCR and LDLR, among other genes.[26] Glycerol kinase 5 (GK5) inhibits SREBP processing; however, the mechanism through which this occurs is unknown.[107] Mutations to MBTPS2 are associated with IFAP and KFSD in which alopecia is present.[116–118,120–127] C, Representation of putative cholesterol transport and trafficking routes in hair follicle keratinocytes. Uptake of cholesterol is represented by the presence of the LDL receptor (LDLR) and scavenger receptor class B member 1 (SRB1) on the plasma membrane.[26,29] Cholesterol synthesis predominantly occurs in the endoplasmic reticulum, with a secondary site being the peroxisome.[26,189] ABC transporters mediate the efflux of excess cholesterol from cells to apolipoproteins (apo), in particular ABCA1 and ABCG1.[27,28] Other potential cholesterol transporters are ABCA2, ABCA5, ABCA7, ABCB1.[22,25,190,191] Mitochondria trafficking of cholesterol is represented by StAR Related Lipid Transfer Domain Containing 4 (STARD4).[10] Congenital hypertrichosis has been associated with mutations to ABCA5[22,108]

matrix keratinocyte in the hair bulb is distinct from that of epidermal keratinocytes, the roles for cholesterol in epidermal physiology can nevertheless provide pointers to the control of keratinocyte behaviour in the HF. This is further discussed below.

Figure labels: Infundibulum, Capillary, Isthmus, Sebaceous gland, Hair Shaft, Bulge, IRS, ORS, CTS, Suprabulbar, Matrix, Bulb, DP, Adipocytes

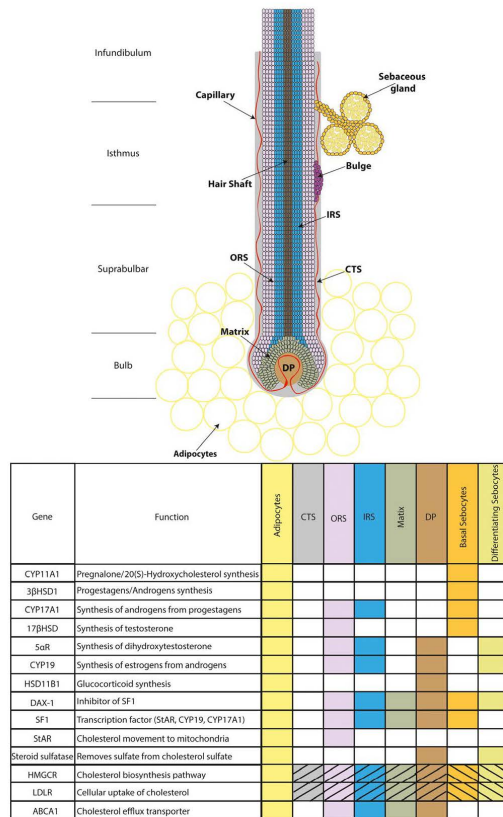| Gene	Function	Adipocytes	CTS	ORS	IRS	Matrix	DP	Basal Sebocytes	Differentiating Sebocytes
CYP11A1	Pregnalone/20(S)-Hydroxycholesterol synthesis								
3βHSD1	Progestagens/Androgens synthesis								
CYP17A1	Synthesis of androgens from progestagens								
17βHSD	Synthesis of testosterone								
5αR	Synthesis of dihydroxytestosterone								
CYP19	Synthesis of estrogens from androgens								
HSD11B1	Glucocorticoid synthesis								
DAX-1	Inhibitor of SF1								
SF1	Transcription factor (StAR, CYP19, CYP17A1)								
StAR	Cholesterol movement to mitochondria								
Steroid sulfatase	Removes sulfate from cholesterol sulfate								
HMGCR	Cholesterol biosynthesis pathway								
LDLR	Cellular uptake of cholesterol								
ABCA1	Cholesterol efflux transporter								

FIGURE 2 Schematic drawing representing Anagen hair follicle (HF). The HF is comprised of multiple concentric keratinocyte layers outer root sheath (ORS), inner root sheath (IRS) and hair shaft, surrounded by a mesenchymal central tissue sheath (CTS). Surrounding the bulb of anagen HFs, the adipocytes contain the largest source of free (unesterified) cholesterol.[192] Circulatory lipoproteins (LDL and HDL) are present in the capillary loop of the DP (dermal papilla) and vessels located throughout the CTS. LDL in particular is therefore available for LDLR-mediated uptake. The associated table provides the colour-coded localisation of enzymes involved in steroidogenesis, including some proteins involved in cholesterol biosynthesis (HMGCR) and uptake (LDLR). Filled boxes indicated know localisation of gene/protein. Striped boxes indicated that the gene/protein is known to be present in pilosebaceous unit but the pattern of expression is yet to be defined. Empty boxes indicate the expression of a specific gene/protein is yet to be reported[46,56,165,192,193]

3.1 | Cholesterol regulates keratinocyte proliferation and differentiation

Lipids are a necessary component of the epidermal barrier, and as such, lipid metabolism has been extensively examined in epidermal keratinocytes (see Feingold, Elias[32]). Many studies have determined that cellular cholesterol levels can modulate and be modified by the proliferative nature of keratinocytes as well as their differentiation status.[33–38] To this end, Sporl, et al[12] previously demonstrated that cyclodextrin-mediated depletion of membrane cholesterol in primary human keratinocytes disrupts lipid raft formation, causing a loss of both early and terminal differentiation markers, keratins 1, 2 and 10, coupled to an increase in proliferation.[12] In parallel, Mathay, et al[39] showed that disruption of lipid rafts resulted in the downregulation of filaggrin gene expression.[39] Intrinsically, these studies tell us that cholesterol status is innately linked to normal keratinocyte behaviour.

It is, however, important to distinguish between different sterol forms when discussing biological activity. In this regard, oxysterols (25-hydroxycholesterol and 22R-hydroxycholesterol) but not free cholesterol or its precursor mevalonate have been shown to induce keratinocyte differentiation through upregulation of involucrin and transglutaminase 1.[33] Oxysterols activate the α and β isoforms of LXR, a transcription factor previously reported to regulate keratinocyte differentiation.[33,40] Activation of LXR by the specific agonist T0901317 reduces proliferation in epidermal keratinocytes and is reported to reduce hair growth in ex vivo human HFs.[41]

Of importance in epidermal keratinocyte function is cholesterol sulphate (CS), present at high levels in the stratum granulosum. CS increases the expression of differentiation markers, filaggrin, loricrin, involucrin and transglutaminase 1, as well as regulating desquamation in the stratum corneum.[42–44] CS itself is an inhibitor of cholesterol synthesis and, if present in excess, leads to reduced cholesterol levels and a mild impairment of barrier function in X-linked ichthyosis, a disease associated with loss-of-function mutations in the gene coding for the steroid sulphatase normally responsible for reducing CS levels.[44] Activators of LXR and PPAR, both of which stimulate keratinocyte differentiation in addition to controlling cholesterol metabolism, also regulate cholesterol sulphotransferase type 2B isoform 1b (SULT2B1b), an enzyme involved in CS synthesis.[11] Mutation in SULT2B1b leads to a congenital ichthyosis, in this case autosomal-recessive congenital ichthyosis.[45]

Cholesterol metabolism and the maintenance of sterol isoforms with defined levels are therefore required to maintain skin health, yet the precise role for both oxysterols and CS in regulating the activity of HF matrix keratinocytes remains to be elucidated. Indeed, 25-hydroxycholesterol can, for example, reduce HMGCR activity in human HFs[46] and CS is an integral lipid of hair fibres,[47] but the functional significance is unclear. A study by Brosche, et al[48] showed an increase in CS levels in hair clippings from patients with elevated serum LDL levels, despite total cholesterol levels remaining constant. In the HF, CS is not involved in desquamation and therefore must have alternative roles in regulating or controlling differentiation and/or adhesion of trichocytes in the hair shaft.

Current evidence shows that cholesterol; its products and intermediates are associated with epidermal keratinocyte differentiation, defects in which can result in epidermal barrier impairment. As such, it is reasonable to suggest that cholesterol may have an equally important role in the control of HF matrix keratinocyte differentiation

and hair shaft formation. Indeed, some insights as to the direct or indirect impact of cholesterol have already been reported, as outlined below.

3.2 | Sources of cholesterol in the HF: uptake vs de novo biosynthesis

As with other organs and tissues, HF cell populations likely obtain cholesterol via intrafollicular *de novo* biosynthesis. The enzyme 24-dehydrocholesterol reductase (DHCR24), which functions in the final step of the Bloch pathway to convert desmosterol to cholesterol (Figure 1A), is highly expressed in HFs.[46,49,50] In addition, when examined in mice, the presence of both cholesterol and its precursor desmosterol were found to be present at higher levels in the hair shaft than the skin,[23,50,51] with particularly high levels of desmosterol reported in relation to both the serum and skin, with a cholesterol/desmosterol ratio of close to 1.2:1.[51] The same authors imply that cholesterol must be incorporated into the hair shaft during formation, rather than as a coating. This suggests that substantial cholesterol synthesis occurs in the hair bulb, where the hair shaft and inner root sheath (IRS) are formed through the proliferation and differentiation of matrix keratinocytes, rather than added as a coating via sebaceous gland secretions.

It is not, however, clear whether carrier-mediated uptake from the circulation is a pathway of any importance for HF biology. As part of the pilosebaceous unit, the HF is in close proximity to multiple sources of exogenous cholesterol (Figure 2). The sebaceous gland is capable of de novo cholesterol synthesis, as are the adipocytes surrounding the proximal HF.[52] Both tissues contain substantial stores of cholesterol (Table 1), and it has been suggested that cholesterol efflux from adipocytes could be capable of modulating HF cycling.[53] Although sebocytes express HMGCR, the cholesterol biosynthetic pathway is halted at the production of squalene, which is present at high levels.[54]

Cholesterol can be delivered to the HF via uptake of circulatory lipoproteins, primarily LDL, which would be present in the microvasculature of the connective tissue sheath (CTS), including capillary loops penetrating into the dermal papilla (DP).[55] Despite these exogenous sources of cholesterol, it perhaps remains more likely that the HF furnishes its cholesterol requirements through de novo synthesis without the requirement for additional uptake from the circulation, as has been suggested in the epidermis.[56] In support of this, Brannan, et al[49] observed no difference in HMGCR activity in hypercholesterolaemic patients vs healthy controls, suggesting the

HF did not have the capacity for the uptake of excess serum LDL.[49] However, given the fact that HFs appear to express LDLRs, these studies do not exclude that, under circumstances where intrafollicular cholesterol is lacking, the HF might obtain cholesterol via LDLR-mediated endocytosis.

The full complement of cholesterol transporting proteins present in the HF is yet to be defined, although we know that the activity of at least one cholesterol transporter (ABCA5) has important biological consequences in the HF, as discussed later in this review.[22] As such, understanding routes for cholesterol movement will provide key insights into how the HF regulates levels of this important lipid.

3.3 | Does cholesterol modulate common signalling pathways for regulation of HF growth and cycling?

Numerous signalling pathways interact to control HF growth and cycling, disruption of which result in the development of hair pathologies. Examples include alopecia caused by treatment of basal cell carcinoma with Hh inhibitors,[57] mutations in a WNT inhibitor (APC downregulated 1) leading to hypotrichosis simplex[58] and the downregulation of Wnt/β catenin signalling in androgenic alopecia (AGA),[59] alopecia areata (AA) and universalis.[60] One common factor in these signalling pathways is the role played by cholesterol and cholesterol-rich lipid rafts, which can facilitate signal transduction.[2]

Members of the Hh family provide a relevant example of lipid-raft-associated signalling proteins[2] and act as regulators of HF cycling and morphogenesis, in particular the progression into anagen phase.[22,61] Cholesterol is a cofactor of the Hh protein, and reduced sterol levels are associated with a concomitant decrease in Shh (sonic Hh) transduction, as demonstrated in a mouse model of Smith-Lemli-Opitz syndrome, which results from defective cholesterol biosynthesis.[62] Cholesterol acts at downstream targets of the Hh signalling pathway at the point of smoothened and patched 1, which initiate transcription of Hh target genes.[63] Cholesterol is involved in the release of Hh ligand,[64] along with post-translational modification of Hh proteins.[65] Therefore, alterations in levels of cholesterol could alter HF cycling, that is, through delayed anagen onset.

Cholesterol status has also been associated with expression of bone morphogenic protein (BMP) family members. Disruption of lipid rafts in keratinocytes via methyl-β-cyclodextrin caused a rapid upregulation of BMP6,[39] which inhibits proliferation of bulge stem cells during telogen,[66] delaying anagen onset.[67] BMP signalling is a regulator of post-natal HF cycling[68] and is involved in bulge stem

Lipid	Hair shaft	IRS	HF	Sebum	SG
Cholesterol	3.9%-5.5%	2.5%	3.7%	7.0%	3.4%
Cholesterol esters	8.5%-19.1%			27.8%	
Cholesterol sulphate	5.7%-17.0%			1.4%	
Squalene	2.9%				19.0%
References	[5,194-197]	[194]	[194]	[195]	[198]

TABLE 1 Composition of sterols as percentage of total lipids in the HF and sebaceous gland

cell activation.[69] Upregulation of BMP signalling reduces cholesterol efflux in macrophages (via inhibition of ABCA1 and ABCG1),[70] which could point to a role for BMPs in controlling HF cholesterol status at key points during the hair cycle. Analysis of cholesterol homeostasis in BMP-ablated mouse mutants would be a crucial step in determining this.

Wnt/β catenin and Notch pathways are also important signalling elements in the control of HF cycling. Lipid modification to these proteins signals for membrane targeting[2,71] and cholesterol is involved in the activity of the canonical Wnt pathway specifically.[3] Furthermore, a cholesterol binding site has been noted on the dishevelled protein, leading to localisation of Wnt to the plasma membrane.[72] Inhibition of cholesterol synthesis by simvastatin enhanced Wnt signalling[73] and reduced levels of the Wnt inhibitor dickkopf-1 (DKK1),[74] a known inducer of catagen.[75]

One could reach the conclusion that impairment of intrafollicular cholesterol homeostasis would disrupt normal HF cycling via modulation of these sterol-sensitive signalling pathways. Yet other factors may also play a role, including that of cholesterol-dependent steroid biosynthesis.

3.4 | Importance of cholesterol homeostasis in steroid hormone biosynthesis

Skin is reported to be a steroidogenic tissue, although it is important to highlight that this activity is substantially lower than that observed in the gonads and adrenal glands (<1%).[56] Importantly, numerous steroidogenic enzymes including CYP450 side chain cleavage enzyme (CYP11A1), which catalyses the rate-limiting step (conversion of cholesterol into pregnenolone) in steroid hormone production, are expressed in the HF (Figure 2).[7,56] Steroid biosynthesis occurs in the inner mitochondrial membrane, where cholesterol levels are comparatively low. Increased delivery of cholesterol to this inner membrane (mediated by members of the StAR family; Figure 1C) leads to a concomitant increase in pregnenolone production, which can then be utilised by steroidogenic enzymes.[56] Hu, et al[76] have reviewed the utilisation of cholesterol sources in the production of steroid hormones, which will not be covered in as much detail here.

In the skin, the major steroid hormone products of cholesterol are glucocorticoids, androgens and estrogens.[9,77-79] In particular, the testosterone metabolite dihydrotestosterone (DHT) is formed in cutaneous tissues, including the HF. Here, it plays a role in the onset of androgenetic alopecia, as discussed in more detail later. There is a notable lack of information regarding the importance of de novo steroidogenesis within the HF vs. uptake of circulating steroid hormones produced in endocrine tissue such as the gonads and adrenal glands, which are subsequently metabolised in situ (for example to DHT). Evidence from prepubertal castration, which results in a large reduction in circulating androgens, shows that these individuals do not develop AGA and also lack androgen-driven vellus to terminal formation of secondary sexual hair.[80,81] The fact that injection of testosterone can induce AGA in castrated individuals would suggest that metabolism of circulating testosterone is the primary source of

increased follicular DHT levels. In this respect, de novo synthesis from cholesterol precursors does not seem sufficient to replace the loss of circulatory testosterone, in driving secondary hair formation or AGA.

It has been suggested that de novo steroid hormone synthesis in peripheral tissues plays a role in autocrine or paracrine signalling.[82] In this way, the comparatively low levels of intrafollicular androgen production in the HF could provide a modulatory signal that regulates hair growth and cycling. Indeed, cross-over in androgen receptor (AR) and Wnt/β-catenin signalling has been observed, with AR activation inhibiting this important HF growth and development pathway.[83] The high levels of DHT observed in balding scalp would therefore increase AR activity and concomitantly reduce Wnt/β-catenin signalling. In this way, changes in intrafollicular cholesterol levels and subsequent fluctuations in steroidogenesis could be linked to alterations in signalling pathways linked to hair growth or cycling. In support of this, recent preliminary evidence has suggested that increased cholesterol release from dermal adipocytes, which would be available for uptake into HF cell populations, might increase HF steroidogenesis and impact on anagen to catagen transition.[53]

A recent study examining women with evidence of female pattern hair loss (FPHL) observed that despite normal levels of circulating androgens, the expression of 5α-reductase (5αR) isoforms was increased in the HF, which might serve to enhance intrafollicular DHT levels.[84] This fits with a role for enhanced steroid hormone metabolism in the onset of FPHL rather than any increase in de novo synthesis.

Given the ability of cutaneous tissues to utilise cholesterol for steroidogenesis, alongside the dependence on rate-limiting cholesterol trafficking, it is clear that alterations in cholesterol homeostasis have the potential to severely impair this process. A role for this local steroid hormone synthesis, vs. in situ metabolism of circulating androgens, oestrogens or glucocorticoids, in defective HF development or function remains to be conclusively shown. Future studies utilising the targeted knockout of specific enzymes within the HF would go some way to elucidating this.

4 | ASSOCIATIONS BETWEEN CHOLESTEROL AND HAIR PATHOLOGIES

4.1 | Cholesterol synthesis is dysregulated in primary cicatricial alopecia

Associations have been made between altered cholesterol status and the group of inflammatory hair loss disorders, termed primary cicatricial alopecias (PCAs), characterised by permanent HF loss and formation of scar-like fibrous tissue.[24] Inflammation and the influx of immune cells is a hallmark of PCA, yet the underlying cause remains unclear. Recent evidence has suggested that altered lipid homeostasis may have a role to play.

In particular, Panicker, et al[24] noted a significant downregulation of genes involved in cholesterol biosynthesis, in both affected and unaffected scalp tissue from PCA patients. This included

7-dehydrocholesterol reductase (7-DHCR), which catalyses the final step in cholesterol biosynthesis (Figure 1) as well as emopamil-binding protein (EBP), mutations in which cause Conradi-Hunermann syndrome, a disorder where scarring hair loss is seen (see section 4.74.7). Inhibition of 7-DHCR, or addition of exogenous 7-dehydrocholesterol (7-DHC) to human primary outer root sheath keratinocytes (ORSK) or via topical application to mouse back skin, resulted in a pro-inflammatory response, including upregulation of Toll-like receptor and interferon signalling networks. Inhibition of cholesterol biosynthesis also upregulated transforming growth factor β (TGFβ1),[24] an established inducer of catagen[85] and fibrosis.[86]

Ultimately, inhibition of cholesterol synthesis in these murine models resulted in loss of HF growth and abnormal cycling, with evidence of follicular plugging and epidermal thickening, alongside an increase in markers associated with catagen induction (TGFβ1) and downregulation of stem cell marker (SOX9).[24] The conclusion is that in PCA patients, accumulation of cholesterol precursors mediates the inflammatory response associated with macrophage recruitment and ultimately, HF destruction.[24] As such, a direct link between HF sterol status and PCA is apparent.

Of relevance to this is evidence suggesting that frontal fibrosing alopecia (FFA), a form of PCA primarily observed in women, may be linked to sex steroid responses.[87] Indeed, postmenopausal decline in DHEA/estrogen activity or levels may predispose individuals to FFA development.[87–89]

Furthermore, a recent GWAS identified a missense mutation in the xenobiotic and steroid hormone metabolising enzyme, CYP1B1, linked with pathogenesis of FFA.[88] CYP1B1, which has been associated with alopecia X in Pomeranian dogs,[90] plays a role in the oxidative metabolism of estradiol and estrone, but may also metabolise xenobiotics such as the oral contraceptive.[88] Although this could again point to a role for steroid hormone metabolism in development of hair disorders such as FFA, it does not provide direct evidence of a role for intrafollicular steroidogenesis. Whether changes in intrafollicular cholesterol levels, coupled to reduced *de novo* steroid hormone production have a role in the pathogenesis of FFA is therefore yet to be determined, but remains a possibility.

4.2 | PPAR dysregulation in PCA pathogenesis

Dysregulation or dysfunction in the PPAR family of ligand-activated nuclear receptors is also suggested to be a causative factor in PCA.[91,92] Regulation of cholesterol homeostasis is the domain of numerous nuclear hormone receptors and the PPARs represent one such important pathway.[93,94] PPAR heterodimerisation with retinoid X receptor (RXR) initiates binding to PPRE (peroxisome proliferator response element), enhancing proliferation of peroxisomes, which act as secondary sites for cholesterol synthesis.[91,93] Beyond lipid homeostasis, PPAR activation is also associated with immune regulation and anti-inflammatory affects.[95] These transcription factors have numerous downstream targets, including but not limited to genes associated with cholesterol catabolism, lipoprotein metabolism, mitochondrial oxidation, glucogenesis and ketogenesis.[96]

In the HF, specific PPAR isoforms have roles in HF survival (PPARα),[97] morphogenesis (PPARβ/δ)[98,99] and keratinocyte differentiation (PPARγ).[100] PPARγ agonism can reduce IL-6 and increases keratin 15 levels in the bulge, as well as inducing catagen.[94]

In scalp tissue from patients with lichen planopilaris (LPP, a form of PCA characterised by follicular inflammation and fibrosis), a significant reduction in PPARγ expression is found in both affected and unaffected HFs.[91] This is associated with a downregulation of the cholesterol homeostasis genes HMGCR, hydroxymethylglutaryl-CoA synthase (HMGCS1) and acetyl CoA acetyltransferase (ACAT), as well as decreased peroxisome numbers, resulting in reduced cholesterol synthesis.[91] Furthermore, PPARγ KO mice develop a scarring alopecia phenotype, along with a downregulation of HMGCR, HMGCS1, sterol O-acyltransferase 1 and 24-dehydrocholesterol reductase[91] supporting dysregulation of cholesterol homeostasis as a potential factor in LPP pathogenesis.

However, other properties of PPARγ activity (ie anti-inflammatory effects[95] and epithelial to mesenchymal transition inhibition[86,101]) are also likely play an important role in disease development.[87] Interestingly, the PPARγ agonist pioglitazone is now being successfully used to treat this disorder, with response rates of over 50% reported.[102] Together, these results suggest a more detailed examination of the role of PPARγ in intrafollicular cholesterol homeostasis is warranted, which may provide pointers towards the development of other therapeutic targets for these disorders.

4.3 | Mutations in cholesterol synthesis cause autosomal-recessive hypotrichosis simplex

A number of studies have also identified mutations in genes linked with cholesterol homeostasis and hair phenotypes, as shown in Table 2. Indeed, a recent publication employing whole-exome sequencing identified mutations in lanosterol synthase (LSS), linked to autosomal-recessive hypotrichosis simplex.[103] LSS is involved in the production of lanosterol during cholesterol biosynthesis (Figure 1A).[104] Patients present with sparse hair on the scalp and in some cases eyebrows and eyelashes. The authors identified 5 LSS mutations, leading to either loss of protein or mislocalisation from the endoplasmic reticulum to the cytoplasm.

The resulting dysfunction is suggested to lead to accumulation of cholesterol precursors, resulting in inflammation and disruption of Wnt/BMP signalling.[103] As the authors did not specifically investigate intrafollicular sterol levels in these patients, a role for the accumulation of potential toxic cholesterol precursors remains to be conclusively shown.

4.4 | Accumulation of cholesterol precursors causes abnormal hair growth in mice

Insulin-induced gene 1 (Insig) modulates cholesterol synthesis through proteolytic degradation of HMGCR, as well as binding to SREBP cleavage-activating protein (SCAP) and preventing SREBP-mediated transcription of cholesterol synthesis genes.[105]

TABLE 2 Mutations in cholesterol homeostasis leading to hair and skin diseases

Mutation	Gene function	Disease	Hair phenotype	References
ABCA12	Ceramide transporter, regulatory function in ABCA1 expression	Harlequin ichthyosis	Sparse and brittle hair shafts	[109]
ABCA5	Putative cholesterol transporter	Congenital hypertrichosis	Excessive hair growth throughout the body	[22,108]
EBP	Conversion of zymosterol in cholesterol biosynthesis pathway	Conradi–Hünermann syndrome	Follicular atrophoderma and patchy scarring alopecia	[129–135]
LSS	Synthesis of lanosterol from squalene-2,3-epoxide	Autosomal-recessive hypotrichosis simplex	Sparse scalp hair may include eyebrows and eyelashes	[103]
MBTPS2	Cleavage of SREBP2	IFAP KFSD	Non-progressive alopecia Cicatricial alopecia	[115–126]
Steroid Sulphatase	Reduces cholesterol sulphate levels	X-linked ichthyosis	Normal	[199]
SULT2B1b	Synthesis enzyme of cholesterol sulphate	Congenital ichthyosis	Normal	[45]

Epidermal specific double knockout of Insig (epi-*Insig*-DKO) prevented normal HF morphogenesis. Histologically, hair kinking, keratin plugging and dissociation of the DP from the hair bulbs were observed.[105] Evers, et al[23] hypothesised that the significant increase in sterol precursors identified in the epi-*Insig*-DKO mice was a causative factor. Supporting this, inhibition of cholesterol biosynthesis with simvastatin significantly reduced levels of sterol precursors in these animals and reversed the morphological HF defects. Although the mechanism by which accumulation of sterol precursors impacted on hair morphogenesis was not described, the authors suggest impaired Shh signalling, given similarities to the hair phenotype displayed by $Shh^{-/-}$ mice. This ties in well with the known role for cholesterol in modulating the Shh pathways, as previously described.

Additionally accumulation of desmosterol in the epidermis and hair of DHCR24$^{-/-}$ mice was found to cause epidermal thickening and reduced HF number, although this knockout was fatal within 24 hours.[50] Another reported DHCR24$^{-/-}$ mouse was viable; however, no skin or hair phenotypes were described.[106] This mouse showed accumulation of serum and liver desmosterol, with very low levels of cholesterol.[106] Accumulation of 7-dehydrodesmosterol in DHCR7-deficient mice is described by Serra et al,[51] with no changes in the levels of upstream lanosterol; however, desmosterol levels were significantly reduced as were levels of cholesterol in the hair.[51]

4.5 | SREBP-mediated dysregulation of cholesterol homeostasis causes murine alopecia

Mutations in murine glycerol kinase 5 (GK5) result in the *toku* phenotype, typified by progressive hair loss and accumulation of dermal lipids.[107] Binding of GK5 to SREBPs inhibits their transcriptional activity, which is therefore increased in the GK5$^{toku/}$^{toku} mice resulting in increased levels of free cholesterol and cholesterol esters, as well as the expression of SREBP1, SREBP2 and HMGCR. Statin treatment partially restores hair growth and reduces cutaneous cholesterol levels in the mutant mice, though

not to wild type levels. Although the authors did not expand on these findings, the study adds further weight to the premise that disruption of cholesterol homeostasis, leading to accumulation of precursors, is detrimental to normal HF function.

4.6 | Congenital hypertrichosis and cholesterol

In addition to hair loss, dysregulation of cholesterol homeostasis has also been observed in a form of congenital hypertrichosis. Of particular note is identification of mutations in the ABCA5 gene, resulting in a condition typified by an excessive overgrowth of hair across the body.[22,108]

DeStefano, et al[22] demonstrated widespread expression of ABCA5 in the HF, which was substantially reduced in patients with a mutated form of the transporter. Keratinocytes isolated from the affected patient showed enhanced accumulation of endolysosomal cholesterol as well as lysosomal dysfunction.[22] Although this study was unable to provide a direct link between defective ABCA5-mediated cholesterol transport and associated hair overgrowth, the work nonetheless highlights the likely importance of cholesterol transport and trafficking in maintaining intrafollicular cholesterol levels and normal hair growth.

4.7 | Hair phenotype in harlequin ichthyosis

Mutations in another ABC transporter, namely ABCA12, are linked with a cutaneous disorder of lipid homeostasis. Loss of ABCA12 results in harlequin ichthyosis (HI), a rare and extreme congenital skin condition characterised by massive epidermal hyperkeratosis causing a hard, plate-like stratum corneum to encasing the neonate from birth. Abnormal epidermal development in which barrier function is impaired leads to life-threatening transepidermal water loss and a heightened risk of infection.[109] The lack of epidermal barrier in HI patients stems from abnormal lamellar granule formation, packaging of which is dependent on the ceramide transport activity of ABCA12.[28,110] ABCA12 has also been shown to play

an important role in the post-transcriptional regulation of ABCA1, a cell membrane transporter involved in the efflux of cellular free cholesterol.[111]

Both ABCA1 and ABCA12 have been localised to epithelial and mesenchymal compartments in the HF, though their functional significance is currently unknown.[112] In relation to HI, a commonly observed hair phenotype exists in which a lower hair density (sparseness) and brittle hair shafts are observed.[113] The belief is that keratotic plugging of the hair canal, caused by epidermal thickening,[114] disrupts the penetration of the hair shaft through the skin. Yet, given the expression of both ABCA12 and ABCA1 in the HF,[112] it may be that intrafollicular dysregulation of lipid (including cholesterol) metabolism also impedes normal HF development, resulting in abnormal hair shaft formation. To date, direct investigations into HF morphology in these patients are lacking.

4.8 | Rare skin diseases associated with lipid homeostasis

Mutations in Membrane Bound Transcription Factor Peptidase, Site 2 (MBTPS2), a protein required for cholesterol homeostasis through cleavage of SREBP2, have been linked to two rare skin diseases, ichthyosis follicularis with alopecia and photophobia (IFAP) syndrome[115-123] and keratosis follicularis spinulosa decalvans (KFSD).[124-126] IFAP presents with non-progressive non-cicatricial alopecia, which can include the scalp, eyebrows and eyelashes and, in some cases, alopecia universalis. KFSD is distinguished by a progressive cicatricial alopecia with follicular hyperkeratosis, eyebrow loss and photophobia.[120,122] Another rare skin disease with a MBTPS2 mutation is the X-linked form of Olmsted syndrome, characterised by mutilating palmoplantar keratoderma and periorificial hyperkeratotic plaques.[127] Although alopecia is a symptom, keratotic plaques could provide an explanation for the sparse, brittle hair that is present, much in the same way that this explanation is given for a similar phenotype in HI patients.[128]

Mutations in EBP, which functions in the cholesterol biosynthesis pathway (see Figure 1A) and is suppressed in cases of PCA,[24] causes Conradi-Hünermann syndrome.[129-132] Phenotypically, Conradi-Hünermann syndrome presents with chondrodysplasia punctata (premature calcification of the long bones) in the surviving patients (the dominant X-linked disease is lethal in the majority of males). Early skin changes including erythema and hyperkeratosis are replaced later in childhood by follicular atrophoderma and patchy scarring alopecia.[130-134] Cholesterol intermediates accumulate due to the impairment of endogenous synthesis pathways. This is somewhat similar to the build-up of intermediates as described by Panicker, et al[24] in cases of PCA. It is thought that the cause of the osteous condition is through the absence of cholesterol in maintaining Hh signalling for bone development.[135] Given the importance of Hh signalling in HF development and cycling, this may also provide some explanation as to the hair phenotype observed.

4.9 | Dyslipidaemia, cholesterol and steroid hormone synthesis in AGA

A number of studies have examined links between AGA and cholesterol levels, in particular focusing on cardiovascular disease risk[136-143] and metabolic syndrome.[136,144-150] Recent meta-analysis by Kim, et al[151] highlighted the association between dyslipidaemia and AGA. The findings show significant increases in both total cholesterol and LDL levels, coupled to lower HDL, though the picture for HDL is less clear with some individual case studies reporting no changes or only small, non-significant reductions in HDL.[137-140,143-145,150,152] Total cholesterol and LDL levels were more consistently increased across the studies.[136,138-141,143-145,147,148,153-155]

As detailed earlier, cholesterol is a common precursor for steroid hormones, including sex steroids. Androgens have many effects on HF biology, including driving location-specific vellus to terminal hair transformation during puberty[156] and changes in sex steroids in women during pregnancy, post-partum and during menopause have also been linked with alterations in HF growth and cycling.[157] AGA is the most common form of hair loss[158] characterised by an androgen-driven terminal to vellus hair transformation on the vertex scalp manifesting as progressive hair thinning. Specifically, the sensitivity to androgens is increased in the frontal region of the scalp in patients with AGA explaining the typical distribution of hair loss.[158] Higher levels of 5αR types I and II are also associated with the frontal region,[159,160] which converts testosterone into DHT.[161] DHT subsequently binds to AR, enhancing the transcription of the catagen inducer, TGFβ.[162] Inhibition of 5αR is targeted in treatment of AGA (eg Finasteride),[163] though alternative AGA therapies include androgen antagonists.[164]

Recent observations in scalp skin have also demonstrated increased expression of StAR in the frontal area of the scalp, which was associated with decreased hair density.[9] The higher level of StAR expression also correlated with oestrogen and testosterone levels.[9] Furthermore, regulatory elements SF-1 (steroidogenic factor 1) and DAX1 (nuclear receptor subfamily 0 group B member 1), which function in the regulation of StAR, and thus steroid hormone production, have been identified in the HF, localised to cells in the outer root sheath (ORS), IRS, matrix and DP[165] (Figure 2). Patel, et al[165] speculate that these transcription factors may be activated by oxysterols and thus play a role in the conversion of sterols into DHT. Whilst this might suggest that StAR-mediated cholesterol trafficking is closely linked to androgen synthesis, patients with AGA show little if any difference in circulatory DHT levels and, as mentioned earlier, intrafollicular androgen production does not appear sufficient to cause DHT-sensitive AGA.[56,160,166-168] That said increased follicular metabolism of testosterone to DHT, combined with enhanced intrafollicular steroidogenesis could be occurring. Confirmation of this would require further systematic investigation.

4.10 | The role of cholesterol biosynthesis in the formation of vitamin D3 and associated hair loss

Within epidermal keratinocytes, exposure to UV light stimulates the synthesis of vitamin D3 from the cholesterol precursor 7-DHC.[169]

As such, the cholesterol biosynthetic pathway may also be important in relation to the supply of vitamin D3 to the HF. Indeed, vitamin D receptors (VDR) are expressed in the HF,[170–172] and alopecia totalis has been observed in patients with VDR mutations.[173] What is more, VDR knockout in mice prevents initiation of new hair cycles following morphogenesis.[172] Evidence also suggests vitamin D deficiency is associated with female hair loss disorders[170] and AA.[174–176] Hair growth was shown to increase with the presence of synthetic vitamin D3 analogues (calcitriol/calcipotriol) in alopecia totalis,[177] AA[178] and in chemotherapy-induced alopecia mouse models.[179] It could be suggested that dysfunction in the cholesterol biosynthesis pathway, which would alter levels of 7-DHC, might play a role in hair loss related to vitamin D3 deficiency.

5 | MODULATION OF CHOLESTEROL HOMEOSTASIS IN THE HF

5.1 | Can statins impact on hair loss?

Statins, a class of drug used to lower serum cholesterol levels through inhibition of HMGCR, have come under close scrutiny for the treatment of certain alopecias, as well as reports that they may in themselves cause hair loss.

The evidence linking statin use and hair loss is, however, far from conclusive. A case study published by Segal[180] reported hair loss in a 38-year-old woman with no unusual medical history, taking daily atorvastatin (10 mg, oral) alongside other medications. Hair loss was reversed upon discontinuation of the statin and returned 2 weeks after re-introduction of the medication. The authors therefore suggest a causal link between the alopecia and atorvastatin treatment. The timeframe of reported hair loss in this instance could indicate stimulation of anagen effluvium, rather than the more commonly observed drug-induced telogen effluvium, given the rapid pace of onset.

Similar case studies have been reported, particularly for atorvastatin use, with alopecia reported in the parietal and vertex regions of a female patients scalp.[181] As with the previous study, atorvastatin was not the only medication administered.

In contrast to these individual cases, larger cohort studies have found no direct causative relationship between alopecia and statin use. Smeeth, et al[182] examined 129 288 statin users against 600 241 controls. In considering a range of potential adverse effects, the authors did not find any evidence to suggest that statins can be linked to alopecia. The evidence for statins causing hair loss does not therefore suggest any direct relationship and drug-drug interactions cannot be ruled out as a factor in any individual cases observed.

Juxtaposed to this, some studies have suggested a role for statins in reversing hair loss in certain patients. Combinations of simvastatin and ezetimibe (commonly used to block Niemann-Pick C1-like 1-mediated uptake of dietary cholesterol when treating hypercholesterolaemia) were found to regrow hair in patients with AA, totalis and universalis.[17] It should be stated that this case study[17] was not

a randomised control trial and care should be taken in interpreting these observations, considering the potential for spontaneous regrowth in this disorder. Indeed, the extent of regrowth in response to this therapy varies significantly between studies, ranging from <20% to 'significant',[16–19] with patients displaying more severe AA receiving no benefit.[183,184]

Loi, et al[183] conducted a small prospective study to examine simvastatin/ezetimibe treatment in patients with AA totalis/universalis, noting no benefit. A similarly small study by Lattouf, et al[185] did, however, observe hair regrowth in a number of AA patients, in addition to possible prevention of relapse. Combination treatment involving simvastatin and ezetimibe remains, therefore, a potentially beneficial therapy for some AA patients.

Whereas both statins and ezetimibe are cholesterol-lowering therapies, the hair growth restoration observed in AA patients is most likely to occur as a result of both the immunomodulatory activity of these drugs and their inhibitory activity against the JAK/STAT pathway.[19] Infiltration of CD4$^+$ and CD8$^+$ lymphocytes is a key feature of AA.[186] CD4$^+$ lymphocytic infiltration increases the expression of intercellular adhesion molecule-1 (ICAM-1) and MHC (major histocompatibility complex) class II molecules in HFs. Statin treatment can inhibit the expression of ICAM-1 and can bind to lymphocyte function-associated antigen 1 (LFA-1), interfering with LFA-1-ICAM-1 interactions.[17,187] Statins can also interfere with MHC class II expression and may limit the effects of CD4$^+$ lymphocytes.

In addition, JAK/STAT inhibitors have proven useful in restoring hair growth in AA patients, by attenuating production of inflammatory cytokines (IL-2, IL-15 and interferon-γ) by cytotoxic T lymphocytes.[19,51,188] It is likely that, as seen with JAK/STAT inhibitors, statin-mediated inhibition of inflammatory cytokine signalling is a mechanism by which statins can help treat acute episodes of AA.[19]

As such, it cannot be claimed that the benefits of statin treatment in AA result from direct cholesterol modulatory activity and additional work is required to understand whether intrafollicular modulation of cholesterol homeostasis in itself is beneficial in the treatment of alopecia.

6 | CONCLUSIONS

Cholesterol is a hugely important component of all cells and accumulated evidence suggests a principal role in HF biology. Whether as a structural element of lipid rafts, a modulator of intrafollicular signalling pathways or a precursor for androgen synthesis, cholesterol can intersect with numerous areas of HF biology and pathology. Currently, there is a dearth of information relating to how HF cell populations handle cholesterol, relating synthesis, transport, trafficking and regulation. It is clear that altered cholesterol levels are commonly observed alongside hair disorders (both alopecias and hirsutism). Yet, whether these changes are directly responsible for, or have an influence on, the observed hair phenotypes remain to be conclusively determined. Additional efforts to understand the impact of cholesterol across all

levels of HF cell biology would undoubtedly yield important information as to potential targets for development of future therapies.

ACKNOWLEDGEMENTS

CONFLICT OF INTEREST

The authors have declared no conflicting interest.

AUTHOR CONTRIBUTION

ISH and MAP designed the concept for the Review manuscript. All authors contributed to the writing of the manuscript. ISH edited the final contributions. All authors read and approved the final manuscript.

ORCID

Iain S. Haslam https://orcid.org/0000-0002-1008-2447

REFERENCES

[1] H. Ohvo-Rekilä, B. Ramstedt, P. Leppimäki, S. J. Peter. *Prog. Lipid Res.* **2002**, *41*, 66.
[2] J. P. Incardona, S. Eaton. *Curr. Opin. Cell Biol.* **2000**, *12*, 193.
[3] R. Sheng, H. Kim, H. Lee, Y. Xin, Y. Chen, W. Tian, Y. Cui, J.-C. Choi, J. Doh, J.-K. Han, W. Cho. *Nat. Commun.* **2014**, *5*, 4393.
[4] K. R. Feingold. *J. Lipid Res.* **2009**, *50*, S417.
[5] P. W. Wertz. *Acta Derm. Venereol. Suppl. (Stockh).* **2000**, *208*, 7.
[6] A. H. Payne, D. B. Hales. *Endocr. Rev.* **2004**, *25*, 947.
[7] D. Thiboutot, K. Gilliland, Z. Cong, S. Jabara, J. M. McAllister, A. Sivarajah, G. Clawson. *J. Invest. Dermatol.* **2003**, *120*, 905.
[8] V. A. Cortes, D. Busso, A. Maiz, A. Arteaga, F. Nervi, A. Rigotti. *Front. Biosci. (Landmark Ed).* **2014**, *19*, 416.
[9] T. Inoue, Y. Miki, K. Abe, M. Hatori, M. Hosaka, Y. Kariya, S. Kakuo, T. Fujimura, A. Hachiya, S. Honma, S. Aiba, H. Sasano. *Mol. Cell. Endocrinol.* **2012**, *362*, 19.
[10] H. M. Elbadawy, F. Borthwick, C. Wright, P. E. Martin, A. Graham. *Br. J. Dermatol.* **2011**, *164*, 628.
[11] Y. J. Jiang, P. Kim, P. M. Elias, K. R. Feingold. *J. Lipid Res.* **2005**, *46*, 2657.
[12] F. Spörl, M. Wunderskirchner, O. Ullrich, G. Bömke, U. Breitenbach, T. Blatt, H. Wenck, K.-P. Wittern, A. Schrader. *J. Invest. Dermatol.* **2010**, *130*, 1268.
[13] H. Tsuruoka, W. Khovidhunkit, B. E. Brown, J. W. Fluhr, P. M. Elias, K. R. Feingold. *J. Biol. Chem.* **2002**, *277*, 2916.
[14] K. U. Schallreuter, S. Hasse, H. Rokos, B. Chavan, M. Shalbaf, J.D. Spencer, J. M. Wood. *Exp. Dermatol.* **2009**, *18*, 680.
[15] J. S. Lee, E. Seppanen, J. Patel, M. P. Rodero, K. Khosrotehrani. *Exp. Dermatol.* **2016**, *25*, 71.
[16] A. Ali, J. M. Martin. *J. Drugs Dermatol.* **2010**, *9*, 62.
[17] C. Lattouf, J. J. Jimenez, A. Tosti, M. Miteva, T. C. Wikramanayake, C. Kittles, I. Herskovitz, M. Z. Handler, G. Fabbrocini, L. A. Schachner. *J. Am. Acad. Dermatol.* **2015**, *72*, 359.
[18] D. N. Robins. *J. Drugs Dermatol.* **2007**, *6*, 946.
[19] J. Cervantes, J. J. Jimenez, G. M. DelCanto, A. Tosti. *J. Investig. Dermatol. Symp. Proc.* **2018**, *19*, S25.
[20] T. H. Lee. *Harv. Health Lett.* **2000**, *25*, 8.
[21] C. Robb-Nicholson. *Harv. Womens Health Watch* **1998**, *5*, 8.
[22] G. M. DeStefano, M. Kurban, K. Anyane-Yeboa, C. Dall'Armi, G. Di Paolo, H. Feenstra, N. Silverberg, L. Rohena, L. D. López-Cepeda, V. Jobanputra, K. A. Fantauzzo, M. Kiuru, M. Tadin-Strapps, A. Sobrino, A. Vitebsky, D. Warburton, B. Levy, J. C. Salas-Alanis, A. M. Christiano.. *PLoS Genet.* **2014**, *10*, e1004333.
[23] B. M. Evers, M. S. Farooqi, J. M. Shelton, J. A. Richardson, J. L. Goldstein, M. S. Brown, G. Liang. *J. Invest. Dermatol.* **2010**, *130*, 1237.
[24] S. P. Panicker, T. Ganguly, M. Consolo, V. Price, P. Mirmirani, K. Honda, P. Karnik. *PLoS One* **2012**, *7*, e38449.
[25] I. L. Aye, A. T. Singh, J. A. Keelan. *Chem. Biol. Interact.* **2009**, *180*, 327.
[26] E. Ikonen. *Nat. Rev. Mol. Cell Biol.* **2008**, *9*, 125.
[27] K. Klappe, I. Hummel, D. Hoekstra, J. W. Kok. *Chem. Phys. Lipids.* **2009**, *161*, 57.
[28] F. Quazi, R. S. Molday. *Essays Biochem.* **2011**, *50*, 265.
[29] D. Rhainds, L. Brissette. *Int. J. Biochem. Cell Biol.* **2004**, *36*, 39.
[30] R. E. Soccio, J. L. Breslow. *Arterioscler. Thromb. Vasc. Biol.* **2004**, *24*, 1150.
[31] J. W. Oh, J. Kloepper, E. A. Langan, Y. Kim, J. Yeo, M. J. Kim, T.-C. Hsi, C. Rose, G. S. Yoon, S.-J. Lee, J. Seykora, J. C. Kim, Y. K. Sung, M. Kim, R. Paus, M. V. Plikus. *J. Invest. Dermatol.* **2016**, *136*, 34.
[32] K. R. Feingold, P. M. Elias. *Biochim. Biophys. Acta.* **2014**, *1841*, 280.
[33] K. Hanley, D. C. Ng, S. S. He, P. Lau, K. Min, P. M. Elias, D. D. Bikle, D. J. Mangelsdorf, M. L. Williams, K. R. Feingold. *J. Invest. Dermatol.* **2000**, *114*, 545.
[34] K. Hanley, L. Wood, D. C. Ng, S. S. He, P. Lau, A. Moser, P. M. Elias, D. D. Bikle, M. L. Williams, K. R. Feingold. *J. Lipid Res.* **2001**, *42*, 390.
[35] O. Hanyu, H. Nakae, T. Miida, Y. Higashi, H. Fuda, M. Endo, A. Kohjitani, H. Sone, C. A. Strott. *Biochem. Biophys. Res. Comm.* **2012**, *428*, 99.
[36] R. Jans, L. Mottram, D. L. Johnson, A. M. Brown, S. Sikkink, K. Ross, N. J. Reynolds. *J. Invest. Dermatol.* **2013**, *133*, 793.
[37] M. Ponec, L. Havekes, J. Kempenaar, S. Lavrijsen, M. Wijsman, J. Boonstra, B. J. Vermeer. *J. Cell. Physiol.* **1985**, *125*, 98.
[38] M. Ponec, J. Kempenaar, J. Boonstra. *Biochim. Biophys. Acta.* **1987**, *921*, 512.
[39] C. Mathay, M. Pierre, M. R. Pittelkow, E. Depiereux, A. F. Nikkels, A. Colige, Y. Poumay. *J. Invest. Dermatol.* **2011**, *131*, 46.
[40] M. Schmuth, P. M. Elias, K. Hanley, P. Lau, A. Moser, T. M. Willson, D. D. Bikle, K. R. Feingold. *J. Invest. Dermatol.* **2004**, *123*, 41.
[41] L. E. Russell, W. J. Harrison, A. W. Bahta, C. C. Zouboulis, J. M. Burrin, M. P. Philpott. *Exp. Dermatol.* **2007**, *16*, 844.
[42] K. R. Feingold, Y. J. Jiang. *Dermatoendocrinol.* **2011**, *3*, 113.
[43] C. A. Strott, Y. Higashi. *J. Lipid Res.* **2003**, *44*, 1268.
[44] P. M. Elias, M. L. Williams, W. M. Holleran, Y. J. Jiang, M. Schmuth. *J. Lipid Res.* **2008**, *49*, 697.
[45] L. Heinz, G. J. Kim, S. Marrakchi, J. Christiansen, H. Turki, M. A. Rauschendorf, M. Lathrop, I. Hausser, A. D. Zimmer, J. Fischer. *Am. J. Hum. Genet.* **2017**, *100*, 926.
[46] C. D. W. Smythe, M. Greenall, T. Kealey. *J. Invest. Dermatol.* **1998**, *111*, 139.
[47] P. W. Wertz, D. T. Downing. *Lipids* **1988**, *23*, 878.
[48] T. Brosche, S. Dressler, D. Platt. *Aging (Milano).* **2001**, *13*, 131.
[49] P. G. Brannan, J. L. Goldstein, M. S. Brown. *J. Lipid. Res.* **1975**, *16*, 7.
[50] R. Mirza, S. Qiao, Y. Murata, H. Seo. *Am. J. Dermatopathol.* **2009**, *31*, 446.
[51] M. Serra, X. Matabosch, L. Ying, G. Watson, C. Shackleton. *J. Steroid Biochem. Mol. Biol.* **2010**, *122*, 318.

[52] G. Rivera-Gonzalez, B. Shook, V. Horsley. *Cold Spring Harbor Perspect. Med.* **2014**, *4*(3), a015271.

[53] C. Nicu, J. A. Hardman, J. Pople, R. Paus. *Exp. Dermatol.* **2019**;28:432.

[54] M. Picardo, M. Ottaviani, E. Camera, A. Mastrofrancesco. *Dermatoendocrinol.* **2009**, *1*, 68.

[55] R. A. Ellis, G. Moretti. *Ann. N. Y. Acad. Sci.* **1959**, *83*, 448.

[56] A. Slominski, B. Zbytek, G. Nikolakis, P. R. Manna, C. Skobowiat, M. Zmijewski, W. Li, Z. Janjetovic, A. Postlethwaite, C. C. Zouboulis, R. C. Tuckey. *J. Steroid Biochem. Mol. Biol.* **2013**, *137*, 107.

[57] L. A. Fecher, W. H. Sharfman. *Biologics.* **2015**, *9*, 129.

[58] Y. Shimomura, D. Agalliu, A. Vonica, V. Luria, M. Wajid, A. Baumer, S. Belli, L. Petukhova, A. Schinzel, A. H. Brivanlou, B. A. Barres, A. M. Christiano. *Nature* **2010**, *464*, 1043.

[59] G. Q. Lu, Z. B. Wu, X. Y. Chu, Z. G. Bi, W. X. Fan. *Medicine* **2016**, *95*, e4297.

[60] Y. Y. Lim, S. Y. Kim, H. M. Kim, K. S. Li, M. N. Kim, K.-C. Park, B. J. Kim. *Clin. Exp. Dermatol.* **2014**, *39*, 368.

[61] K. Krause, K. Foitzik. *Semin. Cutan. Med. Surg.* **2006**, *25*, 2.

[62] M. K. Cooper, C. A. Wassif, P. A. Krakowiak, J. Taipale, R. Gong, R. I. Kelley, F. D. Porter, P. A. Beachy. *Nat. Genet.* **2003**, *33*, 508.

[63] J. Y. Tang, P. L. So, E. H. Epstein Jr. *Toxicol. Appl. Pharmacol.* **2007**, *224*, 257.

[64] R. Burke, D. Nellen, M. Bellotto, E. Hafen, K.-A. Senti, B. J. Dickson, K. Basler. *Cell* **1999**, *99*, 803.

[65] J. A. Porter, K. E. Young, P. A. Beachy. *Science* **1996**, *274*, 255.

[66] J. Lee, T. Tumbar. *Semin. Cell Dev. Biol.* **2012**, *23*, 906.

[67] Y.-C. Hsu, H. A. Pasolli, E. Fuchs. *Cell* **2011**, *144*, 92.

[68] U. Guha, L. Mecklenburg, P. Cowin, L. Kan, W. M. O'Guin, D. D'Vizio, R. G. Pestell, R. Paus, J. A. Kessler. *Am. J. Pathol.* **2004**, *165*, 729.

[69] M. V. Plikus, J. A. Mayer, D. de laCruz, R. E. Baker, P. K. Maini, R. Maxson, C.-M. Chuong. *Nature* **2008**, *451*, 340.

[70] J. Feng, J. Gao, Y. Li, Y. Yang, L. Dang, Y. Ye, J. Deng, A. Li. *Int. J. Mol. Sci.* **2014**, *15*, 5536.

[71] K. S. Stenn, P. Karnik. *J. Invest. Dermatol.* **2010**, *130*, 1205.

[72] R. Sheng, H. Kim, H. Lee, Y. Xin, Y. Chen, W. Tian, Y. Cui, J.-C. Choi, J. Doh, J.-K. Han, W. Cho. *Nat. Commun.* **2014**, *5*, 4393.

[73] K. Gao, Z. Shen, Y. Yuan, D. Han, C. Song, Y. Guo, X. Mei. *J. Neurochem.* **2016**, *138*, 139.

[74] M. Pontremoli, M. Brioschi, R. Baetta, S. Ghilardi, C. Banfi. *Sci. Rep.* **2018**, *8*, 16671.

[75] M. H. Kwack, M. K. Kim, J. C. Kim, Y. K. Sung. *J. Invest. Dermatol.* **2012**, *132*, 1554.

[76] J. Hu, Z. Zhang, W.-J. Shen, S. J. N. Azhar. *Nutr. Metab. (Lond).* **2010**, *7*, 47.

[77] C. C. Zouboulis. *Dermatoendocrinol.* **2009**, *1*, 250.

[78] C. C. Zouboulis, W. C. Chen, M. J. Thornton, K. Qin, R. Rosenfield. *Hormone Metab. Res.* **2007**, *39*, 85.

[79] K. R. Feingold, B. E. Brown, S. R. Lear, A. H. Moser, P. M. Elias. *J. Invest. Dermatol.* **1983**, *81*, 365.

[80] J. B. Hamilton. *J. Clin. Endocrinol. Metab.* **1960**, *20*, 1309.

[81] R. S. English Jr. *Med. Hypotheses* **2018**, *111*, 73.

[82] M. D. Taves, C. E. Gomez-Sanchez, K. K. Soma. *Am. J. Physiol. Endocrinol. Metab.* **2011**, *301*, E11.

[83] K. Kretzschmar, D. L. Cottle, P. J. Schweiger, F. M. Watt. *J. Invest. Dermatol.* **2015**, *135*, 2753.

[84] P. Sánchez, C. Serrano-Falcón, J. Torres, S. Serrano. *Arch. Dermatol. Res.* **2018**, *310*, 77.

[85] T. Hibino, T. Nishiyama. *J. Dermatol. Sci.* **2004**, *35*, 9.

[86] H. Imanishi, D. M. Ansell, J. Chéret, M. Harries, M. Bertolini, N. Sepp, T. Bíró, E. Poblet, F. Jimenez, J. Hardman, S. P. Panicker, C. M. Ward, R. Paus. *J. Invest. Dermatol.* **2018**, *138*, 511.

[87] M. J. Harries, F. Jimenez, A. Izeta, J. Hardman, S. P. Panicker, E. Poblet, R. Paus. *Trends Mol. Med.* **2018**, *24*, 435.

[88] C. Tziotzios, C. M. Stefanato, D. A. Fenton, M. A. Simpson, J. A. McGrath. *Exp. Dermatol.* **2016**, *25*, 847.

[89] N. K. Gaspar. *An. Bras. Dermatol.* **2016**, *91*, 776.

[90] M. A. T. Brunner, V. Jagannathan, D. P. Waluk, P. Roosje, M. Linek, L. Panakova, T. Leeb, D. J. Wiener, M. M. Welle. *PLoS One* **2017**, *12*, e0186469.

[91] P. Karnik, Z. Tekeste, T. S. McCormick, A. C. Gilliam, V. H. Price, K. D. Cooper, P. Mirmirani. *J. Invest. Dermatol.* **2009**, *129*, 1243.

[92] S. Harnchoowong, P. Suchonwanit. *PPAR Res.* **2017**, *2017*, 12.

[93] M. Gupta, V. K. Mahajan, K. S. Mehta, P. S. Chauhan, R. Rawat. *Arch. Dermatol. Res.* **2015**, *307*, 767.

[94] Y. Ramot, A. Mastrofrancesco, E. Camera, P. Desreumaux, R. Paus, M. Picardo. *Exp. Dermatol.* **2015**, *24*, 245.

[95] D. S. Straus, C. K. Glass. *Trends Immunol.* **2007**, *28*, 551.

[96] S. Mandard, F. Zandbergen, N. S. Tan, P. Escher, D. Patsouris, W. Koenig, R. Kleemann, A. Bakker, F. Veenman, W. Wahli, M. Müller, S. Kersten. *J. Biol. Chem.* **2004**, *279*, 34411.

[97] N. Billoni, B. Buan, B. Gautier, C. Collin, O. Gaillard, Y. F. Mahé, B. A. Bernard. *Acta dermatovenereol.* **2000**, *80*, 329.

[98] N. Di-Poï, L. Michalik, B. Desvergne, W. Wahli. *Lipids* **2004**, *39*, 1093.

[99] G. Icre, W. Wahli, L. Michalik. *J. Investig. Dermatol. Symp. Proc.* **2006**, *11*, 30.

[100] Y. Ramot, A. Mastrofrancesco, E. Herczeg-Lisztes, T. Bíró, M. Picardo, J. E. Kloepper, R. Paus. *J. Invest. Dermatol.* **2014**, *134*, 1128.

[101] A. K. Reka, H. Kurapati, V. R. Narala, G. Bommer, J. Chen, T. J. Standiford, V. G. Keshamouni. *Mol. Cancer Ther.* **2010**, *9*, 3221.

[102] N. A. Mesinkovska, A. Tellez, D. Dawes, M. Piliang, W. Bergfeld. *J. Am. Acad. Dermatol.* **2015**, *72*, 355.

[103] M.-T. Romano, A. Tafazzoli, M. Mattern, S. Sivalingam, S. Wolf, A. Rupp, H. Thiele, J. Altmüller, P. Nürnberg, J. Ellwanger, R. Gambon, A. Baumer, N. Kohlschmidt, D. Metze, S. Holdenrieder, R. Paus, D. Lütjohann, J. Frank, M. Geyer, M. Bertolini, P. Kokordelis, R. C. Betz. *Am. J. Hum. Genet.* **2018**, *103*, 777.

[104] L. J. Sharpe, A. J. Brown. *J. Biol. Chem.* **2013**, *288*, 18707.

[105] N. Sever, T. Yang, M. S. Brown, J. L. Goldstein, R. A. DeBose-Boyd. *Mol. Cell* **2003**, *11*, 25.

[106] A. Wechsler, A. Brafman, M. Shafir, M. Heverin, H. Gottlieb, G. Damari, S. Gozlan-Kelner, I. Spivak, O. Moshkin, E. Fridman, Y. Becker, R. Skaliter, P. Einat, A. Faerman, I. Björkhem, E. Feinstein. *Science* **2003**, *302*, 2087.

[107] D. Zhang, W. Tomisato, L. Su, L. Sun, J. H. Choi, Z. Zhang, K.-W. Wang, X. Zhan, M. Choi, X. Li, M. Tang, J. M. Castro-Perez, S. Hildebrand, A. R. Murray, E. M. Y. Moresco, B. Beutler. *Proc. Natl. Acad. Sci. USA.* **2017**, *114*, E5197.

[108] R. Hayashi, K. Yoshida, R. Abe, H. Niizeki, Y. Shimomura. *J. Dermatol. Sci.* **2017**, *85*, 63.

[109] H. Ahmed, E. A. O'Toole. *Pediatr. Dermatol.* **2014**, *31*, 539.

[110] A. C. Thomas, T. Cullup, E. E. Norgett, T. Hill, S. Barton, B. A. Dale, E. Sprecher, E. Sheridan, A. E. Taylor, R. S. Wilroy, C. DeLozier, N. Burrows, H. Goodyear, P. Fleckman, K. G. Stephens, L. Mehta, R. M. Watson, R. Graham, R. Wolf, A. Slavotinek, M. Martin, D. Bourn, C. A. Mein, E. A. O'Toole, D. P. Kelsell. *J. Invest. Dermatol.* **2006**, *126*, 2408.

[111] Y. Fu, N. Mukhamedova, S. Ip, W. D'Souza, K. J. Henley, T. DiTommaso, R. Kesani, M. Ditiatkovski, L. Jones, R. M. Lane, G. Jennings, I. M. Smyth, B. T. Kile, D. Sviridov. *Cell Metab.* **2013**, *18*, 225.

[112] I. S. Haslam, C. El-Chami, H. Faruqi, A. Shahmalak, C. A. O'Neill, R. Paus. *Br. J. Dermatol.* **2015**, *172*, 1562.

[113] L. Basel-Vanagaite, R. Attia, A. Ishida-Yamamoto, L. Rainshtein, D. Ben Amitai, R. Lurie, M. Pasmanik-Chor, M. Indelman, A. Zvulunov, S. Saban, N. Magal, E. Sprecher, M. Shohat. *Am. J. Hum. Genet.* **2007**, *80*, 467.

[114] M. Akiyama. *Biochim. Biophys. Acta* **2014**, *1841*, 435.

[115] C. Araujo, M. Goncalves-Rocha, C. Resende, A. P. Vieira, C. Brito. *Case Rep. Med.* **2015**, *2015*, 450937.

[116] D Bornholdt, TP Atkinson, B Bouadjar, B. Catteau, H. Cox, D. DeSilva, J. Fischer, C. N. Gunasekera, S. Hadj-Rabia, R. Happle, M. Holder-Espinasse, E. Kaminski, A. König, A. Mégarbané, H. Mégarbané, U. Neidel, F. Oeffner, V. Oji, A. Theos, H. Traupe, A. Vahlquist, B. W. vanBon, M. Virtanen, K. H. Grzeschik. *Hum. Mutat.* **2013**, *34*, 587.

[117] K. Fong, T. Takeichi, L. Liu, R. Pramanik, J. Lee, M. Akiyama, J. A. McGrath. *Clin. Exp. Dermatol.* **2015**, *40*, 529.

[118] K. Izumi, A. Wilkens, J. R. Treat, H. B. Pride, I. D. Krantz. *Pediatr. Dermatol.* **2013**, *30*, e263.

[119] H. Megarbane, A. Megarbane. *Orphanet. J. Rare Dis.* **2011**, *6*, 29.

[120] A. Ming, R. Happle, K. H. Grzeschik, G. Fischer. *Pediatr. Dermatol.* **2009**, *26*, 427.

[121] G. Nemer, R. Safi, F. Kreidieh, J. Usta, C. Bergqvist, F. Ballout, W. Btadini, N. Hamzeh, O. Abbas, A. G. Kibbi, Y. Shimomura, M. Kurban. *Arch. Dermatol. Res.* **2017**, *309*, 637.

[122] F. Oeffner, G. Fischer, R. Happle, A. König, R. C. Betz, D. Bornholdt, U. Neidel, M. delCarmen Boente, S. Redler, J. Romero-Gomez, A. Salhi, Á. Vera-Casaño, C. Weirich, K.-H. Grzeschik. *Am. J. Hum. Genet.* **2009**, *84*, 459.

[123] H. J. Wang, Z. L. Tang, Z. M. Lin, L. L. Dai, Q. Chen, Y. Yang. *Clin. Exp. Dermatol.* **2014**, *39*, 158.

[124] E. Aten, L. C. Brasz, D. Bornholdt, I. B. Hooijkaas, M. E. Porteous, V. P. Sybert, M. H. Vermeer, R. H. A. M. Vossen, M. J. R. van derWielen, E. Bakker, M. H. Breuning, K.-H. Grzeschik, J. C. Oosterwijk, J. T. denDunnen. *Hum. Mutat.* **2010**, *31*, 1125.

[125] K. Fong, E. K. Wedgeworth, J. E. Lai-Cheong, I. Tosi, J. E. Mellerio, A. M. Powell, J. A. McGrath. *Clin. Exp. Dermatol.* **2012**, *37*, 631.

[126] J. Zhang, Y. Wang, R. Cheng, C. Ni, J. Liang, M. Li, Z. Yao. *Clin. Exp. Dermatol.* **2016**, *41*, 757.

[127] A. Haghighi, C. A. Scott, D. S. Poon, R. Yaghoobi, N. Saleh-Gohari, V. Plagnol, D. P. Kelsell. *J. Invest. Dermatol.* **2013**, *133*, 571.

[128] S. Duchatelet, A. Hovnanian. *Orphanet J. Rare Dis.* **2015**, *10*, 33.

[129] N. Braverman, P. Lin, F. F. Moebius, C. Obie, A. Moser, H. Glossmann, W. R. Wilcox, D. L. Rimoin, M. Smith, L. Kratz, R. I. Kelley, D. Valle. *Nat. Genet.* **1999**, *22*, 291.

[130] S. Ikegawa, H. Ohashi, T. Ogata, A. Honda, M. Tsukahara, T. Kubo, M. Kimizuka, M. Shimode, T. Hasegawa, G. Nishimura, Y. Nakamura. *Am. J. Med. Genet.* **2000**, *94*, 300.

[131] F. Morice-Picard, E. Kostrzewa, C. Wolf, P. Benlian, A. Taieb, D. Lacombe. *Arch. Dermatol.* **2011**, *147*, 1073.

[132] P. M. Steijlen, M. vanGeel, M. Vreeburg, D. Marcus-Soekarman, L. J. Spaapen, F. C. Castelijns, M. Willemsen, M. A. vanSteensel. *Br. J. Dermatol.* **2007**, *157*, 1225.

[133] C. Lambrecht, C. Wouters, H. VanEsch, P. Moens, I. Casteels, M. A. Morren. *Pediatr. Dermatol.* **2014**;*31*:493.

[134] H. Martanova, A. Krepelova, A. Baxova, H. Hansíková, Z. Cánský, M. Kvapil, V. Gregor, M. Magner, J. Zeman. *Prague Med. Rep.* **2007**, *108*, 263.

[135] C. Has, L. Bruckner-Tuderman, D. Müller, M. Floeth, E. Folkers, D. Donnai, H. Traupe. *Hum. Mol. Genet.* **2000**, *9*, 1951.

[136] S. Arias-Santiago, M. T. Gutierrez-Salmeron, A. Buendia-Eisman, M. S. Giron-Prieto, R. Naranjo-Sintes. *Acta dermatovenereol.* **2010**, *90*, 485.

[137] S. Arias-Santiago, M. T. Gutierrez-Salmeron, L. Castellote-Caballero, A. Buendia-Eisman, R. Naranjo-Sintes. *Actas Dermosifiliogr.* **2010**, *101*, 248.

[138] J. A. Ellis, M. Stebbing, S. B. Harrap. *Clin. Sci. (Lond).* **2001**, *100*, 401.

[139] C. A. Guzzo, D. J. Margolis, J. Johnson. *Dermatol. Surg.* **1996**, *22*, 481.

[140] S. Sasmaz, M. Senol, A. Ozcan, G. Dogan, C. Tuncer, O. Akyol, S. Sener. *J. Eur. Acad. Dermatol. Venereol.* **1999**, *12*, 123.

[141] K. H. Sharma, A. Jindal. *Int. J. Trichology.* **2014**, *6*, 5.

[142] L. Sharma, A. Dubey, P. R. Gupta, A. Agrawal. *Indian Dermatol. Online J.* **2013**, *4*, 283.

[143] M. Trevisan, E. Farinaro, V. Krogh, F. Jossa, D. Giumetti, G. Fusco, S. Panico, C. Mellone, S. Frascatore, A. Scottoni, M. Mancini. *J. Clin. Epidemiol.* **1993**, *46*, 1213.

[144] F. Acibucu, M. Kayatas, F. Candan. *Singapore Med. J.* **2010**, *51*, 931.

[145] N. F. Agamia, Y. T. Abou, A. El-Hadidy, A. El-Abd. *Arab. J. Urol.* **2016**, *14*, 157.

[146] O. A. Bakry, S. M. ElFarargy, N. Ghanayem, A. Soliman. *Int. J. Dermatol.* **2015**, *54*, e339.

[147] H. S. Banger, S. K. Malhotra, S. Singh, M. Mahajan. *Int. J. Trichology.* **2015**, *7*, 141.

[148] S. Chakrabarty, R. Hariharan, D. Gowda, H. Suresh. *Int. J. Trichology.* **2014**, *6*, 50.

[149] M. H. ElSayed, M. A. Abdallah, D. G. Aly, N. H. Khater. *Int. J. Dermatol.* **2016**, *55*, 1131.

[150] S. A. S. Thakare, A. Early-onset. *Int. J. Recent Surg. Med. Sci.* **2016**, *2*, 5.

[151] M. W. Kim, I. S. Shin, H. S. Yoon, S. Cho, H. S. Park. *J. Eur. Acad. Dermatol. Venereol.* **2017**, *31*, 942.

[152] H. I. El-Sayyad, S. A. Khalifa, Y. A. Fouda, A. S. Yonis. *Nutrition* **2012**, *28*, 698.

[153] S. Arias-Santiago, M. T. Gutierrez-Salmeron, A. Buendia-Eisman, M. S. Giron-Prieto, R. Naranjo-Sintes. *Int. J. Dermatol.* **2010**, *49*, 1340.

[154] S. Arias-Santiago, M. T. Gutierrez-Salmeron, L. Castellote-Caballero, A. Buendia-Eisman, R. Naranjo-Sintes. *J. Am. Acad. Dermatol.* **2010**, *63*, 420.

[155] O. A. Bakry, M. A. Shoeib, M. K. ElShafiee, A. Hassan. *Indian Dermatol. Online J.* **2014**, *5*, 276.

[156] S. Inui, S. Itami. *Exp. Dermatol.* **2013**, *22*, 168.

[157] C. Pierard-Franchimont, G. E. Pierard. *Biomed. Res. Int.* **2013**, *2013*, 957432.

[158] S. Inui, S. Itami. *J. Dermatol. Sci.* **2011**, *61*, 1.

[159] M. E. Sawaya, V. H. Price. *J. Invest. Dermatol.* **1997**, *109*, 296.

[160] G. Nikolakis, C. A. Stratakis, T. Kanaki, A. Slominski, C. C. Zouboulis. *Rev. Endocr. Metab. Disord.* **2016**, *17*, 247.

[161] J.-J. Lai, P. Chang, K.-P. Lai, L. Chen, C. Chang. *Arch. Dermatol. Res.* **2012**, *304*, 499.

[162] T. Hibino, T. Nishiyama. *J. Dermatol. Sci.* **2004**, *35*, 9.

[163] Z. Zhou, S. Song, Z. Gao, J. Wu, J. Ma, Y. Cui. *Clin. Interv. Aging* **2019**, *14*, 399.

[164] Z. Santos, P. Avci, M. R. Hamblin. *Expert Opin. Drug Discov.* **2015**, *10*, 269.

[165] M. V. Patel, I. A. McKay, J. M. Burrin. *J. Invest. Dermatol.* **2001**, *117*, 1559.

[166] R. F. Hannen, A. E. Michael, A. Jaulim, R. Bhogal, J. M. Burrin, M. P. Philpott. *Biochem. Biophys. Res. Comm.* **2011**, *404*, 62.

[167] Y. Zhang, J. Xu, J. Jing, X. Wu, Z. Lv. *Med. Sci. Monit.* **2018**, *24*, 7770.

[168] I. Urysiak-Czubatka, M. L. Kmieć, G. Broniarczyk-Dyła. *Postepy Dermatol. Alergol.* **2014**, *31*, 207.

[169] V. Spustova, R. Dzurik. *Vnitr. Lek.* **2004**, *50*, 537.

[170] D. D. Bikle. *J. Bone Miner. Metab.* **2010**, *28*, 117.

[171] M. B. Demay. *Arch. Biochem. Biophys.* **2012**, *523*, 19.

[172] M. B. Demay, P. N. MacDonald, K. Skorija, D. R. Dowd, L. Cianferotti, M. Cox. *J. Steroid Biochem. Mol. Biol.* **2007**, *103*, 344.

[173] P. J. Malloy, Z. Hochberg, D. Tiosano, J. W. Pike, M. R. Hughes, D. Feldman. *J. Clin. Investig.* **1990**, *86*, 2071.

[174] S. Lee, B. J. Kim, C. H. Lee, W. S. Lee. *J. Eur. Acad. Dermatol. Venereol.* **2018**, *32*, 1214.

[175] R. Ghafoor, M. I. Anwar. *J. Coll. Phys. Surg.-Pak.* **2017**, *27*, 200.

[176] T. Y. Tsai, Y. C. Huang. *J. Am. Acad. Dermatol.* **2018**, *78*, 207.

[177] *Horm. Res. Paediatrics.* **2018**;*90*:1.

[178] D. H. Kim, J. W. Lee, I. S. Kim, S. Y. Choi, Y. Y. Lim, H. M. Kim, B. J. Kim, M. N. Kim. *Ann. Dermatol.* **2012**, *24*, 341.

[179] R. Paus, M. B. Schilli, B. Handjiski, A. Menrad, B. M. Henz, P. Plonka. *Can. Res.* **1996**, *56*, 4438.

[180] A. S. Segal. *Am. J. Med.* **2002**, *113*, 171.

[181] Y. A. Mohammad-Ali, R. Preethi, K. Kenneth, K. Heinz, A. Kortz, C. J. Andrew. *J. Cutan. Pathol.* **2015**, *42*, 746.

[182] L. Smeeth, I. Douglas, A. J. Hall, R. Hubbard, S. Evans. *Br. J. Clin. Pharmacol.* **2009**, *67*, 99.

[183] C. Loi, M. Starace, B. M. Piraccini. *J. Am. Acad. Dermatol.* **2016**, *74*, e99.

[184] G. M. Freitas, R. M. Trueb. *Skin Appendage Disord.* **2017**, *3*, 156.

[185] C. Lattouf, L. A. Schachner, T. C. Wikramanayake, C. Kittles, A. Tosti, M. Miteva, J. J. Jimenez, I. Herskovitz, M. Z. Handler, G. Fabbrocini. *J. Am. Acad. Dermatol.* **2016**, *74*, e101.

[186] K. J. McElwee, P. Freyschmidt-Paul, R. Hoffmann, S. Kissling, S. Hummel, M. Vitacolonna, M. Zöller. *J. Invest. Dermatol.* **2005**, *124*, 947.

[187] M. R. Namazi. *Exp. Dermatol.* **2004**, *13*, 337.

[188] J. Mackay-Wiggan, A. Jabbari, N. Nguyen, J. E. Cerise, C. Clark, G. Ulerio, M. Furniss, R. Vaughan, A. M. Christiano, R. Clynes. *JCI Insight.* **2016**, *1*, e89790.

[189] S. K. Krisans. *Am. J. Respir. Cell Mol. Biol.* **1992**, *7*, 358.

[190] P. Borst, N. Zelcer, A. vanHelvoort. *Biochim. Biophys. Acta.* **2000**, *1486*, 128.

[191] E. J. Tarling, T. Q. deAguiar Vallim, P. A. Edwards. *Trends Endocrinol. Metab.* **2013**, *24*, 342.

[192] S. Chung, J. S. Parks. *Curr. Opin. Lipidol.* **2016**, *27*, 19.

[193] J. Li, V. Papadopoulos, V. Vihma. *Steroids* **2015**, *103*, 89.

[194] W. S. Lee. *J. Dermatol. Sci.* **2011**, *64*, 153.

[195] L. Coderch, S. Mendez, C. Barba, R. Pons, M. Marti, J. L. Parra. *Chem. Phys. Lipids.* **2008**, *155*, 1.

[196] Y. Masukawa, H. Narita, G. Imokawa. *J. Cosmet. Sci.* **2005**, *56*, 1.

[197] C. F. Cruz, M. M. Fernandes, A. C. Gomes, L. Coderch, M. Martí, S. Méndez, L. Gales, N. G. Azoia, U. Shimanovich, A. Cavaco-Paulo. *Int. J. Cosmet. Sci.* **2013**, *35*, 244.

[198] S. M. Puhvel, R. M. Reisner, M. Sakamoto. *J. Invest. Dermatol.* **1975**, *64*, 406.

[199] P. M. Elias, M. L. Williams, E. H. Choi, K. R. Feingold. *Biochim. Biophys. Acta.* **2014**, *1841*, 353.

Appendix 2   Cell counting macro

```
/*
 * Description: Counting cells using ilastik segmentation
 */

//selecting input folder
#@ File (label="Select experiment folder", style="directory") inFolder
inFolder+=File.separator;
//Generate results folder in the inFolder
outFolder = inFolder + File.separator + "counts" + File.separator;
File.makeDirectory(outFolder);
//clearing
run("Clear Results");
run("Close All");
roiManager("reset");
print("\\Clear");
close("Log");
//running without images
setBatchMode(true);
print("Title" + "," + "Cells" + ",");

//loop for files
fileList = getFileList(inFolder);
for (i = 0; i < fileList.length; i++) {
        currentFile =fileList[i];
//opening files in loop
        if (endsWith(currentFile, ".h5")) {
filePath = inFolder + currentFile;
run("Import HDF5", "select=["+ filePath +"] axisorder=[yxc]");
run("Duplicate...", "title=[duplicate] duplicate");
rename(currentFile);
run("Convert to Mask", "method=Otsu background=Dark black");
run("Options...", "iterations=7 count=1 black do=Close stack");
run("Fill Holes", "stack");
run("Analyze Particles...", "size=1000-Infinity pixel add slice");
Title = getTitle();
nRoi = roiManager("count");
print(Title + "," + nRoi + ",");
roiManager("reset");
run("Close All");
        }
}

//save log as CSV
string = getInfo("log");
path = outFolder + "Cell_counts.csv";
File.saveString(string, path);
print("\\Clear");
close("Log")
```

247

Appendix 3   Pixel intensity macro

```
/*
 * Description: Measure pixel intensity per cell using ilastik segmentation
 */

//selecting input folder
#@ File (label="Select experiment folder", style="directory") inFolder
inFolder+=File.separator;
//Generate results folder in the inFolder
outFolder = inFolder + File.separator + "cell" + File.separator;
File.makeDirectory(outFolder);
//clearing
run("Clear Results");
run("Close All");
roiManager("reset");
print("\\Clear");
close("Log");
//running without images
setBatchMode(true);

//loop for files
fileList = getFileList(inFolder);
for (i = 0; i < fileList.length; i++) {
        currentFile =fileList[i];
//opening tif
if (endsWith(currentFile, ".tif")) {
                filePath2 = inFolder + currentFile;
                open(filePath2);
run("Duplicate...", "title=signal duplicate range=2");
}

//opening hdf5 files in loop
        if (endsWith(currentFile, ".h5")) {
filePath = inFolder + currentFile;
run("Import HDF5", "select=["+ filePath +"] axisorder=[cyx]");
run("Duplicate...", "title=[duplicate] duplicate channels=1");
rename(currentFile);
run("Convert to Mask", "method=Otsu background=Dark black");
run("Options...", "iterations=12 count=1 black do=Close stack");
run("Fill Holes", "stack");
run("Watershed");
run("Set Measurements...", "area mean perimeter display redirect=[signal] decimal=3");
run("Analyze Particles...", "size=200-Infinity pixel summarize");
run("Close All");
        }
}

//save as CSV
saveAs("Results", outFolder + File.separator + "cell_results.csv");
```

Appendix 4   Co-localisation macro

```
/*
 * Description: Masking pixel intensity to organelle marker
 */

//selecting input folder
#@ File (label="Select experiment folder", style="directory") inFolder
inFolder+=File.separator;

//Generate results folder in the inFolder
outFolder = inFolder + File.separator + "Masking_Results" + File.separator;
File.makeDirectory(outFolder);

//clearing
run("Clear Results");
run("Close All");
print("\\Clear");
close("Log");

//running without images
setBatchMode(true);

print("Treatment,,,Mean,Count,Total Area,% Area,Average size");

fileList = getFileList(inFolder);
for (i = 0; i < fileList.length; i++) {
        currentFile =fileList[i];

        if (endsWith(currentFile, ".czi")) {
filePath = inFolder + currentFile;
open(filePath);

//naming images
rename("Image");
run("Split Channels");
selectWindow("C1-Image");
rename("organelle");
selectWindow("C2-Image");
rename("signal");

// masking to organelle
selectWindow("organelle");
setAutoThreshold("Otsu dark");
run("Convert to Mask");
run("Set Measurements...", "mean display redirect=signal decimal=3");
run("Analyze Particles...", "size=100-Infinity pixel summarize");


IJ.renameResults("Results");
```

```
Mean = getResult("Mean", 0);
Count = getResult("Count", 0);
TA = getResult("Total Area", 0);
PA = getResult("%Area", 0);
Area = getResult("Average Size", 0);


dotIndex = indexOf(currentFile, ".");
    Title = substring(currentFile, 0, dotIndex);
print(Title + "," + "" + "," + "" + "," + Mean + "," + Count + "," + TA + "," + PA + "," + Area);

run("Close All");
        }
}
//save log as CSV
string = getInfo("log");
path = outFolder + "results.csv";
File.saveString(string, path);


print("\\Clear");
run("Clear Results");
```

Appendix 5 Co-localisation co-efficient macro

```
/*
 * Description: Using BIOP JaCoP plugin to measure co-localisation
 */

#@ File (label="Select experiment folder", style="directory") inFolder
#@ File (label="Select output folder", style="directory") outFolder
#@ String (label="Type folder name", style="text field") folder

inFolder+=File.separator;
outFolder+=File.separator;

//clearing
run("Clear Results");
run("Close All");
//running without images
setBatchMode(true);

fileList = getFileList(inFolder);
for (i = 0; i < fileList.length; i++) {
        currentFile =fileList[i];

//co-loc channel 1 and 2
        if (endsWith(currentFile, ".czi")) {
filePath = inFolder + currentFile;
open(filePath);
run("BIOP JACoP", "channel_a=1 channel_b=2 threshold_for_channel_a=Moments
threshold_for_channel_b=Otsu manual_threshold_a=0 manual_threshold_b=0 get_pearsons
get_manders costes_block_size=5 costes_number_of_shuffling=100");
run("Close All");
        }
}

//savings results
saveAs("Results", outFolder + File.separator + folder + "coloc.csv");
run("Clear Results");
```

Appendix 6   BODIPY cholesterol intensity macro

```
/*
 * Description: Measure intensity of BODIPY channel from maximum intensity projection
*/

//selecting input folder
#@ File (label="Select experiment folder", style="directory") inFolder
inFolder+=File.separator;

//Generate results folder in the inFolder
outFolder = inFolder + File.separator + "Results" + File.separator;
File.makeDirectory(outFolder);

//running without images
setBatchMode(true);

//clearing
run("Clear Results");
run("Close All");
run("Set Measurements...", "mean display redirect=None decimal=3");

//loop for files
fileList = getFileList(inFolder);
for (i = 0; i < fileList.length; i++) {
        currentFile =fileList[i];

        //opening files in loop Note: change file type eg. tif/czi ect.
        if (endsWith(currentFile, ".czi")) {
filePath = inFolder + currentFile;
open(filePath);

//select BODIPY
selectWindow(currentFile + " - C=2");
run("Z Project...", "projection=[Max Intensity]");
run("Measure");
run("Close All");
        }
}

saveAs("Results", outFolder + File.separator + "BODIPY.csv");
run("Clear Results");
run("Close All");

text = "\n%%% Congratulation your file have been successfully processed %%%";
        print(text);
```

Appendix 7   BODIPY co-localisation macro

```
/*
 * Description: Masking pixel intensity to organelle marker using maximum intensity projection
 */

//selecting input folder
#@ File (label="Select experiment folder", style="directory") inFolder
inFolder+=File.separator;

//Generate results folder in the inFolder
outFolder = inFolder + File.separator + "Masking_Results" + File.separator;
File.makeDirectory(outFolder);

//clearing
run("Clear Results");
run("Close All");
print("\\Clear");
close("Log");

//running without images
setBatchMode(true);

print("Donor_Treatment_Time,,,Lysosome,Count,Total        Area,%        Area,Average
size,ER,Count,Total Area,% Area,Average size,Mitochondria,Count,Total Area,% Area,Average
size");

fileList = getFileList(inFolder);
for (i = 0; i < fileList.length; i++) {
        currentFile =fileList[i];

        if (endsWith(currentFile, ".czi")) {
filePath = inFolder + currentFile;
open(filePath);

//naming images
run("Z Project...", "projection=[Max Intensity]");
rename("Image");
run("Split Channels");
selectWindow("C1-Image");
rename("lysosome");
selectWindow("C2-Image");
rename("ER");
selectWindow("C3-Image");
rename("Bodipy");
selectWindow("C4-Image");
rename("mitochondria");

// masking to C1
selectWindow("lysosome");
```

```
setAutoThreshold("Otsu dark");
run("Convert to Mask");
run("Set Measurements...", "mean display redirect=Bodipy decimal=3");
run("Analyze Particles...", "size=100-Infinity pixel summarize");

// masking to C2
selectWindow("ER");
setAutoThreshold("Moments dark");
run("Convert to Mask");
run("Set Measurements...", "mean display redirect=Bodipy decimal=3");
run("Analyze Particles...", "size=100-Infinity pixel summarize");

// masking to C4
selectWindow("mitochondria");
setAutoThreshold("Default dark");
run("Convert to Mask");
run("Set Measurements...", "mean display redirect=Bodipy decimal=3");
run("Analyze Particles...", "size=10-Infinity pixel summarize");

IJ.renameResults("Results");
Lysosome = getResult("Mean", 0);
LCount = getResult("Count", 0);
LTA = getResult("Total Area", 0);
LPA = getResult("%Area", 0);
LA = getResult("Average Size", 0);

ER = getResult("Mean", 1);
ERCount = getResult("Count", 1);
ERTA = getResult("Total Area", 1);
ERPA = getResult("%Area", 1);
ERA = getResult("Average Size", 1);

Mitochondria = getResult("Mean", 2);
MCount = getResult("Count", 2);
MTA = getResult("Total Area", 2);
MPA = getResult("%Area", 2);
MA = getResult("Average Size", 2);

dotIndex = indexOf(currentFile, ".");
    Title = substring(currentFile, 0, dotIndex);
print(Title + "," + "" + "," + "" + "," + Lysosome + "," + LCount + "," + LTA + "," + LPA + "," + LA +
"," + ER + "," + ERCount + "," + ERTA + "," + ERPA +
"," + ERA + "," + Mitochondria + "," + MCount + "," + MTA + "," + MPA + "," + MA);
run("Close All");
        }
}
//save log as CSV
string = getInfo("log");
path = outFolder + "results.csv";
File.saveString(string, path);
print("\\Clear");
```

Appendix 8   Manufactures protocols

Protocol	Manufactures instructions link
MTT assay	https://www.thermofisher.com/uk/en/home/references/protocols/cell-culture/mtt-assay-protocol/vybrant-mtt-cell-proliferation-assay-kit.html
RNA extraction (Promega)	https://www.promega.co.uk/-/media/files/resources/protcards/reliaprep-rna-cell-miniprep-system-quick-protocol.pdf?la=en
RNA extraction (Qiagen mini)	https://www.qiagen.com/gb/resources/download.aspx?id=1d882bbe-c71d-4fec-bdd2-bc855d3a4b55&lang=en
RNA extraction (Qiagen micro)	https://www.qiagen.com/gb/resources/download.aspx?id=f6f13ba4-0991-45f3-ab5d-0b7b2c9f4799&lang=en
cDNA synthesis	https://www.bioline.com/mwdownloads/download/link/id/3308/
Lysotracker	https://www.thermofisher.com/document-connect/document-connect.html?url=https%3A%2F%2Fassets.thermofisher.com%2FTFS-Assets%2FLSG%2Fmanuals%2Fmp07525.pdf&title=THlzb1RyYWNrZXIgYW5kIEx5c29TZW5zb3IgUHJvYmVz
ER Cytopainter	https://www.abcam.com/ps/products/139/ab139482/documents/ab139482%20-%20CytoPainter%20ER%20Staining%20kit%20red%20fluorescence%20v2b%20(website).pdf
Mitochondria Cytopainter	https://www.abcam.com/ps/products/219/ab219940/documents/MitoBlue-staining-protocol-book-v2-ab219940%20(website).pdf
Bradford assay	https://www.thermofisher.com/document-connect/document-connect.html?url=https%3A%2F%2Fassets.thermofisher.com%2FTFS-Assets%2FLSG%2Fmanuals%2FMAN0011203_CoomassiePlus_Bradford_Asy_UG.pdf&title=VXNlciBHdWlkZTogIENvb21hc3NpZSBQbHVzIChCcmFkZm9yZCkgQXNzYXkgS2l0
Nuclear extraction	https://www.abcam.com/ps/products/113/ab113474/documents/ab113474%20Nuclear%20Extraction%20Kit%20v3a%20v2a%20(website).pdf
SREBP2 transcription factor assay	https://www.abcam.com/ps/products/133/ab133111/documents/ab133111%20-%20SREBP-2%20Transcription%20Factor%20Assay%20Kit%20-%20protocol%20v3%20(website).pdf